Contributions to the Chemistry of Higher-Coordinate Silicon: Synthesis, Structure, and Stereodynamics of New Silicon(IV) Complexes with SiO_2N_2C, SiO_4C, or SiO_6 Skeletons

---

Dissertation

zur Erlangung des naturwissenschaftlichen Doktorgrades

der Bayerischen Julius-Maximilians-Universität Würzburg

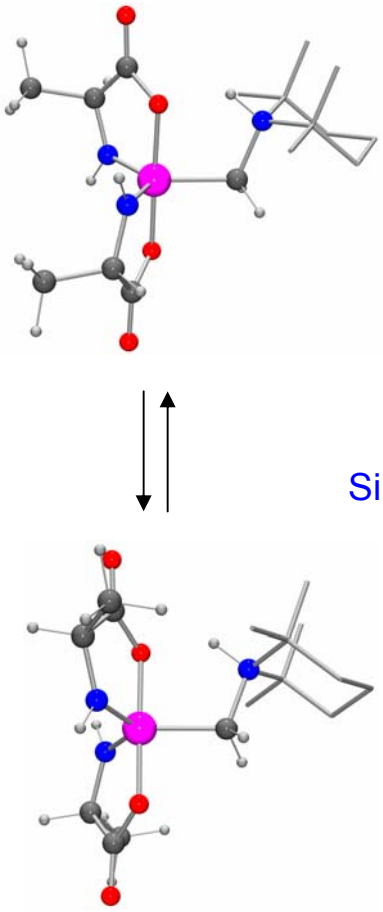

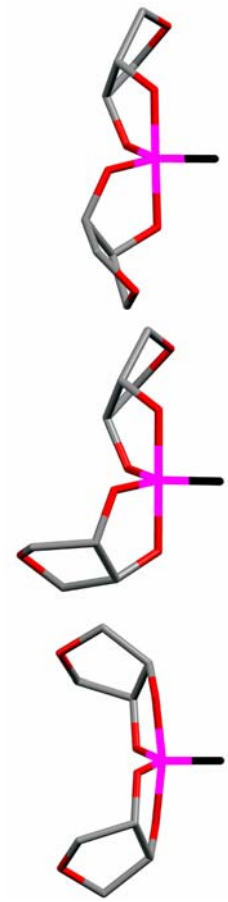

Vorgelegt von

Diplom-Chemikerin

Simona Olimpia Dragota

aus Sibiu/Rumänien

Würzburg 2005

Contributions to the Chemistry of Higher-Coordinate Silicon: Synthesis, Structure, and Stereodynamics of New Silicon(IV) Complexes with $Si O_2N_2C$, $Si O_4C$, or $Si O_6$ Skeletons

Dissertation

zur Erlangung des naturwissenschaftlichen Doktorgrades
der Bayerischen Julius-Maximilians-Universität Würzburg

Vorgelegt von
Diplom-Chemikerin
Simona Olimpia Dragota
aus Sibiu/Rumänien

Würzburg 2005

Eingereicht am: .....
bei der Fakultät für Chemie und Pharmazie

1. Gutachter: Prof. Dr. R. Tacke .....
2. Gutachter: Priv. Doz. Dr. C. Strohmann.....
der Dissertation

1. Prüfer: Prof. Dr. R. Tacke .....
2. Prüfer: .....
des Öffentlichen Promotionskolloquiums

Tag des Öffentlichen Promotionskolloquiums:.....

Doktorurkunde ausgehändigt am:.....

Table of Contents

1 Introduction

Silicon and oxygen are the most abundant elements at the earth's surface, and silicates, including silicon dioxide, are the most common materials. In silicate minerals formed at pressures typical of the Earth's crust, the silicon is usually coordinated by four oxygen atoms. In contrast, silicates formed at higher pressures, typical of the Earth's transition zone and lower mantle, contain predominantly hexacoordinate silicon. Pentacoordinate silicon is not normally found as a structural element in crystalline phases, but is supposed to play a central role in many dynamic processes that occur in silicates: pentacoordinate silicon is probably a component of alumosilicate melts and glasses at mantle temperatures and pressures, where it will dominate their transport properties; it is also believed to act as an intermediate activated state during oxygen diffusion in silicate minerals.[1]

The study of compounds with higher-coordinate silicon atoms is currently one of the main areas of research in silicon chemistry.[2] Silicon is usually tetracoordinate, but has the ability to form higher-coordinate species including heptacoordinate and even octacoordinate silicon complexes.[3] The ligand atoms scale range from strongly electronegative elements like fluorine or oxygen to less electronegative elements like hydrogen, carbon, nitrogen, phosphorus, sulphur, or chlorine. Our group has made substantial contributions to the chemistry of higher-coordinate silicon by investigating the class of zwitterionic pentacoordinate silicates[4] and the class of anionic and neutral hexacoordinate silicon(IV) complexes.[5] Higher-coordinate silicates provide access to a wide variety of new silicon compounds and therefore are in demand in fields ranging from organic synthesis to ceramics to the electronics industry.[6]

Silicon is obviously essential for the growth of animal and plant tissue as is deduced from nutritional and fertilizing experiments.[7] Marine organisms are responsible for the biogeochemical cycling[8] of silicon in the oceans, processing an estimated 6.7 gigatonnes of silicon annually.[9] The organic matter associated with biogenic silica, which controls the silica morphology contains mainly polysaccharides, polyamines, and proteins (silaffins and silicateins), a characteristic feature of silica-associated proteins being the quaternary ammonium cations.[10,11]

2 Objectives

The goal of this thesis was to contribute to the field of silicon chemistry, with a special emphasis on the chemistry of penta- and hexacoordinate silicon.

In continuation of our studies on higher-coordinate silicon compounds, zwitterionic λ^5*Si*-silicates and anionic λ^6*Si*-silicates containing multidentate ligands derived from natural products were to be synthesized and structurally characterized in the solid state and in solution. The goals of this thesis are presented in detail in the following sections.

2.1 Spirocyclic Zwitterionic λ^5*Si*-[(Ammonio)methyl]silicates with an *Si*O_2N_2C Skeleton and Two Identical Bidentate Ligands Derived from α-Amino Acids

The λ^5*Si*-[(ammonio)methyl]silicates of the formula type **A** containing twofold deprotonated α-amino acids (glycine, (*S*)-alanine, (*S*)-phenylalanine, (*S*)-valine, (*S*)-*tert*-leucine, or (*S*)-proline) were to be synthesized and structurally characterized in the solid state (crystal structure analyses; ^{15}N and ^{29}Si VACP/MAS NMR experiments) and in solution (^{1}H, ^{13}C, ^{15}N, and ^{29}Si NMR experiments).

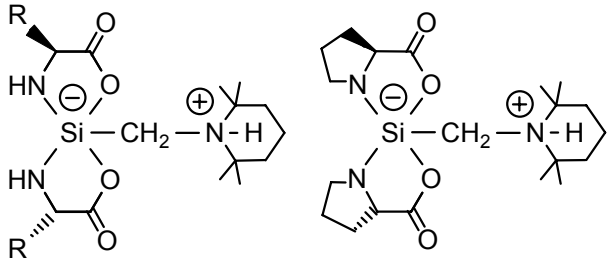

R = H, Me, CH_2Ph, *i*-Pr, *t*-Bu

A

Dynamic NMR experiments (kinetic or variable temperature NMR studies) were to give more insight into the stereodynamic processes of the Si-coordination polyhedra of the zwitterionic compounds of the formula type **A** in solution.

2.2 Spirocyclic Zwitterionic λ^5*Si*-[(Ammonio)methyl]silicates with an *Si*O_4*C* Skeleton and Two Identical Bidentate Ligands Derived from α-Hydroxycarboxylic Acids

The λ^5*Si*-[(ammonio)methyl]silicates of the formula type **B** containing twofold deprotonated α-hydroxycarboxylic acids ((*S*)-lactic acid, (*S*)-3-phenyllactic acid, or (*S*)-mandelic acid) were to be synthesized and structurally characterized in the solid state (crystal structure analyses; ^{15}N and ^{29}Si VACP/MAS NMR experiments) and in solution (^{1}H, ^{13}C, ^{15}N, and ^{29}Si NMR experiments). To find out more information about the stereodynamics of the Si-coordination polyhedra in solution, dynamic NMR experiments were to be performed.

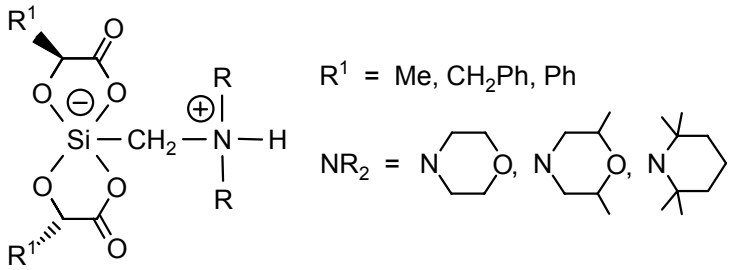

B

2.3 Spirocyclic Zwitterionic λ^5*Si*-[(Ammonio)methyl]silicates with an *Si*O_4*C* Skeleton and Two Identical Bidentate Ligands Derived from *meso*-Oxolane-3,4-diol

The λ^5*Si*-[(ammonio)methyl]silicates of the formula type **C** containing two bidentate *meso*-oxolane-3,4-diolato(2–) ligands were to be synthesized and structurally characterized in the solid state (crystal structure analyses; ^{29}Si VACP/MAS NMR experiments) and in solution (^{1}H, ^{13}C, ^{15}N, and ^{29}Si NMR experiments).

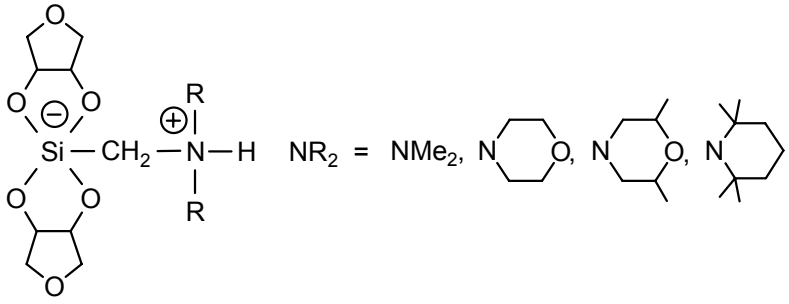

C

The synthesis of bis[*meso*-oxolane-3,4-diolato(2–)][(morpholinio)methyl]silicate has already been reported.[12] This compound was to be synthesized by a new path including Si–C cleavage reactions in aqueous and nonaqueos solutions, and its molecular structure in the crystal was to be determined by X-ray diffraction.

The stability of the λ^5*Si*-silicates of the formula type **C** was to be investigated by NMR spectroscopy in aqueous solutions under mild physiological conditions, with respect to their role as potential model systems for the silicon biochemistry. *meso*-Oxolane-3,4-diol can be regarded as a model system for related diolato(2–) ligands that derive from carbohydrates with *cis*-furanoidic diol moieties.

2.4 Spirocyclic Zwitterionic λ^5*Si*-[(Ammonio)methyl]silicates with an *Si*O_4C Skeleton and Two Identical Bidentate Ligands Derived from Benzoin

The already known bis[*cis*-1,2-diphenylethene-1,2-diolato(2–)][(morpholinio)methyl]-silicate[2o,13] of the formula type **D** was to be synthesized by new methods including Si–C cleavage reactions with benzoin. Furthermore, the dynamic behavior of the derivative bis[*cis*-1,2-diphenylethene-1,2-diolato(2–)][(2,2,6,6-tetramethylpiperidinio)methyl]silicate[14] in solution was to be studied by VT ^{1}H NMR experiments.

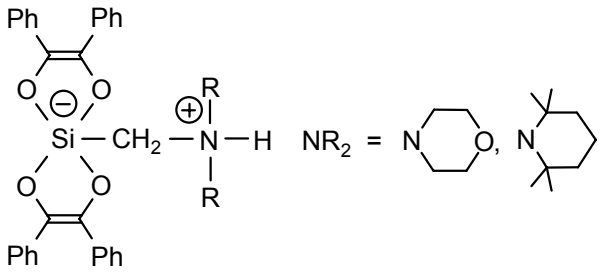

D

2.5 Anionic λ^6*Si*-Silicates with *Si*O_6 Skeletons and Multidentate Ligands Derived from Citric Acid or Malic Acid

Hexacoordinate silicon(IV) complexes of the formula type **E** were to be synthesized and structurally characterized in the solid state (crystal structure analyses; ^{13}C, ^{15}N, and ^{29}Si VACP/MAS NMR experiments). The stability of the λ^6*Si*-silicates in aqueous and

nonaqueous solutions was to be investigated by NMR spectroscopy (^{1}H, ^{13}C, ^{15}N, and ^{29}Si NMR experiments).

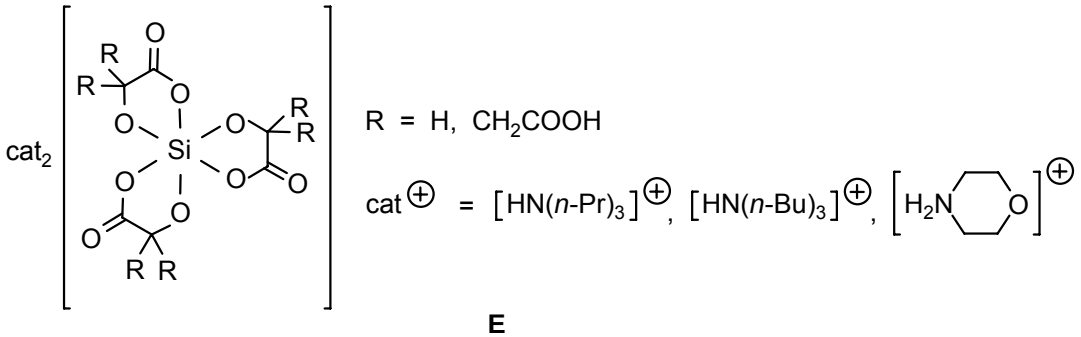

E

These studies were to be performed as part of our research program dealing with hexacoordinate silicon(IV) complexes containing *Si*O$_6$ skeletons, with a special emphasis on the stereochemistry of those λ^6*Si*-silicates that contain unsymmetric multidentate ligands. Hexacoordinate silicon(IV) complexes with *Si*O$_6$ skeletons and multidentate ligands derived from natural products (such as citric acid and malic acid) are of interest as model systems for silicon biochemistry (in this context, see ref. 5 and literature cited therein).

3 Spirocyclic Zwitterionic λ⁵*Si*-[(Ammonio)methyl]silicates with an SiO_2N_2C Skeleton and Two Identical Bidentate Ligands Derived from α-Amino Acids (Compounds 1–6)

A series of zwitterionic λ⁵*Si*-silicates with an (2,2,6,6-tetramethylpiperidinio)methyl group and two identical bidentate chelate ligands derived from glycine, (*S*)-alanine, (*S*)-phenylalanine, (*S*)-valine, (*S*)-*tert*-leucine, or (*S*)-proline was synthesized and structurally characterized.[15] The spirocyclic zwitterionic λ⁵*Si*-silicates **1**–**6** are characterized by a pentacoordinate (formally negatively charged) silicon atom and a tetracoordinate (formally positively charged) nitrogen atom. Compounds *rac*-**1**, (*Δ*,*S*,*S*)-**2** (**2b**), (*Λ*,*S*,*S*)-**3**·CH_2Cl_2 (**3a**·CH_2Cl_2), (*Λ*,*S*,*S*)-**4**·CH_2Cl_2 (**4a**·CH_2Cl_2), (*Λ*,*S*,*S*)-**5**·CH_2Cl_2 (**5a**·CH_2Cl_2), (*Λ*,*S*,*S*)-**6**·2CH_2Cl_2 (**6a**·2CH_2Cl_2), and (*Λ*,*S*,*S*)-**6**·½CH_2Cl_2 (**6a**·½CH_2Cl_2) were structurally characterized in the solid state (crystal structure analyses; ^{15}N and ^{29}Si VACP/MAS NMR experiments) and in solution (^1H, ^{13}C, ^{15}N, and ^{29}Si NMR experiments, including studies of the stereodynamics).

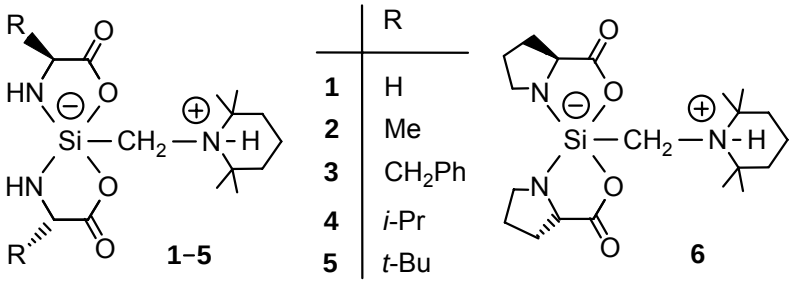

The chiral λ⁵*Si*-[(ammonio)methyl]silicates with ligands derived from optically active α-amino acids were isolated as diastereomerically and enantiomerically pure compounds. Generally, such compounds are characterized by an excellent crystallizability, because they represent polar (zwitterionic) molecules, and they can form intra- and/or intermolecular hydrogen bonds in the crystal. Due to the lipophilic properties of the protonated 2,2,6,6-tetramethylpiperidino group, despite the polar nature of zwitterions, compounds **1**–**6** were expected to be soluble in dichloromethane and, hence, to be accessible to low-temperature solution NMR studies. The experimental investigations were complemented by computational studies of the anionic model species **I** and the related model species **2'**, **4'**, and **6'**.

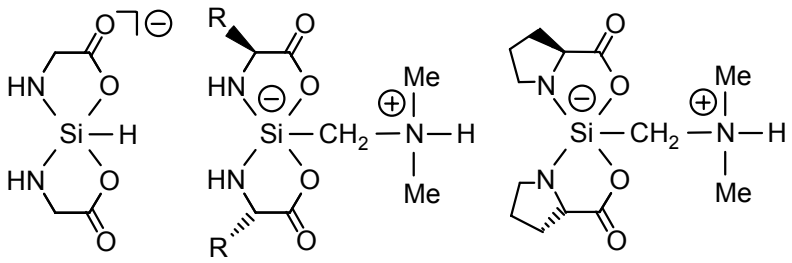

I **2'** (R = Me) **6'**
4' (R = *i*-Pr)

3.1 Syntheses of the λ⁵*Si*-[(Ammonio)methyl]silicates 1–6

Compounds **1**–**3** were prepared according to Scheme 1 by treatment of [(2,2,6,6-tetramethylpiperidino)methyl]silane (**23**) with two molar equivalents of glycine, (*S*)-alanine, or (*S*)-phenylalanine. The syntheses were performed in dichloromethane at 20 °C, and compounds *rac*-**1**, **2b**, and **3a**·CH_2Cl_2 were isolated as colorless crystalline solids (yields: *rac*-**1**, 72%; **2b**, 83%; **3a**·CH_2Cl_2, 77%). Compounds **4**–**6** were prepared analogously according to Scheme 1 by treatment of **23** with two molar equivalents of (*S*)-valine, (*S*)-*tert*-leucine, or (*S*)-proline and were also isolated as colorless crystalline solids (yields: **4a**·CH_2Cl_2, 72%; **5a**·CH_2Cl_2, 78%; **6a**·2CH_2Cl_2, 83%; **6a**·½CH_2Cl_2, 81%). For the preparation of the solvates **6a**·2CH_2Cl_2 and **6a**·½CH_2Cl_2, different synthetic methods were developed (for details, see Chapter 10, Experimental Section).

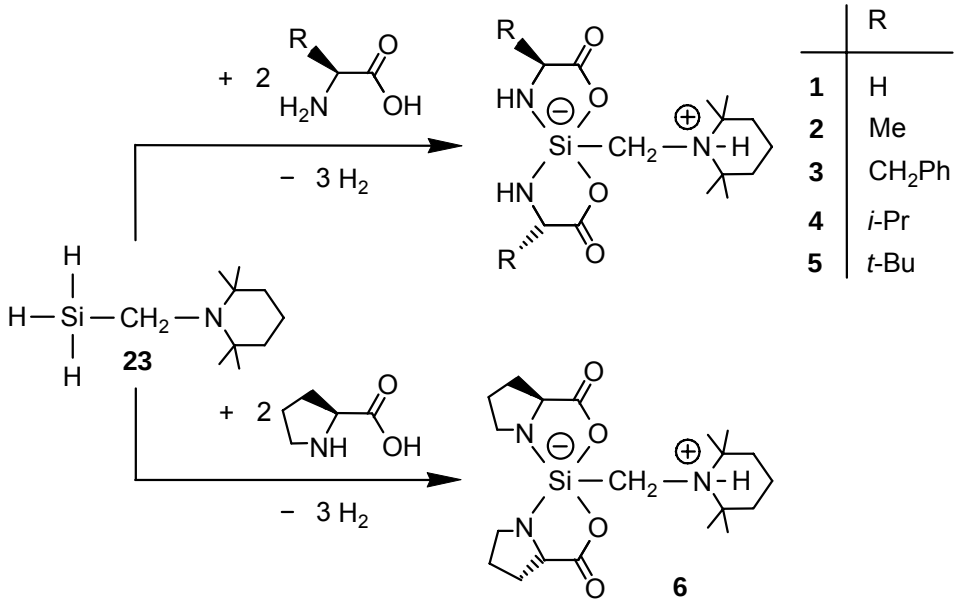

Scheme 1

The identities of *rac*-**1**, **2b**, **3a**·CH_2Cl_2, **4a**·CH_2Cl_2, **5a**·CH_2Cl_2, **6a**·2CH_2Cl_2, and **6a**·½CH_2Cl_2 were established by elemental analyses (C, H, N), single-crystal X-ray

diffraction studies, VACP/MAS NMR experiments (^{15}N, ^{29}Si), and solution NMR studies (^{1}H, ^{13}C, ^{15}N, ^{29}Si).

The resolution of the diastereomers of **2**–**6** by crystallization is quite remarkable, leading to the selective formation of the diastereomerically and enantiomerically pure compounds **2b**, **3a**·CH_2Cl_2, **4a**·CH_2Cl_2, **5a**·CH_2Cl_2, **6a**·2CH_2Cl_2, and **6a**·½CH_2Cl_2.

Theoretically, the formation of the crystalline diastereomerically and enantiomerically pure compounds **2b**, **3a**·CH_2Cl_2, **4a**·CH_2Cl_2, **5a**·CH_2Cl_2, **6a**·2CH_2Cl_2, and **6a**·½CH_2Cl_2 could occur by kinetic or thermodynamic control (kinetic control: selective formation of the respective diastereomers of **2**–**6** in solution, followed by crystallization of the respective solvates without change of absolute configuration of the zwitterionic λ^5*Si*-silicates; thermodynamic control: selective formation of one of the two diastereomers or formation of both diastereomers of **2**–**6**, followed by (*Λ*)/(*Δ*)-epimerization and crystallization of the thermodynamically more stable solvates). In principle, both thermodynamic and kinetic control for this kind of resolution is possible; however, the experimental data available so far do not allow a clear discrimination between these two alternatives.

3.2 Crystal Structure Analyses of the λ^5*Si*-[(Ammonio)methyl]-silicates 1–6

Compounds *rac*-**1**, **2b**, **3a**·CH_2Cl_2, **4a**·CH_2Cl_2, **5a**·CH_2Cl_2, **6a**·2CH_2Cl_2, and **6a**·½CH_2Cl_2 were structurally characterized by single-crystal X-ray diffraction.[16] The crystal data and the experimental parameters used for these studies are given in Appendix A (Tables 25 and 26). Suitable single crystals of *rac*-**1**, **2b**, **3a**·CH_2Cl_2, **4a**·CH_2Cl_2, **5a**·CH_2Cl_2, **6a**·2CH_2Cl_2, and **6a**·½CH_2Cl_2 were isolated directly from the respective reaction mixtures (see Chapter 10, Experimental Section). The crystals were mounted in inert oil (perfluoroalkyl ether, ABCR) on a glass fiber and then transferred to the cold nitrogen gas stream of the diffractometer (Stoe IPDS; graphite-monochromated MoKα radiation (λ = 0.71073 Å)). All structures were solved by direct methods.[17] A riding model was employed in the refinement[18] of the C*H* hydrogen atoms, whereas the N*H* and O*H* hydrogen atoms were localized in difference Fourier syntheses and refined freely. All bond lengths and angles, which are not discussed explicitly in the following sections, are in the expected range and therefore do not need further comments. For reasons of comparison, some selected bond distances and angles are listed in Tables 1 and 2.

Compound *rac*-**1** crystallizes in the space group *Pbca*, and the crystals are built up by (*Λ*)- and (*Δ*)-enantiomers. Compounds **2b**, **3a**·CH_2Cl_2, **4a**·CH_2Cl_2, **5a**·CH_2Cl_2, **6a**·$2CH_2Cl_2$, and **6a**·$½CH_2Cl_2$ crystallize in chiral space groups (Appendix A, Tables 25 and 26), and the crystals investigated contain only one particular diastereomer ((*Δ*,*S*,*S*)-configuration, **2b**; (*Λ*,*S*,*S*)-configuration, **3**–**6**). The molecular structures of the zwitterions **1**–**3** are depicted in Figures 1–3.

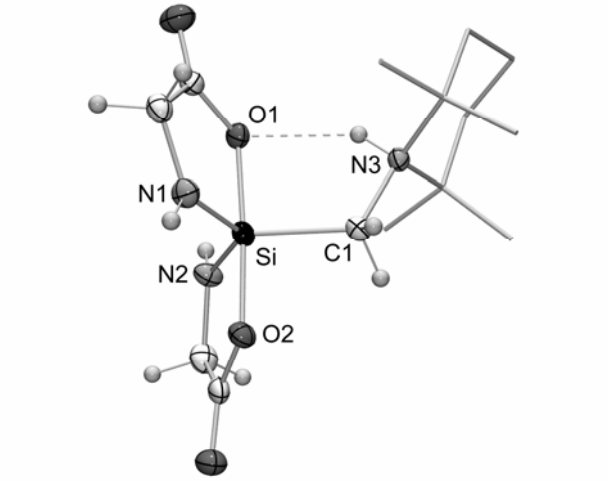

Figure 1. Molecular structure of *rac*-**1** ((*Δ*)-enantiomer) in the crystal (probability level of displacement ellipsoids 50%; CH_2 and $C(CH_3)_2$ moieties of the 2,2,6,6-tetramethylpiperidinio group represented as stick model for clarity).

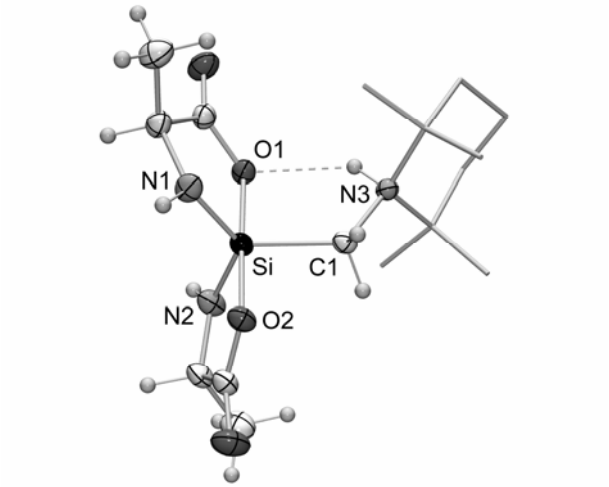

Figure 2. Molecular structure of **2b** ((*Δ*,*S*,*S*)-diastereomer) in the crystal (probability level of displacement ellipsoids 50%; CH_2 and $C(CH_3)_2$ moieties of the 2,2,6,6-tetramethyl-piperidinio group represented as stick model for clarity).

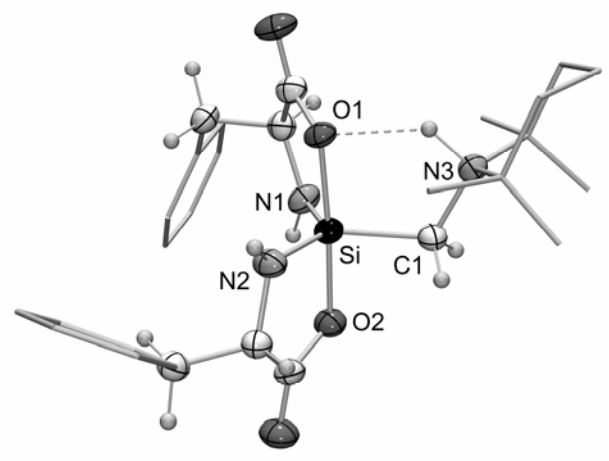

Figure 3. Molecular structure of **3a** ((*Λ*,*S*,*S*)-diastereomer) in the crystal of **3a**·CH_2Cl_2 (probability level of displacement ellipsoids 50%; CH_2 and $C(CH_3)_2$ moieties of the 2,2,6,6-tetramethylpiperidinio and phenyl groups represented as stick models for clarity).

In the case of **4a**·CH_2Cl_2, no crystallographic symmetry was found; the unit cell contains four symmetrically independent zwitterions (*Molecules I–IV*) with very similar structures and four additional disordered dichloromethane molecules. Comparing the orientation of *Molecules I* and *IV* (–178.2 deg) and that of *Molecules II* and *III* (178.4 deg), a nearly 180 deg rotation about [1 0 0] is observed. Furthermore, *Molecules I* and *II*, and in the same sense, Molecules *III* and *IV* are connected to pairs via intermolecular hydrogen bonds (Table 3). Due to their likeness, only one structure of the four molecules is depicted in Figure 4.

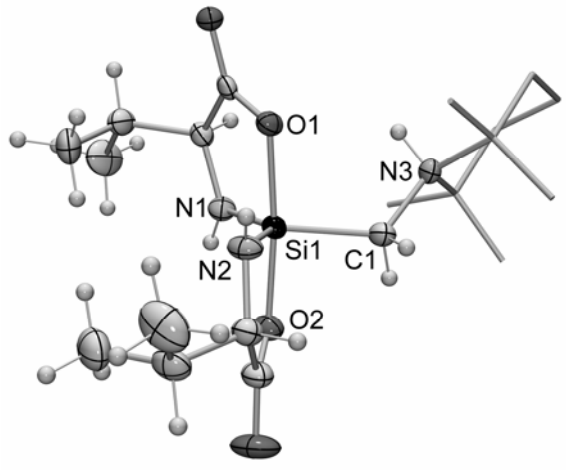

Figure 4. Molecular structure of **4a** (*Molecule I*) in the crystal of **4a**·CH_2Cl_2 ((*Λ*,*S*,*S*)-diastereomers) (probability level of displacement ellipsoids 50%; CH_2 and $C(CH_3)_2$ moieties of the 2,2,6,6-tetramethylpiperidinio group represented as stick model for clarity). The structures of *Molecules II–IV* are very similar.

In the case of **5a**·CH_2Cl_2, the asymmetric unit contains one zwitterion and one additional molecule of dichloromethane, and in the case of **6a**·2CH_2Cl_2, one zwitterion and two additional molecules of dichloromethane. The molecular structures of the zwitterions of **5a**·CH_2Cl_2 and **6a**·2CH_2Cl_2 are depicted in Figures 5 and 6, respectively.

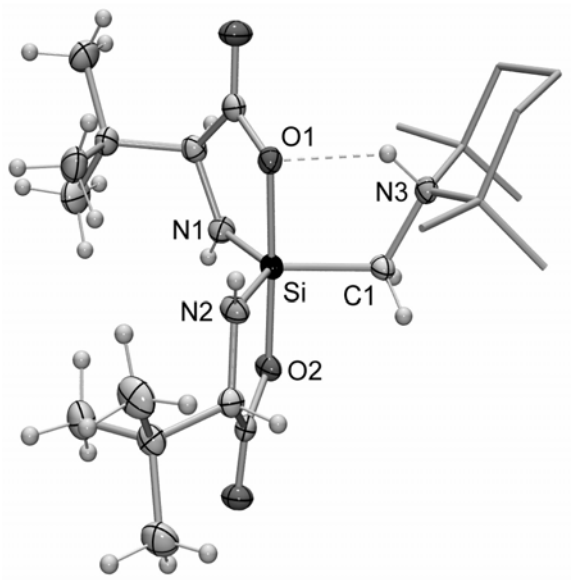

Figure 5. Molecular structure of **5** in the crystal of **5a**·CH_2Cl_2 ((*Λ,S,S*)-diastereomer) (probability level of displacement ellipsoids 50%; CH_2 and $C(CH_3)_2$ moieties of the 2,2,6,6-tetra-methylpiperidinio group represented as stick model for clarity).

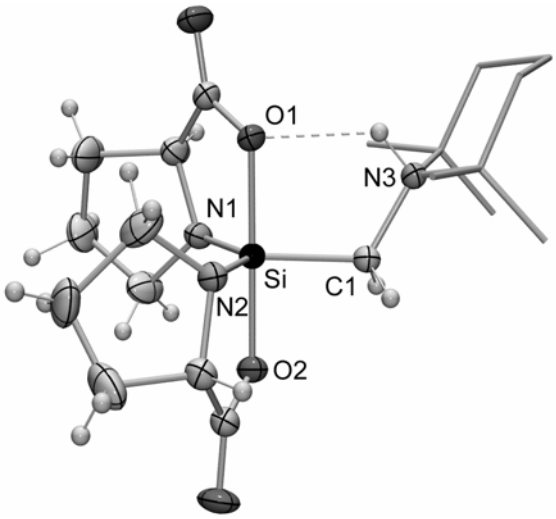

Figure 6. Molecular structure of **6** in the crystal of **6a**·2CH_2Cl_2 ((*Λ,S,S*)-diastereomer) (probability level of displacement ellipsoids 50%; CH_2 and $C(CH_3)_2$ moieties of the 2,2,6,6-tetra-methylpiperidinio group represented as stick model for clarity).

The asymmetric unit of **6a**·½CH_2Cl_2 contains two zwitterions (*Molecules I* and *II*) and one dichloromethane molecule (the molecular structure of the zwitterion is depicted in Figure 7). As can be seen from Figures 1–7, the Si-coordination polyhedra of *rac*-**1**, **2b**, **3a**·CH_2Cl_2, **4a**·CH_2Cl_2, **5a**·CH_2Cl_2, **6a**·2CH_2Cl_2, and **6a**·½CH_2Cl_2 (compounds with an *Si*O_2N_2C skeleton) are distorted trigonal bipyramids, with the oxygen atoms O1 and O2 in the axial positions. The nitrogen atoms N1 and N2 and the carbon atom C1 occupy the equatorial sites. The Si–O distances range from 1.8058(14) Å to 1.8524(13) Å, and the Si–C bond lengths are in the range 1.906(3)–1.9274(19) Å. The Si–N distances range from 1.7087(17) Å to 1.740(2) Å (see Tables 1 and 2).

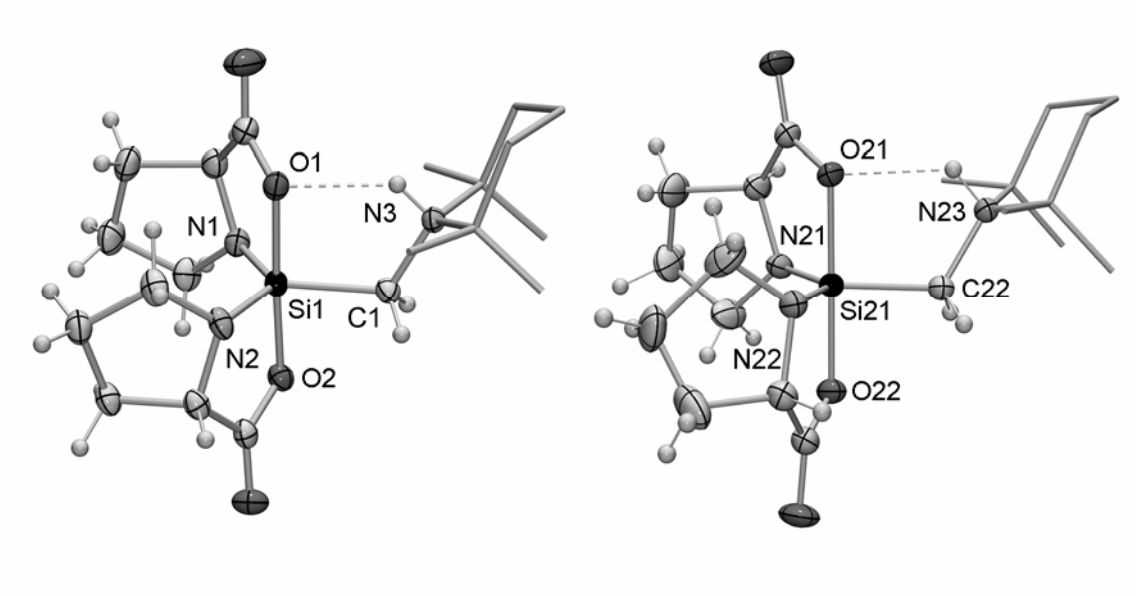

Figure 7. Molecular structures of the two crystallographically independent zwitterions **6a** in the crystal of **6a**·½CH_2Cl_2 ((*Λ*,*S*,*S*)-diastereomers) (*Molecules I* and *II*; probability level of displacement ellipsoids 50%; CH_2 and $C(CH_3)_2$ moieties of the 2,2,6,6-tetramethylpiperidinio groups represented as stick model for clarity).

Table 1. Selected Bond Distances (Å) and Angles (deg) for *rac*-**1**, **2b**, and **3a**·CH_2Cl_2

	rac-**1**	**2b**	**3a**·CH_2Cl_2
Si–O1	1.8356(19)	1.8294(10)	1.835(2)
Si–O2	1.8163(19)	1.8129(10)	1.817(3)
Si–N1	1.717(2)	1.7150(13)	1.725(3)
Si–N2	1.713(2)	1.7146(13)	1.725(3)
Si–C1	1.918(2)	1.9157(14)	1.906(3)
O1–Si–O2	176.25(9)	178.50(5)	175.81(12)
O1–Si–N1	86.45(10)	86.93(5)	86.41(13)
O1–Si–N2	90.94(10)	93.30(5)	91.76(13)
O1–Si–C1	93.58(9)	92.55(5)	94.47(13)
O2–Si–N1	91.64(10)	93.23(5)	91.18(14)
O2–Si–N2	87.60(10)	87.80(6)	86.98(14)
O2–Si–C1	90.15(9)	86.06(5)	89.68(13)
N1–Si–N2	126.59(11)	126.76(6)	127.31(16)
N1–Si–C1	115.30(11)	118.06(6)	117.40(16)
N2–Si–C1	118.10(11)	115.11(7)	115.25(16)

Table 2. Selected Interatomic Distances (Å) and Angles (deg) for **4a**·CH_2Cl_2, **5a**·CH_2Cl_2, **6a**·$2CH_2Cl_2$, and **6a**·$½CH_2Cl_2$

	4a·CH_2Cl_2[a]				**5a**·CH_2Cl_2	**6a**·$2CH_2Cl_2$	**6a**·$½CH_2Cl_2$[b]	
	Molecule I	*Molecule II*	*Molecule III*	*Molecule IV*			*Molecule I*	*Molecule II*
Si–O1	1.8275(13)	1.8116(12)	1.8122(13)	1.8267(13)	1.8258(14)	1.8524(13)	1.8322(14)	1.8227(14)
Si–O2	1.8098(13)	1.8242(13)	1.8251(14)	1.8144(14)	1.8058(14)	1.8105(13)	1.8169(14)	1.8279(15)
Si–N1	1.7146(17)	1.7133(18)	1.7151(18)	1.7162(18)	1.7087(17)	1.7287(17)	1.7378(18)	1.740(2)
Si–N2	1.718(2)	1.7168(17)	1.7135(19)	1.7184(17)	1.7124(16)	1.7381(17)	1.7387(18)	1.7285(19)
Si–C1	1.915(2)	1.918(2)	1.923(2)	1.922(2)	1.9274(19)	1.9142(18)	1.9228(19)	1.919(2)
O1–Si–O2	173.89(7)	174.37(7)	174.47(7)	173.13(7)	176.83(7)	179.25(7)	177.60(7)	178.26(7)
O1–Si–N1	86.23(7)	86.81(7)	86.91(7)	86.33(7)	85.98(7)	86.48(7)	87.27(8)	87.58(8)
O1–Si–N2	90.67(7)	90.13(7)	90.28(8)	90.33(7)	93.25(7)	91.60(7)	93.43(8)	91.51(8)
O1–Si–C1	97.27(7)	97.85(7)	98.09(7)	97.35(7)	92.71(7)	92.74(7)	91.64(7)	95.96(8)
O2–Si–N1	91.26(7)	91.83(7)	91.58(7)	91.02(7)	91.23(8)	92.78(7)	93.38(7)	91.58(8)
O2–Si–N2	86.69(7)	86.38(7)	86.44(8)	86.59(7)	87.24(7)	88.82(7)	88.12(7)	87.79(8)
O2–Si–C1	88.83(7)	87.63(8)	87.33(7)	89.50(8)	89.93(7)	87.64(7)	86.03(7)	85.77(8)
N1–Si–N2	130.18(9)	127.76(9)	127.75(9)	130.73(9)	127.24(9)	126.26(8)	124.24(8)	127.44(9)
N1–Si–C1	117.52(10)	117.41(9)	117.42(10)	116.97(9)	118.17(9)	117.82(8)	119.12(9)	118.54(10)
N2–Si–C1	112.20(9)	114.67(9)	114.63(9)	112.22(9)	114.56(9)	115.92(8)	116.59(8)	113.82(10)

[a]Atoms of *Molecule I*, Si1, O1, O2, N1, N2, and C1; atoms of *Molecule II*, Si21, O21, O22, N21, N22, and C21; atoms of *Molecule III*, Si41, O41, O42, N41, N42, and C41; atoms of *Molecule IV*, Si61, O61, O62, N61, N62, and C61. [b]Atoms of *Molecule I*, Si1, O1, O2, N1, N2, and C1; atoms of *Molecule II*, Si21, O21, O22, N21, N22, and C22.

As expected from the presence of the potential NH donor functions and the potential oxygen acceptor atoms, hydrogen-bonding systems were observed in the crystals of **1**–**6**.[19] As can be seen from Figures 1–7 and Table 3, all compounds studied form intramolecular N–H···O hydrogen bonds between the NH groups of the ammonium moieties and one of the two axial oxygen ligand atoms (except for the intermolecular hydrogen bond formed by *Molecule II* of **6**·½CH_2Cl_2 where a carbonyl oxygen atom acts as the proton acceptor). As result of this interaction, the respective axial Si–O bonds (Si–O1) containing the hydrogen acceptor atom (O1) are slightly longer than the other axial Si–O2 bonds.

Table 3. Hydrogen-Bonding Geometries for *rac*-**1**, **2b**, **3a**·CH_2Cl_2, **4a**·CH_2Cl_2, **5a**·CH_2Cl_2, **6a**·2CH_2Cl_2, and **6a**·½CH_2Cl_2 in the Crystal[a]

	D–H···A	D–H (Å)	H···A (Å)	D···A (Å)	D–H···A (deg)
rac-**1**	N2–H2···O4	0.87(4)	2.42(3)	3.183(3)	146(3)
	N3–H3···O1	0.87(2)	2.06(3)	2.770(3)	138(2)
2b	N2–H2···O4	0.833(19)	2.589(19)	3.3350(19)	149.9(18)
	N3–H3···O1	0.900(17)	2.112(17)	2.7955(15)	132.0(14)
3a·CH_2Cl_2	N3–H3···O1	1.05(5)	1.98(4)	2.807(4)	133(3)
4a·CH_2Cl_2	N3–H3···O23	0.88(2)	2.07(2)	2.922(2)	163.0(18)
	N23–H23···O3 [b]	0.876(17)	2.035(18)	2.866(2)	158(2)
	N23–H23···O21	0.876(17)	2.57(2)	3.110(2)	121.1(18)
	N43–H43···O63	0.858(17)	2.052(17)	2.879(2)	161.7(18)
	N63–H63···O43	0.89(2)	2.08(2)	2.931(2)	161.8(18)
5a·CH_2Cl_2	N3–H3···O1	0.92(2)	2.01(2)	2.742(2)	134.9(17)
6a·2CH_2Cl_2	N3–H3···O1	0.90(2)	2.14(2)	2.7884(18)	128.4(19)
6a·½CH_2Cl_2	N3–H3···O1	0.88(2)	2.06(2)	2.737(2)	134(2)
	N23–H23···O21[c]	0.87(3)	2.55(2)	3.044(2)	116.9(19)
	N23–H23···O23	0.87(3)	2.11(3)	2.947(2)	161(2)

[a]Data calculated by using the program PLATON.[19] [b]Bifurcate N23–H23···O21/O3 interaction; O21···H23···O3 = 78.7(6) deg. [c]Bifurcate N23–H23···O21/O23 interaction; O21···H23···O23 = 80.4 (9) deg.

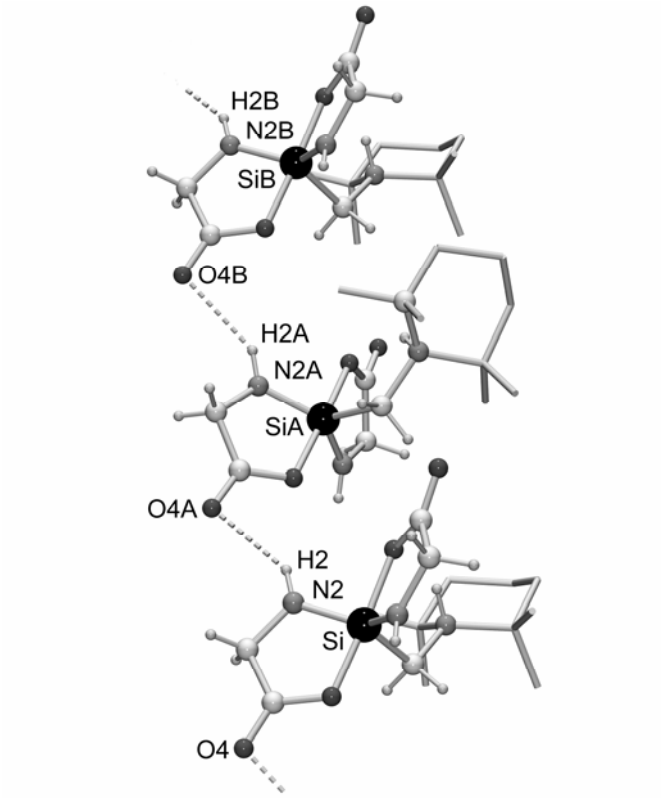

Figure 8. Intermolecular N–H···O hydrogen bonds in the crystal of *rac*-**1** leading to infinite chains along the base [0 1 0] vector (CH_2 and $C(CH_3)_2$ moieties of the 2,2,6,6-tetramethylpiperidinio groups represented as stick model for clarity).[19]

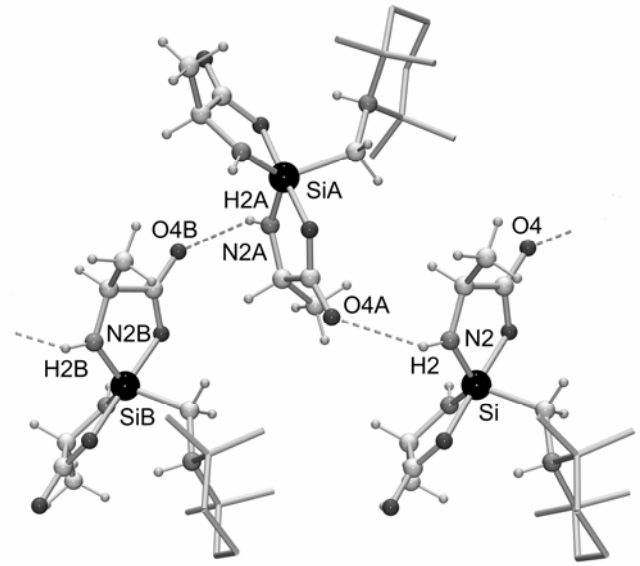

Figure 9. Intermolecular N–H···O hydrogen bonds in the crystal of **2b** leading to infinite chains along the base [1 0 0] vector (CH_2 and $C(CH_3)_2$ moieties of the 2,2,6,6-tetramethylpiperidinio groups represented as stick model).[19,20]

In the case of compounds *rac*-**1** and **2b**, an additional intermolecular N–H···O interaction between one of the two SiNH groups and one of the two carbonyl oxygen atoms was observed.[19] This hydrogen bond leads to the formation of chains in the crystals of *rac*-**1** and **2b** (Figures 8 and 9).[20]

In the case of **4a**·CH_2Cl_2, the two zwitterions of each pair (*Molecule I*/*Molecule II* and *Molecule III*/*Molecule IV*) are connected via intermolecular N–H···O interactions; *Molecule II* is involved in a bifurcate hydrogen-bonding interaction, with one additional intramolecular N–H···O hydrogen bond (see Table 3).

In the case of **6a**·½CH_2Cl_2, *Molecule II* is involved in an additional intermolecular N–H···O interaction with its symmetry equivalent (bifurcate N–H···O/O interaction).

3.3 NMR Studies of the λ⁵*Si*-[(Ammonio)methyl]silicates 1–6

3.3.1 NMR Studies of the λ⁵*Si*-[(Ammonio)methyl]silicates 1–6 in the Solid State

Compounds *rac*-**1**, **2b**, **3a**·CH_2Cl_2, **4a**·CH_2Cl_2, **5a**·CH_2Cl_2, **6a**·2CH_2Cl_2, and **6a**·½CH_2Cl_2 were characterized at 22 °C by solid-state ^{29}Si VACP/MAS NMR spectroscopy (Table 4). The isotropic ^{29}Si chemical shifts obtained clearly characterize the ^{29}Si resonance signals as arising from pentacoordinate silicon atoms.

Table 4. ^{29}Si VACP/MAS NMR Data for *rac*-**1**, **2b**, **3a**·CH_2Cl_2, **4a**·CH_2Cl_2, **5a**·CH_2Cl_2, **6a**·2CH_2Cl_2, and **6a**·½CH_2Cl_2 in the Crystal (Spectra Recorded at 22 °C, Chemical Shifts in ppm)

rac-**1**	–94.1 to –91.8 (m)	**5a**·CH_2Cl_2	–101.2 to –99.1 (m)
2b	–100.5 to –98.0 (m)	**6a**·2CH_2Cl_2	–97.5 to –95.0 (m)
3a·CH_2Cl_2	–98.5 to –96.0 (m)	**6a**·½CH_2Cl_2	–97.0 to –93.0 (m)
4a·CH_2Cl_2	–98.8 to –95.6 (m)		

The solid-state ^{29}Si NMR resonance signals of *rac*-**1**, **2b**, **3a**·CH_2Cl_2, **4a**·CH_2Cl_2, **5a**·CH_2Cl_2, **6a**·2CH_2Cl_2, and **6a**·½CH_2Cl_2 (compounds with an *Si*O_2N_2C skeleton) are split or are broad (only slightly structured) due to $^1J(^{14}N,^{29}Si)$ couplings. As an example, a representative partial spectrum obtained in a ^{29}Si VACP/MAS NMR experiment with **6a**·2CH_2Cl_2 is depicted in Figure 10. We were not able to simulate these spectra and to extract the $^1J(^{14}N,^{29}Si)$ coupling constants because these couplings were poorly resolved. The line width of the ^{29}Si signals depends on the magnitude of $^1J(^{14}N,^{29}Si)$ and the quadrupole

relaxation time of the ^{14}N nucleus Tq(^{14}N). When Tq(^{14}N) becomes comparable with $1/^1J(^{14}N,^{29}Si)$, splitting of the ^{29}Si resonance signals due to ^{14}N,^{29}Si coupling can be observed directly.[21]

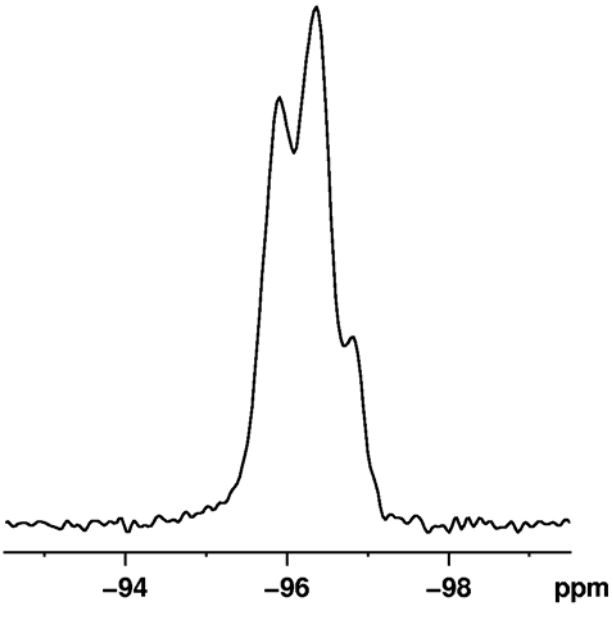

Figure 10. Partial spectrum obtained in a ^{29}Si VACP/MAS NMR experiment with **6a**·2CH_2Cl_2 (79.5 MHz, 22 °C, ν_{rot} = 5 kHz).

The zwitterionic λ^5*Si*-silicates **1**–**6** were also characterized at 22 °C by solid-state ^{15}N VACP/MAS NMR spectroscopy (see Chapter 10, Experimental Section). The solid-state ^{15}N NMR resonance signals of **1**–**6** were sharp due to the high crystallinity of the bulk materials used for these experiments. A representative partial spectrum obtained in a ^{15}N VACP/MAS NMR experiment with **3a**·CH_2Cl_2 is depicted in Figure 11 as an example.

The spectra obtained in the ^{15}N and ^{29}Si VACP/MAS NMR experiments were compatible with the crystal structures of these compounds and demonstrated that compounds **2b**, **3a**·CH_2Cl_2, **4a**·CH_2Cl_2, **5a**·CH_2Cl_2, **6a**·2CH_2Cl_2, and **6a**·½CH_2Cl_2 were diastereomerically and enantiomerically pure.

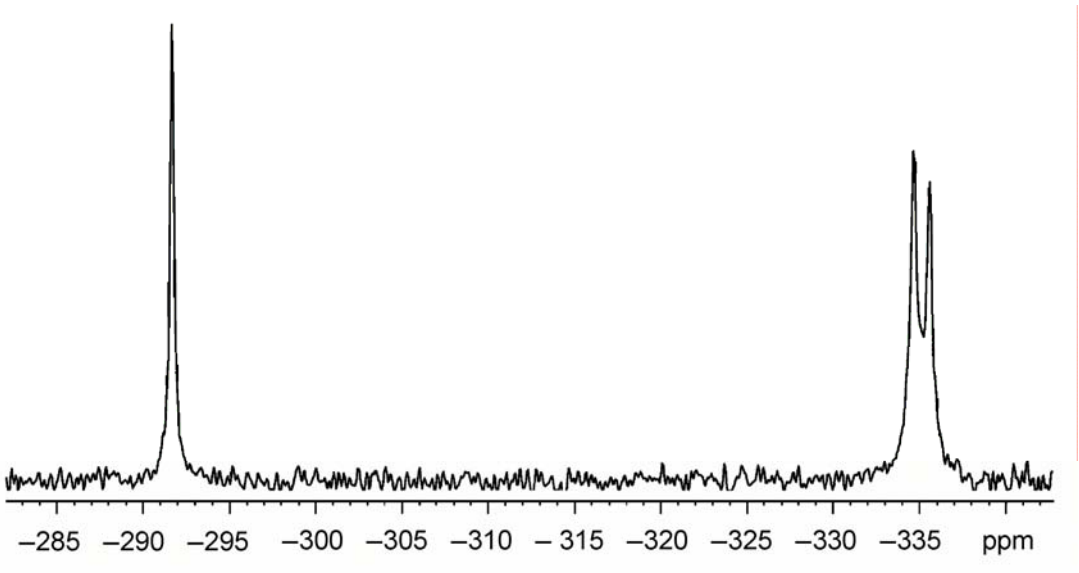

Figure 11. A representative partial spectrum obtained in a ^{15}N VACP/MAS NMR experiment with **3a**·CH_2Cl_2 (40.6 MHz, 22 °C, ν_{rot} = 5 kHz).

3.3.2 NMR Studies of the λ^5*Si*-[(Ammonio)methyl]silicates 1–6 in Solution

Compounds *rac*-**1**, **2b**, **3a**·CH_2Cl_2, **4a**·CH_2Cl_2, **5a**·CH_2Cl_2, **6a**·2CH_2Cl_2, and **6a**·½CH_2Cl_2 were additionally characterized by solution ^{1}H, ^{13}C, and ^{29}Si NMR spectroscopy. Furthermore, 2D ^{15}N,^{1}H HMQC NMR spectra were recorded for all these compounds. All these solution NMR studies were performed at 23 °C using CD_2Cl_2 as the solvent. As can be seen from Table 5, the ^{29}Si chemical shifts are very similar to the isotropic ^{29}Si chemical shifts obtained in the solid-state NMR experiments (Table 4), indicating that the λ^5*Si*-silicate skeletons of compounds **1**–**6** exist in solution as well. In contrast to the solid-state ^{29}Si NMR spectra, the solution-state ^{29}Si NMR spectra of *rac*-**1**, **2b**, **3a**·CH_2Cl_2, **4a**·CH_2Cl_2, **5a**·CH_2Cl_2, **6a**·2CH_2Cl_2, and **6a**·½CH_2Cl_2 (compounds with an *Si*O_2N_2C skeleton) are characterized by sharp resonance signals (full-width at half height ca. 15–25 Hz). When the spin-lattice relaxation time of the ^{14}N nuclei Tq(^{14}N) is much faster than ^1J(^{14}N,^{29}Si), the splitting of the ^{29}Si resonance signals due to the ^{14}N,^{29}Si coupling cannot be observed. In this case, the ^{14}N nuclei have a strong quadrupolar interaction with a strong EFG (Electric Field Gradient).

Furthermore, the ^{1}H chemical shifts observed for the SiCH_2N*H* protons (δ = 5.7–6.0 ppm) indicate the presence of the ammonium moieties. Thus, these NMR experiments unequivocally demonstrate that the zwitterions **1**–**6** also exist in solution (for further details, see Chapter 10, Experimental Section).

Table 5. ^{29}Si NMR Data for *rac*-**1**, **2b**, **3a**·CH_2Cl_2, **4a**·CH_2Cl_2, **5a**·CH_2Cl_2, **6a**·$2CH_2Cl_2$, and **6a**·$½CH_2Cl_2$ in Solution (CD_2Cl_2, Spectra Recorded at 23 °C, Chemical Shifts in ppm)

rac-**1**	–91.9	**5a**·CH_2Cl_2	–100.3
2b	–97.1 (**2a**)/–98.4 (**2b**)	**6a**·$2CH_2Cl_2$	–97.8
3a·CH_2Cl_2	–97.36 (**3a**)/–97.45 (**3b**)	**6a**·$½CH_2Cl_2$	–97.8
4a·CH_2Cl_2	–98.0		

As the trigonal-bipyramidal structure, with the carboxylato oxygen atoms in the axial sites, is the energetically most favorable one for the zwitterionic λ⁵*Si*-silicates **1**–**6** (see Chapter 3.2, Crystal Structure Analyses), it is likely that this particular structure is also dominant in solution.

The chiral nature of the zwitterions is reflected by the ABX spin systems observed for the $SiCH_AH_BNH_X$ protons in the ^{1}H NMR spectra. In the case of *rac*-**1** (*chiral* λ⁵*Si*-silicate skeleton with *achiral* bidentate ligands), diastereotopism of the $SiCH_AH_BN$ protons indicates that this zwitterion is configurationally stable on the NMR time scale at 23 °C. It is likely that all the other compounds studied (*chiral* λ⁵*Si*-silicate skeletons with *chiral* bidentate ligands) are also configurationally stable on the NMR time scale at 23 °C, but this information cannot be extracted directly from the ^{1}H NMR spectra because the chiral nature of the configurationally stable bidentate ligands ((*S*)-configuration) could already be sufficient for the existence of ABX spin systems for the $SiCH_AH_BNH_X$ protons; i.e., the ABX spin systems observed cannot be correlated exclusively with the chirality of the λ⁵*Si*-silicate skeletons ((*Λ*)- and (*Δ*)-configuration; for the (*Λ*)/(*Δ*)-nomenclature see refs 22 and 23) of **2**–**6**.

3.3.3 Dynamic NMR Studies of the λ⁵*Si*-[(Ammonio)methyl]silicates 1–6 in Solution

To learn more about the behavior of the zwitterionic compounds **1**–**6** in solution, ^{1}H, ^{13}C, and ^{29}Si NMR cross-experiments at 300.1 MHz were carried out. For this purpose, *rac*-**1** (76 mmol) and **6a**·$½CH_2Cl_2$ (44 mmol) were dissolved in CD_2Cl_2 (750 μL). The NMR spectra, recorded at 23 °C and supported by correlation experiments, indicated that the zwitterions of *rac*-**1** and **6a**·$½CH_2Cl_2$ undergo an intermolecular ligand exchange, leading to the formation of a new zwitterionic λ⁵*Si*-silicate containing one glycinato(2–) ligand and one prolinato(2–) ligand. Figure 12 shows a representative partial spectrum obtained in a ^{29}Si,^{1}H

HMQC experiment. Related cross-experiments with **4a**·CH_2Cl_2/**6a**·½CH_2Cl_2, **2b**/**3a**·CH_2Cl_2, and **5a**·CH_2Cl_2/**6a**·½CH_2Cl_2 demonstrated an intermolecular ligand exchange between the respective zwitterions as well.

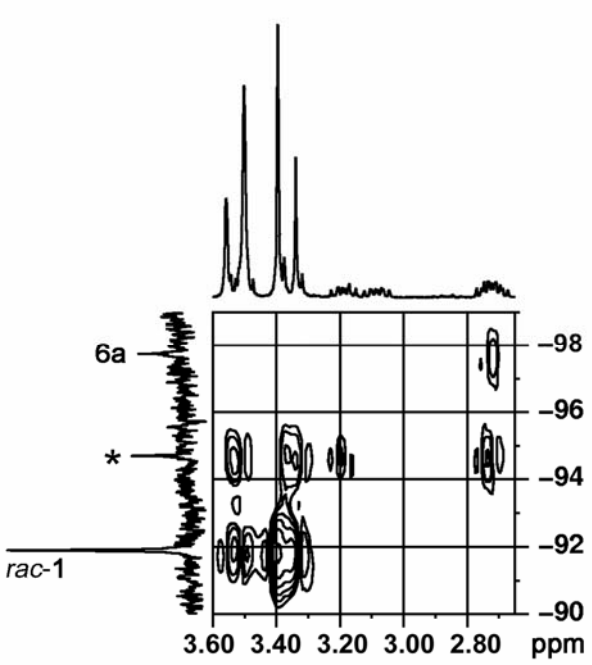

Figure 12. Partial spectrum obtained in a $^{29}Si,^1H$ HMQC experiment (23 °C, 300.1 MHz) with a solution of *rac*-**1** (76 mmol) and **6a**·½CH_2Cl_2 (44 mmol) in CD_2Cl_2 (750 μL). The spectrum was recorded ca. 2 h after dissolution of *rac*-**1** and **6a**·½CH_2Cl_2. *Top*: ^1H NMR resonance signals. *Left*: ^{29}Si NMR resonance signals; the signal marked with an asterisk corresponds to the cross product.

In the neutral pentacoordinate silicon compounds **1**–**3**, one (2,2,6,6-tetramethylpiperidinio)methyl group and two bidentate chelate ligands derived from the α-amino acids glycine (**1**), (*S*)-alanine (**2b**), or (*S*)-phenylalanine (**3a**·CH_2Cl_2) are bound to the silicon(IV) coordination center. Upon dissolution in dichloromethane, the diastereomerically and enantiomerically pure compounds **2b** and **3a**·CH_2Cl_2 undergo a (*Λ*)/(*Δ*)-epimerization to give an equilibrium mixture of the respective (*Λ*,*S*,*S*)- and (*Δ*,*S*,*S*)-diastereomers. Compound **2b** was found to be configurationally stable in dichloromethane at –40 °C over a period of 24 h; however, at 23 °C (*Λ*)/(*Δ*)-epimerization was observed, with an equilibration time of ca. 2 h. In the case of **3a**·CH_2Cl_2, the equilibration time was ca. 3 h. In both cases, molar (*Λ*)/(*Δ*)-equilibration ratios of 0.7:0.3 were observed, the respective (*Λ*)-isomers being thermodynamically more stable than the (*Δ*)-isomers. It is likely that the enantiomers of *rac*-**1**

undergo an analogous (*Λ*)/(*Δ*)-enantiomerization. The (*Λ*)/(*Δ*)-epimerization process of **2b** and **3a**·CH_2Cl_2, respectively, will be discussed in detail (see below).

In the zwitterionic λ⁵*Si*-silicates **4**–**6**, one (2,2,6,6-tetramethylpiperidinio)methyl group and two bidentate chelate ligands derived from the α-amino acids (*S*)-valine (**4a**), (*S*)-*tert*-leucine (**5a**), or (*S*)-proline (**6a**) are bound to the silicon(IV) coordination center. These bidentate ligands are sterically more demanding than those derived from (*S*)-alanine and (*S*)-phenylalanine (compounds **2b** and **3a**·CH_2Cl_2). Most surprisingly, the λ⁵*Si*-silicates **4a**, **5a**, and **6a** were demonstrated to exist as diastereo- and enantiomerically pure zwitterions in solution as well (dichloromethane, temperature range –100 °C to 23 °C).

Upon dissolution of **2b** and **3a**·CH_2Cl_2 in CD_2Cl_2, (*Λ*)/(*Δ*)-epimerization was observed, leading to equilibrium mixtures of the respective diastereomers (**2a** ⇄**2b**; **3a** ⇄**3b**). In the case of **2** and **3**, the absolute configurations of the respective diastereomers in solution could be assigned because the kinetics of the epimerization process at the silicon atom could be monitored by ^{1}H NMR spectroscopy (see below).

The (*Λ*)/(*Δ*)-epimerization of compound **2** as monitored by ^{1}H NMR spectroscopy is depicted in Figure 13.

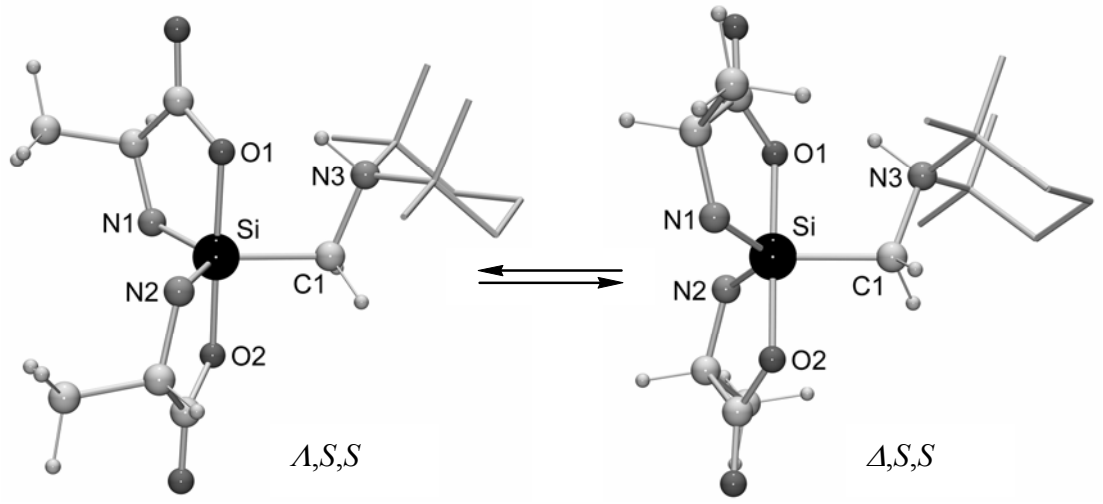

Figure 13. (*Λ*)/(*Δ*)-epimerization of compound **2** as monitored by ^{1}H NMR spectroscopy (23 °C, 300.1 MHz).

The kinetics of the epimerization processes **2a** ⇄ **2b** and **3a** ⇄ **3b** were studied at 23 °C by ^{1}H NMR spectroscopy at 300.1 MHz. For this purpose, the diastereomerically and enantiomerically pure compounds **2b** and **3a**·CH_2Cl_2 were dissolved in CD_2Cl_2 (**2b**, *c* = 30

mM; **3a**·CH_2Cl_2, *c* = 78 mM), and the integrals of the NC*H*C_2 resonance signals of the two bidentate ligands of **2a**/**2b** and **3a**/**3b** were measured as a function of time (see Figures 14 and 16). The first ^{1}H NMR spectra were recorded 5 and 6 min, respectively, after dissolution of **2b** and **3a**·CH_2Cl_2 and revealed already partial epimerization, with the following molar ratios: **2a**:**2b**, 0.23:0.77; **3a**:**3b**, 0.95:0.05. To follow the epimerization processes, ^{1}H NMR spectra were recorded every 300 and 135 seconds, respectively. After a period of ca. 2 and ca. 3 hours, respectively, the equilibration was completed, with the following molar equilibrium ratios: **2a**:**2b**, 0.71:0.29; **3a**:**3b**, 0.73:0.27. These data indicate that the energy differences between the respective (*Λ,S,S*)- and (*Δ,S,S*)-diastereomers are small, the (*Λ,S,S*)-isomers being somewhat more stable than the corresponding (*Δ,S,S*)-epimers. The experimentally established energy differences amount to ca. 2.2 kJ mol^{-1} and ca. 2.5 kJ mol^{-1}. These values match with the calculated energy difference obtained for the respective (*Λ*)- and (*Δ*)-isomers of the model specie **2'** (2.3 kJ mol^{-1}; see Chapter 3.4 Computational Studies). It is interesting to note that the more stable (*Λ,S,S*)-epimer is also found in the crystal of **3a**·CH_2Cl_2, whereas crystalline **2b** contains the less stable (*Δ,S,S*)-epimer.

The kinetics of the epimerization processes studied are depicted in Figures 15 and 17. In these Figures, the percentages of **2a** and **3b** in the respective mixtures of epimers are plotted against the time. The experimental curves could be fitted with a monoexponential function of the type $f(t) = m_1[1–\exp(–t/m_2)]$.

The kinetics of the epimerization process **2a** ⇄ **2b** were additionally studied by VT ^{1}H NMR experiments at 300.1 MHz in the temperature range –60 °C to 0 °C using CD_2Cl_2 as the solvent. For this purpose, a sample of diastereomerically and enantiomerically pure **2b** was dissolved in CD_2Cl_2 at different temperatures, and ^{1}H NMR spectra were recorded every 300 seconds (monitoring of the epimerization process by integration of the respective NC*H*C_2 resonance signals). Compound **2b** was found to be configurationally stable at –60 °C and –40 °C: no changes of the NMR spectra were observed over a period of ca. 24 hours. However, upon dissolution of **2b** at –20 °C, a very slow epimerization process took place which was partially monitored at this particular temperature over a period of ca. 32 hours, revealing the following molar ratio after that period: **2a**:**2b**, 0.27:0.73. After dissolution of **2b** at –10 °C, ^{1}H NMR spectra were recorded over a period of ca. 67 hours, leading to the following molar ratio: **2a**:**2b**, 0.61:0.39. According to analogous kinetic studies at 0 °C, the thermodynamic equilibrium was reached after ca. 4 hours (molar equilibrium ratio **2a**:**2b**, 0.71:0.29).

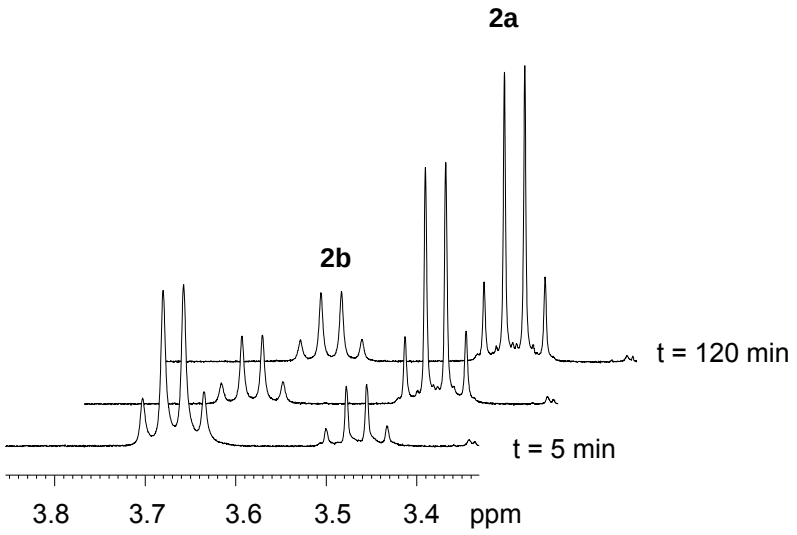

Figure 14. Partial ^{1}H NMR spectra of **2** as a function of time (CD_2Cl_2, 23 °C, 300.1 MHz).

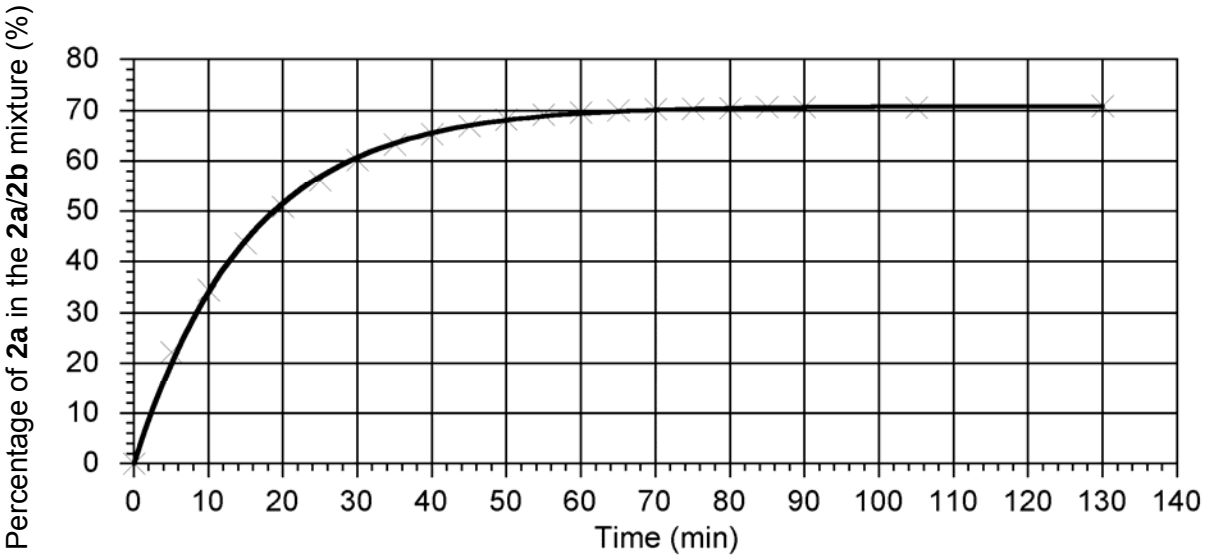

Figure 15. Kinetics of the epimerization process of **2a** ⇄ **2b** after dissolution of **2b** in CD_2Cl_2 (c = 30 mM). The experimental data were extracted from ^{1}H NMR spectra (23 °C, 300.1 MHz). The solid line represents a fit of the experimental curve with the monoexponential equation $f(t) = m_1[1 - \exp(-t/m_2)]$, with $m_1 = 70.9 \pm 0.2$ and $m_2 = 15.4 \pm 0.2$.

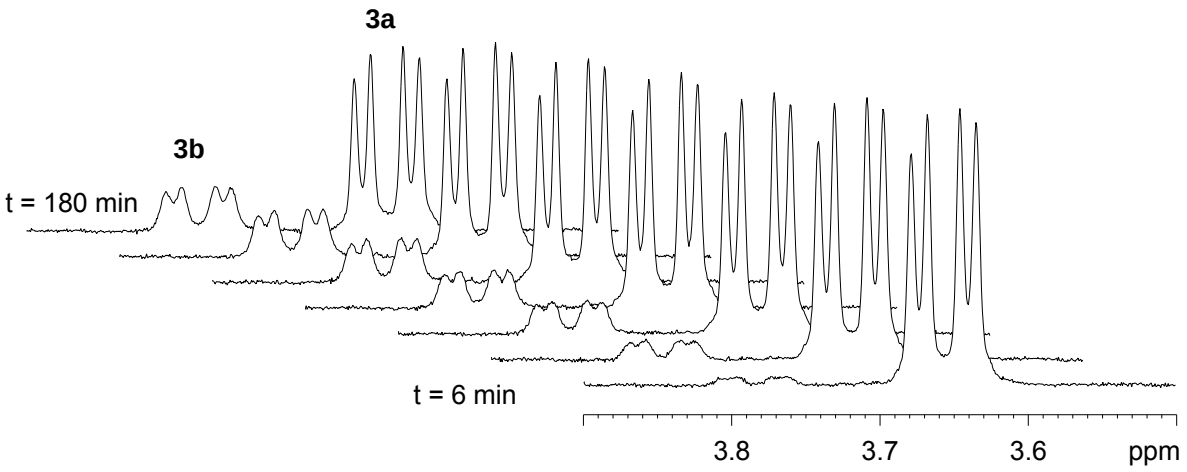

Figure 16. Partial ^{1}H NMR spectra of **3** as a function of time (CD_2Cl_2, 23 °C, 300.1 MHz).

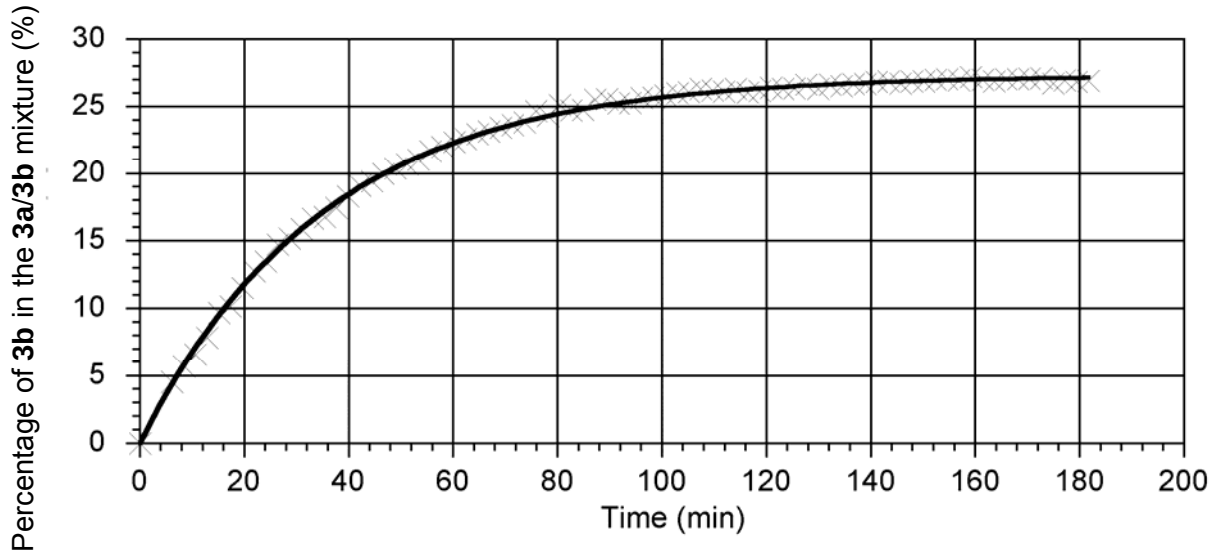

Figure 17. Kinetics of the epimerization process of **3a** ⇄ **3b** after dissolution of **3a**·CH_2Cl_2 in CD_2Cl_2 (c = 78 mM). The experimental data were extracted from ^{1}H NMR spectra (23 °C, 300.1 MHz). The solid line represents a fit of the experimental curve with the monoexponential equation $f(t) = m_1[1 - \exp(-t/m_2)]$, with $m_1 = 27.3 \pm 0.1$ and $m_2 = 35.5 \pm 0.2$.

A comparison of the kinetics of the epimerization processes studied at –20 °C, –10 °C, and 0 °C is depicted in Figure 18, in which the percentages of **2a** in the respective mixtures of epimers are plotted against the time. The experimental curves could be fitted with a monoexponential function of the type $f(t) = m_1[1–\exp(–t/m_2)])$.

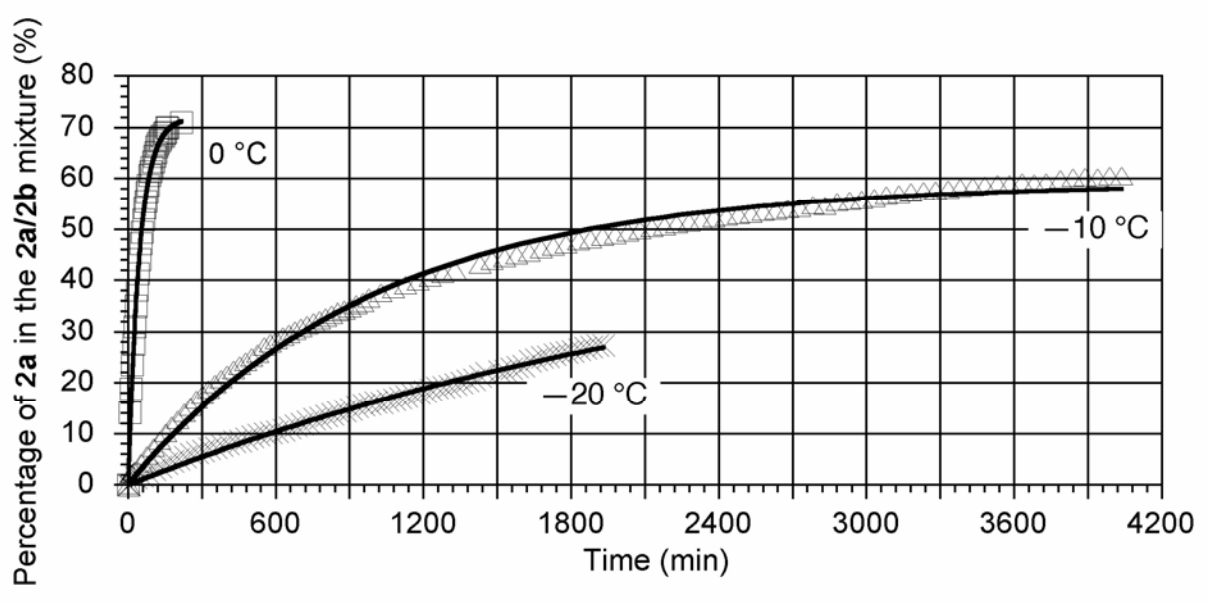

Figure 18. Comparison of the kinetics of the epimerization process of **2a** ⇄ **2b** after dissolution of **2b** in CD_2Cl_2 (c = 30 mM) at different temperatures. The experimental data were extracted from ^{1}H NMR spectra (300.1 MHz). The solid lines represent fits of the experimental curves with monoexponential equations of the type $f(t) = m_1[1 - \exp(-t/m_2)]$; –20 °C, $m_1 = 54.5 \pm 3.0$, $m_2 = 2825 \pm 197.0$; –10 °C, $m_1 = 59.0 \pm 0.4$, $m_2 = 997 \pm 18.2$; 0 °C, $m_1 = 71.9 \pm 0.5$, $m_2 = 46.9 \pm 1.0$. The errors of the fit for the experiment at –20 °C are relatively large because only the beginning of the epimerization process was observed due to its long duration.

Additionally, low-temperature ^{1}H NMR experiments at 300.1 MHz with solutions of **4a**·CH_2Cl_2 (20 mM), **5a**·CH_2Cl_2 (32 mM), and **6a**·½CH_2Cl_2 (44 mM) in CD_2Cl_2 were performed at –100 °C. The ^{1}H NMR spectra were recorded every 300 seconds; the first spectra were obtained ca. 6 min after dissolution of the zwitterionic λ^5*Si*-silicates. In all cases, only one single diastereomer could be detected, and no changes of the NMR spectra were observed over a period of 1 h. Compared to the ^{1}H NMR spectra obtained at 23 °C, no line-broadening was observed at –100 °C.

Furthermore, VT ^{1}H NMR experiments with a 12 mM solution of **6a**·½CH_2Cl_2 in CD_2Cl_2 were carried out in the temperature range –60 °C to 23 °C. For this purpose, five ^{1}H NMR spectra were recorded every 180 seconds at this temperature (the first spectrum was recorded ca. 5 min after dissolution of the compound), followed by measurement of further five ^{1}H NMR spectra each every 180 seconds at –40 °C, –20 °C, and 0 °C. After the sample was kept undisturbed for a period of 3 days at 23 °C, and ^{1}H, ^{13}C, and 2D ^{29}Si,^{1}H HMQC NMR spectra were recorded every 24 hours, further ^{1}H NMR spectra were measured upon

cooling to 0 °C, –20 °C, –40 °C, and –60 °C. No changes of the ^{1}H NMR spectra were observed in all these NMR experiments; i.e., only one single diastereomer could be detected in the temperature range and over the time period studied (see Figure 19). Attempts to perform VT NMR experiments with **4a**, **5a**, and **6a** at higher temperatures failed because these zwitterions decompose at temperatures above 27 °C. Thus, no information about a potential (*Λ*)/(*Δ*)-epimerization of these compounds at higher temperatures could be obtained by NMR spectroscopy.

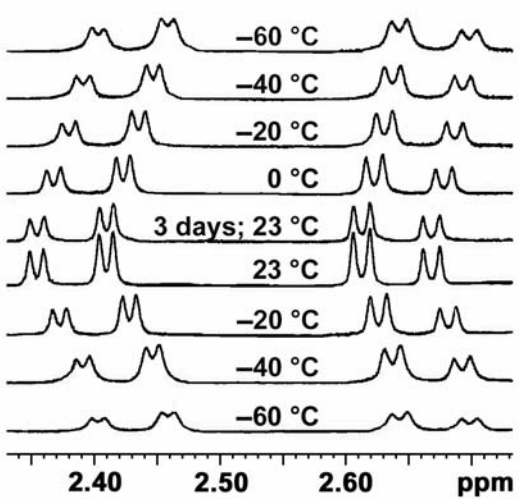

Figure 19. Partial ^{1}H NMR spectra (resonance signals of the $SiCH_2N$ protons) of a 12 mM solution of **6a**·½CH_2Cl_2 in CD_2Cl_2 at 300.1 MHz in the temperature range –60 °C to 23 °C (warming from –60 °C to 23 °C and subsequent cooling to –60 °C).

The presence of only one data set in all the solution NMR spectra of **4a**, **5a**, and **6a** could be interpreted in terms of a rapid (*Λ*)/(*Δ*)-epimerization that is very fast on the NMR time scale. However, no coalescence phenomena (line broadening) were observed upon cooling to –100 °C. As the derivatives **2b** and **3a** (compounds with sterically less demanding bidentate ligands) were demonstrated to undergo a relatively slow (*Λ*)/(*Δ*)-epimerization at 23 °C (equilibration times: **2**, ca. 2 h; **3**, ca. 3 h), a rapid (*Λ*)/(*Δ*)-epimerization of **4a**, **5a**, and **6a** at 23 °C, and especially at –100 °C, is very unlikely.

The presence of only one data set in all the solution NMR spectra of **4a**, **5a**, and **6a** could be alternatively interpreted in terms of (*Λ*)/(*Δ*)-equilibrium ratios that do not allow the detection of both diastereoisomers. In the case of **2** and **3**, molar (*Λ*)/(*Δ*)-equilibrium ratios of **2a**:**2b** = 0.71:0.29 and **3a**:**3b** = 0.73:0.27 were determined at 23 °C (solvent, CD_2Cl_2), with the (*Λ*)-isomer being the thermodynamically more stable one. This ratio corresponds to an energy

difference between the respective (*Λ*)- and (*Δ*)-isomers of ca. 2.2 kJ mol^{-1} and ca. 2.5 kJ mol^{-1}, respectively. This values match with the calculated energy differences obtained for the respective (*Λ*)- and (*Δ*)-isomers of the model species **2'** (2.3 kJ mol^{-1}) and **4'** (2.1 kJ mol^{-1}) (see Chapter 3.4, Computational Studies). Thus, it is unlikely that the molar (*Λ*)/(*Δ*)-equilibrium ratios of **4** and **5** differ totally from those of **2** and **3**; i.e., the (*Δ*,*S*,*S*)-isomers of **4** and **5** should also be detectable at 23 °C. However, it is unlikely that the derivative (*Δ*,*S*,*S*)-**6**, with its two more rigid prolinato(2–) ligands, can be detected by ^{1}H NMR spectroscopy in solution at 23 °C: Geometry optimizations for the model species **6'** demonstrated the (*Λ*)-isomer to be more stable than the (*Δ*)-isomer by 12.3 kJ mol^{-1} (see Chapter 3.4, Computational Studies). This energy difference corresponds to a theoretical molar (*Λ*)/(*Δ*)-equilibrium ratio of 0.993:0.007.

As the bidentate ligands of **4a**, **5a**, and **6a** are sterically more demanding than those of **2b** and **3a**, one could speculate that the steric bulkiness of the bidentate ligands controls the stereochemistry of these zwitterionic λ^5*Si*-silicates in solution. However, further studies are necessary to confirm this hypothesis. As the compounds studied were found to undergo an intermolecular ligand exchange between λ^5*Si*-silicates with different bidentate ligands on the hours time scale (NMR cross-experiments), one could speculate about an intermolecular (*Λ*)/(*Δ*)-epimerization process of **3**–**6**; however, such kind of process could not be detected under the experimental conditions used. In all NMR experiments with solutions of **4a**, **5a**, and **6a**, only one single diastereomer could be detected in the temperature range –100 °C to 23 °C.

3.4 Computational Studies of the Anionic Model I and Related Model Species

To get more information about the structure of the zwitterions **1**–**6**, quantum-chemical investigations were performed.[24] For this purpose, computational studies of the anionic model species **I** (SCF/TZP+ level) were carried out using the TURBOMOLE program system (version 5.6).[25] Critical points of the potential energy surfaces were characterized as local minima (zero imaginary frequencies) and saddle points (one imaginary frequency), respectively, by calculation of the vibrational frequencies. The calculated energies include the zero-point vibrational energy obtained by SCF calculations and the single-point MP2 energy. The transition state **ID** was found using the module statpt implemented in TURBOMOLE.

The TZP (triple-ζ plus polarization) basis set given in ref 26a is suitable to describe molecules with moderately polarized chemical bonds. To get a more accurate description of pentacoordinate silicon species containing distinctly polarized silicon-element bonds, the exponents of the most diffuse s, p, and d GTOs (Gauss-type orbitals) for Si, F, O, N, C, and H were additionally optimized at the SCF level. For this purpose, a TZP basis set optimization with additional diffuse s and p functions (TZP+) was performed for the SiF_2ONH skeleton of the anion [ethene-1-aminato-2-olato(2–)]difluorohydridosilicate(1–) (model for the anion **I**), whereas the carbon and hydrogen atoms in the outer spheres of the Si-coordination polyhedra were not considered in these TZP and TZP+ basis set optimizations (see below).

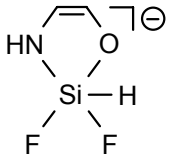

This particular anion with an SiF_2ONH framework was chosen because it shall also serve as a model for theoretical studies of related anionic monocyclic λ^5*Si*-silicates containing one bidentate ethene-1-aminato-2-olato ligand, two fluoro ligands, and one hydrido ligand bound to the Si-coordination center.

As shown in Figure 20, four different structures (**IA**–**ID**) were studied for the anionic model species **I**. For energetic reasons, square pyramids with the hydrogen atom in a basal position were not considered. The trigonal-bipyramidal species **IA** and **IB** and the square-pyramidal species **IC** are chiral and therefore exist as (*Λ*)- and (*Δ*)-enantiomers. Calculations of the vibrational frequencies demonstrated that **IA** and **IB** represent local minima (a third possible minimum, with both nitrogen atoms occupying the axial sites, could not be located as a stationary point), whereas **IC** represents a geometry nearby the expected Berry-type square-pyramidal transition state (no stationary point; the sum of the basal angles had to be fixed in internal coordinates during the geometry optimization), and **ID** is a transition state (for selected geometric parameters for **IA**–**ID**, see Table 6). The trigonal-bipyramidal structure, with the two oxygen atoms in the axial sites, is the energetically most favorable one. This result is in agreement with the experimentally established structures of the Si-coordination polyhedra in the crystals of *rac*-**1**, **2b**, and **3a**·CH_2Cl_2, **4a**·CH_2Cl_2, **5a**·CH_2Cl_2, **6a**·$2CH_2Cl_2$, and **6a**·$½CH_2Cl_2$. The energy barrier between the trigonal-bipyramidal local minima **IA** and **IB** and **IC** and **ID** are relatively high (38.8 and 56.4 kJ mol^{-1}, respectively), indicating that Berry-type distortions of the trigonal-bipyramidal Si-coordination polyhedra of *rac*-**1**, **2b**, and **3a**·CH_2Cl_2, **4a**·CH_2Cl_2, **5a**·CH_2Cl_2, **6a**·$2CH_2Cl_2$, and **6a**·$½CH_2Cl_2$ cannot be achieved so easy.

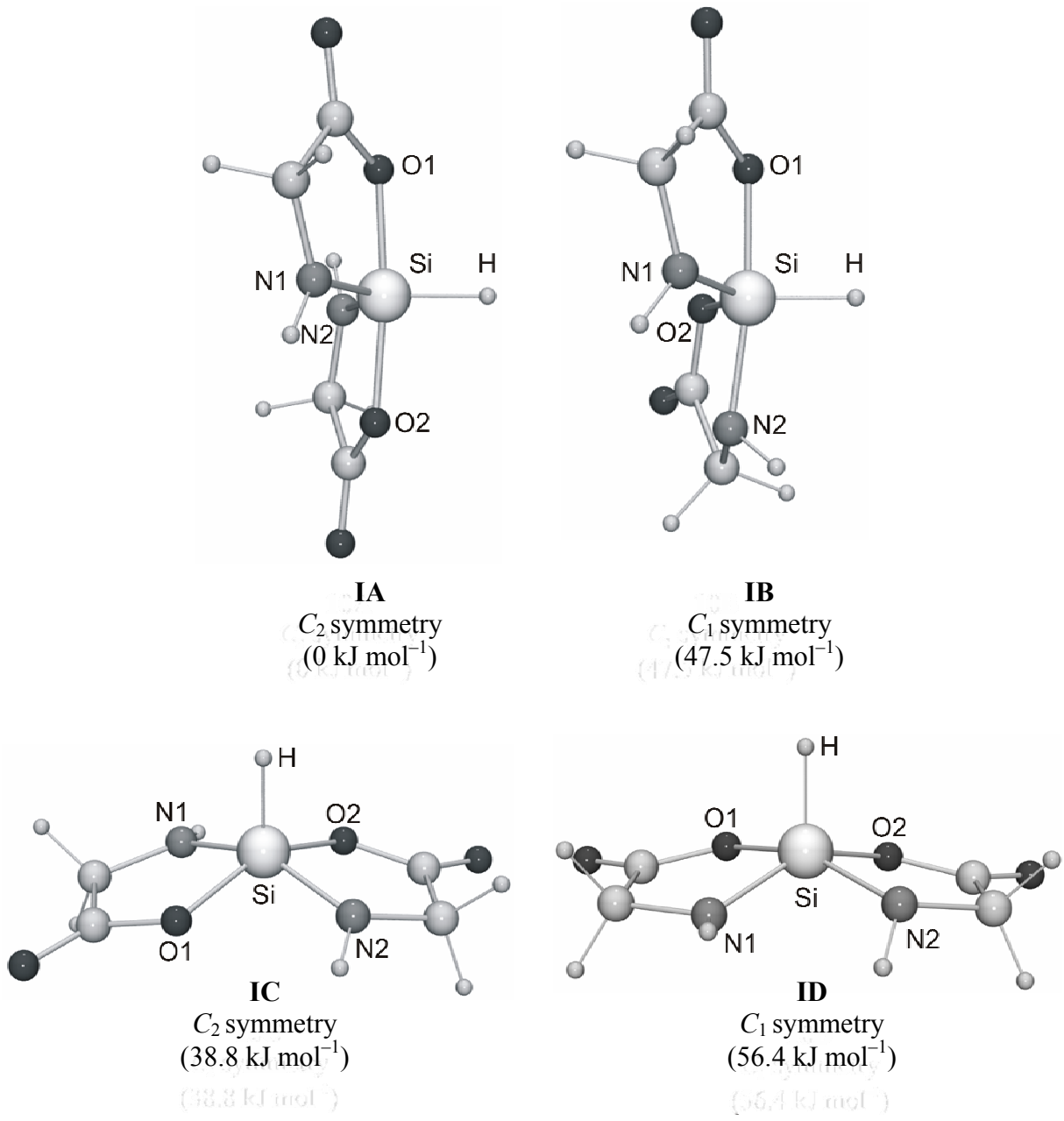

Figure 20. Calculated structures and relative energies of **IA** and **IB** (local minima), **IC** (a geometry nearby the expected Berry-type square-pyramidal transition state), and **ID** (transition state) as obtained by SCF/TZP+ geometry optimizations. **IC** does not represent a stationary point (the gradient does not vanish); however, test calculations indicate that the potential energy surface in the vicinity of this particular geometry is quite flat. The anion **ID** with a possible C_s symmetry does not represent a critical point.

Table 6. Selected Calculated Bond Distances (Å) and Angles (deg) for the Local Minima **IA** and **IB,** for the idealized Geometry **IC,** and for the Transition State **ID** as obtained by SCF/TZP+ Geometry Optimizations

	IA	**IB**	**IC**	**ID**
Si–O1	1.818	1.821	1.798	1.790
Si–O2	1.818	1.725	1.798	1.764
Si–N1	1.730	1.731	1.759	1.771
Si–N2	1.730	1.827	1.759	1.795
Si–H	1.479	1.488	1.483	1.482
O1–Si–O2	173.6	87.7	150.8	84.4
O1–Si–N1	85.7	85.0	85.1	84.4
O1–Si–N2	91.4	171.9	87.9	157.4
O1–Si–H	93.2	89.7	104.6	97.9
O2–Si–N1	91.4	126.0	87.9	145.6
O2–Si–N2	85.7	86.5	85.1	86.4
O2–Si–H	93.2	113.0	104.6	102.5
N1–Si–N2	125.7	93.9	151.8	91.7
N1–Si–H	117.1	120.4	104.1	111.3
N2–Si–H	117.1	97.7	104.1	104.2

In addition, geometry optimizations for the (*Λ*,*S*,*S*)- and (*Δ*,*S*,*S*)-isomers of **2'**, **4'**, and **6'** (model systems with the (dimethylammonio)methyl group instead of the (2,2,6,6-tetramethylpiperidinio)methyl moiety) were performed at the RI-MP2 level[27] using a TZP basis set[26a] and a TZVP auxiliary basis for the fit of the charge density.[26b] The calculations were performed using the TURBOMOLE program system.[25] The optimized structures were characterized as minima on the potential energy surfaces by harmonic vibrational frequency analysis. The reported energy differences include the MP2 energies and zero-point vibrational energies obtained by HF calculations.

The structures of the calculated minima are shown in Figures 21–23, with selected calculated distances and angles in Table 7. As can be seen from Figures 2, 4, 6 (Chapter 3.2.1) and 21–23 and from Tables 1, 2 (Chapter 3.2.1), and 7, the calculated structures of **2'**, **4'**, and **6'** and the respective experimentally established structures of **2b**, **4a**·CH_2Cl_2, and **6a**·$2CH_2Cl_2$

are in reasonable agreement (a perfect agreement between the calculated and experimentally established structures cannot be expected since the latter are influenced by intermolecular interactions in the crystal). The Si-coordination polyhedra of all local minimum structures are slightly distorted trigonal bipyramids, with the oxygen ligand atoms in the axial positions and the nitrogen and carbon ligand atoms occupying the equatorial sites.

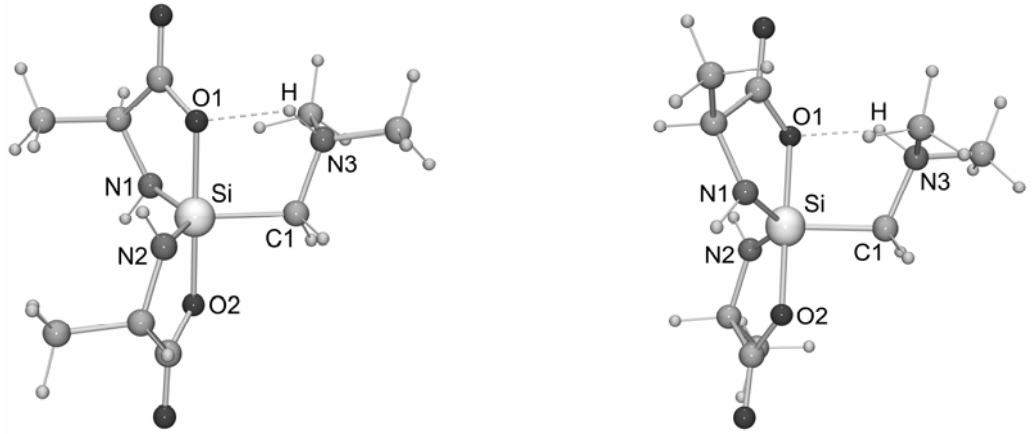

Figure 21. Calculated structures of **2a'** (left) and **2b'** (right). The dashed lines indicate intramolecular N3–H···O1 hydrogen bonds.

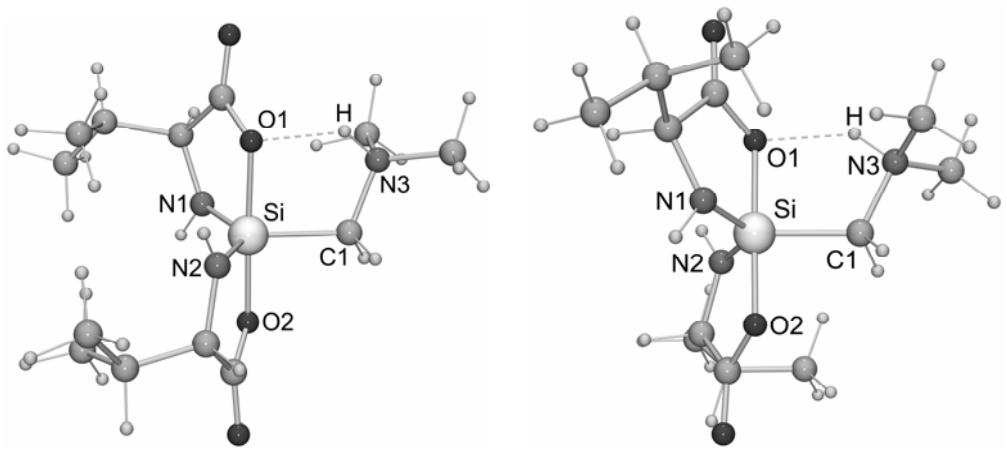

Figure 22. Calculated structures of **4a'** (left) and **4b'** (right). The dashed lines indicate intramolecular N3–H···O1 hydrogen bonds.

The calculated energy differences between the respective (*Λ*,*S*,*S*)- and (*Δ*,*S*,*S*)-isomers amount to 2.3 kJ mol^{-1} (**2'**), 2.1 kJ mol^{-1} (**4'**), and 12.3 kJ mol^{-1} (**6'**), with the (*Λ*)-isomers being energetically more stable than the (*Δ*)-isomers. In the case of a (*Λ*)/(*Δ*)-epimerization,

these energy differences would result in molar (*Λ*)/(*Δ*)-equilibrium ratios of 0.72:0.28 (**2'**), 0.70:0.30 (**4'**), and 0.993:0.007 (**6'**) at 23 °C.

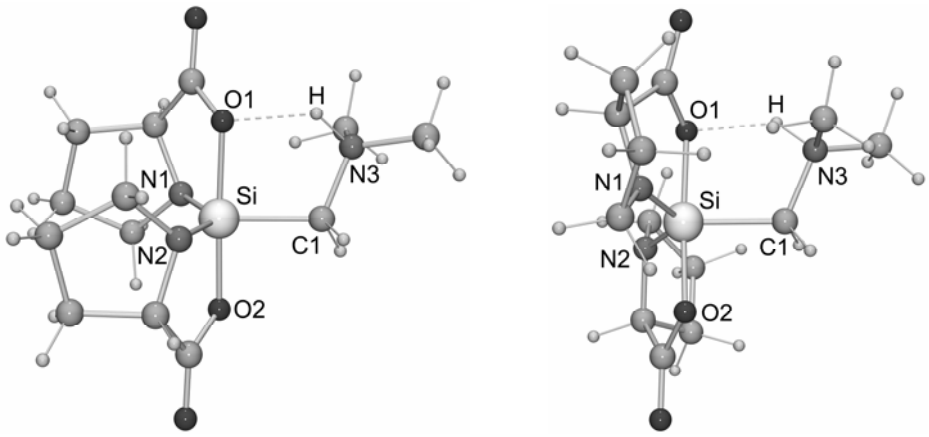

Figure 23. Calculated structures of **6a'** (left) and **6b'** (right). The dashed lines indicate intramolecular N3–H···O1 hydrogen bonds.

Table 7. Selected Interatomic Distances (Å) and Angles (deg) for the Calculated Structures of the (*Λ*,*S*,*S*)- and (*Δ*,*S*,*S*)-Isomers of **2'**, **4'**, and **6'**

	2a'	**2b'**	**4a'**	**4b'**	**6a'**	**6b'**
Si–O1	1.871	1.871	1.872	1.870	1.874	1.882
Si–O2	1.788	1.788	1.789	1.790	1.792	1.788
Si–N1	1.750	1.751	1.739	1.753	1.765	1.734
Si–N2	1.734	1.731	1.729	1.735	1.749	1.742
Si–C1	1.939	1.940	1.948	1.936	1.939	1.955
O1–Si–O2	179.9	179.5	178.4	179.3	177.8	176.6
O1–Si–N1	85.4	85.4	85.4	85.4	86.0	85.1
O1–Si–N2	91.4	91.6	92.3	91.6	91.8	92.8
O1–Si–C1	88.9	88.7	88.6	89.0	88.2	87.4
O2–Si–N1	94.7	95.0	95.2	95.0	95.0	95.4
O2–Si–N2	88.6	88.5	88.5	88.6	88.9	89.7
O2–Si–C1	91.0	90.9	89.9	90.4	89.6	89.4
N1–Si–N2	130.7	129.9	129.1	128.4	130.3	126.1
N1–Si–C1	114.2	114.4	116.0	116.6	114.8	117.2
N2–Si–C1	114.9	115.5	114.8	114.8	114.8	116.5

4 Spirocyclic Zwitterionic λ⁵*Si*-[(Ammonio)methyl]silicates with an *SiO₄C* Skeleton and Two Identical Bidentate Ligands Derived from α-Hydroxycarboxylic Acids (Compounds 7–12)

4.1 Spirocyclic Zwitterionic λ⁵*Si*-[(Ammonio)methyl]silicates with an *SiO₄C* Skeleton and Two Identical Bidentate Ligands Derived from (*S*)-Lactic Acid (Compounds 7–9)

The spirocyclic zwitterionic λ⁵*Si*-[(ammonio)methyl]silicates (*Δ*,*S*,*S*)-**7**·CH_3CN (**7b**·CH_3CN), (*Λ*,*S*,*S*)-**8** (**8a**), (*Δ*,*S*,*S*)-**8** (**8b**), and (*Δ*,*S*,*S*)-**9** (**9b**)[15a] were synthesized and structurally characterized in the solid state (crystal structure analyses; ^{15}N and ^{29}Si VACP/MAS NMR experiments) and in solution (^{1}H, ^{13}C, ^{15}N, and ^{29}Si NMR experiments, including studies of the stereodynamics). The chiral λ⁵*Si*-silicates with ligands derived from optically active (*S*)-lactic acid were isolated as diastereomerically and enantiomerically pure compounds that undergo a (*Λ*)/(*Δ*)-epimerization in solution to give an equilibrium mixture of the respective (*Λ*,*S*,*S*)- and (*Δ*,*S*,*S*)-diastereomers.

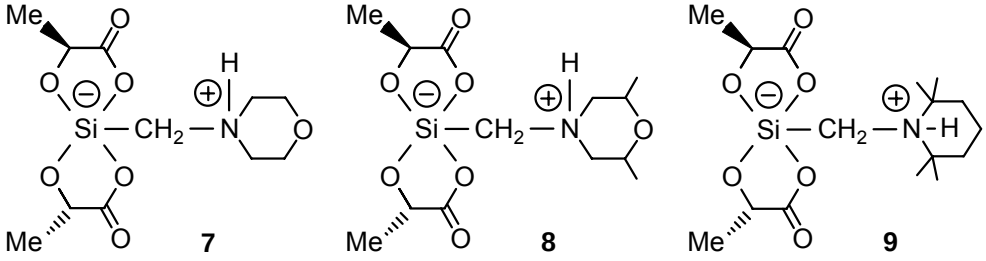

The studies presented here were performed as part of our research program dealing with pentacoordinate silicon(IV) complexes containing *Si*O_4C skeletons, with a special emphasis on the stereochemistry of such complexes containing bidentate ligands derived from α-hydroxycarboxylic acids (in this context see ref. 2o and literature cited therein).

4.1.1 Syntheses of the λ⁵*Si*-[(Ammonio)methyl]silicates 7–9

The zwitterionic λ⁵*Si*-silicate **7** was prepared according to Scheme 2 by treatment of trimethoxy[(morpholino)methyl]silane (**25**) with two molar equivalents of (*S*)-lactic acid at 20 °C in tetrahydrofuran and was isolated, after recrystallization from acetonitrile, as the crystalline solvate **7b**·CH_3CN (yield: 79%).

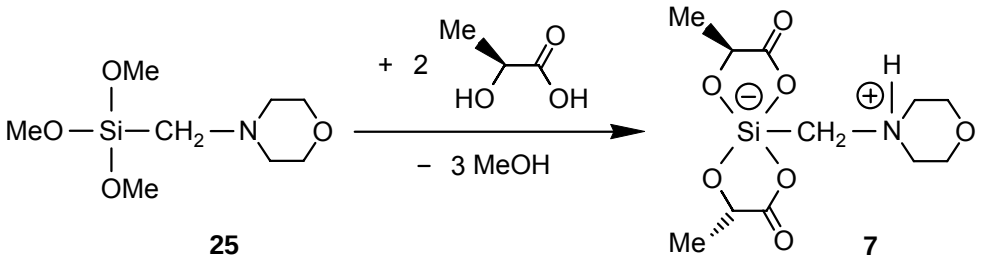

25 **7**

Scheme 2

The zwitterionic λ^5*Si*-silicate **8** was prepared according to Scheme 3 by treatment of [(*cis*-2,6-dimethylmorpholino)methyl]trimethoxy silane (**29**) with two molar equivalents of (*S*)-lactic acid at 20 °C in tetrahydrofuran and was isolated, after recrystallization from tetrahydrofuran/acetonitrile/diethyl ether (1:1:1 (v/v/v)), as the crystalline solid **8a** (yield: 90%). The λ^5*Si*-silicate **8b** was prepared analogously to **8a** using tetrahydrofuran as the solvent and was isolated as a crystalline solid (yield 88%).

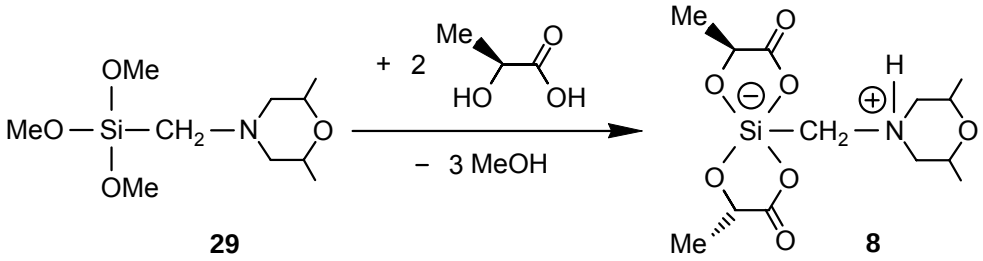

29 **8**

Scheme 3

The zwitterionic λ^5*Si*-silicate **9** was prepared according to Scheme 4 by treatment of trimethoxy[(2,2,6,6-tetramethylpiperidino)methyl]silane (**24**) with two molar equivalents of (*S*)-lactic acid at 20 °C in acetonitrile and was isolated as the crystalline solid **9b** (yield: 91%).

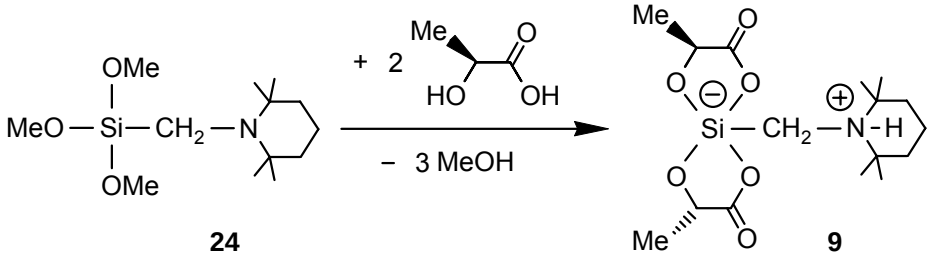

24 **9**

Scheme 4

The identities of **7b**·CH_3CN, **8a**, **8b**, and **9b** were established by elemental analyses (C, H, N), single-crystal X-ray diffraction studies, VACP/MAS NMR experiments (^{15}N, ^{29}Si), and solution NMR studies (^{1}H, ^{13}C, ^{15}N, ^{29}Si).

4.1.2 Crystal Structure Analyses of the λ^5*Si*-[(Ammonio)methyl]-silicates 7–9

The zwitterionic λ^5*Si*-silicates **7b**·CH_3CN, **8a**, and **9b** were structurally characterized by single-crystal X-ray diffraction.[16] The crystal data and experimental parameters used for these studies are given in Appendix A (Table 27). For reasons of comparison, selected bond distances and angles are listed in Table 8. Suitable single crystals of **7b**·CH_3CN, **8a**, and **9b** were isolated directly from the respective reaction mixtures (see Chapter 10, Experimental Section). In the case of **8b**, the quality of the crystals used for the X-ray diffraction experiment was not sufficient for the completely refinement of the structure; however, this experiment clearly indicated the (*Δ*,*S*,*S*)-configuration of the Si-coordination polyhedron of **8b**. The crystals were mounted in inert oil (perfluoroalkyl ether, ABCR) on a glass fiber and then transferred to the cold nitrogen gas stream of the diffractometer (Stoe IPDS; graphite-monochromated MoKα radiation (λ = 0.71073 Å)). All structures were solved by direct methods.[17] A riding model was employed in the refinement[18] of the C*H* hydrogen atoms, whereas the N*H* and O*H* hydrogen atoms were localized in difference Fourier syntheses and refined freely. All bond lengths and angles that are not discussed explicitly in the following sections are in the expected range and therefore do not need further discussion.

The zwitterionic λ^5*Si*-silicates **7b**·CH_3CN, **8a**, and **9b** crystallize in chiral space groups (Appendix A, Table 27), and the crystals investigated contain only one particular diastereomer ((*Δ*,*S*,*S*)-configuration in the case of **7b**·CH_3CN and **9b**, and (*Λ*,*S*,*S*)-configuration in the case of **8a**). The molecular structures of the zwitterions are depicted in Figures 24–26.

As can be seen from Figures 24–26, the Si-coordination polyhedra of **7b**·CH_3CN, **8a**, and **9b** (compounds with an *Si*O_4C framework) are distorted trigonal bipyramids, with the carboxylato oxygen atoms O1 and O3 in the axial positions. The alcoholato oxygen atoms O2 and O4 and the carbon atom C1 occupy the equatorial sites. The Si–O distances range from 1.6582(10) Å to 1.8233(12) Å, the axial Si–O bonds (1.7875(11)–1.8233(12) Å) being significantly longer than the equatorial ones (1.6582(10)–1.6747(12) Å). The Si–C bond lengths are in the range 1.8958(16)–1.9090(17) Å. Generally, the Si–O and the Si–C distances are similar to those reported for related zwitterionic λ^5*Si*-silicates with *Si*O_4C skeletons and ligands derived from α-hydroxycarboxylic acids (in this context, see refs. 2o, 4f,k,o, and 28).

As expected from the presence of the potential NH donor functions and the potential oxygen acceptor atoms, hydrogen-bonding systems were observed in the crystals of **7b**·CH_3CN, **8a**, and **9b**.[19] As can be seen from Figure 27 and Table 9, the zwitterion of **7b**·CH_3CN forms a bifurcate N–H···O/O hydrogen bond with one intramolecular and one intermolecular interaction leading to the formation of infinite one-dimensional chains along the [0 1 0] base vector.

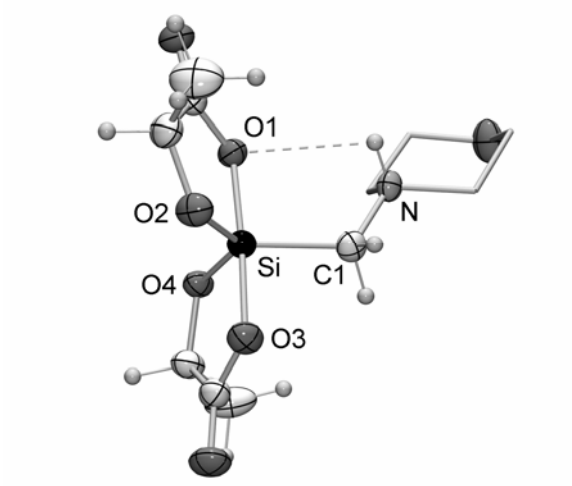

Figure 24. Molecular structure of **7b** ((*Λ*,*S*,*S*)-diastereomer) in the crystal of **7b**·CH_3CN (probability level of displacement ellipsoids 50%; CH_2 moieties of the morpholinio group represented as stick model for clarity).

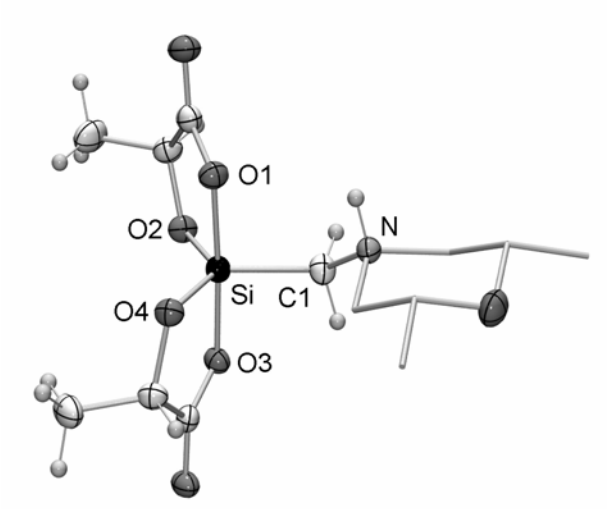

Figure 25. Molecular structure of **8a** ((*Λ*,*S*,*S*)-diastereomer) in the crystal (probability level of displacement ellipsoids 50%; CH_2CHCH_3 moieties of the *cis*-2,6-dimethylmorpholinio group represented as stick model for clarity).

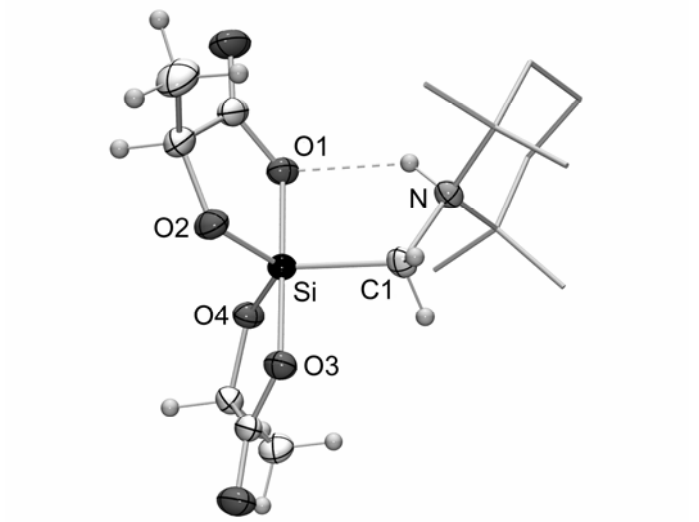

Figure 26. Molecular structure of **9b** ((*Δ*,*S*,*S*)-diastereomer) in the crystal (probability level of displacement ellipsoids 50%; CH_2 and $C(CH_3)_2$ moieties of the tetramethylpiperidinio group represented as stick model for clarity).

Table 8. Selected Bond Distances (Å) and Angles (deg) for **7b**·CH_3CN, **8a**, and **9b**

	7b·CH_3CN	**8a**	**9b**
Si–O1	1.7971(9)	1.8017(12)	1.8077(11)
Si–O2	1.6616(10)	1.6606(11)	1.6624(12)
Si–O3	1.8188(10)	1.8233(12)	1.7875(11)
Si–O4	1.6582(10)	1.6747(12)	1.6643(12)
Si–C1	1.8958(16)	1.9087(17)	1.9090(17)
O1–Si–O2	89.09(5)	89.87(6)	88.96(5)
O1–Si–O3	175.96(5)	176.69(6)	178.32(6)
O1–Si–O4	90.74(5)	89.49(5)	90.97(5)
O1–Si–C1	94.64(5)	93.22(6)	92.45(6)
O2–Si–O3	87.36(5)	88.96(6)	89.47(5)
O2–Si–O4	123.68(6)	125.25(6)	119.94(7)
O2–Si–C1	122.31(6)	112.81(7)	121.60(7)
O3–Si–O4	89.64(5)	88.65(5)	90.32(6)
O3–Si–C1	88.88(6)	90.09(6)	87.87(6)
O4–Si–C1	113.83(6)	121.88(7)	118.40(7)

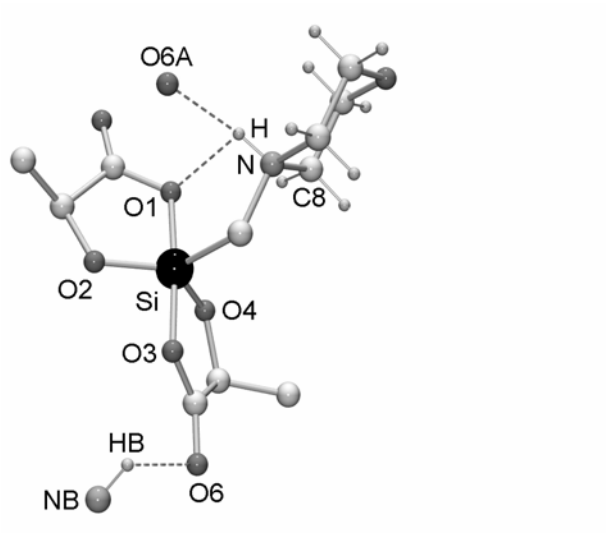

Figure 27. Hydrogen-bonding system in the crystal of **7b**·CH_3CN leading to infinite chains along the base [0 1 0] base vector (the hydrogen atoms of the lactato(2–) ligands are omitted for clarity).

In the case of **8a**, intermolecular hydrogen bonds of the N–H···O type lead to the formation of infinite one-dimensional chains along the [1 0 0] base vector (Figure 28, Table 9). As can be seen from Figure 26 and Table 9, the zwitterion **9b** forms an intramolecular N–H···O hydrogen bond.

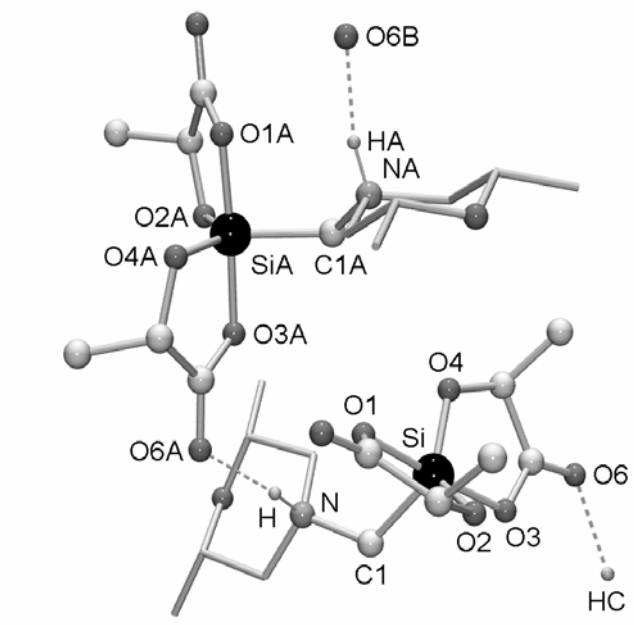

Figure 28. Intermolecular N–H···O hydrogen bonds in the crystal of **8a** leading to infinite chains along the base [1 0 0] base vector (CH_2CHCH_3 moieties of the *cis*-2,6-dimethylmorpholinio groups represented as stick model for clarity).[19]

Table 9. Hydrogen-Bonding Geometries for **7b**·CH_3CN, **8a**, and **9b** in the Crystal[a]

	D–H···A	D–H (Å)	H···A (Å)	D···A (Å)	D–H···A (deg)
7b·CH_3CN	N–H···O1	0.888(16)	2.492(15)	2.8117(17)	101.8(11)
	N–H···O6[b]	0.888(16)	2.222(17)	2.8918(16)	131.9(13)
8a	N–H···O6	0.95(2)	1.84(2)	2.7666(18)	162.9(18)
9b	N–H···O1	0.89(2)	2.07(2)	2.7463(17)	133(2)

[a]Data calculated by using the program PLATON.[19] [b]Bifurcate N–H···O1/O6 interaction; O1···H···O6 = 106.5(6) deg.

4.1.3 NMR Studies of the λ⁵*Si*-[(Ammonio)methyl]silicates 7–9

4.1.3.1 NMR Studies of the λ⁵*Si*-[(Ammonio)methyl]silicates 7–9 in the Solid State

The zwitterionic λ⁵*Si*-silicates **7b**·CH_3CN, **8a**, **8b**, and **9b** were characterized at 22 °C by solid-state ^{29}Si VACP/MAS NMR spectroscopy (Table 10). The isotropic ^{29}Si chemical shifts obtained clearly characterize the ^{29}Si resonance signals as arising from pentacoordinate silicon atoms. Compared to the solid-state ^{29}Si NMR resonance signals of compounds **1**–**6** (compounds with an *Si*O_2N_2C skeleton), the solid-state ^{29}Si NMR resonance signals of **7b**·CH_3CN, **8a**, **8b**, and **9b** are sharp (compounds with an *Si*O_4C skeleton).

Table 10. ^{29}Si VACP/MAS NMR Data for **7b**·CH_3CN, **8a**, **8b**, and **9b** in the Crystal (Spectra Recorded at 22 °C; Chemical Shifts in ppm)

7b·CH_3CN	–94.7
8a	–94.1
8b	–94.4
9b	–96.6

In addition, the zwitterionic λ⁵*Si*-silicates **7b**·CH_3CN, **8a**, **8b**, and **9b** were characterized at 22 °C by solid-state ^{15}N VACP/MAS NMR spectroscopy (see Chapter 10, Experimental Section). The solid-state ^{15}N NMR resonance signals were sharp due to the high crystallinity of the bulk materials used for these experiments. The solid-state NMR spectra obtained were compatible with the crystal structures of these compounds and demonstrated

that the non-racemic compounds **7b**·CH_3CN, **8a**, **8b**, and **9b** were diastereomerically and enantiomerically pure.

4.1.3.2 NMR Studies of the λ⁵*Si*-[(Ammonio)methyl]silicates 7–9 in Solution

Compounds **7b**·CH_3CN, **8a**, **8b**, and **9b** were additionally characterized by solution ^1H, ^{13}C, and ^{29}Si NMR spectroscopy. All these solution NMR studies were performed at 23 °C using [D_6]DMSO or CD_2Cl_2 as solvents. As can be seen from Table 11, the ^{29}Si chemical shifts are very similar to the isotropic ^{29}Si chemical shifts obtained in the solid-state NMR experiments, indicating that the λ⁵*Si*-silicate skeletons of all these compounds exist in solution as well. Furthermore, the ^1H chemical shifts observed for the $SiCH_2NH$ protons (δ = 5.7–6.0 ppm) indicate the presence of the ammonium moieties. Thus, these NMR experiments unequivocally demonstrate that the zwitterions also exist in solution (for further details, see Chapter 10, Experimental Section).

Table 11. ^{29}Si NMR Data for **7b**·CH_3CN, **8a**, **8b**, and **9b** in Solution (Spectra Recorded at 23 °C, Chemical Shifts in ppm)[a]

7b·CH_3CN	–95.94 (major isomer)/–95.98 (minor isomer)
8a, **8b**	–96.22 (**8a**)/–96.24 (**8b**)
9b	–96.3 (major isomer)/–97.5 (minor isomer)

[a] **7b**·CH_3CN, [D6]DMSO; **8a**, **8b**, **9b**, CD_2Cl_2.

As the trigonal-bipyramidal structure, with the carboxylato oxygen atoms in the axial sites, is the energetically most favorable one for all the zwitterionic λ⁵*Si*-silicates studied (see Chapter 4.1.2, Crystal Structure Analyses), it is likely that this particular structure is also dominant in solution. The chiral nature of the zwitterions is reflected by the ABX spin systems observed for the $SiCH_AH_BNH_X$ protons in the ^1H NMR spectra.

Stability in Water. Upon dissolution of compounds **7b**·CH_3CN, **8a**, and **9b** in water, a partial hydrolysis of the zwitterionic λ⁵*Si*-silicates was observed. ^{29}Si NMR experiments (23 °C, 300.1 MHz) with aqueous solutions (D_2O) of **7b**·CH_3CN (c = 500 mM), **8a** (c = 290 mM), and **9b** (c = 185 mM) were performed at room temperature. The ^{29}Si NMR spectra indicated

that a thermodynamic equilibrium between the pentacoordinate silicates and related tetracoordinate silicon species exists in aqueous solution.

4.1.3.3 Dynamic NMR Studies of the λ^5*Si*-[(Ammonio)methyl]-silicates 7–9 in Solution

Upon dissolution of the zwitterionic λ^5*Si*-silicates **7b**·CH_3CN, **8a**, **8b**, and **9b** in organic solvents a (*Λ*)/(*Δ*)-epimerization was observed. This isomerization process leads to equilibrium mixtures of the respective diastereomers (**7a** ⇄**7b**; **8a** ⇄**8b**; **9a** ⇄**9b**).

In the case of compound **7**·CH_3CN, the absolute configurations of the diastereomers could not be assigned because the epimerization process was too fast and could not be monitored by ^{1}H NMR spectroscopy; even upon dissolution of **7b**·CH_3CN in CD_3CN at –40 °C, spontaneous equilibration was observed (attempts to study the epimerization process in CD_2Cl_2 at temperatures between –40 °C and –90 °C failed due to the poor solubility of this compound).

Interestingly, compound **8a** does not undergo an epimerization in solution (CD_2Cl_2) at low temperatures (only one set of resonance signals was observed in the ^{1}H NMR spectra). This compound was studied by ^{1}H NMR spectroscopy at 300.1 MHz in the temperature range –94 °C to 23 °C, using CD_2Cl_2 as the solvent. For this purpose, a sample of diastereomerically and enantiomerically pure **8a** was dissolved in CD_2Cl_2 at –94 °C, (*c* = 72 mM), and ^{1}H NMR spectra were recorded every 300 s at this temperature for one hour (the first spectrum was recorded ca. 270 s after dissolving the sample).

Furthermore, ^{1}H NMR spectra were subsequently recorded with the same sample at –60 °C, –50 °C, –40 °C, and –30 °C, and no significant changes of the NMR spectra were observed in the temperature range studied. However at –20 °C a very slow epimerization process took place which was monitored at this temperature over a period of ca. 10 h (monitoring of the epimerization process by using the respective N*H*, SiOCC*H*$_3$, or NCCC*H*$_3$ resonance signals as the chemical sonds). The thermodynamic equilibrium at –20 °C was reached after ca. 5 h (molar equilibrium ratio: **8a**:**8b**, 0.30:0.70). At 23 °C a different molar equilibrium ratios was observed (**8a**:**8b**, 0.44:0.56). Representative partial ^{1}H NMR spectra of **8** as a function of temperature and time are depicted in Figure 29. The ^{1}H NMR resonance signals of the NCCC*H*$_3$ (–94 °C, 1.10–1.20 ppm) and SiOCC*H*$_3$ groups (–94 °C, 1.23–1.33

ppm) are plotted as a function of temperature and time. The epimerization process **8a** ⇄ **8b** is depicted in the Scheme below.

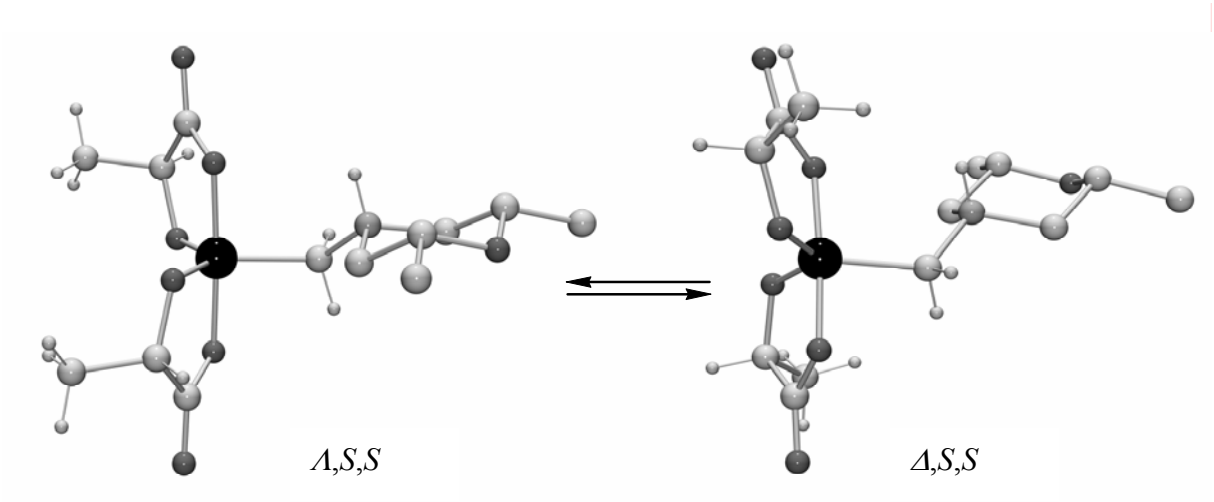

In the case of compound **9b**, the absolute configurations of the diastereomers could not be assigned because the epimerization process was too fast and could not be monitored by ^{1}H NMR spectroscopy; even upon dissolution of this compound in CD_2Cl_2 at –90 °C, a spontaneous equilibration was observed.

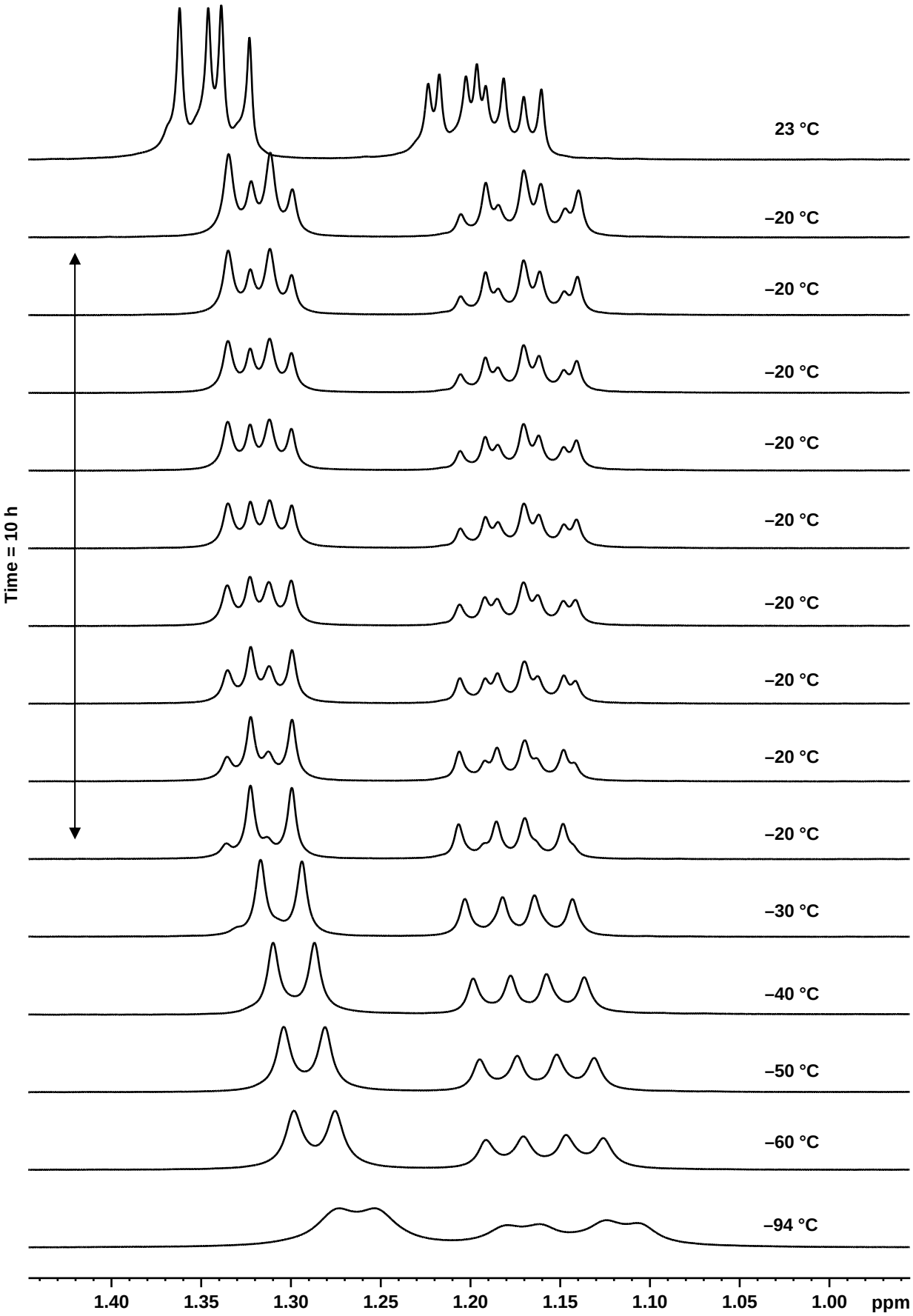

Figure 29. Representative partial ^{1}H NMR spectra (resonance signals of the NCCC*H*$_3$ and SiOCC*H*$_3$ groups) of **8** in CD_2Cl_2 at 300.1 MHz as a function of temperature (warming from –94 °C to 23 °C) and time (monitoring at –20 °C for 10 hours).

4.2 Spirocyclic Zwitterionic λ⁵*Si*-[(Ammonio)methyl]silicates with an SiO_4C Skeleton and Two Identical Bidentate Ligands Derived from (*S*)-3-Phenyllactic Acid (Compounds 10 and 11) or (*S*)-Mandelic Acid (Compound 12)

A series of zwitterionic λ⁵*Si*-silicates with an (ammonio)methyl ligand and two bidentate chelate ligands derived from (*S*)-3-phenyllactic acid ((*Λ*,*S*,*S*)-**10** and (*Λ*,*S*,*S*)-**11**·CH_3CN[15a]) or (*S*)-mandelic acid ((*Λ*,*S*,*S*)-**12**[15a]) was synthesized as diastereomerically and enantiomerically pure products. Compounds (*Λ*,*S*,*S*)-**10** (**10a**), (*Λ*,*S*,*S*)-**11**·CH_3CN (**11a**·CH_3CN), and (*Λ*,*S*,*S*)-**12** (**12a**) were structurally characterized in the solid state (crystal structure analyses; ^{15}N and ^{29}Si VACP/MAS NMR experiments), and compounds **11a**·CH_3CN and **12a** were additionally characterized in solution (^{1}H, ^{13}C, and ^{29}Si NMR experiments).

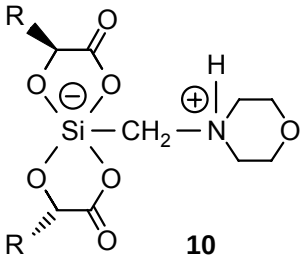

10

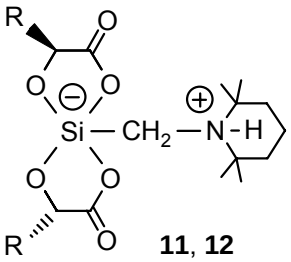

11, **12**

	R
10, **11**	CH_2Ph
12	Ph

The zwitterionic λ⁵*Si*-silicates **11a** and **12a** undergo a (*Λ*)/(*Δ*)-epimerization in solution to give an equilibrium mixture of the respective (*Λ*,*S*,*S*)- and (*Δ*,*S*,*S*)-diastereomers. Due to the poor solubility of **10a** in polar or unpolar organic solvents, solution NMR experiments with this compound failed.

4.2.1 Syntheses of the λ⁵*Si*-[(Ammonio)methyl]silicates 10–12

The zwitterionic λ⁵*Si*-silicate **10** was prepared according to Scheme 5 by treatment of trimethoxy[(morpholino)methyl]silane (**25**) with two molar equivalents of (*S*)-3-phenyllactic acid. The synthesis was performed at 20 °C in acetonitrile (method a) or in water (method b), and compound **10a** was isolated as a colorless crystalline solid (yield: 88% and 71%, respectively).

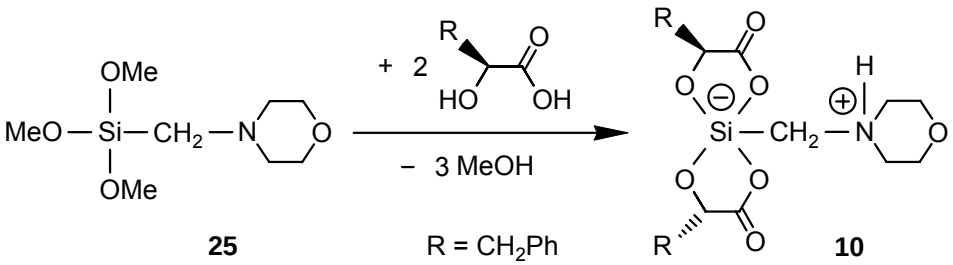

Scheme 5

The zwitterionic λ⁵*Si*-silicates **11** and **12** were prepared according to Scheme 6 by treatment of trimethoxy[(2,2,6,6-tetramethylpiperidino)methyl]silane (**24**) with two molar equivalents of (*S*)-3-phenyllactic acid or (*S*)-mandelic acid. The syntheses were performed at 20 °C in acetonitrile, and compounds **11a**·CH_3CN and **12a** were isolated as colorless crystalline solids (yields: **11a**·CH_3CN, 85%; **12a**, 81%).

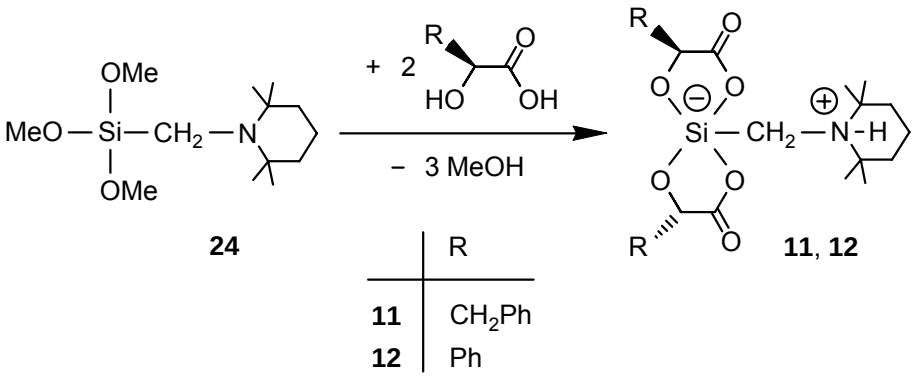

Scheme 6

The identities of **10a**, **11a**·CH_3CN, and **12a** were established by elemental analyses (C, H, N), single-crystal X-ray diffraction studies, VACP/MAS NMR experiments (^{15}N, ^{29}Si), and solution NMR studies (^{1}H, ^{13}C, ^{15}N, ^{29}Si; except for **10a**).

4.2.2 Crystal Structure Analyses of the λ⁵*Si*-[(Ammonio)methyl]-silicates 10–12

The λ⁵*Si*-silicates **10a**, **11a**·CH_3CN, and **12a** were structurally characterized by single-crystal X-ray diffraction.[16] The crystal data and experimental parameters used for these studies are given in Appendix A (Table 28). For reason of comparison, selected bond distances and angles are listed in Table 12. Suitable single crystals of **10a**, **11a**·CH_3CN, and **12a** were isolated directly from the respective reaction mixtures (see Chapter 10, Experimental Section). The crystals were mounted in inert oil (perfluoroalkyl ether, ABCR) on a glass fiber and then transferred to the cold nitrogen gas stream of the diffractometer (Stoe IPDS; graphite-monochromated MoKα radiation (λ = 0.71073 Å)). All structures were solved

by direct methods.[17] A riding model was employed in the refinement[18] of the C*H* hydrogen atoms, whereas the N*H* and O*H* hydrogen atoms were localized in difference Fourier syntheses and refined freely. All bond lengths and angles that are not discussed explicitly in the following sections are in the expected range and therefore do not need further discussion.

The zwitterionic λ^5*Si*-silicates **10a**, **11a**·CH_3CN, and **12a** crystallize in chiral space groups (Appendix A, Table 28), and the crystals investigated contain only one particular diastereomer (*Λ*,*S*,*S*)-configuration). The molecular structures of the zwitterions are depicted in Figures 30–32.

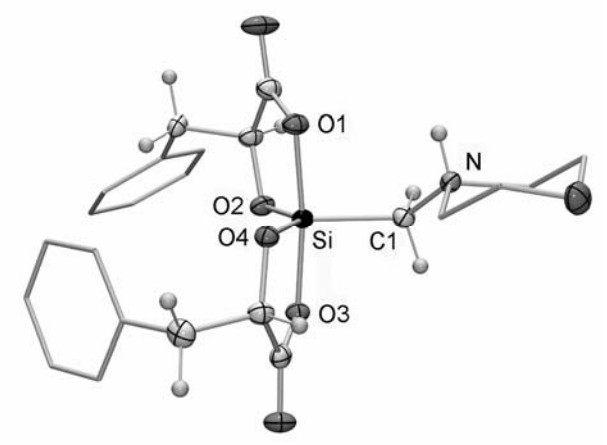

Figure 30. Molecular structure of **10a** ((*Λ*,*S*,*S*)-diastereomer) in the crystal (probability level of displacement ellipsoids 50%; CH_2 moieties of the morpholinio group and phenyl groups represented as stick models for clarity).

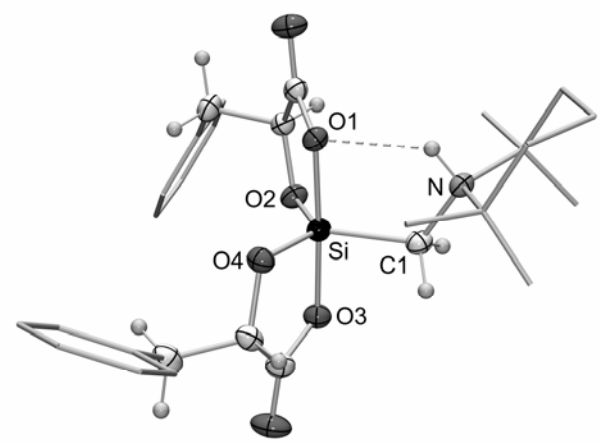

Figure 31. Molecular structure of **11a** ((*Λ*,*S*,*S*)-diastereomer) in the crystal of **11a**·CH_3CN (probability level of displacement ellipsoids 50%; CH_2 and $C(CH_3)_2$ moieties of the 2,2,6,6-tetramethylpiperidinio group and phenyl groups represented as stick models for clarity).

As can be seen from Figures 30–32 and Table 12, the Si-coordination polyhedra of **10a**, **11a**·CH_3CN, and **12a** are distorted trigonal bipyramids, with the carboxylato oxygen atoms O1 and O3 in the axial positions. The alcoholato oxygen atoms O2 and O4 and the carbon atom C1 occupy the equatorial sites. The Si–O distances range from 1.659(2) Å to 1.8229(11) Å, the axial Si–O bonds (1.787(2)–1.8229(11) Å) being significantly longer than the equatorial ones (1.659(2)–1.6668(10) Å). The Si–C bond lengths are in the range 1.8949(16)–1.9052(14) Å. Generally, the Si–O and the Si–C distances are similar to those

reported for the related zwitterionic λ^5*Si*-silicates **7**–**9** with *Si*O$_4$C skeletons and ligands derived from α-hydroxycarboxylic acids (in this context, see Chapter 4.1.2).

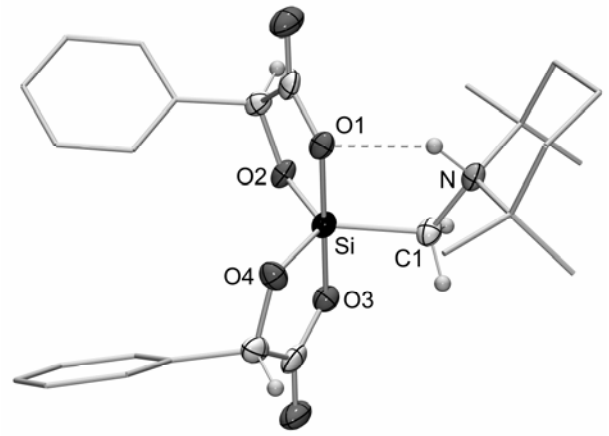

Figure 32. Molecular structure of **12a** ((*Λ*,*S*,*S*)-diastereomer) in the crystal (probability level of displacement ellipsoids 50%; CH_2 and $C(CH_3)_2$ moieties of the 2,2,6,6-tetramethylpiperidinio and phenyl groups represented as stick model for clarity).

Table 12. Selected Bond Distances (Å) and Angles (deg) for **10a**, **11a**·CH_3CN, and **12a**

	10a	**11a**·CH_3CN	**12a**
Si–O1	1.8015(11)	1.8131(11)	1.811(2)
Si–O2	1.6665(11)	1.6667(11)	1.666(2)
Si–O3	1.8229(11)	1.8017(12)	1.787(2)
Si–O4	1.6668(10)	1.6654(11)	1.659(2)
Si–C1	1.9052(14)	1.8949(16)	1.896(3)
O1–Si–O2	89.76(5)	88.72(5)	88.94(10)
O1–Si–O3	172.80(5)	176.22(5)	179.51(10)
O1–Si–O4	88.53(5)	90.15(5)	90.18(10)
O1–Si–C1	94.27(6)	94.08(6)	92.84(11)
O2–Si–O3	87.35(5)	88.19(5)	90.57(10)
O2–Si–O4	129.43(6)	124.49(6)	120.70(11)
O2–Si–C1	112.72(6)	119.65(6)	121.28(12)
O3–Si–O4	88.22(5)	89.82(5)	90.14(10)
O3–Si–C1	92.94(6)	89.33(6)	87.35(11)
O4–Si–C1	117.81(6)	115.79(7)	117.98(12)

As expected from the presence of the potential NH donor functions and the potential oxygen acceptor atoms, hydrogen-bonding systems were observed in the crystals of **10a**, **11a**·CH_3CN, and **12a**. As can be seen from Figure 33 and Table 13, the zwitterion of **10a** forms an intermolecular N–H···O hydrogen bond leading to the formation of infinite one-dimensional chains along the [0 1 0] base vector.

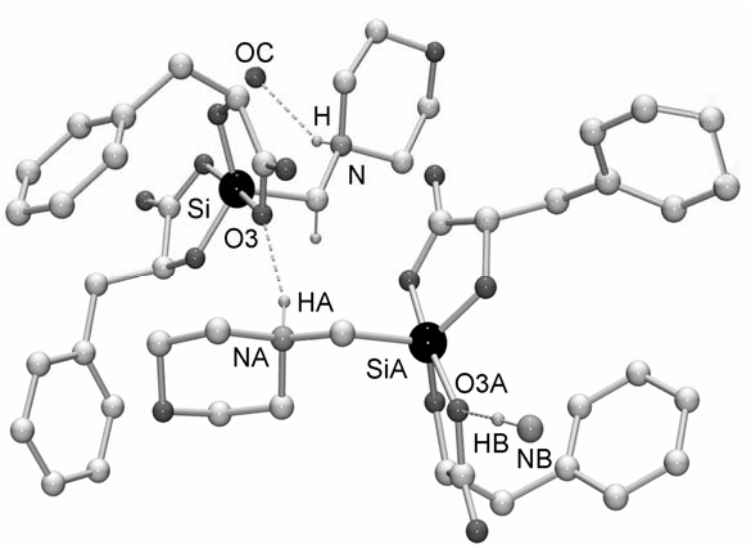

Figure 33. Intermolecular N–H···O hydrogen bonds in the crystal of **10a** leading to infinite chains along the base [0 1 0] base vector (hydrogen atoms except that involved in the hydrogen-bonding system are omitted for clarity).[19]

As can be seen from Figures 31 and 32 and Table 13, compounds **11a**·CH_3CN and **12a** form an intramolecular hydrogen bond between the ammonium NH group and one of two axial oxygen atoms.

Table 13. Hydrogen-Bonding Geometries for **10a**, **11a**·CH_3CN, and **12a** in the Crystal[a]

	D–H···A	D–H (Å)	H···A (Å)	D···A (Å)	D–H···A (deg)
10a	N–H···O3	0.92(2)	2.02(2)	2.9060(17)	161.3(17)
11a·CH_3CN	N–H···O1	0.87(2)	2.197(19)	2.8202(17)	128.7(16)
12a	N–H···O1	0.96(3)	1.98(3)	2.732(3)	134(2)

[a]Data calculated by using the program PLATON.[19]

4.2.3 NMR Studies of the λ⁵*Si*-[(Ammonio)methyl]silicates 10–12

4.2.3.1 NMR Studies of the λ⁵*Si*-[(Ammonio)methyl]silicates 10–12 in the Solid State

The zwitterionic λ⁵*Si*-silicates **10a**, **11a**·CH_3CN, and **12a** were characterized at 22 °C by solid-state ^{29}Si VACP/MAS NMR spectroscopy (Table 14). The isotropic ^{29}Si chemical shifts obtained clearly characterize the ^{29}Si resonance signals as arising from pentacoordinate silicon atoms. The ^{29}Si NMR chemical shifts of **10a**, **11a**·CH_3CN, and **12a** are very similar to those of compounds **7b**·CH_3CN, **8a**, and **9b** (compounds with an *Si*O_4C skeleton).

Table 14. ^{29}Si VACP/MAS NMR Data for **10a**, **11a**·CH_3CN, and **12a** in the Crystal (Spectra Recorded at 22 °C; Chemical Shifts in ppm)

10a	–95.9
11a·CH_3CN	–95.3
12a	–94.5

All zwitterionic λ⁵*Si*-silicates were also characterized at 22 °C by solid-state ^{15}N VACP/MAS NMR spectroscopy (see Chapter 10, Experimental Section). The ^{15}N NMR resonance signals were sharp due to the high crystallinity of the bulk materials used for these experiments. The solid-state NMR spectra obtained were compatible with the crystal structures of these compounds and demonstrated that the non-racemic compounds **10a**, **11a**·CH_3CN, and **12a** were diastereomerically and enantiomerically pure.

4.2.3.2 NMR Studies of the λ⁵*Si*-[(Ammonio)methyl]silicates 10–12 in Solution

Compound **10a** was found to be insoluble in polar or unpolar organic solvents and therefore solution NMR experiments could not be performed. However, compounds **11a**·CH_3CN and **12a** could be characterized by solution ^{1}H, ^{13}C, and ^{29}Si NMR spectroscopy. Furthermore, 2D ^{15}N,^{1}H HMQC NMR spectra were recorded for compounds **11a**·CH_3CN and **12a**. All these solution NMR studies were performed at 23 °C using CD_2Cl_2 as the solvent. As can be seen from Table 15, the ^{29}Si chemical shifts are very similar to the isotropic ^{29}Si

chemical shifts obtained in the solid-state NMR experiments (Table 14), indicating that the λ^5*Si*-silicate skeletons of all these compounds exist in solution as well. Furthermore, the ^{1}H chemical shifts observed for the SiCH$_2$N*H* protons (δ = 5.7–6.0 ppm) indicate the presence of the ammonium moieties. Thus, these NMR experiments unequivocally demonstrate that the zwitterions **11a** and **12a** exist in solution as well (for further details, see Chapter 10, Experimental Section).

Table 15. ^{29}Si NMR Data for **11a**·CH$_3$CN and **12a** in Solution (Spectra Recorded at 23 °C, Chemical Shifts in ppm)[a]

11a·CH$_3$CN	–96.5 (major isomer)/–96.5 (minor isomer)
12a	–95.9 (major isomer)/–96.4 (minor isomer)

[a] **11a**·CH$_3$CN, **12a**, CD$_2$Cl$_2$.

As the trigonal-bipyramidal structure, with the carboxylato oxygen atoms in the axial sites, is the energetically most favorable one for all the zwitterionic λ^5*Si*-silicates studied (see Chapter 4.2.2, Crystal Structure Analyses), it is likely that this particular structure is also dominant in solution. The chiral nature of the zwitterions is reflected by the ABX spin systems observed for the SiCH$_A$H$_B$NH$_X$ protons in the ^{1}H NMR spectra. Upon dissolution of **11a**·CH$_3$CN and **12a**, a (*Λ*)/(*Δ*)-epimerization was observed. This isomerization process leads to equilibrium mixtures of the respective diastereomers (**11a** ⇄ **11b**; **12a** ⇄ **12b**). In the case of **11a**·CH$_3$CN and **12a** (compounds with an *Si*O$_4$C skeleton), the absolute configurations of the diastereomers could not be assigned because the epimerization process was too fast and could not be monitored by ^{1}H NMR spectroscopy; even upon dissolution of **11a**·CH$_3$CN and **12a** in CD$_2$Cl$_2$ at –90 °C, a spontaneous equilibration was observed.

5 Spirocyclic Zwitterionic λ⁵*Si*-[(Ammonio)methyl]silicates with an *SiO₄C* Skeleton and Two Identical Bidentate Ligands Derived from *meso*-Oxolane-3,4-diol (Compounds 13–16)

The spirocyclic zwitterionic λ⁵*Si*-[(ammonio)methyl]silicates **13**–**16** with an *Si*O₄C skeleton and two bidentate ligands derived from *meso*-oxolane-3,4-diol were synthesized and structurally characterized (solution and solid-state NMR spectroscopy (**13**–**16**); single-crystal X-ray diffraction (**14**–**16**)).[29] The dynamic behavior of **16** in solution (CD_3CN, [D_6]DMSO, CD_2Cl_2) was studied by VT ^{1}H NMR experiments, with a special emphasis on the isomerization of the *syn*/*syn*, *syn*/*anti*, and *anti*/*anti* isomers and the enantiomerization of the respective (*Λ*)- and (*Δ*)-enantiomers. These experimental studies were complemented by computational studies of a related anionic model species **II**. Higher-coordinate silicon complexes with ligands derived from *meso*-oxolane-3,4-diol, that shares its ligand properties with furanosides and furanoses have already been described in the literature, and anionic λ⁵*Si*-silicates with two bidentate *meso*-oxolane-3,4-diolato(2–) ligands were demonstrated to be stable in water under strongly alkaline conditions.[30] In context with this findings, the behaviour of compounds **13**–**16** in aqueous solution was also studied.

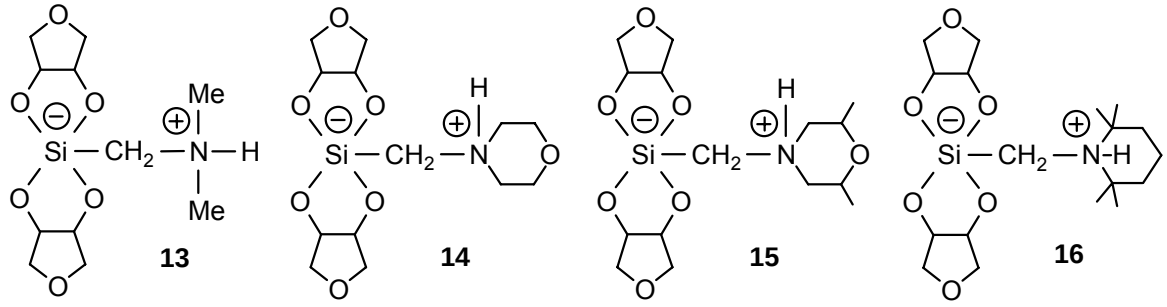

Taking into account the relative orientation of the oxolane rings and the (ammonio)methyl ligand *syn*/*syn*, *syn*/*anti*, and *anti*/*anti* isomers have to be considered for compounds **13**–**16**. As example, the three possible arrangements of the anionic model species **II** are depicted below (*syn* and *anti* refer to the orientation of the oxolane ring relative to the hydrido ligand).

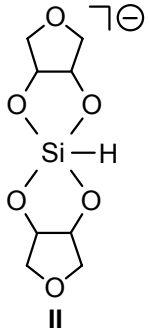

II

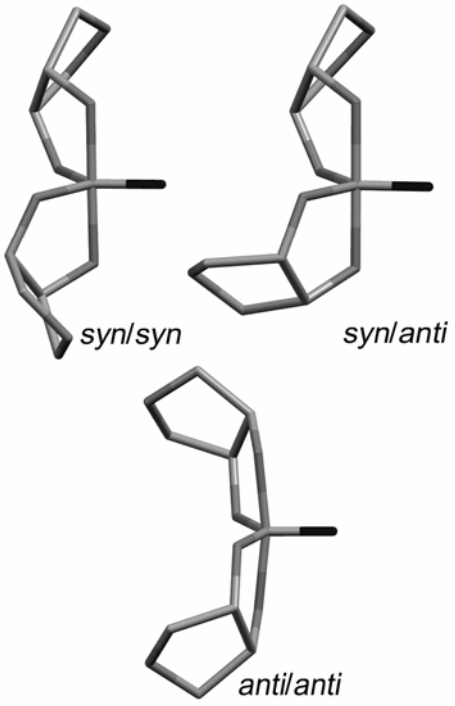

Figure 34. The three possible isomeric structures of the λ⁵*Si*-silicate skeletons of **13**–**16** (*syn*/*syn*, *syn*/*anti*, *anti*/*anti*) as demonstrated for the three isomers of the anionic model species **II**.

5.1 Syntheses of the λ⁵*Si*-[(Ammonio)methyl]silicates 13–16

The zwitterionic λ⁵*Si*-silicate **13** was synthesized according to Scheme 7 by reaction of [(dimethylamino)methyl]trimethoxy silane (**28**) with two molar equivalents of *meso*-oxolane-3,4-diol (1,4-anhydroerythritol) in water at 20 °C and isolated in 88% yield as a colorless crystalline solid.

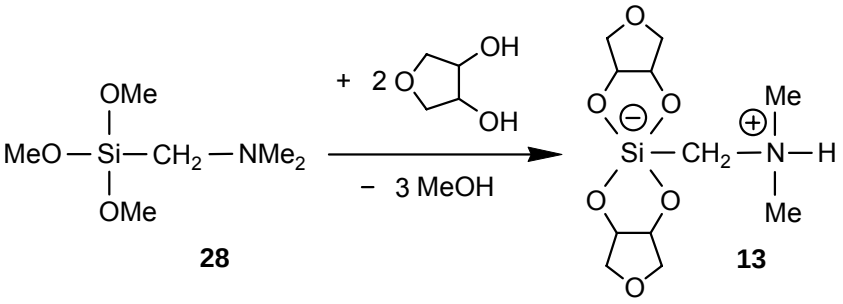

Scheme 7

The zwitterionic λ⁵*Si*-silicate **14** was synthesized according to Scheme 8, method a (cleavage of three Si–O bonds), by reaction of trimethoxy[(morpholino)methyl]silane (**25**) with two molar equivalents of *meso*-oxolane-3,4-diol in acetonitrile at 20 °C and isolated, after recrystallization from acetonitrile and then from dichloromethane/diethyl ether/*n*-

pentane, in 87% yield as a colorless crystalline solid. Alternatively, compound **14** was synthesized according to Scheme 8, method b (cleavage of one Si–C bond and two Si–O bonds), by reaction of dimethoxy(morpholinomethyl)phenylsilane (**26**) with two molar equivalents of *meso*-oxolane-3,4-diol in water at 20 °C and isolated, after crystallization from acetonitrile and subsequent recrystallization from dichloromethane/diethyl ether/*n*-pentane, in 53% yield as a colorless crystalline solid. As the synthesis according to method b involves a relatively slow Si–C cleavage reaction as the rate-determining step, product formation was significantly slower than that observed for method a (see Experimental Section).

The hydrate **14**·H_2O was synthesized analogously to **14** (Scheme 8, method a) using water instead of acetonitrile as the solvent and was isolated, after crystallization from water, in 93% yield as a colorless crystalline solid.

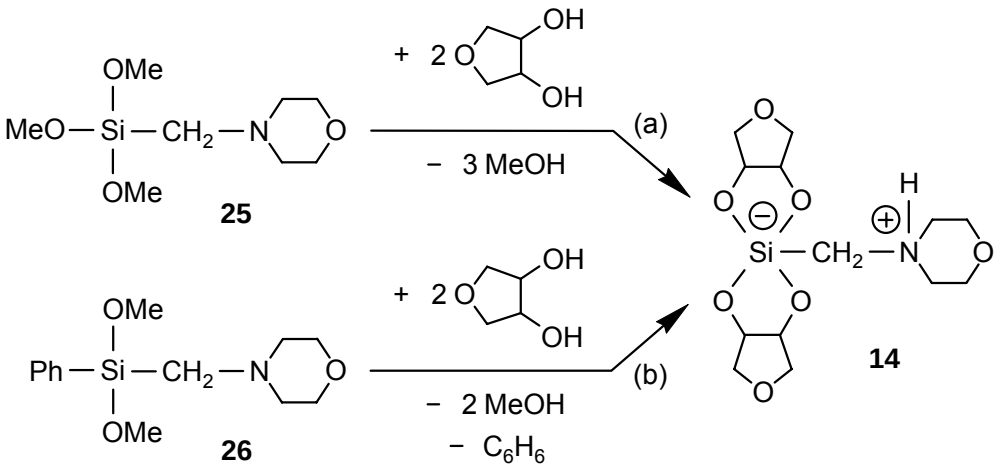

Scheme 8

The zwitterionic λ⁵*Si*-silicate **15**·$C_4H_8O_3$ ($C_4H_8O_3$ = *meso*-3,4-oxolane-diol) was synthesized according to Scheme 9 by reaction of [(*cis*-2,6-dimethylmorpholino)methyl]-trimethoxy silane (**29**) with two molar equivalents of *meso*-oxolane-3,4-diol in tetrahydrofuran/diethyl ether at 20 °C and was isolated in 72% yield as a colorless crystalline solid.

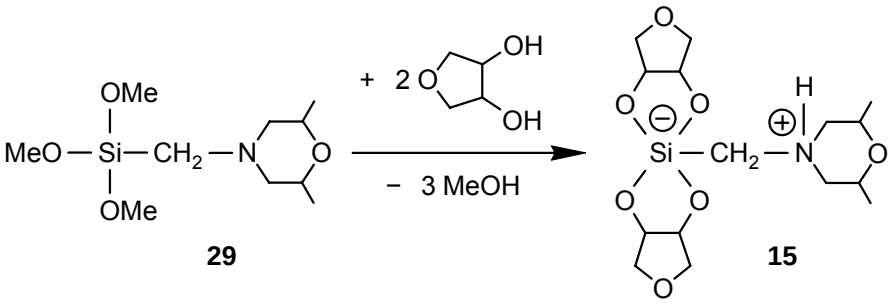

Scheme 9

The zwitterionic λ⁵*Si*-silicate **16** was prepared according to Scheme 10 by reaction of trimethoxy[(2,2,6,6-tetramethyl-piperidino)methyl]silane (**24**) with two molar equivalents of

meso-oxolane-3,4-diol in diethyl ether/*n*-pentane at 20 °C and isolated, after recrystallization from dichloromethane/diethyl ether, in 82% yield as a colorless crystalline solid.

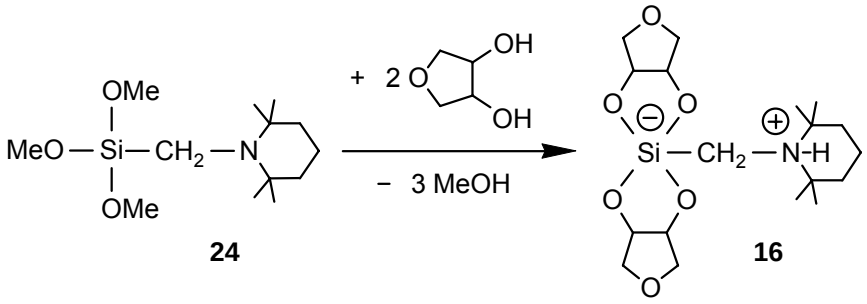

24 **16**

Scheme 10

The identities of **13**, **14**, **14**·H_2O, **15**·$C_4H_8O_3$, and **16** were established by elemental analyses (C, H, N), single-crystal X-ray diffraction studies (except for **13**), VACP/MAS NMR experiments (^{13}C, ^{15}N, ^{29}Si), and solution NMR studies (^{1}H, ^{13}C, ^{29}Si).

5.2 Crystal Structure Analyses of the λ⁵*Si*-[(Ammonio)methyl]-silicates 14–16

Compounds **14**, **14**·H_2O, **15**·$C_4H_8O_3$, and **16** were structurally characterized by single-crystal X-ray diffraction.[16] The crystal data and experimental parameters used for these studies are given in Appendix A (Table 29). For reason of comparison, selected bond distances and angles are listed in Table 16. Suitable single crystals of **14** could be obtained by crystallization from dichloromethane/diethyl ether/*n*-pentane (1:1:1 (v/v/v); addition of diethyl ether and *n*-pentane to a solution of **14** in dichloromethane at 20 °C). Suitable single crystals of **14**·H_2O could be obtained by crystallization from water (slow evaporation of the solvent at 20 °C over a period of two months; before starting the evaporation, a pH value of pH 7 was adjusted by addition of concentrated hydrochloric acid). The syntheses of compounds **15**·$C_4H_8O_3$ and **16** yielded directly well-crystallized products (see Chapter 10, Experimental Section). The crystals were mounted in inert oil (perfluoroalkyl ether, ABCR) on a glass fiber and then transferred to the cold nitrogen gas stream of the diffractometer (Stoe IPDS; graphite-monochromated MoKα radiation (λ = 0.71073 Å)). All structures were solved by direct methods.[17] A riding model was employed in the refinement[18] of the C*H* hydrogen atoms, whereas the N*H* and O*H* hydrogen atoms were localized in difference Fourier syntheses and refined freely. The investigations of **14** and **16** were complicated by twinning and partial disorder.[31] All bond lengths and angles which are not discussed explicitly in the following sections are in the expected range and therefore do not need further discussion.

The chiral λ^5*Si*-silicates **14**–**16** crystallize in the space groups $P2_1/c$ (**14** and **16**), *Cc* (**14**·H_2O), and $P2_1/n$ (**15**·$C_4H_8O_3$), respectively, and thus their crystals contain equal amounts of the respective (*Λ*)- and (*Δ*)-enantiomers. The asymmetric units contain one zwitterion in the case of **14**, and one zwitterion and one water molecule in the case of **14**·H_2O. As can be seen from Figures 35 and 36 and Table 16, the molecular structures of **14** and **14**·H_2O are very similar. The asymmetric unit of **15**·$C_4H_8O_3$ contains one zwitterion and one *meso*-oxolane-3,4-diol molecule. The molecular structure of **15** is depicted in Figure 37. As can be seen from Figure 38 and Table 16, compound **16** contains three crystallographically independent zwitterions in the unit cell (*Molecules I*, *II*, and *III*), with very similar structures.

The Si-coordination polyhedron of **15**·$C_4H_8O_3$ is a strongly distorted square pyramid, whereas the Si-coordination polyhedra of **14**, **14**·H_2O, and of the three crystallographically independent zwitterions of **16** are slightly distorted trigonal bipyramids (transition trigonal bipyramid → square pyramid:[32,33] **14**, 26.8%; **14**·H_2O, 49.0%; **15**·$C_4H_8O_3$, 52.8%; **16** (*Molecule I*), 4.3%; **16** (*Molecule II*), 4.4%; **16** (*Molecule III*), 5.3%). Obviously, the energy difference between a trigonal-bipyramidal and a square-pyramidal Si-coordination polyhedron of these compounds is rather small, and, hence, their structure can be easily influenced by intra- and intermolecular hydrogen bonds in the crystal. This finding is in accordance with the small energy difference calculated for the respective conformers of the model species **II** (see Computational Studies).

The Si–O distances of the *Si*O_4C skeletons range from 1.6782(9) Å to 1.7950(9) Å, the axial Si–O bonds (1.7333(12)–1.7950(9) Å) being significantly longer than the equatorial ones 1.6782(9)–1.7114(11) (Å). The Si–C distances range from 1.9120(16) Å (**15**·$C_4H_8O_3$) to 1.9259(13) Å (**16**).

Taking into account the relative orientation of the oxolane ring and the (ammonio)methyl ligand, *syn*/*anti* geometry was observed in the crystals of compounds **14**, **14**·H_2O, and **16**, and *syn*/*syn* geometry in the crystal of compound **15**·$C_4H_8O_3$.

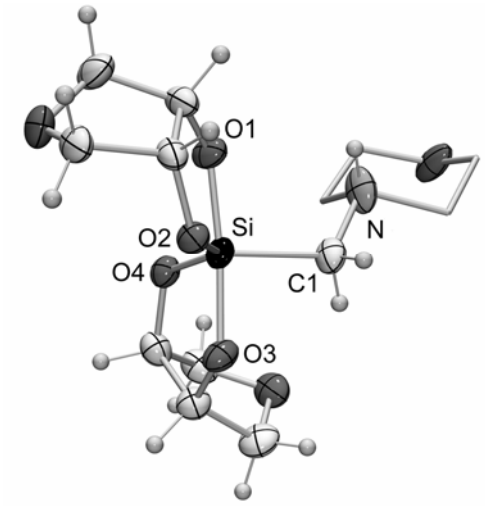

Figure 35. Molecular structure of **14** ((*Δ*)-enantiomer) in the crystal (probability level of displacement ellipsoids 50%; CH_2 moieties of the morpholinio group represented as stick model for clarity).

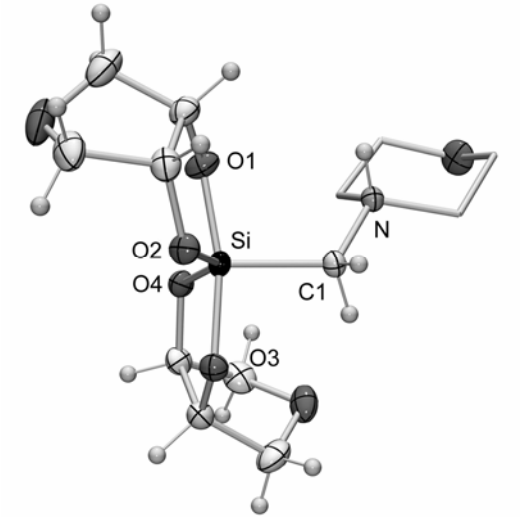

Figure 36. Molecular structure of **14** in the crystal of **14**·H_2O ((*Δ*)-enantiomer) (probability level of displacement ellipsoids 50%; CH_2 moieties of morpholinio group represented as stick model for clarity).

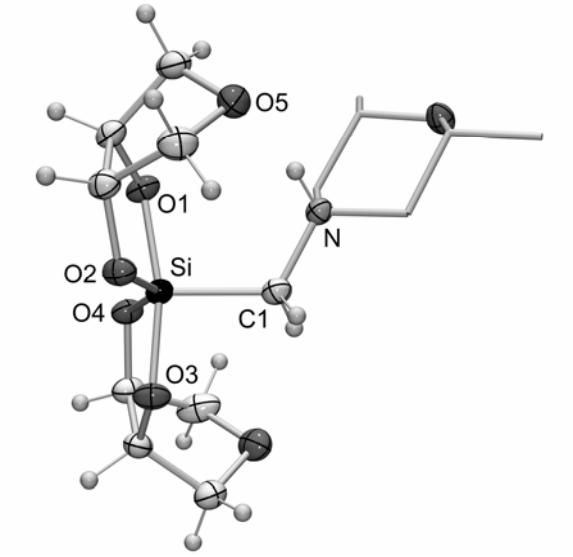

Figure 37. Molecular structure of **15**·$C_4H_8O_3$ ((*Δ*)-enantiomer) in the crystal (probability level of displacement ellipsoids 50%; $CH_2CH(CH_3)$ moieties of the *cis*-2,6-dimethyl-morpholinio group represented as stick model for clarity).

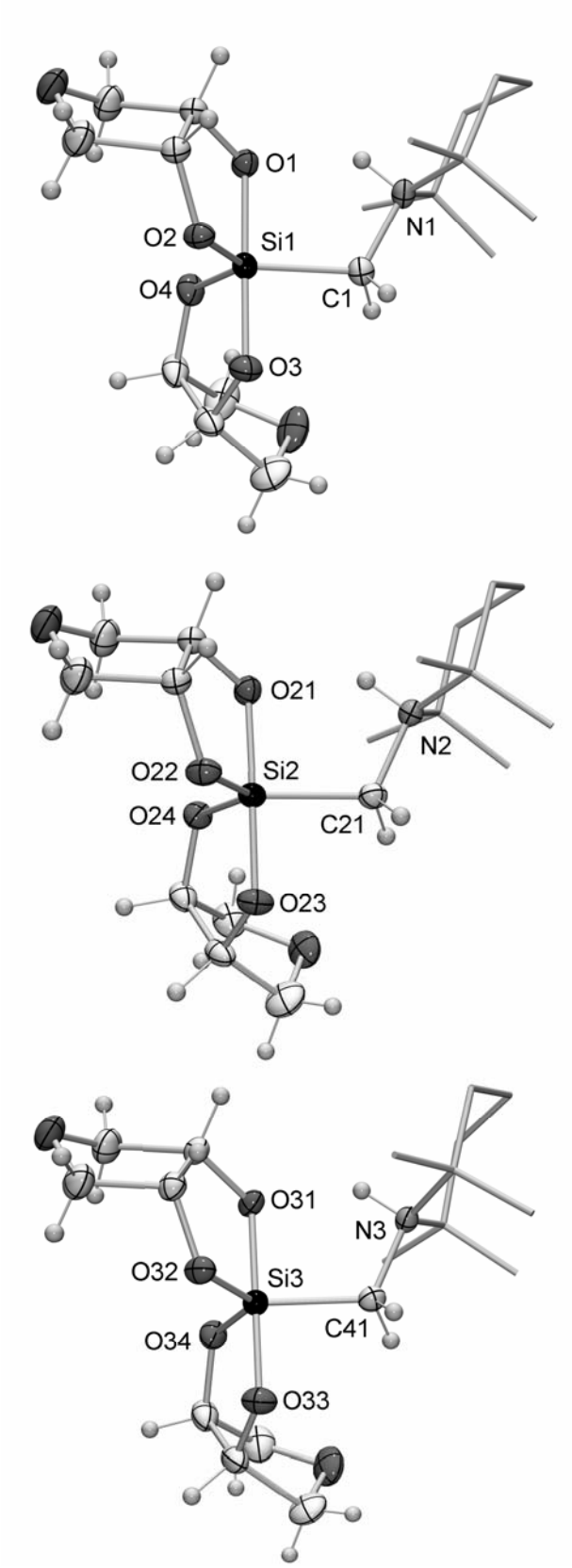

Figure 38. Molecular structures of the three crystallographically independent zwitterions ((*Δ*)-enantiomers) in the crystal of **16** (*Molecules I*, *II*, and *III*; probability level of displacement ellipsoids 50%; CH_2 and $C(CH_3)_2$ moieties of the tetramethylpiperidinio groups represented as stick models for clarity).

Table 16. Selected Interatomic Distances (Å) and Angles (deg) for **14**, **14**·H_2O, **15**·$C_4H_8O_3$, and **16**

	14	**14**·H_2O	**15**·$C_4H_8O_3$	**16**		
				Molecule I[a]	*Molecule II*[b]	*Molecule III*[c]
Si–O1	1.739(2)	1.7333(12)	1.7653(11)	1.7847(9)	1.7932(9)	1.7950(9)
Si–O2	1.702(2)	1.7114(11)	1.6926(12)	1.6873(9)	1.6825(9)	1.6844(9)
Si–O3	1.758(2)	1.7528(11)	1.7353(11)	1.7377(10)	1.7375(9)	1.7360(10)
Si–O4	1.682(2)	1.7007(11)	1.7103(11)	1.6803(10)	1.6782(9)	1.6810(10)
Si–C1	1.913(3)	1.9168(14)	1.9120(16)	1.9199(13)	1.9259(13)	1.9239(13)
O1–Si–O2	89.05(10)	89.01(5)	88.44(5)	88.86(4)	88.76(4)	88.58(4)
O1–Si–O3	172.98(10)	166.88(5)	166.84(6)	178.67(5)	178.96(5)	179.14(5)
O1–Si–O4	90.63(11)	87.96(5)	85.79(5)	90.09(5)	89.65(4)	89.61(5)
O1–Si–C1	95.17(13)	99.27(6)	99.33(6)	91.02(5)	90.85(5)	90.90(5)
O2–Si–O3	85.51(10)	84.85(5)	87.97(5)	90.25(5)	90.32(4)	90.59(5)
O2–Si–O4	130.78(10)	137.66(5)	139.55(6)	121.77(5)	121.99(5)	122.81(5)
O2–Si–C1	116.84(13)	111.59(6)	109.74(6)	120.93(5)	120.54(5)	119.99(5)
O3–Si–O4	89.57(10)	88.79(5)	88.75(5)	91.22(5)	91.24(5)	91.01(5)
O3–Si–C1	91.26(13)	93.78(6)	93.80(6)	88.59(5)	89.21(5)	89.33(5)
O4–Si–C1	112.20(12)	110.58(6)	110.70(6)	117.30(5)	117.46(5)	117.19(5)

[a]Atoms of *Molecule I*: Si1, O1, O2, O3, O4, and C1. [b]Atoms of *Molecule II*: Si2, O21, O22, O23, O24, and C22. [c]Atoms of *Molecule III*: Si3, O31, O32, O33, O34, and C41.

As expected from the presence of the potential NH donor functions and the potential oxygen acceptor atoms, hydrogen-bonding systems were observed in the crystals of **14**–**16** (Table 17, Figures 39–41).[19]

Compound **14** forms a trifurcate N–H···O1/O2/O3 hydrogen bond, with one intramolecular and two intermolecular interactions, leading to the formation of infinite one-dimensional chains along the [0 0 1] base vector (Figure 39).

The zwitterion of **14**·H_2O forms a bifurcate intermolecular N–H···O2/O3 hydrogen bond, leading to the formation of infinite one-dimensional chains along the [0 0 1] base vector.The water molecule is also involved in the hydrogen-bonding system, with intermolecular O8–H1···O4 and O8–H2···O5 interactions between the water molecule and the zwitterion (Figure 40).

The zwitterion of **15**·$C_4H_8O_3$ forms an intramolecular N–H···O5 hydrogen bond, and an additional *meso*-oxolane-3,4-diol molecule is also involved in the hydrogen-bonding system, with one intermolecular O8–H···O4 interaction and one bifurcate O9–H···O1/O8 interaction (Figure 41).

In the case of the three crystallographically independent molecules of **16**, intramolecular N–H···O hydrogen bonds between the NH groups of the ammonium moieties and one of the four oxygen ligand atoms were observed. As a result of this interaction, the axial Si–O1 distances of the three zwitterions are significantly longer than the respective axial Si–O3 bond lengths.

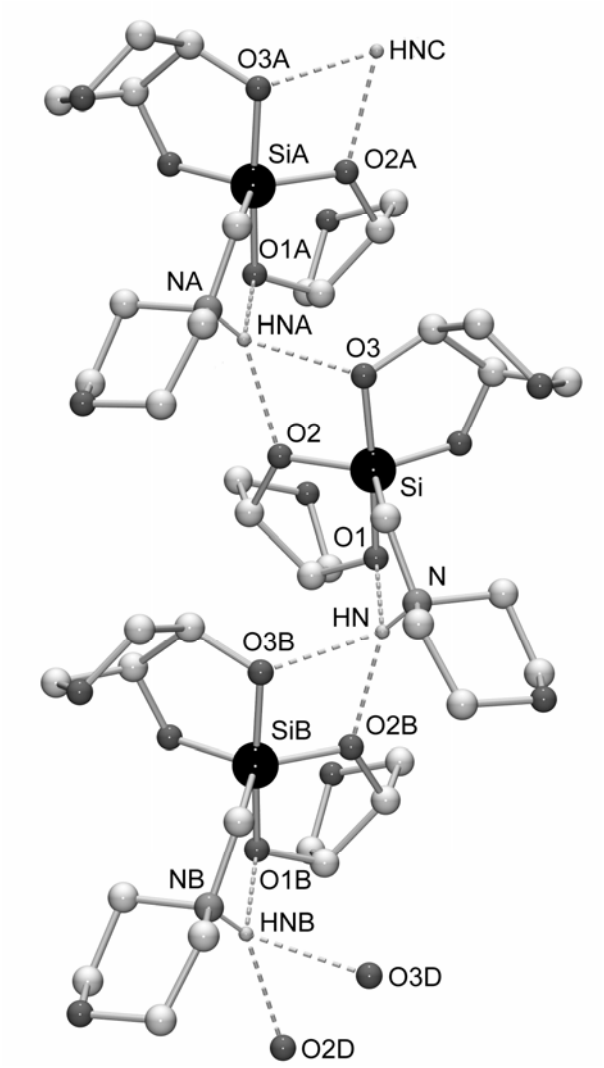

Figure 39. Hydrogen bonds in the crystal of **14** leading to infinite one-dimensional chains along the [0 0 1] base vector. The hydrogen atoms (except for that involved in hydrogen bonds) are omitted for clarity.

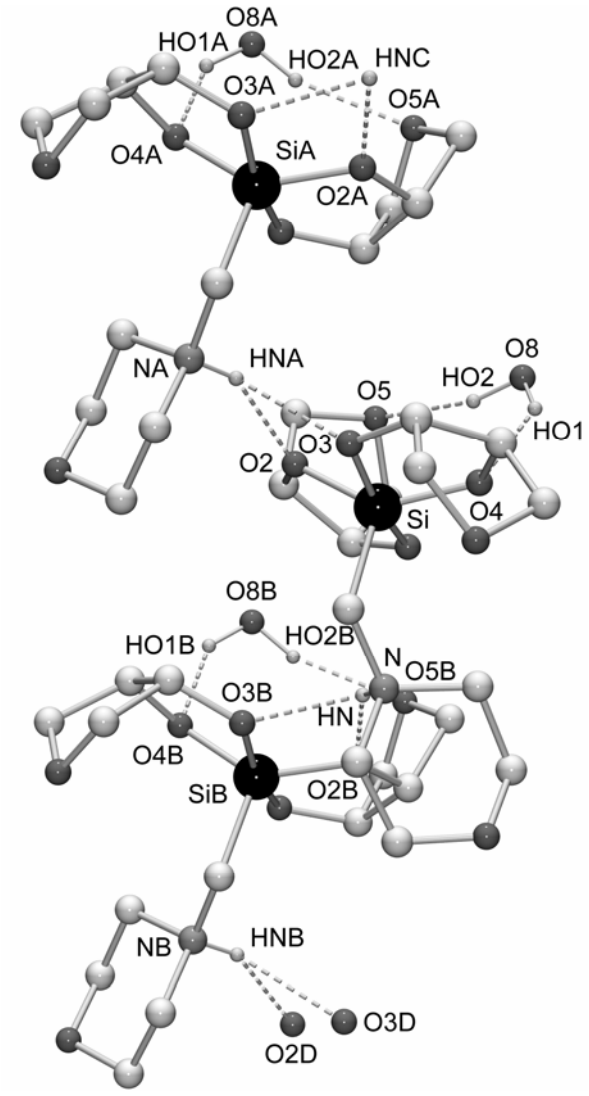

Figure 40. Hydrogen bonds in the crystal of **14**·H_2O leading to infinite one-dimensional chains along the [0 0 1] base vector. The hydrogen atoms (except for those involved in hydrogen bonds) are omitted for clarity.

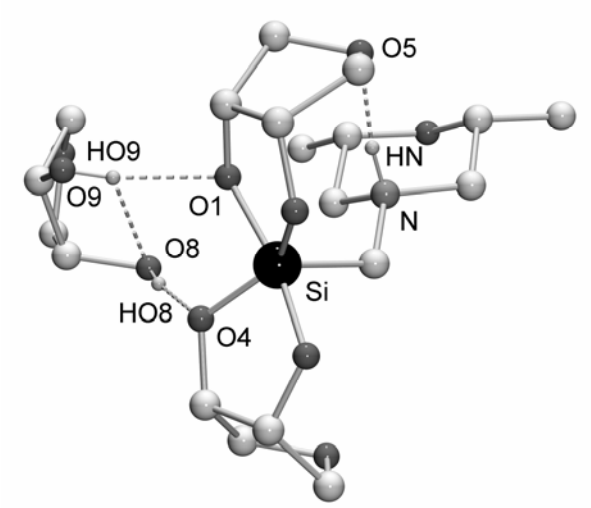

Figure 41. Hydrogen bonds in the crystal of **15**·$C_4H_8O_3$. The hydrogen atoms (except for those involved in hydrogen bonds) are omitted for clarity.

Table 17. Hydrogen-Bonding Geometries for **14**, **14**·H_2O, **15**·$C_4H_8O_3$, and **16**[a]

	D–H···A	D–H (Å)	H···A (Å)	D···A (Å)	D–H···A (deg)
14	N–H···O1[b]	0.85(4)	2.51(4)	2.828(5)	103(3)
	N–H···O2	0.85(4)	2.26(4)	3.024(4)	149(3)
	N–H···O3	0.85(4)	2.19(4)	2.844(4)	133(4)
14·H_2O	N–H···O2[c]	0.926(19)	2.285(19)	3.1244(15)	150.4(16)
	N–H···O3	0.926(19)	2.170(18)	2.8803(16)	132.8(17)
	O8–H1···O4	0.95(3)	2.10(3)	2.913(2)	142(3)
	O8–H2···O5	0.96(3)	2.10(3)	3.007(2)	158(4)
15·$C_4H_8O_3$	N–H···O5	0.889(18)	2.084(18)	2.9387(18)	161(17)
	O8–H···O4	1.08(2)	1.66(2)	2.7189(17)	167(2)
	O9–H···O1[d]	1.00(3)	1.85(3)	2.7822(17)	154(2)
	O9–H···O8	1.00(3)	2.42(3)	2.873(2)	106.8(18)
16	N1–H1···O1[e]	0.889(17)	1.938(16)	2.6718(15)	138.8(13)
	N2–H2···O21[f]	0.887(18)	1.888(17)	2.6317(14)	140.1(14)
	N3–H3···O31[g]	0.912 (17)	1.865(16)	2.6261(14)	139.5(14)

[a]Data calculated by using the program PLATON.[19] [b]Trifurcate N–H···O1/O2/O3 interaction; O1···H···O2 = 94.0(15) deg, O1···H···O3 = 104.5(15) deg, O2···H···O3 = 63.7(10) deg. [c]Bifurcate N–H···O2/O3 interaction; O2···H···O3 = 63.2(5) deg. [d]Bifurcate O9–H···O1/O8 interaction; O1···H···O8 = 98.5(12) deg. [e]*Molecule I*. [f]*Molecule II*. [g]*Molecule III*.

5.3 NMR Studies of the λ⁵*Si*-[(Ammonio)methyl]silicates 13–16

5.3.1 NMR Studies of the λ⁵*Si*-[(Ammonio)methyl]silicates 13–16 in the Solid State

The zwitterionic λ⁵*Si*-silicates **13**, **14**, **14**·H_2O, **15**·$C_4H_8O_3$, and **16** were characterized at 22 °C by solid-state VACP/MAS NMR spectroscopy (^{13}C, ^{15}N, ^{29}Si; see Experimental Section). The spectra obtained were compatible with the crystal structures of these compounds; however, it should be mentioned that the solid-state NMR studies of **16** at 22 °C revealed the existence of only one type of zwitterion in the crystal, whereas the crystal structure analysis at –100 °C revealed the existence of three zwitterions (with very similar structures) in the asymmetric unit. The isotropic ^{29}Si chemical shifts of **13**, **14**, **14**·H_2O, **15**·$C_4H_8O_3$, and **16** obtained in the solid-state VACP/MAS NMR experiments clearly characterize the sharp ^{29}Si resonance signals (full width at half height ca. 7.5–20 Hz) as arising from pentacoordinate silicon atoms (Table 18). It is interesting to note that in the case of **13** the $^1J_{NC}$ coupling could be resolved in the ^{13}C VACP/MAS NMR spectrum.

Table 18. ^{29}Si VACP/MAS NMR Data for **13**, **14**, **14**·H_2O, **15**·$C_4H_8O_3$, and **16** in the Crystal (Spectra Recorded at 22 °C; Chemical Shifts in ppm)

13	–87.0	**15**·$C_4H_8O_3$	–90.1
14, **14**·H_2O	–87.5	**16**	–85.0

5.3.2 NMR Studies of the λ⁵*Si*-[(Ammonio)methyl]silicates 13–16 in Dichloromethane (CD_2Cl_2)

As can be seen from Table 19, the ^{29}Si chemical shifts in solution (CD_2Cl_2) are very similar to those determined in the solid state (Table 18). The ^1H and ^{13}C solution-state NMR data are also compatible with the zwitterionic structures of **13**–**16** (see Experimental Section). Furthermore, $^1H,^1H$ COSY NMR experiments (solvent, CD_2Cl_2) gave evidence for a coupling of the $SiCH_2N$ protons with the NH proton and thus unequivocally indicate the presence of an ammonium group (^1H chemical shifts of the $SiCH_2NH$ protons, δ 7.6–8.1 ppm). Thus, these NMR experiments clearly demonstrate that the zwitterions **13**–**16** exist in solution as well (for further details, see Chapter 10, Experimental Section). As the trigonal-bipyramidal structure is

the energetically most favorable one (see Crystal Structure Analyses and Computational Studies), it is to be supposed that this particular structure is also dominant in solution.

Table 19. ^{29}Si NMR Data for **13**, **14**, **14**·H_2O, **15**·$C_4H_8O_3$, and **16** in Solution (Chemical Shifts in ppm; Spectra Recorded at 24 °C)

	δ (CD_2Cl_2)	δ (D_2O)
13	–89.4	–88.7, –88.2, –87.4
14, **14**·H_2O	–89.3, –89.2	–89.2, –88.7, –87.9
15·$C_4H_8O_3$	–89.3	–88.9, –88.5, –87.7
16	–86.1, –85.7, –85.3	–86.3, –86.1, –85.2

As can be seen from Table 19 and from the Experimental Section, a different stereochemistry of the zwitterionic λ^5*Si*-silicates **13**–**16** in aqueous and nonaqueous solutions was observed.

Upon dissolution of compounds **13** and **15**·$C_4H_8O_3$ in CD_2Cl_2 at 20 °C (**13**, *c* = 435 mM; **15**·$C_4H_8O_3$, *c* = 23 mM), the presence of only one species in solution was detected (one data set was observed in the NMR spectra of **13** and **15**·$C_4H_8O_3$).

Upon dissolution of compound **14** or **14**·H_2O in CD_2Cl_2 at 20 °C (**14**, *c* = 32 mM; **14**·H_2O, *c* = 475 mM), the presence of two NMR-spectroscopically distinguishable species in solution was observed (molar equilibrium ratio major isomer:minor isomer, 0.80:0.20).

However, upon dissolution of **16** in CD_2Cl_2 at 23 °C (*c* = 102 mM), an equilibrium mixture of the respective *syn*/*syn*, *syn*/*anti*, and *anti*/*anti* isomers was observed (three NMR-spectroscopically distinguishable species in solution), with the following molar equilibrium ratio: **16a**:**16b**:**16c**, 0.24:0.63:0.13. As can be seen from Figure 42, the partial ^{1}H,^{1}H COSY NMR spectrum (300.1 MHz, 23 °C, CD_2Cl_2) gave evidence for a coupling of the $SiCH_2N$ protons with the NH protons of the three isomeric zwitterionic structures of **16** in solution, and thus clearly indicate the presence of three ammonium groups.

This finding is in agreement with the results of ab initio studies of the related anionic model system bis[*meso*-oxolane-3,4-diolato(2–)]hydridosilicate(1–) **II** (see Chapter 5.4, Computational Studies of the Anionic Model System II).

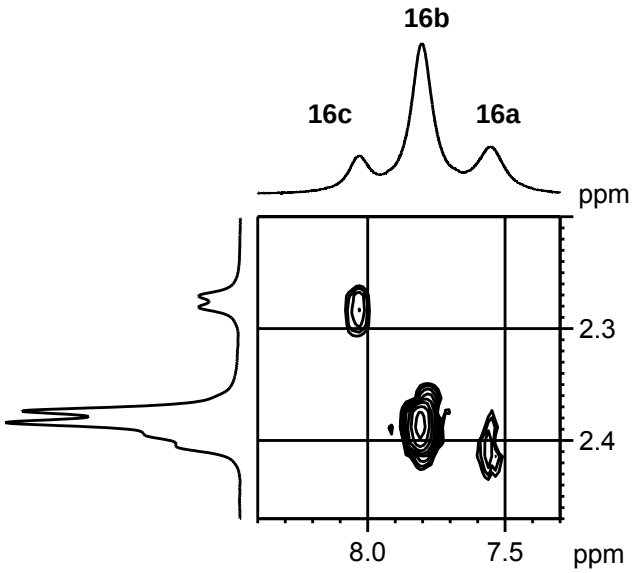

Figure 42. Partial $^{1}H,^{1}H$ COSY NMR spectrum (CD_2Cl_2, 23 °C, 300.1 MHz). *Top*: resonance signals of the NH ammonium protons of **16a**–**16c**. *Left*: resonance signals of the $SiCH_2N$ protons of **16a**–**16c**, respectively.

As the isomers **IIA**–**IIC** represent local minima with a maximum energy difference of only 5.8 kJ mol^{-1}, it is likely that the three isomers **16a–16c** observed in solution (solvent, CD_2Cl_2) correspond to the three isomeric structures **IIA**–**IIC**. As can be seen from Figure 57, the energetically preferred structures **IIA**–**IIC** differ only in the position of the two oxolane rings relative to the hydrido ligand (**IIA**, *syn*/*syn* isomer; **IIB**, *syn*/*anti* isomer; **IIC**, *anti*/*anti* isomer). In the case of **IIA** and **IIC** (C_2 symmetry), only one ^{1}H and one ^{13}C NMR resonance signal is expected for the CH moieties of the two oxolane rings, whereas in the case of **IIB** (C_1 symmetry) two resonance signals each are expected. The analysis of the ^{1}H and ^{13}C NMR data of the major isomer **16b** (supported by $^{1}H,^{1}H$, $^{13}C,^{1}H$, and $^{29}Si,^{1}H$ correlation experiments) clearly indicate that this particular isomer (observation of two separated ^{1}H and ^{13}C resonance signals for the CH moieties of the oxolane rings) corresponds to the model species **IIB**. For the isomers **16a** and **16c**, one single ^{1}H and one single ^{13}C NMR resonance signal was observed for the CH moieties of the oxolane rings. The assignment of the configuration of these isomers (correlation with the model species **IIA** and **IIB**) is based on the results of VT NMR experiments with **16** (see Chapter 5.3.4 VT ^{1}H NMR Studies) and ab initio studies of the model species **II** (see Chapter 5.4 Computational Studies).

As can be seen from the Experimental Section and Figure 43, two separate ^{1}H NMR resonance signals for the C*H* protons and two separate ^{13}C NMR resonance signals for the *C*H atoms of **16b** (solvent CD_2Cl_2) were observed (a representative partial $^{1}H,^{13}C$ HMQC NMR spectrum is depicted in Figure 43).

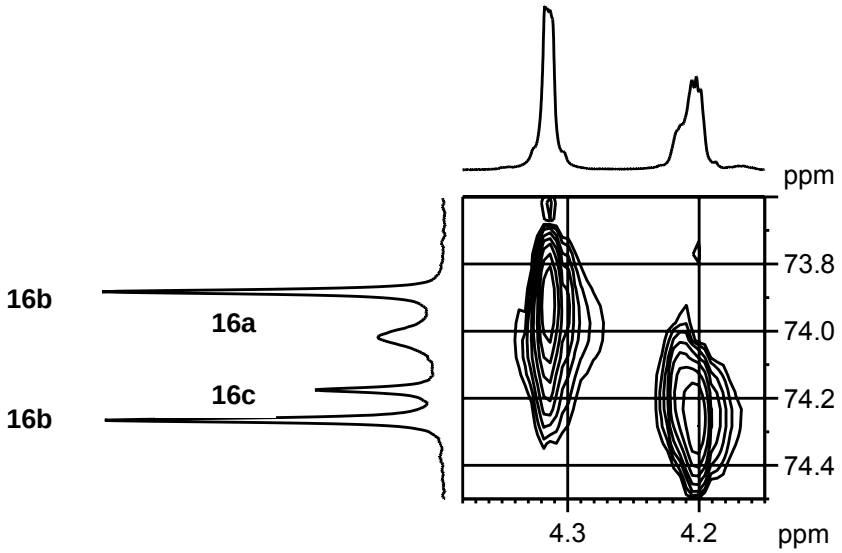

Figure 43. Partial $^{1}H,^{13}C$ HMQC NMR spectrum (CD_2Cl_2, 24 °C, 600.1 MHz). *Top*: resonance signals of the C*H* protons of **16a**–**16c**. *Left*: resonance signals of the *C*H atoms of **16a**–**16c**.

5.3.3 NMR Studies of the λ⁵*Si*-[(Ammonio)methyl]silicates 13–16 in Water (D_2O)

Upon dissolution of **13**, **14**, **14**·H_2O, **15**·$C_4H_8O_3$, and **16** in water (D_2O), an equilibrium mixture of the *syn*/*syn*, *syn*/*anti*, and *anti*/*anti* isomers of the zwitterionic λ⁵*Si*-silicates was observed (Table 19). Further species could not be detected, indicating that the two bidentate *meso*-oxolane-3,4-diolato(2–) ligands strongly stabilize the *Si*O_4C skeletons of these zwitterions against hydrolysis; i.e., in contrast to the hydrolytically sensitive compounds **1**–**12**, no decomposition was observed upon dissolution of the λ⁵*Si*-silicates **13**–**16** in water. This remarkable hydrolytic stability of the zwitterions **13**–**16** is emphasized by their direct synthesis in water using an NMR tube as the reaction vessel: Upon addition of the silanes **28**, **25**, **29**, or **24** to a solution of two molar equivalents of *meso*-oxolane-3,4-diol in D_2O, ^{1}H, ^{13}C, and ^{29}Si NMR spectra were measured and found to be identical with those obtained upon dissolution of **13**–**16** in D_2O. Figures 44–47 show representative partial spectra obtained in $^{29}Si,^{1}H$ HMQC experiments with **13**–**16** in D_2O, demonstrating the existence of the zwitterions.

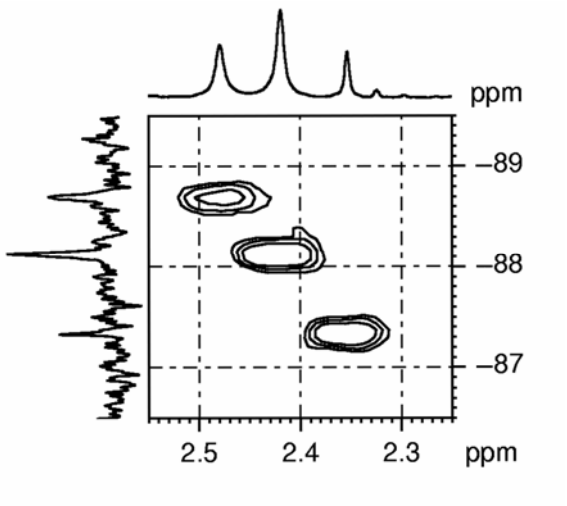

Figure 44. Partial spectrum obtained in a ^{29}Si,^{1}H HMQC experiment (23 °C, 300.1 MHz) with a 302 mM solution of **13** in water (D_2O) (pH 7.0 ± 0.1). Compound **13** was synthesized as described in the Experimental Section. *Top*: ^{1}H NMR resonance signals of the SiC*H*$_2$N protons of the three isomers of **13**. *Left*: ^{29}Si NMR signals of the three isomers of **13**.

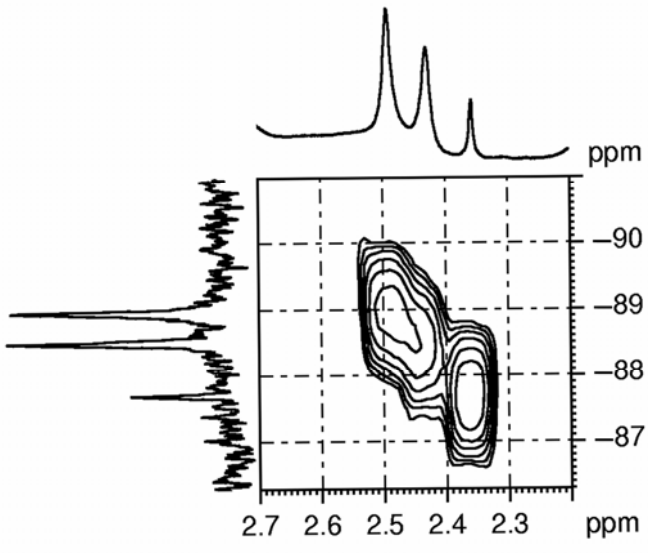

Figure 45. Partial spectrum obtained in a ^{29}Si,^{1}H HMQC experiment (23 °C, 300.1 MHz) with a 475 mM solution of **14** (pH 8.0 ± 0.1) synthesized directly in D_2O. The spectrum was measured 4 hours after combining the reactants in an NMR tube. *Top*: ^{1}H NMR resonance signals of the SiC*H*$_2$N protons of the three isomers of **14**. *Left*: ^{29}Si NMR signals of the three isomers of **14**.

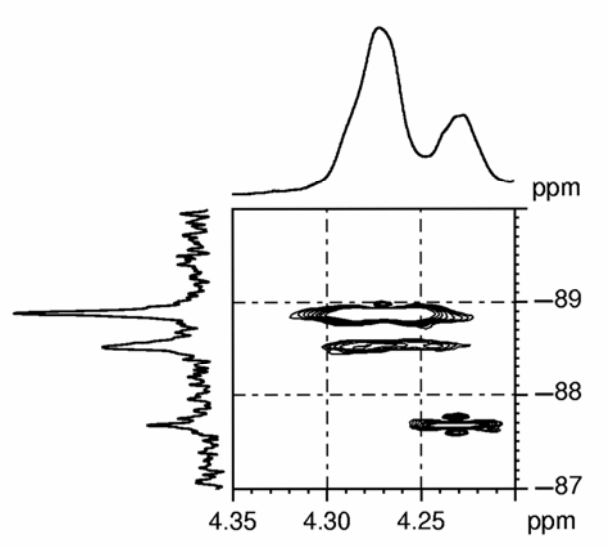

Figure 46. Partial spectrum obtained in a ^{29}Si,^{1}H HMQC experiment (23 °C, 300.1 MHz) with a 468 mM solution of **15** in water (D_2O) (pH 8.4 ± 0.1). Compound **15** was synthesized directly in D_2O; the spectrum was measured ca. 10 hours after combining the reactants in an NMR tube. *Top*: ^{1}H NMR resonance signals of the SiC*H*$_2$N protons of the three isomers of **15**. *Left*: ^{29}Si NMR resonance signals of the three isomers of **15**.

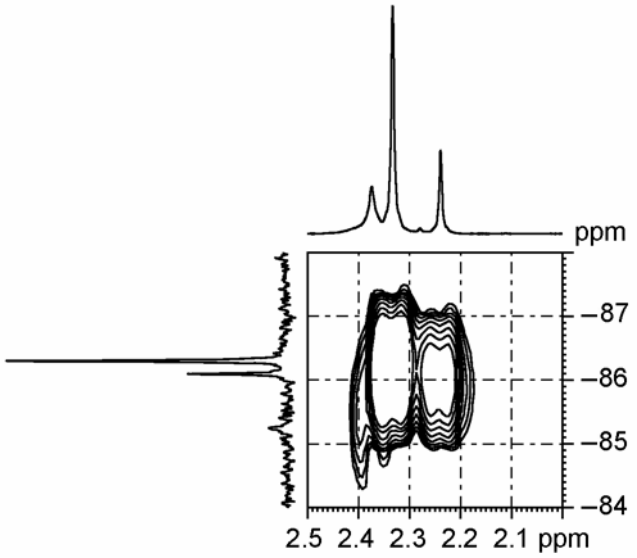

Figure 47. Partial spectrum obtained in a ^{29}Si,^{1}H HMQC experiment (23 °C, 300.1 MHz) with a 512 mM solution of **16** in water (D_2O) (pH 9.2 ± 0.1). Compound **16** was synthesized as described in the Experimental Section. *Top*: ^{1}H NMR resonance signals of the SiC*H*$_2$N protons of the three isomers of **16**. *Left*: ^{29}Si NMR resonance signals of the three isomers of **16**.

To get more information about the stability of compounds **13**–**16** in water, ^{1}H, ^{13}C, ^{29}Si NMR experiments were carried out at various pH values.

Upon dissolution of **13** in D_2O, a pH value of pH 8.9 was measured. This pH value was decreased stepwise by addition of small amounts of concentrated hydrochloric acid, and ^1H, ^{13}C, and ^{29}Si NMR experiments were performed at pH 8.9, pH 7.4, and pH 7.0. As can be seen from Figure 48, the resulting partial ^{29}Si NMR spectra indicate the existence of the three isomers of **13** in aqueous solution at all pH values studied (no tetracoordinate silicon species could be detected), clearly demonstrating the hydrolytic stability of **13** in the range pH 7.0–8.9.

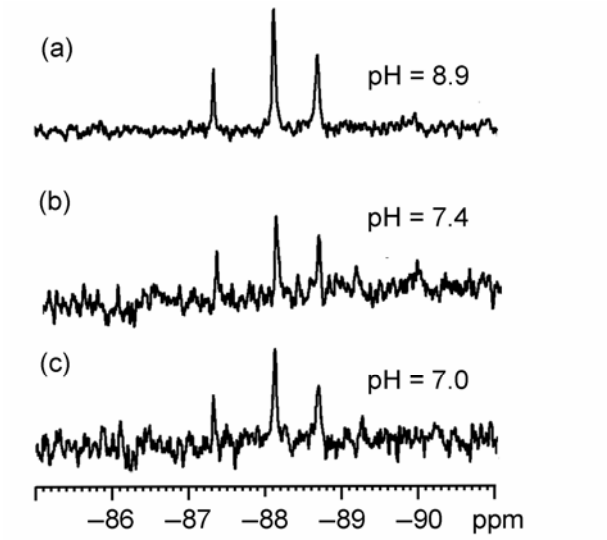

Figure 48. Partial spectra obtained in ^{29}Si NMR experiments (23 °C, 300.1 MHz) with 302 mM or 435mM solutions of **13** (synthesized according Scheme 1, method a) in D_2O at (a) pH 8.9 ± 0.1, (b) pH 7.4 ± 0.1, and (c) pH 7.0 ± 0.1. The ^{29}Si NMR spectrum obtained for a 435 mM aqueous solution (D_2O) of **13** synthesized directly in an NMR tube was identical with spectrum a.

Furthermore, ^1H, ^{13}C, and ^{29}Si NMR experiments with a 475 mM solution of **14** in D_2O were carried out at various pH values. Upon dissolution of **14** in D_2O, a value of pH 8.0 was measured. This pH value was decreased stepwise by addition of small amounts of concentrated hydrochloric acid, and ^1H, ^{13}C, and ^{29}Si NMR experiments were performed at pH 7.4 and pH 7.0. As can be seen from Figure 49, the resulting partial ^{29}Si NMR spectra indicate the existence of the three isomers of **14** in aqueous solution at all pH values studied (no tetracoordinate silicon species could be detected), clearly demonstrating the stability of the λ^5*Si*-silicate **14** in the range pH 7.0–8.0. The integrals extracted from the ^1H spectra indicated that the ratio of the three isomers of **14** does not significantly depend on the pH value. Upon further acidification to pH 6, partial hydrolysis of **14** was observed (formation of

tetracoordinate silicon species), and at pH 5, no ^{29}Si resonance signals for **14** could be detected at all (complete hydrolysis of **14**).

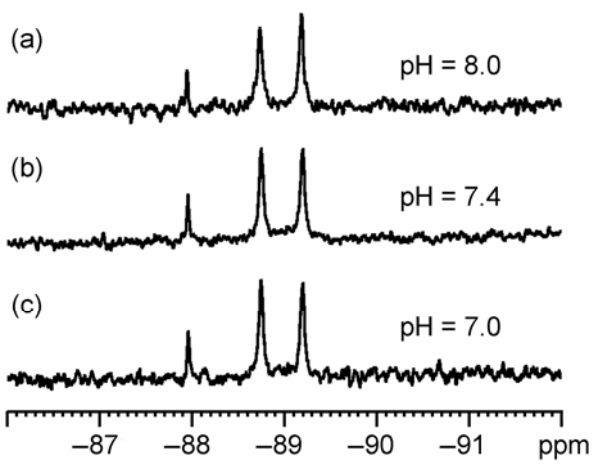

Figure 49. Partial spectra obtained in ^{29}Si NMR experiments (23 °C, 400.1 MHz) with 475 mM solutions of **14** (synthesized according Scheme 1, method a) in D_2O at (a) pH 8.0 ± 0.1, (b) pH 7.4 ± 0.1, and (c) pH 7.0 ± 0.1. The ^{29}Si NMR spectrum obtained for a 475 mM aqueous solution (D_2O) of **14** synthesized directly in an NMR tube was identical with spectrum a.

Upon dissolution of compound **15**·$C_4H_8O_3$ in D_2O, a value of pH 8.4 was measured. This pH value was decreased stepwise by addition of small amounts of concentrated hydrochloric acid, and ^{1}H, ^{13}C, and ^{29}Si NMR experiments were performed at pH 7.4 and pH 7.0. As can be seen from Figure 50, the resulting partial ^{29}Si NMR spectra indicate the existence of the three isomers of **15** in aqueous solution at all pH values studied (no tetracoordinate silicon species could be detected), clearly demonstrating the stability of the λ⁵*Si*-silicate **15** in the range pH 7.0–8.4.

Compound **16** was synthesized directly in an NMR tube, and the pH value was decreased stepwise by addition of small amounts of concentrated hydrochloric acid, and ^{1}H, ^{13}C, and ^{29}Si NMR experiments were performed at pH 7.4 and pH 7.0. As can be seen from Figure 51, the resulting partial ^{29}Si NMR spectra indicate the existence of the three isomers of **16** in aqueous solution at all pH values studied (no tetracoordinate silicon species could be detected), clearly demonstrating the stability of the λ⁵*Si*-silicate **16** in the range pH 7.0–9.2. Except for small differences in the chemical shifts due to the change of the solvent, the spectra of **16** recorded in D_2O were analogous to those obtained in CD_2Cl_2 or CD_3CN at room temperature, and indicate the presence of three isomers (**16a**, **16b**, **16c**) that correspond to the model species **IIA**, **IIB**, and **IIC**. The integrals extracted from the ^{1}H spectra indicated that the ratio of the three isomers of **16** does not significantly depend on the pH value.

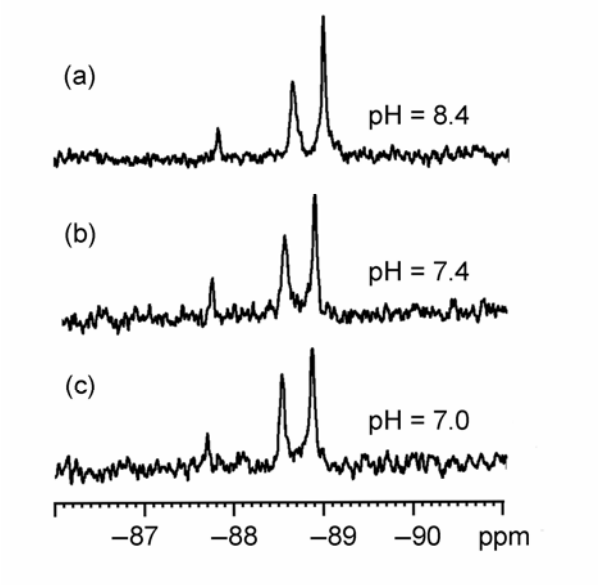

Figure 50. Partial spectra obtained in ^{29}Si NMR experiments (23 °C, 400.1 MHz) with 468 mM solutions of **15**·$C_4H_8O_3$ in water (D_2O) at (a) pH 8.4 ± 0.1, (b) pH 7.4 ± 0.1, and (c) pH 7.0 ± 0.1. Compound **15**·$C_4H_8O_3$ was synthesized as described in the Experimental Section; the pH values pH 7.4 and 7.0 were adjusted by addition of concentrated hydrochloric acid directly before starting the NMR measurements. The ^{29}Si NMR spectrum obtained for a 468 mM aqueous solution (D_2O) of **15** synthesized directly in an NMR tube was identical with spectrum a.

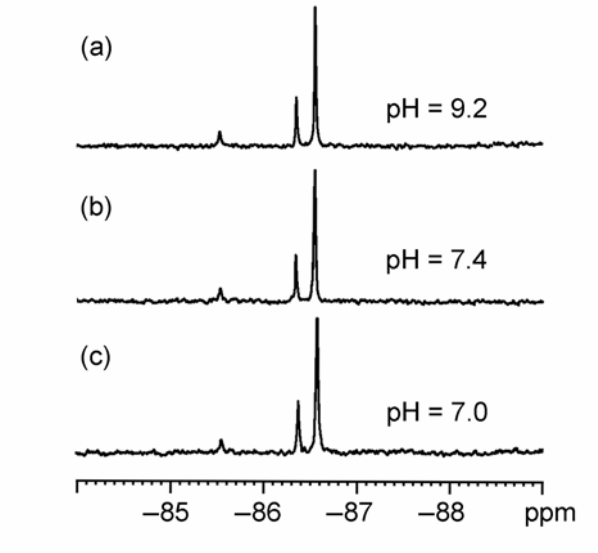

Figure 51. Partial spectra obtained in ^{29}Si NMR experiments (23 °C, 400.1 MHz) with 520 mM solutions of **16** (synthesized directly in D_2O). The spectra were measured ca. 12–14 hours after combining the reactants in an NMR tube. (a) pH 9.2 ± 0.1, (b) pH 7.4 ± 0.1, and (c) pH 7.0 ± 0.1. The ^{29}Si NMR spectrum obtained for a 512 mM aqueous solution (D_2O) of **16** synthesized as described in Experimental Section was identical with spectrum a.

As can be seen from Figures 48–51, an equilibrium mixture of the *syn*/*syn*, *syn*/*anti*, and *anti*/*anti* isomers of the zwitterionic λ^5*Si*-silicates of **13**–**16** could be detected in aqueous solution, clearly demonstrating the stability of these spirocyclic zwitterions in D_2O in the pH ranges 7.0–9.2. The aqueous solutions of **13**–**16** did not undergo gel formation (observation over two months (**13**, **15**, **16**), or six months (**14**).

The integrals extracted from the ^1H spectra measured in D_2O at pH = 8.9–7.0 (**13**), pH = 8.0–7.0 (**14**), pH = 8.4–7.0 (**15**), and pH = 9.2–7.0 (**16**) indicate that the ratio of the three isomers of **13**–**16** does not significantly depend on the pH value.

Due to partial overlapping of the indicative resonance signals for the CH moieties of the *meso*-oxolane-3,4-diolato(2–) ligands, the data extracted from the ^1H and ^{13}C NMR spectra of aqueous solutions (D_2O) of **13** and **14** did not allow an assignment of the configuration of the respective three isomers (correlation with the model species **IIa**–**IIc**). In the case of **16**, however, assignment of the configurations was possible. Except for small differences in the chemical shifts due to the change of the solvent, the spectra of **16** recorded in D_2O at 296 K were similar to those obtained in CD_2Cl_2 and CD_3CN, and, hence, the assignment of the configurations of the three isomers **16a**–**16c** in aqueous solution were performed analogously to the assignment in the organic solvents (see Chapter 5.3.2).

At the first glance, the basic reaction upon dissolution of **13**–**16** in water is quite surprising, because the ammonium groups of these zwitterions should lead to an acidic reaction. However, the basic reaction of **13**–**16** in water might be explained by a hydrolytic Si–OC cleavage of the zwitterions to give the tetracoordinate silicon species **13'**–**16'** and hydroxide ions; i.e., one could speculate about equilibria of the type **13** ⇄ **13'**, **14** ⇄ **14'**, **15** ⇄ **15'**, and **16** ⇄ **16'**. However, as can be seen from the pH values measured, these equilibria should lie far to the left, and, hence, the detection of **13'**–**16'** by NMR spectroscopy should not be possible (see Scheme below).

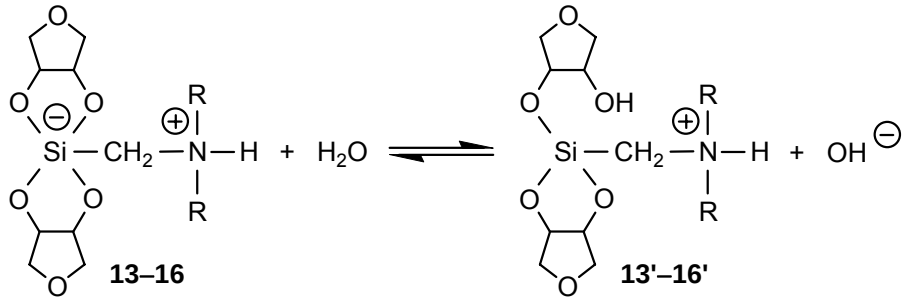

	13, 13'	14, 14'	15, 15'	16, 16'
NR_2	NMe_2	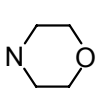	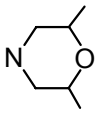	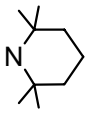

The hydrolytic stability of **13**–**16** in the pH ranges studied is quite remarkable, but cannot be satisfactorily explained so far. Taking into account that the related λ^5*Si*-silicates **7**–**12** decompose upon dissolution in water, special structural and/or electronic features of the *meso*-oxolane-3,4-diolato(2–) ligand have to be considered to explain this hydrolytic stability. This particular ligand and related ligands that derive from carbohydrates with *cis*-furanoidic diol moieties have already been reported to form anionic pentacoordinate silicon species in aqueous solution;[30] however, these anionic λ^5*Si*-silicates are only stable in strongly alkaline solutions. Thus, it is likely that the zwitterionic nature of **13**–**16** (i.e., the presence of the (ammonio)methyl group) also accounts for their hydrolytic stability.

Interestingly, the shape of the recipient (flat or spherical) where the aqueous solutions of compounds **13**–**16** were kept, influences the crystallization process (form of the crystals (needlelike or rosettelike); timeperiod for a quantitative crystallization (two days – one week)), i.e. the surface area acts like a template. For example, the crystals obtained by deposition of a saturated aqueous solution of **14** on a flat glass surface are depicted in Figure 52. The best results concerning the quality of the crystals and the yield were obtained using flat flasks.

Figure 52. Crystals of **14** obtained by crystallization on a flat glass surface.

The investigations presented here were carried out as part of our studies on higher-coordinate silicon (IV) complexes with chelate ligands derived from organic hydroxy compounds with respect to their potential role in silicon biochemistry.[34] Taking into account all these findings, it is an open question whether λ⁵*Si*-silicates with bidentate ligands derived from *meso*-oxolane-3,4-diol and related diols may play a role for transport and storage of silicon in biological systems.

5.3.4 VT ^{1}H NMR Studies with the λ⁵*Si*-[(Ammonio)methyl]silicates 14 and 16

To get more information about the isomerism at the silicon center of compounds **13**–**16** in solution, variable temperature ^{1}H NMR experiments with **14** and **16** were performed.

Compound **14** was studied by VT ^{1}H NMR experiments at 300.1 MHz in the temperature range 178–296 K using CD_2Cl_2 as a solvent (c = 28 mM). The occurrence of two ^{1}H resonance signals corresponding to the $SiCH_2N$ protons and two ^{1}H resonance signals corresponding to the protons of the NH moieties of the zwitterion clearly indicate the existence of two isomers in the temperature range studied. Furthermore, ^{1}H, ^{13}C, ^{29}Si NMR experiments, supported by ^{1}H,^{1}H COSY, ^{1}H,^{13}C HMQC, ^{1}H,^{13}C HMBC, and ^{1}H,^{29}Si HMQC NMR experiments at 193 K (300.1 MHz, CD_2Cl_2) clearly demonstrated the presence of two isomers of **14** in solution at this particular temperature. A representative partial spectrum obtained in a ^{1}H,^{1}H COSY NMR experiment (300.1 MHz, 193 K) is depicted in Figure 53.

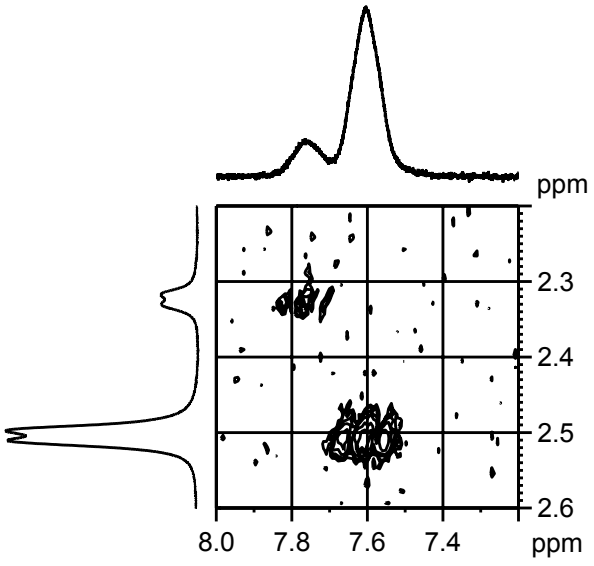

Figure 53. Partial spectrum obtained in a ^{1}H,^{1}H COSY NMR experiment (193 K, 300.1 MHz) with a 28 mM solution of **14** in CD_2Cl_2. *Top*: resonance signals of the NH protons. *Left*: resonance signals of the $SiCH_2N$ protons.

Compound **16** was also studied by VT ^{1}H NMR experiments at 300.1 MHz in the temperature range 233–343 K (solvent, CD_3CN), 296–393 K (solvent, [D_6]DMSO), and 190–298 K (solvent, CD_2Cl_2).

As can be seen from Figure 54, the partial ^{1}H NMR spectra of **16** in CD_3CN (c = 102 mM) clearly indicate the presence of three isomers in solution (molar ratio: **16a**:**16b**:**16c**, 0.17:0.75:0.08; integrals extracted from the ^{1}H spectrum measured at 296 K). The ^{1}H NMR spectra of solutions of **16** in CD_3CN and CD_2Cl_2 at 296 K are very similar, and, hence, the configurations of the three isomers **16a**–**16c** in these solutions can be assigned in the same manner.

Upon cooling of solutions of **16** in CD_3CN below 296 K, splitting of the SiCH_2N signals of all three isomers (coupling with the ammonium proton, $^3J_{HH}$ = 3.1–3.3 Hz) was observed. As can be seen from Figure 54, separate resonance signals for the two diastereotopic $SiCH_2N$ protons of the (*Λ*)- and (*Δ*)-enantiomers of **16a**–**16c** could not be observed in the temperature range studied. Instead of three $SiCH_AH_BNH_X$ spin systems, three $SiC(H_A)_2NH_X$ spin systems were observed, indicating that the enantiomers of **16a**–**16c** are not configurationally stable on the NMR time scale in the temperature range studied. This finding is in agreement with the results of ab initio studies of the model system **II** (see Chapter 5.4, Computational Studies): The energies of the Berry-type transition states **IID**–**IIF** that allow a (*Λ*)/(*Δ*)-enantiomerization of the enantiomers of the respective isomers **IIA**–**IIC** are very low (maximum energy barrier 11.3 kJ mol^{-1}).

At ca. 296 K, coalescence of the $SiCH_2N$ signals of **16a** and **16b** was observed, followed by another coalescence phenomenon upon further heating to 318 K. Based on the results of ab initio studies of the model system **II**, these coalescence phenomena can be interpreted in terms of isomerization processes of the types **16a** ⇄ **16b** and **16b** ⇄ **16c** (see Chapter 5.4, Computational Studies). As determined by line-shape analysis, the activation free enthalpies for these isomerization processes amount to 65 ± 3 kJ mol^{-1} (**16a** ⇄ **16b**) and 66 ± 2 kJ mol^{-1} (**16b** ⇄ **16c**).[35] These activation barriers are very similar to the calculated energy differences between the model species **IIA** and **IIB** (59.0 kJ mol^{-1}) and **IIB** and **IIC** (63.5 kJ mol^{-1}) and, hence, support the interpretation of the coalescence phenomena in terms of “twist”-type isomerization processes via transition states related to the model species **IIG** and **IIH** (see Chapter 5.4, Computational Studies).

The dynamic behavior of the isomers of **16** in solution was further studied by VT ^{1}H NMR experiments in the temperature range 296–393 K using [D_6]DMSO as the solvent. The ^{1}H spectrum measured at 296 K is similar to those obtained for solutions in CD_3CN or CD_2Cl_2

at the same temperature, again demonstrating the existence of the three isomers **16a**–**16c** in solution (molar ratio: **16a**:**16b**:**16c**, 0.18:0.67:0.15; integrals extracted from the ^{1}H spectrum measured at 296 K). As can be seen from Figure 55, coalescence points were observed at ca. 296 K and ca. 316 K, the coalescence temperatures being almost identical with those obtained for solutions of **16** in CD_3CN.

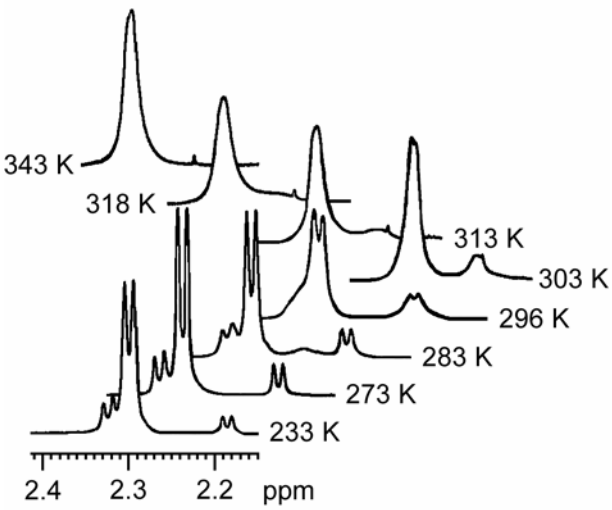

Figure 54. Partial ^{1}H NMR spectra (resonance signals of the SiCH_2N protons) of **16** in CD_3CN (c = 55 mM) as a function of temperature in the range 233–343 K (300.1 MHz).

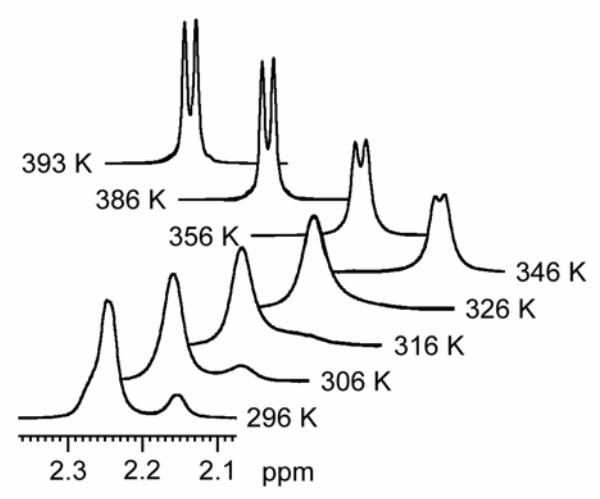

Figure 55. Partial ^{1}H NMR spectra (resonance signals of the SiCH_2N protons) of **16** in [D_6]DMSO (c = 80 mM) as a function of temperature in the range 296–393 K (300.1 MHz).

Upon further heating to 393 K, splitting of the broad resonance signal for the $SiCH_2N$ group into a dublett ($^3J_{HH}$ = 3.2 Hz) was observed, indicating that all three isomers are not configurationally stable on the NMR time scale at this temperature.

As the three isomers **16a**–**16c** found in the solution of **16** represent no coalescence states at room temperature (no other species appeared in the solution of **16** upon cooling to 233 K), the VT ^{1}H NMR experiments at 300.1 MHz support the assignment of the three isomers **16a**–**16c** to the three calculated local minima **IIA**–**IIC**.

Further VT ^{1}H NMR experiments were performed with a solution of **16** in CD_2Cl_2 in the temperature range 190–298 K. The ^{1}H NMR spectrum did not change significantly upon cooling from 298 K to 190 K (no change from the $SiC(H_A)NH_X$ spin systems to $SiCH_AH_BNH_X$ spin systems; no significant change of the NH resonance signals), indicating that the respective (*Λ*)- and (*Δ*)-enantiomers of the three isomers **16a**–**16c** are not configurationally stable on the NMR time scale in the temperature range studied.

Representative partial NMR spectra obtained by these VT ^{1}H NMR experiments in the temperature range 190–298 K are depicted in Figure 56.

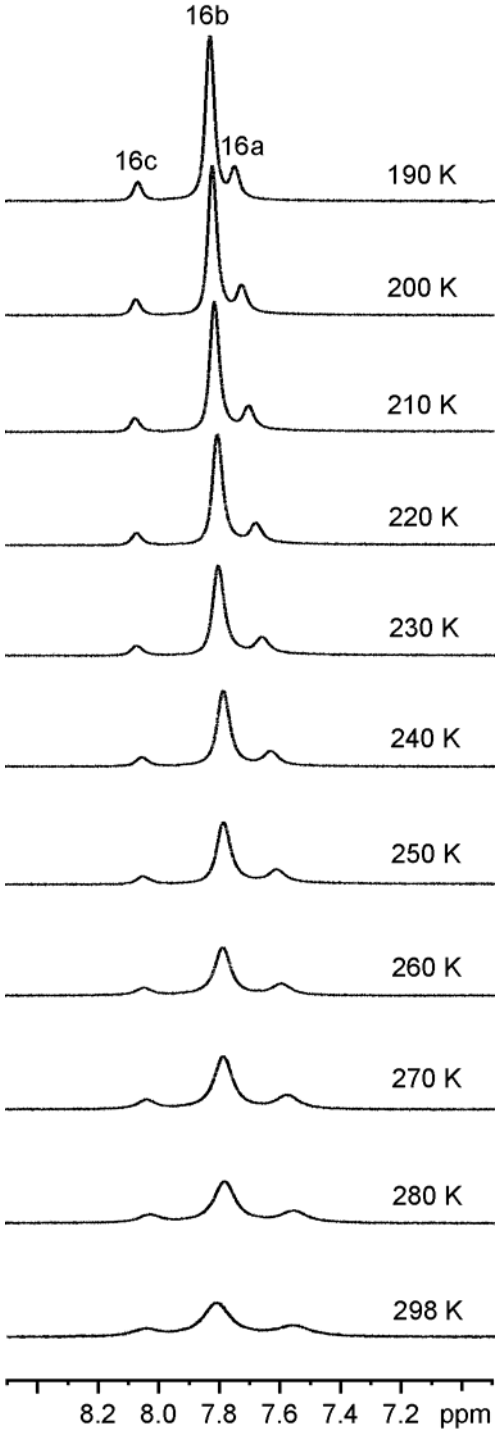

Figure 56. Partial ^{1}H NMR spectra (resonance signals of the N*H* ammonium protons) of **16** in CD_2Cl_2 (c = 45 mM) at 300.1 MHz as a function of temperature in the range 190–298 K (cooling from 298 K to 190 K).

5.4 Computational Studies of the Anionic Model System II

To get more information about the structure and dynamic behavior of the zwitterions **13**–**16** in solution, quantum-chemical investigations were performed.[24] For this purpose, computational studies of the anionic model species **II** (SCF/TZP+level) were carried out using the TURBOMOLE program system.[36a,b]

Critical points of the potential energy surface were characterized as local minima (zero imaginary frequencies) and saddle points (one imaginary frequency), respectively, by calculation of the vibrational frequencies. The relative energies given for **II** include the zero-point vibrational energy obtained by SCF calculations and the single-point MP2 energy. Transition states **IIG** and **IIH** were found using the module statpt implemented in TURBOMOLE. The TZP (triple-ζ plus polarization) basis set given in ref 36b is suitable to describe molecules with moderately polarized chemical bonds.

Earlier results of quantum-chemical studies of several related zwitterionic λ^5*Si*-silicates with an *Si*O$_4$C skeleton have already been reported elesewhere.[37]

As can be seen from Figure 57, eight different structures (**IIA**–**IIH**) were studied for the anionic model species **II**. For energetic reasons, square pyramids with the hydrogen atom in a basal position were not considered. Calculations of the vibrational frequencies demonstrated that the isomers **IIA** (*syn*/*syn*), **IIB** (*syn*/*anti*), and **IIC** (*anti*/*anti*) represent local minima, whereas **IID**–**IIH** are transition states (for selected geometric parameters for **IIA**–**IIH**, see Table 20). The three trigonal-bipyramidal minimum structures differ only slightly in their energy (maximum energy difference, 5.8 kJ mol^{-1}). The isomer **IIB** with the *syn*/*anti* geometry matches with the experimentally established structures of the Si-coordination polyhedra of **16** (*Molecules I–III*) in the crystal, whereas the experimentally established structure of the Si-coordination polyhedron of **15**·C$_4$H$_8$O$_3$ (*syn*/*syn* geometry) can be best described as a structure that lies on the Berry-pseudorotation coordinate between the trigonal-bipyramidal local minimum **IIA** and the square-pyramidal transition state **IID**. The energy barriers between the trigonal-bipyramidal local minimum **IIA** and the Berry-type square-pyramidal transition states **IID**–**IIF** are relatively small (maximum energy difference, 11.9 kJ mol^{-1}), which fits with the large range of distortions of the Si-coordination polyhedra of **15** and **16** observed in the crystal. The (*Λ*)- and (*Δ*)-enantiomers **IIA**–**IIC** can be converted into each other via the respective Berry-type transition states **IID**–**IIF** ((*Λ*)-**IIA** ⇄ **IID** ⇄ (*Δ*)-**IIA**, (*Λ*)-**IIB** ⇄ **IIE** ⇄ (*Δ*)-**IIB**, (*Λ*)-**IIC** ⇄ **IIF** ⇄ (*Δ*)-**IIC**). The calculated energies for the respective barriers amount to 11.3, 9.4 and 6.1 kJ mol^{-1}, respectively.

In addition to the Berry-type mechanism for the (*Λ*)/(*Δ*)-enantiomerization of **IIA**–**IIC**, there is a "twist"-type mechanism that allows the conversions (*Λ*)-**IIA** ⇄ (*Δ*)-**IIB** and (*Λ*)-**IIB** ⇄ (*Δ*)-**IIC** via the transition states **IIG** and **IIH**, respectively ((*Λ*)-**IIA** ⇄ **IIG** ⇄ (*Δ*)-**IIB**, (*Λ*)-**IIB** ⇄ **IIH** ⇄ (*Δ*)-**IIC**). A one-step mechanism for the direct isomerization **IIA** ⇄ **IIC** does not exist. The calculated energies for the "twist"-type barriers (59.0 and 63.5 kJ mol^{-1}) are significantly higher than the Berry-type barriers; i.e., an experimental separation of these two processes should be possible on the NMR time scale (in this context, see Chapter 5.3, VT ^{1}H NMR Studies).

Table 20. Selected Calculated Interatomic Distances (Å) and Angles (deg) for the Local Minima **IIA**–**IIC** and for the Transition States **IID**–**IIH** as Obtained by SCF/TZP+ Geometry Optimizations

	IIA	**IIB**	**IIC**	**IID**	**IIE**	**IIF**	**IIG**	**IIH**
Si–O1	1.755	1.758	1.761	1.726	1.726	1.726	1.783	1.742
Si–O2	1.699	1.695	1.695	1.726	1.726	1.726	1.718	1.718
Si–O3	1.755	1.757	1.761	1.726	1.727	1.726	1.703	1.702
Si–O4	1.699	1.699	1.695	1.726	1.727	1.726	1.699	1.704
Si–H	1.484	1.484	1.485	1.492	1.492	1.491	1.507	1.530
O1–Si–O2	88.4	88.5	88.4	87.3	87.4	87.4	85.0	86.2
O1–Si–O3	179.1	179.6	179.3	86.1	86.2	86.3	91.4	93.7
O1–Si–O4	92.2	91.9	91.3	152.3	152.6	153.0	91.2	93.3
O1–Si–H	89.5	90.1	90.3	103.9	103.8	103.5	170.0	170.5
O2–Si–O3	92.2	91.8	91.3	152.3	152.6	153.0	133.9	132.5
O2–Si–O4	112.8	114.2	116.5	86.1	86.2	86.3	131.4	132.6
O2–Si–H	123.6	123.4	121.8	103.9	103.8	103.5	85.0	84.4
O3–Si–O4	88.4	88.2	88.4	87.3	87.3	87.4	94.6	94.9
O3–Si–H	89.5	89.5	90.3	103.9	103.6	103.5	94.9	93.0
O4–Si–H	123.6	122.4	121.8	103.9	103.6	103.5	96.0	92.8

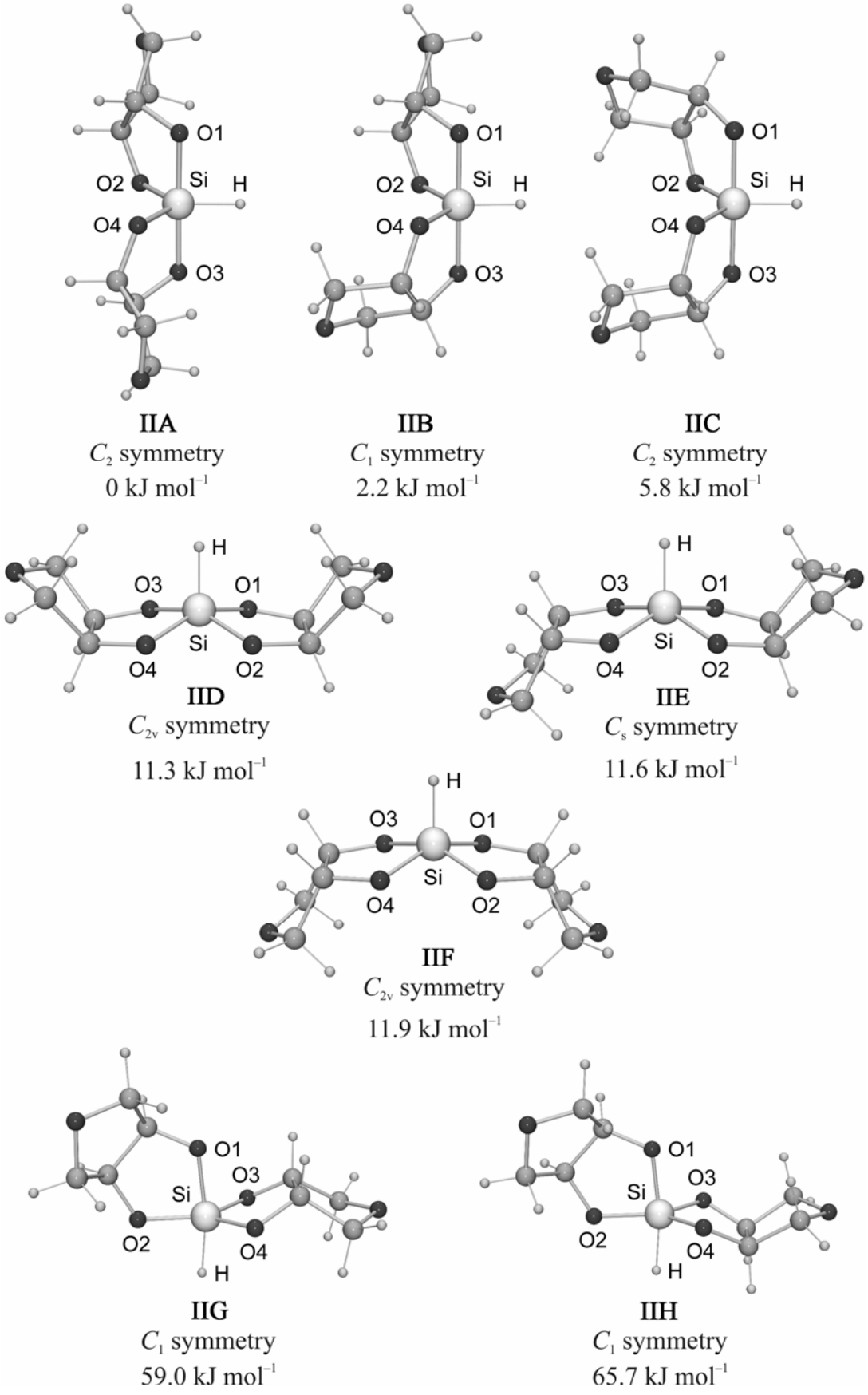

Figure 57. Calculated structures and relative energies of **IIA**–**IIC** (local minima) and **IID**–**IIH** (transition states) as obtained by SCF/TZP+ geometry optimizations.

6 Spirocyclic Zwitterionic λ^5*Si*-[(Ammonio)methyl]silicates with an *SiO*$_4$*C* Skeleton and Two Identical Bidentate Ligands Derived from Benzoin (Compounds 17 and 18)

The synthesis and structural characterization of pentacoordinate silicon compounds of the formula type **D**, with two bidentate ligands of the *cis*-ethene-1,2-diolato(2–) type, have been reported recently (see refs. 2o, 4i, 13, and 14). The *cis*-1,2-diphenylethene-1,2-diolato(2–) ligand formally derives from the tautomeric benzoin species *cis*-HO(Ph)C=C(Ph)OH.

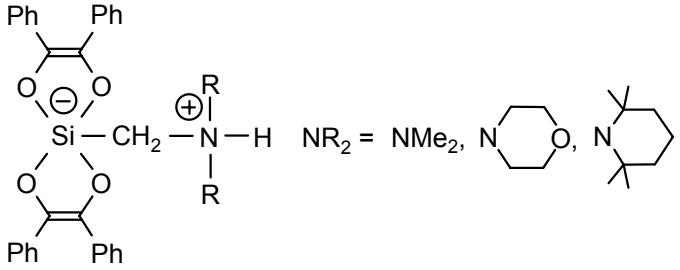

D

As part of this thesis, quite remarkable Si–C cleavage reactions with benzoin have been used for the synthesis of bis[*cis*-1,2-diphenylethene-1,2-diolato(2–)][(morpholinio)methyl]-silicate (**17**).[38] Bis[*cis*-1,2-diphenylethene-1,2-diolato(2–)][(2,2,6,6-tetramethylpiperidinio)-methyl]silicate–dioxane (**18**·3/2$C_4H_8O_2$) was prepared according to ref 14. Compound **18**·3/2$C_4H_8O_2$ with its lipophilic (2,2,6,6-tetramethylpiperidinio)methyl moiety exhibited a good solubility in dichloromethane and therefore allowed low-temperature solution NMR experiments.[38] Preliminary results concerning the syntheses and crystal structures of compounds **17** and **18**·3/2$C_4H_8O_2$ have already been reported in refs 13 and 14.

Si–C cleavage reactions mediated by organic dihydroxy compounds such as benzene-1,2-diols,[4a,b,g,39] α-hydroxycarboxylic acids,[4k,28a,39b] salicylic acid,[4j] or ethane 1,2-diol[4n] have already been used for the synthesis of various λ^5*Si*-silicates with an *Si*O$_4$C framework. Recently, Si–C cleavage reactions were applied to a novel silicon-based linkage and cleavage strategy for solid-phase synthesis of aromatic organic compounds.[39b,40]

6.1 Synthesis of the λ^5*Si*-[(Ammonio)methyl]silicate 17 by Si–C Cleavage Reactions with Benzoin

The zwitterionic λ^5*Si*-silicate **17** was prepared according to Scheme 11, method a (cleavage of three Si–O bonds), by treatment of trimethoxy[(morpholino)methyl]silane (**25**) with two molar equivalents of benzoin in acetonitrile at 20 °C and was isolated as a crystalline solid (yield: 81%). Alternatively, compound **17** was synthesized according to methods b and c (cleavage of one Si–C bond and two Si–O bonds) by treatment of dimethoxy[(morpholino)-methyl]phenylsilane (**26**) and dimethoxy(methyl)[(morpholino)methyl]silane (**27**), respectively, with two molar equivalents of benzoin in acetonitrile at 20 °C (yield: 42% (method b) and 35% (method c)). As the syntheses according to methods b and c involve a relatively slow Si–C cleavage reaction as the rate-determining step, product formation was significantly slower than that observed for method a (see Chapter 10, Experimental Section). All three methods yielded well-crystallized products that did not need further purification by recrystallization.

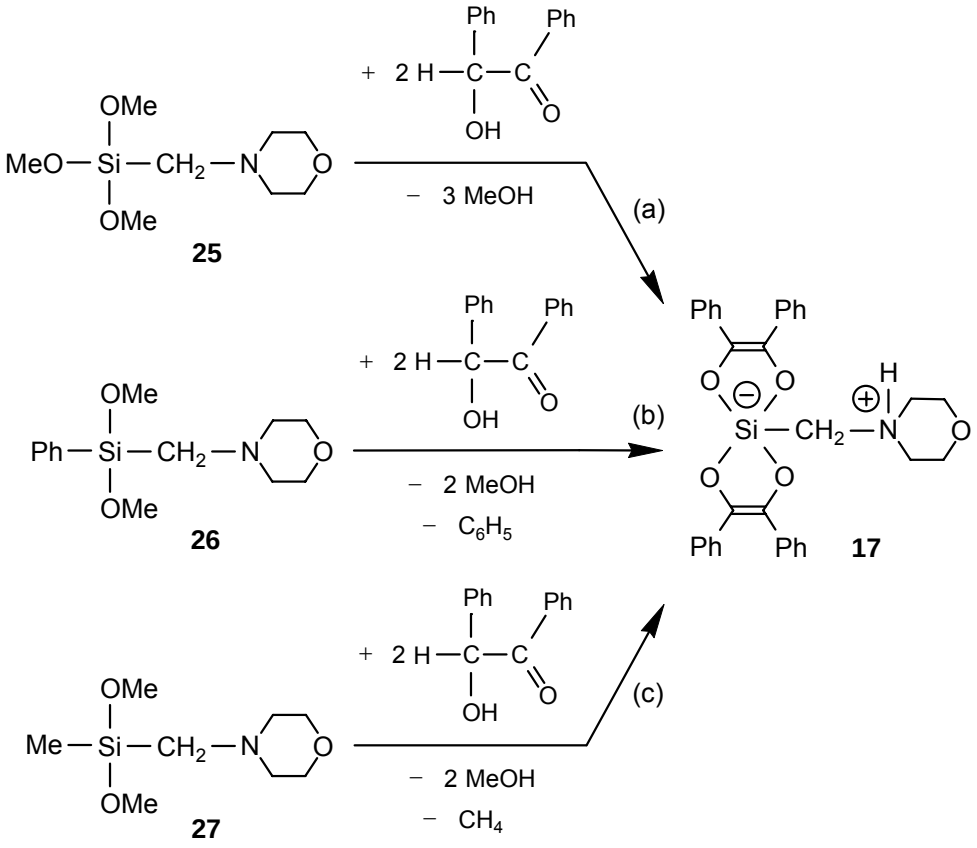

Scheme 11

The synthesis of **18** was carried out according to ref 14 to afford the crystalline solvate **18**·3/2$C_4H_8O_2$.

The identities of the racemic compounds **17** and **18**·3/2$C_4H_8O_2$ were established by elemental analyses (C, H, N), solution NMR studies (^{1}H, ^{13}C, ^{29}Si), solid-state ^{29}Si VACP/MAS NMR experiments (the NMR data obtained for **18**·3/2$C_4H_8O_2$ are very similar to those reported in ref. 14). The isotropic ^{29}Si chemical shifts of **17** and **18**·3/2$C_4H_8O_2$ obtained in the solid-state VACP/MAS NMR experiments clearly characterize the ^{29}Si resonance signals as arising from pentacoordinate silicon atom and are very similar to those determined in solution ([D_6]DMSO). The ^{1}H and ^{13}C NMR data are also compatible with the zwitterionic structure of **17** and **18** (see Chapter 10, Experimental Section and ref. 14). Furthermore, ^{1}H,^{1}H COSY NMR experiments gave evidence for a coupling of the SiC*H*$_2$N protons with the N*H* proton and thus unequivocally indicate the presence of an ammonium group. In conclusion, the NMR studies clearly demonstrate that the zwitterionic λ^5*Si*-silicate **17** and **18** exist in solution as well.

6.2 VT ^{1}H NMR Studies with the λ^5*Si*-[(Ammonio)methyl]silicate 18

Compound **18** was additionally studied by VT ^{1}H NMR experiments at 300.1 MHz in the temperature range 173–296 K using CD_2Cl_2 as the solvent. The temperature dependence of the ^{1}H NMR spectra of **18** is characterized by complete reversibility. As shown in Figure 58, separate resonance signals for the two diastereotopic $SiCH_2N$ protons of the (*Λ*)- and (*Δ*)-enantiomers of **18** could not be observed in the temperature range studied. Instead of an $SiCH_AH_BNH_X$ spin system, we observed an $SiC(H_A)_2NH_X$ spin system, indicating that the enantiomers of **18** are not configurationally stable on the NMR time scale. This finding is in agreement with the results of ab initio studies of the related anionic model system bis[*cis*-ethene-1,2-diolato(2–)]hydridosilicate(1–): The energy difference between the trigonal-bipyramidal geometry (C_2 symmetry, local minimum) and the square-pyramidal geometry (C_{2v} symmetry, transition state) of this species amounts only to 6.9 kJ mol^{-1}, the square-pyramidal structure being a Berry-type transition state for the (*Λ*)/(*Δ*)-enantiomerization of the anion [*cis*-(O(Ph)C=C(Ph)O)]$_2$SiH$^-$.[4i]

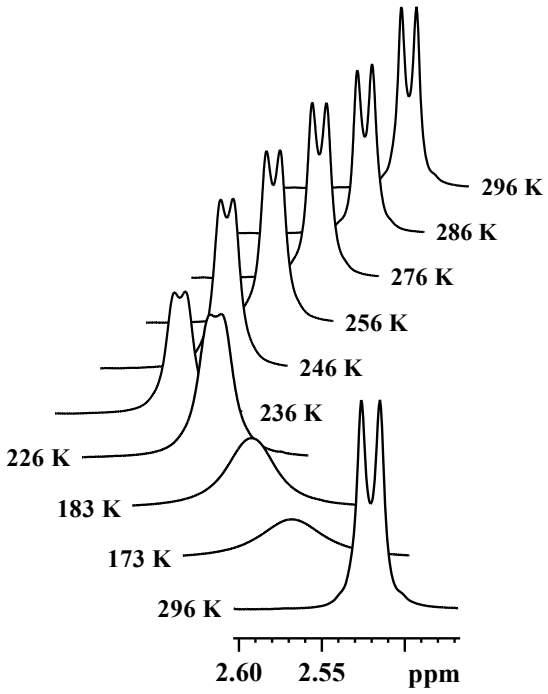

Figure 58. Partial ^{1}H NMR spectrum (resonance signals of the SiCH_2N protons) of **18** in CD_2Cl_2 (c = 12 mM) at 300.1 MHz as a function of temperature in the range 173–296 K.

7 Anionic λ⁶*Si*-Silicates with *Si*O₆ Skeletons and Multidentate Ligands Derived from Citric Acid or Malic Acid (Compounds 19–22)

In recent studies in our group, the synthesis of the hexacoordinate silicon(IV) complexes of the formula type **E** and their structural characterization in the solid state and in solution have been performed.[5c] The λ⁶*Si*-silicate dianions of these compounds contain three bidentate ligands (glycolato(2–) or benzilato(2–) ligands) that derive from α-hydroxycarboxylic acids.

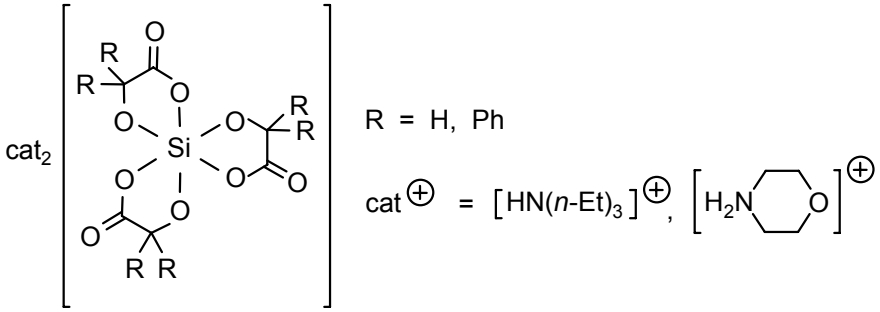

E

Interestingly, all attempts to prepare related compounds of the formula type **E**, with three bidentate citrato(2–) ligands, failed so far (see below).

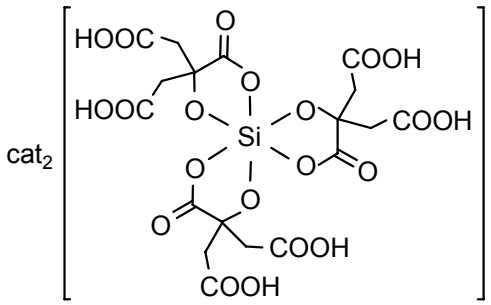

Instead, only a hexacoordinate silicon(IV) complex, in which two tridentate citrato(3–) ligands are bound to the silicon coordination center, could be synthesized (see below).[5d,e]

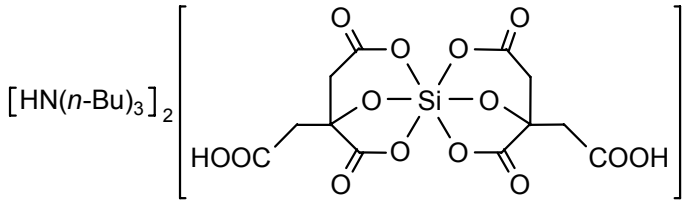

In continuation of these studies, the hitherto unknown hexacoordinate silicon compounds *meso*-**19**·2CH_3OH and *rac*-**20**·1.73CH_3OH, with two tridentate citrato(3–) ligands

or two tridentate citrato(4–) ligands bound to the silicon(IV) coordination center, were synthesized and structurally characterized in the solid state.[41] Compound *meso*-**19**·2CH_3OH, with its achiral λ6*Si*-silicate dianion (center of inversion), displays a different coordination mode as observed for the racemic tri(*n*-butyl)ammonium bis[citrato(3–)-O^1,O^3,O^6]silicate[5d,e] with its chiral λ6*Si*-silicate dianion, whereas compound **20**·1.73CH_3OH shows the same coordination mode, but with an additional negative charge at each of the two tridentate ligands.

In addition, the hitherto unknown compounds (*Λ*,*S*,*S*,*S*)-*mer*-**21** and (*Λ*,*S*,*S*,*S*)-*mer*-**22**·2CH_3CN were synthesized and structurally characterized in the solid state.[41] These compounds contain three bidentate malato(2–) ligands, with an analogous coordination mode as observed for the λ6*Si*-silicate dianions of the hexacoordinate silicon(IV) complexes of the formula type **E**. The solid-state ^{13}C, ^{15}N, ^{29}Si NMR experiments and the crystal structure analyses of the non-racemic compounds *meso*-**19**·2CH_3OH, (*Λ*,*S*,*S*,*S*)-*mer*-**21**, and (*Λ*,*S*,*S*,*S*)-*mer*-**22**·2CH_3CN demonstrated their diastereomeric purity (for the *fac*/*mer* nomenclature, see ref. 42).

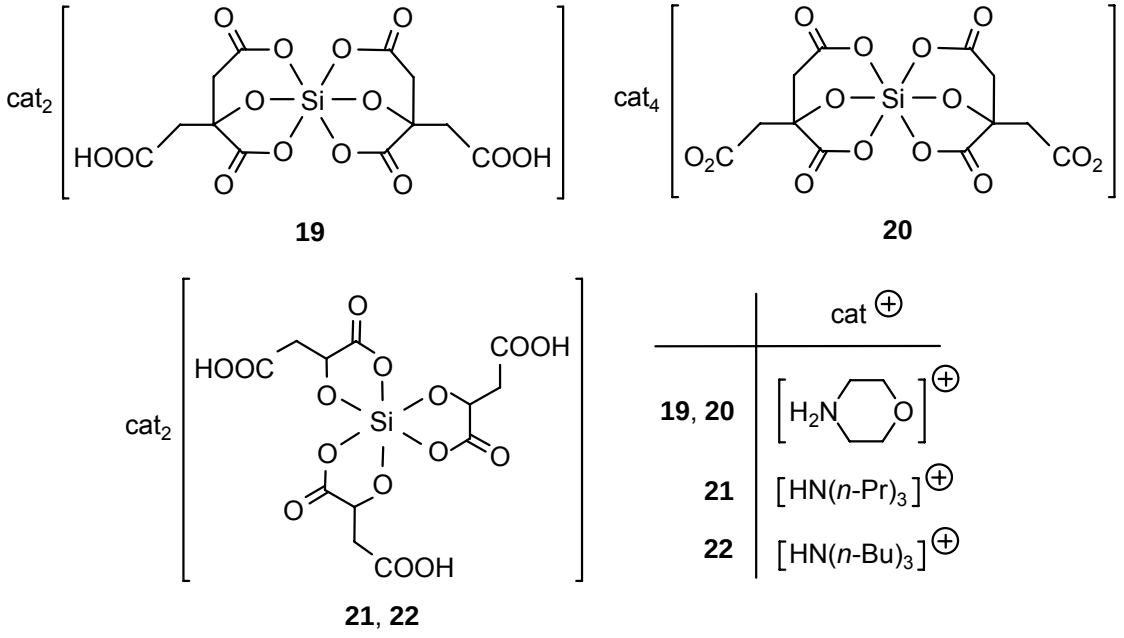

7.1 Syntheses of the λ6*Si*-Silicates 19–22

Compound *meso*-**19** was synthesized according to Scheme 12 by treatment of tetramethoxysilane with citric acid and morpholine (molar ratio 1:2:2) in methanol at 20 °C and was isolated as the crystalline solvate *meso*-**19**·2CH_3OH (yield: 91%). Compound *rac*-**20** was prepared by reaction of tetramethoxysilane with citric acid and morpholine (molar ratio

1:2:4) in tetrahydrofuran/methanol at 20 °C and was isolated in 75% yield as the crystalline solvate *rac*-**20**·1.73CH_3OH (Scheme 12).[43]

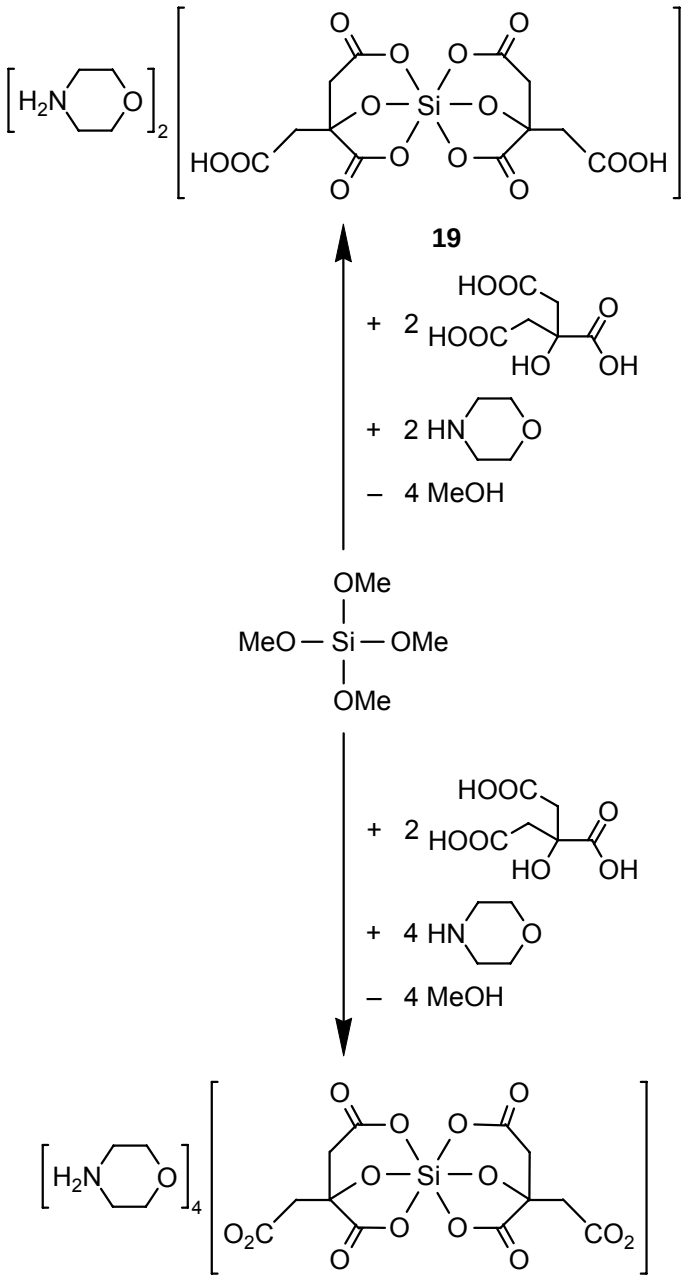

Scheme 12

Compound (*Λ*,*S*,*S*,*S*)-*mer*-**21** was synthesized according to Scheme 13 by treatment of tetramethoxysilane with (*S*)-malic acid and tri(*n*-propyl)amine (molar ratio 1:3:2) in tetrahydrofuran at 20 °C and was isolated in 89% yield as a crystalline solid. Compound (*Λ*,*S*,*S*,*S*)-*mer*-**22** was prepared analogously by reaction of tetramethoxysilane with (*S*)-malic acid and tri(*n*-butyl)amine (molar ratio 1:3:2) in tetrahydrofuran/diethyl ether at 20 °C and was isolated, after recrystallization from acetonitrile, in 86% yield as the solvate (*Λ*,*S*,*S*,*S*)-*mer*-**22**·2CH_3CN (Scheme 13).

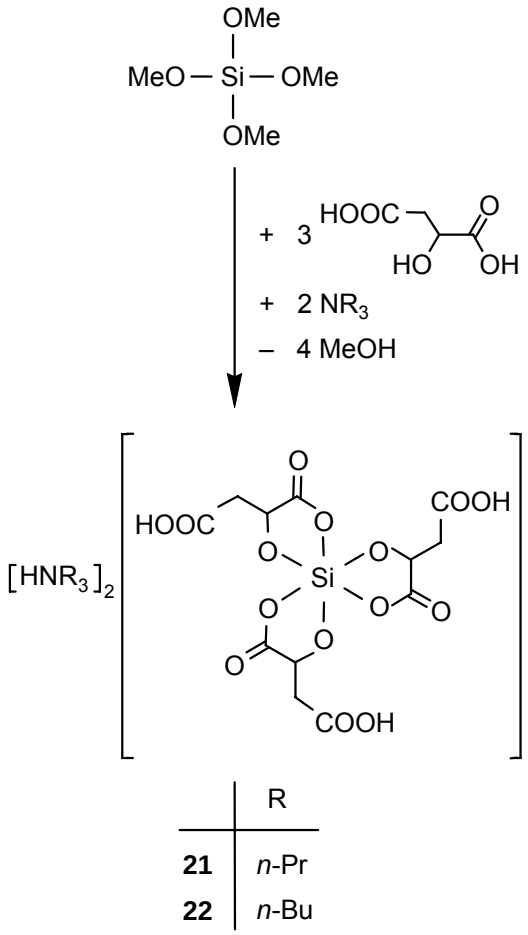

Scheme 13

The identities of *meso*-**19**·2CH_3OH, *rac*-**20**·1.73CH_3OH, (*Λ*,*S*,*S*,*S*)-*mer*-**21**, and (*Λ*,*S*,*S*,*S*)-*mer*-**22**·2CH_3CN were established by elemental analyses (C, H, N), solid-state NMR studies, and crystal structure analyses.

7.2 Crystal Structure Analyses of the λ⁶*Si*-Silicates 19–22

Compounds *meso*-**19**·2CH_3OH, *rac*-**20**·1.73CH_3OH, (*Λ*,*S*,*S*,*S*)-*mer*-**21**, and (*Λ*,*S*,*S*,*S*)-*mer*-**22**·2CH_3CN were structurally characterized by single-crystal X-ray diffraction.[16] The crystal data and experimental parameters used for these studies are given in Appendix A (Table 30). For reason of comparison, selected bond distances and angles are listed in Tables 21 and 22. Suitable single crystals of *meso*-**19**·2CH_3OH, *rac*-**20**·1.73CH_3OH, (*Λ*,*S*,*S*,*S*)-*mer*-**21**, and (*Λ*,*S*,*S*,*S*)-*mer*-**22**·2CH_3CN were isolated directly from the respective reaction mixtures (see Chapter 10, Experimental Section). The crystals were mounted in inert oil (perfluoroalkyl ether, ABCR) on a glass fiber and then transferred to the cold nitrogen gas stream of the diffractometer (Stoe IPDS diffractometer; graphite-monochromated MoK_α

radiation, λ = 0.71073 Å). The structures were solved by direct methods.[17] The non-hydrogen atoms were refined anisotropically.[18] A riding model was employed in the refinement of the CH hydrogen atoms. The NH hydrogen atoms were localized in difference Fourier syntheses and refined freely (except for *rac*-**20**·1.73CH_3OH). Except for *rac*-**20**·1.73CH_3OH and (*Λ*,*S*,*S*,*S*)-*mer*-**21**, the OH hydrogen atoms were also localized in difference Fourier syntheses and refined freely. All bond lengths and angles which are not discussed explicitly in the following sections are in the expected range and therefore do not need further discussion.

Compound *meso*-**19**·2CH_3OH crystallizes in the space group $P2_1/n$, with one morpholinium cation, one half of the centrosymmetric λ⁶*Si*-silicate dianion, and one methanol molecule in the asymmetric unit. Compound *rac*-**20**·1.73CH_3OH crystallizes in the space group $P\bar{1}$ as a 1:1 mixture of (*R*,*R*)- and (*S*,*S*)-enantiomers, with four morpholinium cations, one chiral λ⁶*Si*-silicate tetraanion, and additional methanol molecules in the asymmetric unit. The solvent molecules are distributed over two different sites, one of which is only partially occupied (occupation factor 0.73). The molecular structures of the λ⁶*Si*-silicate anions of *meso*-**19**·2CH_3OH and *rac*-**20**·1.73CH_3OH are depicted in Figures 59 and 60.

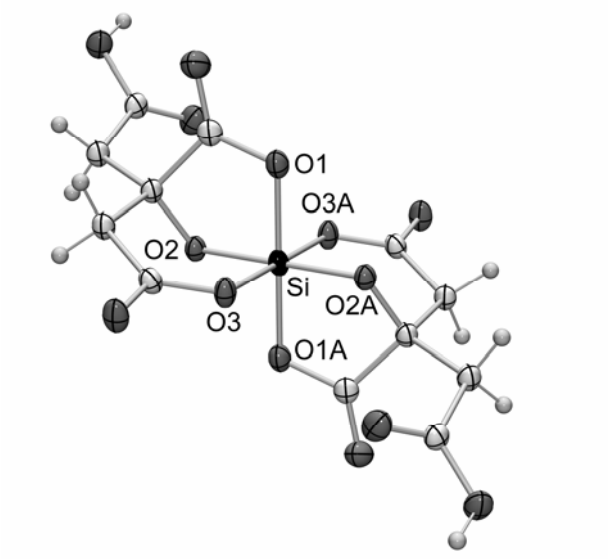

Figure 59. Structure of the λ⁶*Si*-silicate dianion in the crystal of *meso*-**19**·2CH_3OH (probability level of displacement ellipsoids 50%).

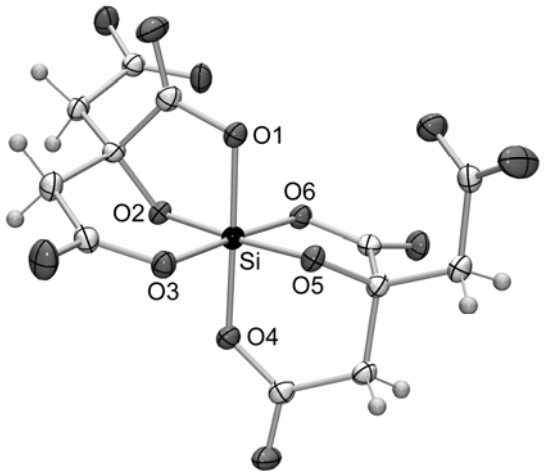

Figure 60. Structure of the λ6*Si*-silicate tetraanion ((*S*,*S*)-enantiomer) in the crystal of *rac*-**20**·1.73CH_3OH (probability level of displacement ellipsoids 50%).

Table 21. Selected Bond Lengths (Å) and Angles (deg) for the λ6*Si*-Silicate Dianion of *meso*-**19**·2CH_3OH and the λ6*Si*-Silicate Tetraanion of *rac*-**20**·1.73CH_3OH

meso-**19**·2CH_3OH		*rac*-**20**·1.73CH_3OH	
Si–O1	1.7835(13)	Si–O1	1.8266(13)
Si–O2	1.7203(12)	Si–O2	1.7156(13)
Si–O3	1.8509(13)	Si–O3	1.7910(14)
Si–O1A	1.7835(13)	Si–O4	1.8319(13)
Si–O2A	1.7203(12)	Si–O5	1.7140(13)
Si–O3A	1.8509(13)	Si–O6	1.8125(13)
O1–Si–O2	89.67(6)	O1–Si–O2	88.14(6)
O1–Si–O3	90.46(6)	O1–Si–O3	90.80(6)
O1–Si–O1A	180.00(4)	O1–Si–O4	178.80(6)
O1–Si–O2A	90.33(6)	O1–Si–O5	88.88(6)
O1–Si–O3A	89.54(6)	O1–Si–O6	91.15(6)
O2–Si–O3	91.35(6)	O2–Si–O3	92.66(6)
O2–Si–O1A	90.33(6)	O2–Si–O4	90.82(6)
O2–Si–O2A	180.000(1)	O2–Si–O5	176.59(7)
O2–Si–O3A	88.65(6)	O2–Si–O6	89.53(6)
O3–Si–O1A	89.54(6)	O3–Si–O4	88.67(6)
O3–Si–O2A	88.65(6)	O3–Si–O5	89.04(6)
O3–Si–O3A	180.0	O3–Si–O6	177.11(6)
O1A–Si–O2A	89.67(6)	O4–Si–O5	92.18(6)
O1A–Si–O3A	90.46(6)	O4–Si–O6	89.42(6)
O2A–Si–O3A	91.35(6)	O5–Si–O6	88.87(6)

As can be seen from Figures 59 and 60, the two tridentate citrato(3–) ligands of *meso*-**19**·2CH_3OH and the two tridentate citrato(4–) ligands of *rac*-**20**·1.73CH_3OH coordinate to the silicon(IV) coordination center through one alcoholato group and two carboxylato groups. The Si-coordination polyhedron of *meso*-**19**·2CH_3OH is a nearly ideal octahedron, with O–Si–O angles in the ranges 88.65(6)–91.35(6) (deg) and 180.0–180.00(4) (deg) and Si–O distances in the range 1.7203(12)–1.8509(13) Å. The octahedral Si-coordination polyhedron of *rac*-**20**·1.73CH_3OH is somewhat more distorted. The O–Si–O angles are in the ranges 88.14(6)–92.66(6) deg and 176.59(7)–178.80(6) deg, and the Si–O bond lengths amount to 1.7140(13)–1.8319(13) Å (see Table 21). The Si–O(carboxylato) distances of both compounds are significantly longer than the Si–O(alcoholato) bond lengths.

Compounds (*Λ*,*S*,*S*,*S*)-*mer*-**21** and (*Λ*,*S*,*S*,*S*)-*mer*-**22**·2CH_3CN crystallize in the space group $P2_12_12_1$ and $P2_1$, respectively. The asymmetric units contain two ammonium cations and one chiral λ^6*Si*-silicate dianion, and in the case of (*Λ*,*S*,*S*,*S*)-*mer*-**22**·2CH_3CN there are two additional acetonitrile molecules. The molecular structures of the λ^6*Si*-silicate dianions of (*Λ*,*S*,*S*,*S*)-*mer*-**21** and (*Λ*,*S*,*S*,*S*)-*mer*-**22**·2CH_3CN are depicted in Figures 61 and 62.

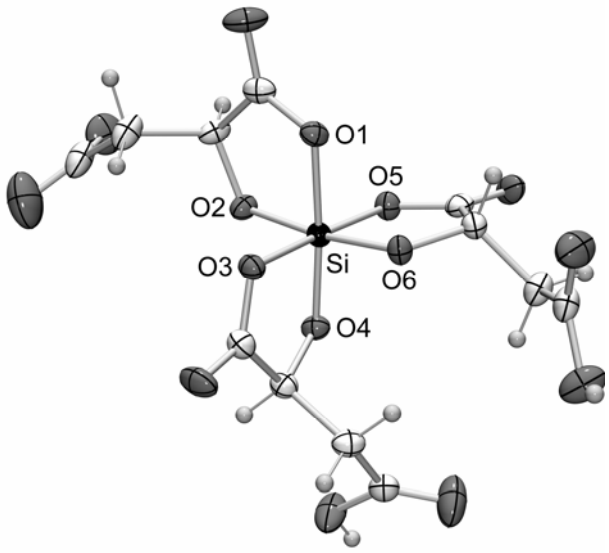

Figure 61. Structure of the λ^6*Si*-silicate dianion in the crystal of (*Λ*,*S*,*S*,*S*)-*mer*-**21** (probability level of displacement ellipsoids 50%).

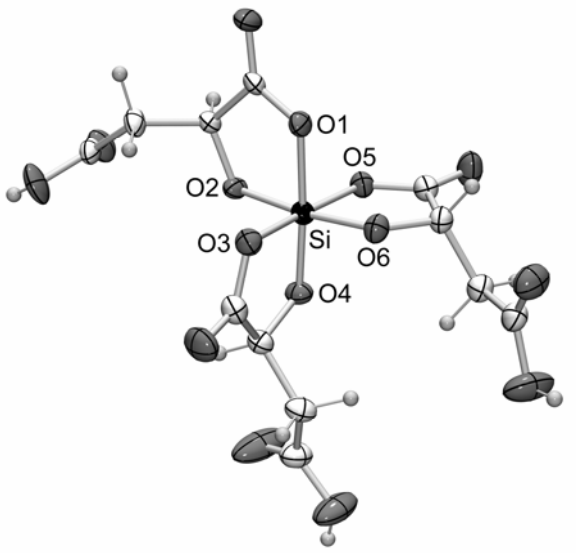

Figure 62. Structure of the λ^6*Si*-silicate dianion in the crystal of (*Λ*,*S*,*S*,*S*)-*mer*-**22**·2CH_3CN (probability level of displacement ellipsoids 50%).

As can be seen from Figures 61 and 62, the bidentate malato(2–) ligands of both compounds coordinate to the silicon(IV) coordination center through one alcoholato group and one carboxylato group. The Si-coordination polyhedra are slightly distorted octahedra, with O–Si–O angles in the ranges 85.49(6)–96.70(6) deg and 172.35(6)–175.90(7) deg and Si–O distances in the range 1.7255(13)–1.8350(13) Å (see Table 22). As in the case of *meso*-**19**·2CH_3OH and *rac*-**20**·1.73CH_3OH, the Si–O (carboxylato) bond lengths are significantly longer than the Si–O (alcoholato) distances.

Table 22. Selected bond lengths (Å) and angles (deg) for the λ⁶*Si*-silicate dianions of (*Λ*,*S*,*S*,*S*)-*mer*-**21** and (*Λ*,*S*,*S*,*S*)-*mer*-**22**·2CH_3CN

	(*Λ*,*S*,*S*,*S*)-*mer*-**21**	(*Λ*,*S*,*S*,*S*)-*mer*-**22**·2CH_3CN
Si–O1	1.8300(12)	1.8350(13)
Si–O2	1.7472(13)	1.7317(13)
Si–O3	1.8249(12)	1.7911(16)
Si–O4	1.7328(12)	1.7255(13)
Si–O5	1.8007(12)	1.8099(16)
Si–O6	1.7537(13)	1.7463(14)
O1–Si–O2	86.98(5)	86.55(6)
O1–Si–O3	87.43(5)	88.46(7)
O1–Si–O4	175.27(6)	175.90(7)
O1–Si–O5	92.09(6)	89.88(7)
O1–Si–O6	85.49(6)	87.29(6)
O2–Si–O3	94.24(6)	95.39(7)
O2–Si–O4	90.91(6)	89.68(6)
O2–Si–O5	90.68(6)	90.56(7)
O2–Si–O6	172.35(6)	173.39(7)
O3–Si–O4	88.50(6)	90.30(7)
O3–Si–O5	175.02(6)	173.71(7)
O3–Si–O6	86.77(6)	86.82(7)
O4–Si–O5	92.17(6)	91.76(7)
O4–Si–O6	96.70(6)	96.54(7)
O5–Si–O6	88.25(6)	87.04(7)

As expected from the presence of the potential N–H and O–H donor functions and the potential oxygen acceptor atoms, the crystal structures of all compounds studied contain very complex hydrogen-bonding systems.[19] In the case of *meso*-**19**·2CH_3OH, N–H···O interactions

connect the morpholinium cations with the λ⁶*Si*-silicate dianions, and intermolecular O–H···O interactions connect the λ⁶*Si*-silicate dianions with each other, leading to an infinite two-dimensional network (base vectors: [1 0 1], [0 1 0]; plane: (1 0 –1)).

In the case of *rac*-**20**·1.73CH_3OH, N–H···O interactions connect the morpholinium cations with the λ⁶*Si*-silicate tetraanions, leading to infinite one-dimensional chains along the [1 0 –1] base vector.

The methanol molecules of *meso*-**19**·2CH_3OH and *rac*-**20**·1.73CH_3OH are also involved in the hydrogen-bonding systems, with intermolecular O–H···O interactions between the solvent molecules and the λ⁶*Si*-silicate dianions.

The bond lengths and angles of the hydrogen-bonding systems in the crystals of *meso*-**19**·2CH_3OH and *rac*-**20**·1.73CH_3OH are not discussed explicitly due to their complexity.

In the case of (*Λ*,*S*,*S*,*S*)-*mer*-**21** and (*Λ*,*S*,*S*,*S*)-*mer*-**22**·2CH_3CN, N–H···O interactions connect the ammonium cations with the λ⁶*Si*-silicate dianions, and intermolecular O–H···O interactions connect the λ⁶*Si*-silicate dianions with each other, leading to an infinite three-dimensional framework and to an infinite two-dimensional network (base vectors: [1 0 1], [0 1 0]; plane (1 0 –1)), respectively (see Figures 63 and 64 and Table 23).

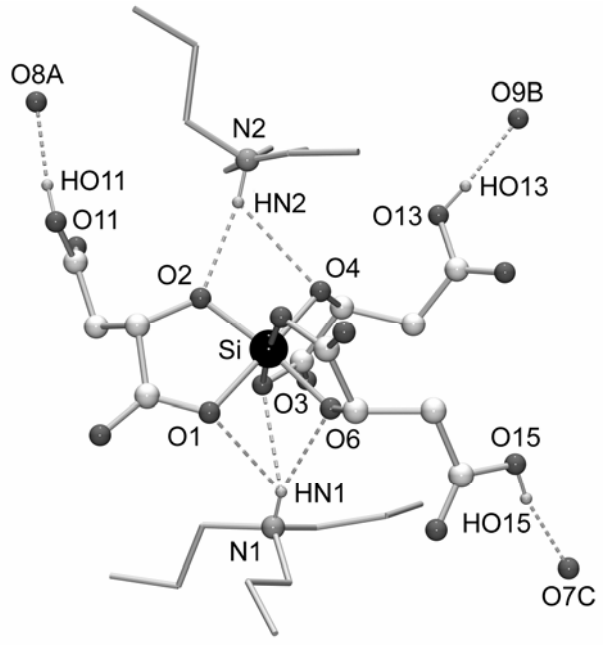

Figure 63. Hydrogen bonds in the crystal of (*Λ*,*S*,*S*,*S*)-*mer*-**21** leading to leading to an infinite three-dimensional framework. The hydrogen atoms (except for those involved in hydrogen bonds) are omitted for clarity. The CH_2 and CH_3 moieties of the ammonium cations are represented as stick model for clarity.

Interestingly, in the case of both compounds trifurcate hydrogen bonds (N1–HN1···O1/O3/O6) and bifurcate hydrogen bonds (N2–HN2···O2/O4) connect the ammonium cations with the λ⁶*Si*-silicate dianions. The acetonitrile molecules of (*Λ*,*S*,*S*,*S*)-*mer*-**22**·2CH_3CN are also involved in the hydrogen-bonding system, with intermolecular O–H···N interactions between the λ⁶*Si*-silicate dianions and the solvent molecules.

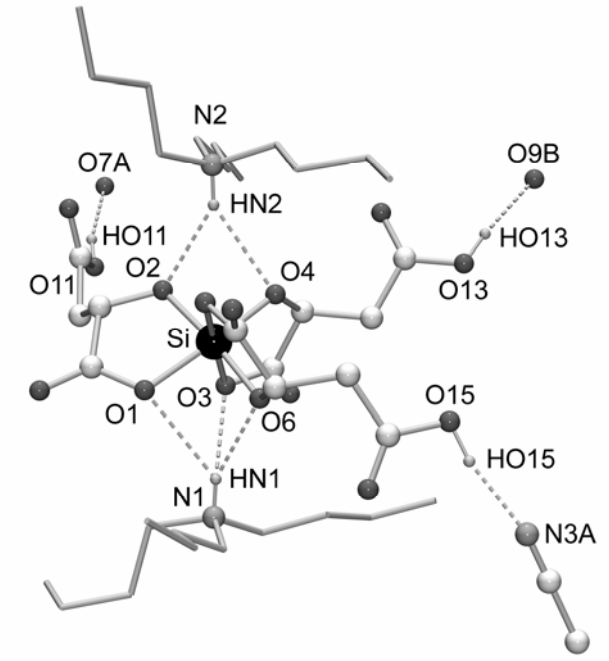

Figure 64. Hydrogen bonds in the crystal of (*Λ*,*S*,*S*,*S*)-*mer*-**22**·2CH_3CN leading to an infinite two-dimensional network (base vectors: [1 0 1], [0 1 0]; plane (1 0 −1)). The hydrogen atoms (except for those involved in hydrogen bonds) are omitted for clarity. The CH_2 and CH_3 moieties of the ammonium cations are represented as stick model for clarity.

Table 23. Hydrogen-Bonding Geometries for (*Λ*,*S*,*S*,*S*)-*mer*-**21** and (*Λ*,*S*,*S*,*S*)-*mer*-**22**·2CH_3CN in the Crystal[a]

	D–H···A	D–H (Å)	H···A (Å)	D···A (Å)	D–H···A (deg)
(*Λ*,*S*,*S*,*S*)-*mer*-**21**	O11–HO11···O8	0.84	1.79	2.620(2)	168
	O13–HO13···O9	0.84	1.85	2.6479(18)	158
	O15–HO15···O7	0.84	1.77	2.5957(19)	166
	N1–HN1···O1	0.85(2)	2.53(2)	3.1796(19)	133.5(17)
	N1–HN1···O3	0.85(2)	2.43(2)	3.008(2)	125.6(17)
	N1–HN1···O6[b]	0.85(2)	2.24(2)	3.0751(19)	164.6(18)
	N2–HN2···O2	0.89(2)	2.08(2)	2.9510(19)	170.6(18)
	N2–HN2···O4[c]	0.89(2)	2.49(2)	3.079(2)	124.4(16)
(*Λ*,*S*,*S*,*S*)-*mer*-**22**·2CH_3CN	O11–HO11···O7	0.74(3)	1.94(3)	2.643(2)	159(4)
	O13–HO13···O9	0.83(3)	1.83(3)	2.656(3)	171(3)
	O15–HO15···N3	0.92(4)	1.92(4)	2.814(3)	167(3)
	N1–HN1···O1	0.84(3)	2.50(3)	3.178(2)	139(2)
	N1–HN1···O3	0.84(3)	2.40(3)	3.079(2)	138(2)
	N1–HN1···O6[d]	0.84(3)	2.21(2)	2.967(3)	150(2)
	N2–HN2···O2	0.86(3)	2.20(2)	2.958(2)	148(2)
	N2–HN2···O4[e]	0.86(3)	2.34(3)	3.101(3)	147(2)

[a]Data calculated by using the program PLATON.[19] [b]Trifurcate N1–HN1···O1/O3/O6 interaction; O1···HN1···O3 = 61.2(5) deg, O1···HN1···O6 = 60.9(5) deg, O3···H···O6 = 63.3(5) deg. [c]Bifurcate N2–HN2···O2/O4 interaction; O2···HN2···O4 = 65.1(6) deg. [d]Trifurcate N1–HN1···O1/O3/O6 interaction; O1···HN1···O3 = 62.1(6) deg, O1···HN1···O6 = 63.0(7) deg, O3···H···O6 = 63.4(7) deg. [e]Bifurcate N2–HN2···O2/O4 interaction; O2···HN2···O4 = 64.9(7) deg.

7.3 NMR Studies of the λ⁶*Si*-Silicates 19–22

Compounds *meso*-**19**·2CH_3OH, *rac*-**20**·1.73CH_3OH, (*Λ*,*S*,*S*,*S*)-*mer*-**21**, and (*Λ*,*S*,*S*,*S*)-*mer*-**22**·2CH_3CN were characterized by solid-state VACP/MAS NMR studies (^{13}C, ^{15}N, ^{29}Si; see Chapter 10, Experimental Section). The isotropic ^{29}Si chemical shifts obtained in these studies clearly indicate the presence of SiO_6 skeletons (Table 24). All ^{13}C, ^{15}N, and ^{29}Si NMR spectra were compatible with the crystal structures of the compounds studied (see Crystal

Structure Analyses) and demonstrated that the non-racemic compounds *meso*-**19**·2CH_3OH, (*Λ*,*S*,*S*,*S*)-*mer*-**21**, and (*Λ*,*S*,*S*,*S*)-*mer*-**22**·2CH_3CN were diastereomerically pure.

Table 24. ^{29}Si VACP/MAS NMR Data for **19**–**22** in the Crystal (Spectra Recorded at 22 °C; Chemical Shifts in ppm, δ values)

meso-**19**·2CH_3OH	−162.4
rac-**20**·1.73CH_3OH	−166.4
(*Λ*,*S*,*S*,*S*)-*mer*-**21**	−148.1
(*Λ*,*S*,*S*,*S*)-*mer*-**22**·2CH_3CN	−146.3

All attempts to characterize *meso*-**19**·2CH_3OH, *rac*-**20**·1.73CH_3OH, (*Λ*,*S*,*S*,*S*)-*mer*-**21**, and (*Λ*,*S*,*S*,*S*)-*mer*-**22** by solution NMR spectroscopy (^{1}H, ^{13}C, ^{29}Si; [D_6]DMSO, 22 °C) gave unsatisfactory results (data not given). In all cases, more than one silicon species was detected, a λ⁶*Si*-silicate being the major species. However, the stereochemistry of these λ⁶*Si*-silicates could not be unequivocally deduced from the NMR spectra.

Upon dissolution of *meso*-**19**·2CH_3OH, *rac*-**20**·1.73CH_3OH, (*Λ*,*S*,*S*,*S*)-*mer*-**21**, and (*Λ*,*S*,*S*,*S*)-*mer*-**22**·2CH_3CN in water at 20 °C, spontaneous hydrolysis of the λ⁶*Si*-silicate anions was observed (no ^{29}Si resonance signal for the λ⁶*Si*-silicate dianions). The resulting clear aqueous solutions (sols) were found to undergo gel formation after a period of ca. three days ((*Λ*,*S*,*S*,*S*)-*mer*-**22**·2CH_3CN), one week ((*Λ*,*S*,*S*,*S*)-*mer*-**21**), or two weeks (*meso*-**19**·2CH_3OH, *rac*-**20**·1.73CH_3OH). Taking into account all these findings, it is unlikely that λ⁶*Si*-silicates with multidentate ligands derived from α-hydroxycarboxylic acids play a role for transport and storage of silicon in biological systems.

8 Summary

This thesis contributes to the field of silicon chemistry, with a special emphasis on the chemistry of penta- and hexacoordinate silicon. The results are summarized in the following sections.

Zwitterionic λ^5*Si*-Silicates with Ligands Derived from α-Amino Acids

The spirocyclic zwitterionic λ^5*Si*-silicates **1**–**6** with a (2,2,6,6-tetramethylpiperidinio)-methyl group and two identical bidentate chelate ligands derived from glycine, (*S*)-alanine, (*S*)-phenylalanine, (*S*)-valine, (*S*)-*tert*-leucine, or (*S*)-proline bound to the silicon(IV) coordination center were synthesized and structurally characterized for the first time.

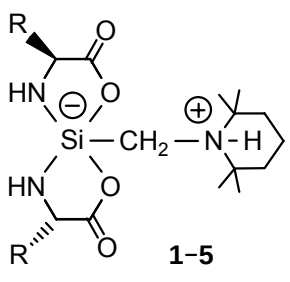

1–**5**

	R
1	H
2	Me
3	CH_2Ph
4	*i*-Pr
5	*t*-Bu

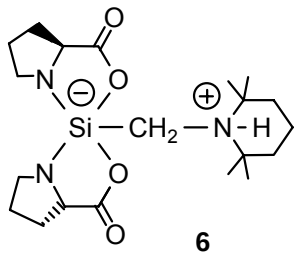

6

Compounds **2**–**6** were isolated as diastereo- and enantiomerically pure crystalline solids: (*Δ*,*S*,*S*)-**2**, (*Λ*,*S*,*S*)-**3**·CH_2Cl_2, (*Λ*,*S*,*S*)-**4**·CH_2Cl_2, (*Λ*,*S*,*S*)-**5**·CH_2Cl_2, (*Λ*,*S*,*S*)-**6**·$2CH_2Cl_2$, and (*Λ*,*S*,*S*)-**6**·½CH_2Cl_2. The identities of **1**–**6** were established by elemental analyses (C, H, N), single-crystal X-ray diffraction studies, VACP/MAS solid-state NMR experiments (^{15}N, ^{29}Si), and solution NMR studies (^{1}H, ^{13}C, ^{15}N, ^{29}Si; including VT NMR and cross-experiments). The experimental investigations were complemented by computational studies of the anionic model species **I**.

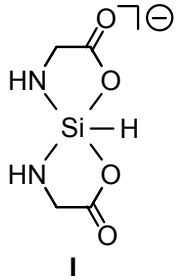

I

Upon dissolution of the diastereo- and enantiomerically pure compounds (*Δ*,*S*,*S*)-**2** and (*Λ*,*S*,*S*)-**3**·CH_2Cl_2 in CD_2Cl_2, the zwitterionic λ^5*Si*-silicates undergo a (*Λ*)/(*Δ*)-epimerization to give an equilibrium mixture of the respective (*Λ*,*S*,*S*)- and (*Δ*,*S*,*S*)-diastereomers, the (*Λ*)-isomers being thermodynamically more stable than the (*Δ*)-isomers. The absolute configurations of the respective diastereomers in solution could be assigned because the

kinetics of the epimerization process at the silicon atom upon dissolution of (*Δ*,*S*,*S*)-**2** and (*Λ*,*S*,*S*)-**3**·CH_2Cl_2 in CD_2Cl_2 could be monitored by ^{1}H NMR spectroscopy.

Upon dissolution of compounds (*Λ*,*S*,*S*)-**4**, (*Λ*,*S*,*S*)-**5**, and (*Λ*,*S*,*S*)-**6** in CD_2Cl_2, the existence of only one diastereomer in solution was observed. Additionally, VT ^{1}H NMR experiments with solutions of (*Λ*,*S*,*S*)-**4**, (*Λ*,*S*,*S*)-**5**, and (*Λ*,*S*,*S*)-**6** in CD_2Cl_2 were performed in the temperature range –100 °C to 23 °C. No additional set of resonance signals indicating a second species could be observed at temperatures down to –100 °C.

Zwitterionic λ^5*Si*-Silicates with Ligands Derived from α-Hydroxycarboxylic Acids

The hitherto unknown spirocyclic zwitterionic λ^5*Si*-silicates **7**–**12** with an (ammonio)-methyl group and two identical bidentate chelate ligands derived from (*S*)-lactic acid, (*S*)-3-phenyllactic acid, or (*S*)-mandelic acid were synthesized and structurally characterized in the solid state (elemental analyses (C, H, N), crystal structure analyses, ^{15}N and ^{29}Si VACP/MAS solid-state NMR experiments) and in solution (except **10**; ^{1}H, ^{13}C, and ^{29}Si NMR experiments).

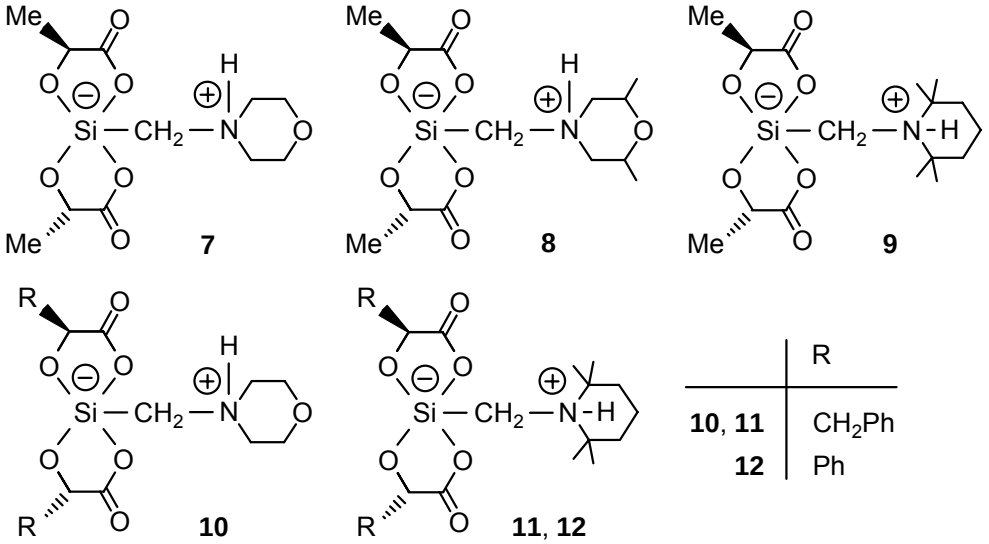

The λ^5*Si*-silicates **7**–**12** were isolated as diastereo- and enantiomerically pure crystalline solids: (*Δ*,*S*,*S*)-**7**·CH_3CN, (*Λ*,*S*,*S*)-**8**, (*Δ*,*S*,*S*)-**8**, (*Δ*,*S*,*S*)-**9**, (*Λ*,*S*,*S*)-**10**, (*Λ*,*S*,*S*)-**11**·CH_3CN, and (*Λ*,*S*,*S*)-**12**. Upon dissolution in CD_2Cl_2 or [D_6]DMSO, the λ^5*Si*-silicates **7**–**9**, **11**, and **12** undergo a (*Λ*)/(*Δ*)-epimerization to give an equilibrium mixture of the respective (*Λ*,*S*,*S*)- and (*Δ*,*S*,*S*)-diastereomers. The stereodynamics of the Si-coordination polyhedra in solution was studied by dynamic ^{1}H NMR experiments. In the case of **7**, **9**, **11**, and **12**, the absolute configurations of the respective diastereomers could not be assigned, because the epimerization process was too fast and could not be monitored by ^{1}H NMR spectroscopy.

Even upon dissolution of (*Δ*,*S*,*S*)-**7**, (*Δ*,*S*,*S*)-**9**, (*Λ*,*S*,*S*)-**11**, and (*Λ*,*S*,*S*)-**12** in CD_2Cl_2 or CD_3CN at low temperatures (–90 °C or –40 °C), a spontaneous equilibration was observed. Interestingly, in the case of **8** the absolute configurations of the diastereomers in solution could be established by monitoring the epimerization process at the silicon atom by low-temperature ^{1}H NMR spectroscopy in CD_2Cl_2 (temperature range –94 °C to 23 °C).

Zwitterionic λ^5*Si*-Silicates with Ligands Derived from *meso*-Oxolane-3,4-diol

The spirocyclic zwitterionic λ^5*Si*-silicates **13**, **15**, and **16** with an (ammonio)methyl group and two bidentate *meso*-oxolane-3,4-diolato(2–) ligands bound to the silicon(IV) coordination center were synthesized for the first time. The already existent compound **14** was resynthesized in order to perform a crystal structure analysis. All compounds were characterized by elemental analyses (C, H, N), ^{29}Si VACP/MAS solid-state NMR experiments, and solution NMR studies (^{1}H, ^{13}C, ^{15}N, and ^{29}Si NMR experiments), and compounds **14–16** were additionally studied by single-crystal X-ray diffraction.

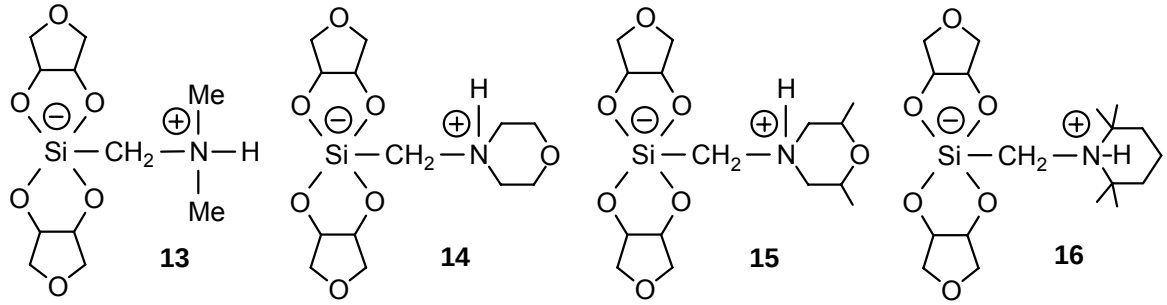

Upon dissolution of **13–16** in water, equilibrium mixtures of the respective *syn*/*syn*, *syn*/*anti*, and *anti*/*anti* isomers were observed, and pH values of pH > 7 were measured. Surprisingly, the zwitterionic λ^5*Si*-silicates **13**–**16** were found to be hydrolytically stable in aqueous solution (no decomposition in the pH range studied: **13**, pH 7.0–8.9; **14**, pH 7.0–8.0; **15**, pH 7.0–8.4; **16**, pH 7.0–9.2) and could even be synthesized in water.

Obviously, special structural and/or electronic features of the *meso*-oxolane-3,4-diolato(2–) ligand, in combination with the zwitterionic nature of the λ^5*Si*-silicates, accounts for this remarkable hydrolytic stability. As this particular diolato(2–) ligand can be regarded as a model system for related diolato(2–) ligands derived from carbohydrates with *cis*-furanoidic diol moieties, the chemistry of hydrolytically stable pentacoordinate silicon compounds in aqueous solution appears to be expandable. The hydrolytic stability under neutral (pH 7.0) and physiological (pH 7.4) conditions is an especially challenging feature of this chemistry.

Some insight into the dynamic stereochemistry of the zwitterionic λ^5*Si*-silicates **13**–**16** was gained through VT ^{1}H NMR experiments with solutions of **16** in organic solvents (CD_2Cl_2, CD_3CN, [D_6]DMSO) in combination with quantum-chemical studies of the related anionic model system **II**.

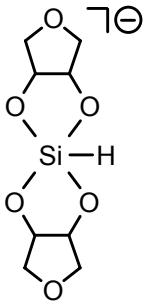

II

Zwitterionic λ^5*Si*-Silicates with Ligands Derived from Benzoin

The already existent zwitterionic λ^5*Si*-silicate **17** was synthesized by new methods, including a remarkable Si–C cleavage reaction with benzoin. To investigate the dynamic behavior of the known zwitterionic λ^5*Si*-silicate **18** in solution, VT ^{1}H NMR experiments in CD_2Cl_2 were performed in the temperature range –100 °C to 23 °C.

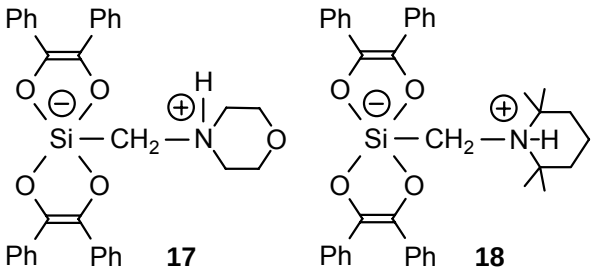

17 **18**

Anionic λ^6*Si*-Silicates with Ligands Derived from Citric Acid or (*S*)-Malic Acid

The hexacoordinate silicon compounds **19**–**22** containing multidentate ligands derived from citric acid or (*S*)-malic acid were synthesized for the first time. The anionic λ^6*Si*-silicates **19**–**22** were structurally characterized in the solid state by single-crystal X-ray diffraction and VACP/MAS NMR spectroscopy (^{13}C, ^{15}N, ^{29}Si). Upon dissolution in water at 20 °C, spontaneous hydrolysis of the λ^6*Si*-silicate anions was observed.

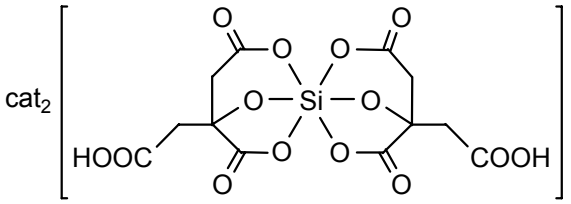

19

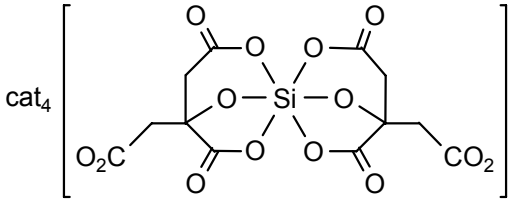

20

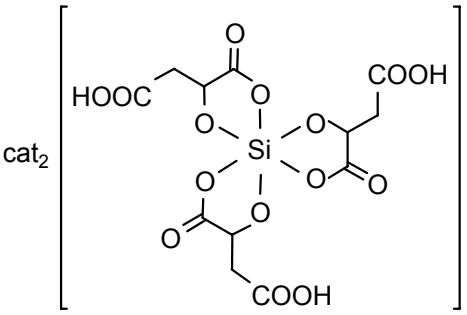

21, **22**

	cat ⊕
19, **20**	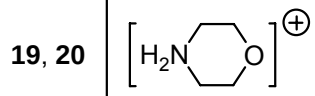
21	$[HN(n\text{-}Pr)_3]^{\oplus}$
22	$[HN(n\text{-}Bu)_3]^{\oplus}$

9 Zusammenfassung

Die vorliegende Arbeit stellt einen Beitrag zur Chemie des penta- und hexakoordinierten Siliciums dar. Als wesentliche Ergebnisse dieser Arbeit seien folgende Punkte herausgestellt:

Zwitterionische λ^5*Si*-Silicate mit Liganden, die sich von α-Aminosäuren ableiten

Erstmalig wurden die spirocyclischen zwitterionischen λ^5*Si*-Silicate **1**–**6** synthetisiert und strukturell charakterisiert. In diesen Verbindungen des pentakoordinierten Siliciums sind eine (2,2,6,6-Tetramethylpiperidinio)methyl-Gruppe und zwei identische zweizähnige Chelat-Liganden, die sich von den α-Aminosäuren Glycin, (*S*)-Alanin, (*S*)-Phenylalanin, (*S*)-Valin, (*S*)-*tert*-Leucin oder (*S*)-Prolin ableiten, an das Si(IV)-Koordinationszentrum gebunden.

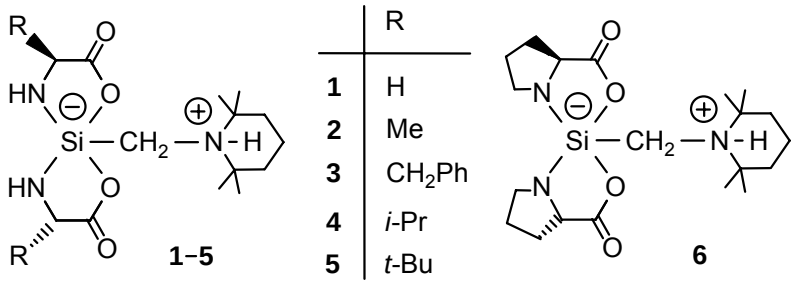

Die Verbindungen **2**–**6** wurden als diastereomeren- und enantiomerenreine kristalline Feststoffe isoliert: (*Δ*,*S*,*S*)-**2**, (*Λ*,*S*,*S*)-**3**·CH_2Cl_2, (*Λ*,*S*,*S*)-**4**·CH_2Cl_2, (*Λ*,*S*,*S*)-**5**·CH_2Cl_2, (*Λ*,*S*,*S*)-**6**·$2CH_2Cl_2$ und (*Λ*,*S*,*S*)-**6**·$½CH_2Cl_2$. Die Charakterisierung von **1**–**6** erfolgte durch Elementaranalysen (C, H, N), Einkristall-Röntgenstrukturanalysen, Festkörper-NMR-Spektroskopie (^{15}N- und ^{29}Si-VACP/MAS-NMR) und NMR-Spektroskopie in Lösung (^{1}H, ^{13}C, ^{15}N und ^{29}Si; einschließlich VT-NMR-Spektroskopie und Kreuzung-Experimenten). Die experimentellen Untersuchungen wurden durch theoretische Studien des anionischen Modellsystems **I** vervollständigt.

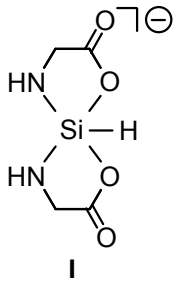

I

Beim Auflösen der diastereomeren- und enantiomerenreinen Verbindungen (*Δ*,*S*,*S*)-**2** bzw. (*Λ*,*S*,*S*)-**3**·CH_2Cl_2 in CD_2Cl_2 wurde jeweils eine (*Λ*)/(*Δ*)-Epimerisierung beobachtet, die zu einer Gleichgewichtseinstellung der entsprechenden (*Λ*,*S*,*S*)- und (*Δ*,*S*,*S*)-Diastereomere

führte, wobei sich zeigte, dass die (*Λ*)-Isomere thermodynamisch stabiler als die (*Δ*)-Isomere sind. Die absolute Konfiguration der entsprechenden Diastereomere konnte bestimmt werden, da die Kinetik der Epimerisierungsprozesse von (*Δ*,*S*,*S*)-**2** und (*Λ*,*S*,*S*)-**3**·CH_2Cl_2 in CD_2Cl_2 mittels ^{1}H-NMR-Spektroskopie beobachtbar war.

Beim Auflösen der Verbindungen (*Λ*,*S*,*S*)-**4**·CH_2Cl_2, (*Λ*,*S*,*S*)-**5**·CH_2Cl_2 und (*Λ*,*S*,*S*)-**6**·$2CH_2Cl_2$ in CD_2Cl_2 wurde das Vorliegen nur eines einzigen Diastereomers beobachtet. ^{1}H-VT-NMR Experimente zwischen –100 °C und 23 °C an Lösungen von **4**–**6** in CD_2Cl_2 ergaben keinen Hinweis auf das Vorliegen weiterer Epimere.

Zwitterionische λ^5*Si*-Silicate mit Liganden, die sich von α-Hydroxycarbonsäuren ableiten

Die spirocyclischen zwitterionischen λ^5*Si*-Silicate **7**–**12** mit einer (Ammonio)methyl-Gruppe und zwei identischen Chelat-Liganden, die sich von (*S*)-Milchsäure, (*S*)-3-Phenylmilchsäure oder (*S*)-Mandelsäure ableiten, wurden erstmals synthetisiert. Die strukturelle Charakterisierung erfolgte durch Elementaranalysen (C, H, N), Festkörper-NMR-Spektroskopie (^{15}N- und ^{29}Si-VACP/MAS-NMR) und durch ^{1}H-, ^{13}C-, ^{15}N- und ^{29}Si-NMR-Experimente in Lösung. Die Existenz dieser Verbindungen wurde zusätzlich mittels Röntgenbeugung an Einkristallen bestätigt.

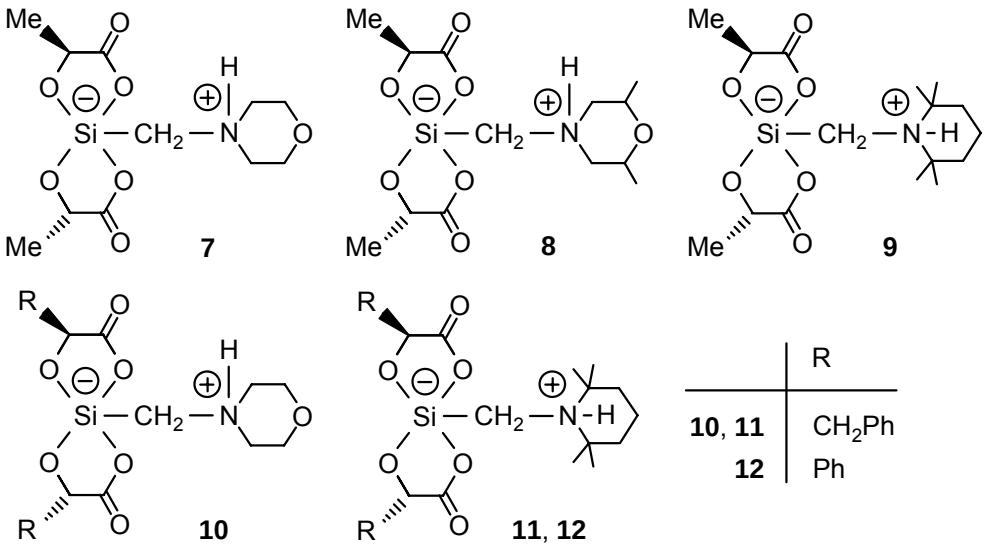

Die λ^5*Si*-Silicate **7**–**12** wurden als diastereomeren- und enantiomerenreine kristalline Feststoffe isoliert: (*Δ*,*S*,*S*)-**7**·CH_3CN, (*Λ*,*S*,*S*)-**8**, (*Δ*,*S*,*S*)-**8**, (*Δ*,*S*,*S*)-**9**, (*Λ*,*S*,*S*)-**10**, (*Λ*,*S*,*S*)-**11**·CH_3CN und (*Λ*,*S*,*S*)-**12**. Beim Auflösen der Verbindungen **7**–**9**, **11** und **12** in CD_2Cl_2 oder [D_6]DMSO epimerisieren diese spontan, bis ein Gleichgewichtsgemisch der entsprechenden (*Λ*,*S*,*S*)- und (*Δ*,*S*,*S*)-Diastereomere entsteht. Die Stereodynamik des Si-Koordinationspolyeders in Lösung wurde mit Hilfe dynamischer NMR-Experimente untersucht. Im Falle

von **7**, **9**, **11** und **12** konnte die Konfiguration der Diastereomere in Lösung nicht aufgeklärt werden. Aufgrund der schnellen Epimerisierung konnten die Prozesse durch ^{1}H-NMR-Spektroskopie nicht verfolgt werden. Sogar beim Auflösen von **7**, **9**, **11** und **12** in CD_2Cl_2 oder CD_3CN bei tiefen Temperaturen (–90 °C oder –40 °C) konnte jeweils nur eine spontane Gleichgewichtseinstellung beobachtet werden. Interessanterweise gelang im Falle von **8** die Bestimmung der absoluten Konfiguration der entsprechenden Diastereomere in Lösung, da die Kinetik des Epimerisierungs-Prozesses am Silicium-Atom beim Auflösen von (*Λ*,*S*,*S*)-**8** oder (*Δ*,*S*,*S*)-**8** in CD_2Cl_2 durch ^{1}H-VT-NMR-Spektroskopie bei tiefen Temperaturen (zwischen –94 °C und 23 °C) verfolgt werden konnte.

Zwitterionische λ^5*Si*-Silicate mit Liganden, die sich von *meso*-Oxolan-3,4-diol ableiten

Die bisher unbekannten spirocyclischen zwitterionischen λ^5*Si*-Silicate **13**, **15** und **16** mit einer (Ammonio)methyl-Gruppe und zwei identischen zweizähnigen *meso*-Oxolan-3,4-diolato(2–)-Liganden wurden synthetisiert. Die bereits bekannte Verbindung **14** wurde zur Anfertigung einer Kristallstrukturanalyse resynthetisiert. Die λ^5*Si*-Silicate **13**–**16** wurden mit Hilfe elementaranalytischer (C, H, N), NMR-spektroskopischer Methoden (^{29}Si-VACP/MAS-NMR; ^{1}H-, ^{13}C-, ^{15}N- bzw. ^{29}Si-NMR) charakterisiert. Die Verbindungen **14–16** wurden zusätzlich durch Einkristall-Röntgenstrukturanalysen charakterisiert.

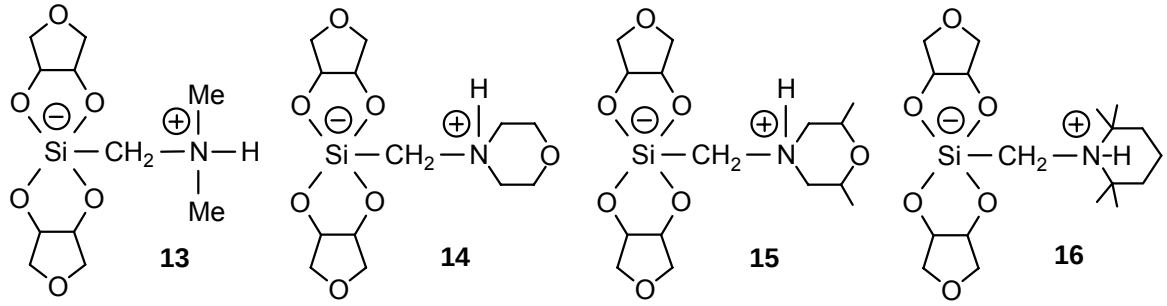

Beim Auflösen von **13–16** in Wasser wurden Gleichgewichtsgemische der entsprechenden *syn*/*syn*-, *syn*/*anti*-, and *anti*/*anti*-Isomere beobachtet und pH-Werte von pH > 7 gemessen. Überraschenderweise sind die zwitterionischen λ^5*Si*-Silicate **13**–**16** in wässriger Lösung stabil (keine Hydrolyse im untersuchten pH-Bereich: **13**, pH 7.0–8.9; **14**, pH 7.0–8.0; **15**, pH 7.0–8.4; **16**, pH 7.0–9.2) und konnten sogar in Wasser synthetisiert werden. Offensichtlich tragen besondere strukturelle und/oder elektronische Merkmale des *meso*-Oxolan-3,4-diolato(2–)-Liganden und die zwitterionische Natur der λ^5*Si*-Silicate zu dieser außerordentlichen hydrolytischen Stabilität bei. Dieser Diolato(2–)-Ligand kann als ein Modell für ähnliche Diolato(2–)-Liganden aufgefasst werden, die sich von Kohlenhydraten mit *cis*-furanoiden Diol-Funktionen ableiten. Die Chemie hydrolysestabiler Verbindungen des

pentakoordinierten Siliciums zeigt damit ein vielversprechendes Potential, wobei die hydrolytische Stabilität unter neutralen (pH 7.0) und physiologischen (pH 7.4) Bedingungen eine besonders interessante Facette dieser Chemie darstellt.

^{1}H-VT-NMR-Experimente von **16** in Lösung in Kombination mit quantenchemichen Untersuchungen an dem verwandten anionischen Modell **II** verschaffen Einblicke in die dynamische Stereochemie der zwitterionischen λ^5*Si*-Silicate **13**–**16**.

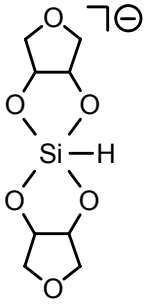

II

Zwitterionische λ^5*Si*-Silicate mit Liganden, die sich vom Benzoin ableiten

Das bereits bekannte zwitterionische λ^5*Si*-Silicat **17** war über neue Syntheserouten zugänglich, die neben Si–O- auch eine bemerkenswerte Si–C-Bindungspaltungsreaktion unter milden Bedingungen beinhalten. Um mehr über das dynamische Verhalten des bereits bekannten zwitterionischen λ^5*Si*-Silicats **18** in Lösung zu erfahren, wurden ^{1}H-VT-NMR-Experimente in dem Temperaturbereich zwischen –100 °C und 23 °C durchgeführt.

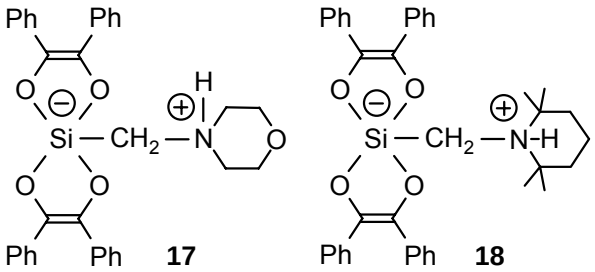

17 **18**

Anionische λ^6*Si*-Silicate mit Liganden, die sich von Zitronensäure oder (*S*)-Äpfelsäure ableiten

Die hexakoordinierten Verbindungen **19**–**22** mit mehrzähnigen Liganden, die sich von Zitronensäure oder (*S*)-Äpfelsäure ableiten, wurden erstmalig synthetisiert. Die anionischen λ^6*Si*-Silicate **19**–**22** wurden durch Einkristall-Röntgenstrukturanalysen und Festkörper-NMR-spektroskopische Untersuchungen (^{13}C-, ^{15}N- bzw. ^{29}Si- VACP/MAS-NMR) strukturell

charakterisiert. Beim Auflösen der Verbindungen **19**–**22** in Wasser bei 20 °C wurde jeweils eine spontane Hydrolyse der λ^6*Si*-Silicat-Anionen beobachtet.

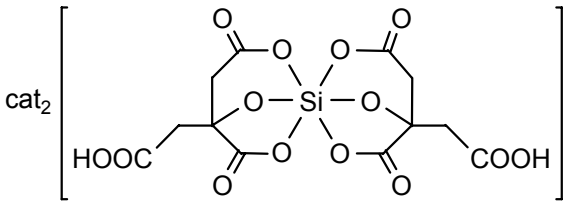

19

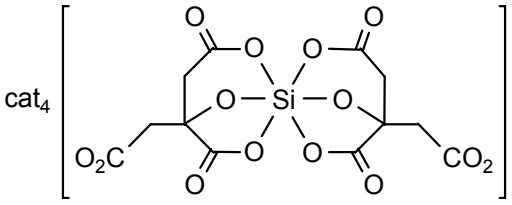

20

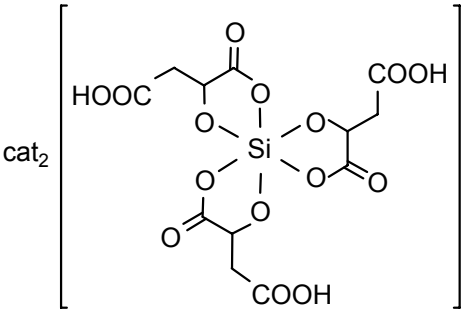

21, **22**

	cat ⊕
19, **20**	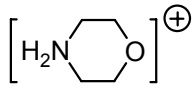
21	$[HN(n\text{-}Pr)_3]^{\oplus}$
22	$[HN(n\text{-}Bu)_3]^{\oplus}$

10 Experimental Section

10.1 General Procedures

All syntheses (except for compounds **13**–**16**) were carried out under dry argon or dry nitrogen. The organic solvents used were dried and purified according to standard procedures and stored under dry nitrogen. The melting points were determined with a Büchi Melting Point B-540 apparatus using samples in sealed capillaries. The pH measurements were performed with a Mettler Toledo MP220 pH meter using a Toledo InLab410 electrode. The elemental analyses were determined with a Leco CHNS-932 apparatus (Leco Instruments).

The ^{1}H, ^{13}C, ^{15}N, and ^{29}Si solution NMR spectra were recorded at 23 °C on a Bruker DRX-300 NMR spectrometer (^{1}H, 300.1 MHz; ^{13}C, 75.5 MHz; ^{15}N, 30.4 MHz; ^{29}Si, 59.6 MHz) or on a Bruker AVANCE-400 NMR spectrometer (^{1}H, 400.1 MHz; ^{13}C, 100.6 MHz; ^{29}Si, 79.5 MHz). Additionally, the ^{1}H and ^{13}C solution NMR spectra of several compounds were recorded at 24 °C on a Bruker DMX-600 NMR spectrometer (^{1}H, 600.1 MHz; ^{13}C, 150.9 MHz). $CDCl_3$, CD_2Cl_2, CD_3CN, [D_6]DMSO, and D_2O were used as the solvents. Chemical shifts (ppm) were determined relative to internal $CHCl_3$ (^{1}H, δ 7.24; $CDCl_3$), $CDHCl_2$ (^{1}H, δ 5.32; CD_2Cl_2), CD_2HCN (^{1}H, δ 1.93; CD_3CN), [D_5]DMSO (^{1}H, δ 2.49; [D_6]DMSO), HDO (^{1}H, δ 4.70; D_2O), $CDCl_3$ (^{13}C, δ 77.0; $CDCl_3$), CD_2Cl_2 (^{13}C, δ 53.8; CD_2Cl_2), CD_3CN (^{13}C, δ 1.3; CD_3CN), [D_6]DMSO (^{13}C, δ 39.5; [D_6]DMSO), external formamide (^{15}N, δ –268.0; $CDCl_3$, CD_2Cl_2, CD_3CN, [D_6]DMSO), or external TMS (^{13}C, δ 0; D_2O; ^{29}Si, δ 0; CD_2Cl_2, CD_3CN, [D_6]DMSO, and D_2O). Analysis and assignment of the ^{1}H NMR data was supported by ^{1}H,^{1}H COSY and ^{13}C,^{1}H, ^{15}N,^{1}H, and ^{29}Si,^{1}H correlation experiments, and the ^{1}H spin systems were partially analyzed by using the program WIN-DAISY 4.05.[44] The $^{2}J_{AB}$ geminal coupling constants reported for the AB parts of the spin systems studied represent absolute values. Assignment of the ^{13}C NMR data was supported by DEPT 135 experiments. The thermocouple used with the probe in the VT ^{1}H NMR experiments was calibrated for low temperatures according to ref. 45a using a 4 % solution of CH_3OH in CD_3OD, and for high temperatures according to ref. 45b using a 80 % solution of ethane-1,2-diol in [D_6]DMSO. The VT ^{1}H NMR spectra were recorded in the temperature ranges 173–296 K (CD_2Cl_2), 233–343 K (CD_3CN), or 296–393 K ([D_6]DMSO); the time required for temperature equilibration was 15 min. Solid-state ^{13}C, ^{15}N, and ^{29}Si VACP/MAS NMR spectra were recorded at 22 °C on a Bruker DSX-400 NMR spectrometer with bottom layer rotors of ZrO_2 (diameter, 7 mm) containing ca. 300 mg of sample (^{13}C, 100.6 MHz; ^{15}N, 40.6 MHz; ^{29}Si, 79.5 MHz; external standard, TMS (^{13}C, ^{29}Si; $\delta = 0$) or glycine (^{15}N, $\delta =$

–342.0); spinning rate, 5–6 kHz; contact time, 1 ms (^{13}C), 3 ms (^{15}N), or 5 ms (^{29}Si); 90° ^{1}H transmitter pulse length, 3.6 μs; repetition time, 4 s).

10.2 Syntheses

Preparation of *rac*-Bis[glycinato(2–)-*N*,*O*][(2,2,6,6-tetramethylpiperidinio)methyl]silicate (*rac*-1). Compound **23** (2.00 g, 10.8 mmol) was added at 20 °C to a stirred suspension of glycine (1.62 g, 21.6 mmol) in dichloromethane (10 mL), and the mixture was stirred at this temperature for 24 h (evolution of hydrogen). The remaining solid was separated by filtration and discarded, *n*-pentane (25 mL) was added to the filtrate, and the resulting solution was kept undisturbed at –20 °C for 48 h (formation of crystals). The precipitate was isolated by filtration and dried in vacuo (0.01 Torr, 60 °C, 2 days) to give *rac*-**1** in 72% yield as a colorless crystalline product (2.56 g, 7.77 mmol); mp 162 °C (dec). ^{15}N VACP/MAS NMR (22 °C, ν_{rot} = 5 kHz) δ –353.1 (SiNHC), –352.4 (SiNHC) –290.6 (C_3NH); ^{29}Si VACP/MAS NMR (22 °C, ν_{rot} = 5 kHz) δ –94.1 to –91.8 (m); ^{1}H NMR (CD_2Cl_2, c = 81 mM, 23 °C, 300.1 MHz) δ 1.28 (br s, 2 H, SiNHC), 1.30 (s, 3 H, CCH_3), 1.33 (s, 6 H, CCH_3), 1.49 (s, 3 H, CCH_3), 1.53–1.92 (m, 6 H, CCH_2C), 2.37 (δ_A) and 2.62 (δ_B) (AB part of an ABX system, $^{2}J_{AB}$ = 16.5 Hz, $^{3}J_{AX}$ = 3.9 Hz, $^{3}J_{BX}$ = 3.5 Hz, 2 H, $SiCH_AH_BNH_X$), 3.44 (δ_A) and 3.59 (δ_B) (AB part of an ABX system, $^{2}J_{AB}$ = 16.9 Hz, $^{3}J_{AX}$ = 0.7 Hz, $^{3}J_{BX}$ = 2.0 Hz, 4 H, $CCH_AH_BNH_XSi$), 5.8 (br s, 1 H, C_3NH); ^{13}C NMR (CD_2Cl_2, c = 81 mM, 23 °C, 75.5 MHz) δ 16.0 ($NCCCH_2C$), 20.1 (CCH_3), 20.3 (CCH_3), 29.8 (CCH_3), 30.9 (CCH_3), 39.5 ($NCCH_2C$), 39.7 ($NCCH_2C$), 40.5 ($SiCH_2N$), 46.5 (NCH_2C), 65.1 (NCC_3), 65.4 (NCC_3), 176.1 (C=O); ^{15}N NMR (CD_2Cl_2, c = 81 mM, 23 °C) δ –357.5 (SiNHC), –298.5 (C_3NH); ^{29}Si NMR (CD_2Cl_2, c = 81 mM, 23 °C, 59.6 MHz) δ –91.9. Anal. Calcd for $C_{14}H_{27}N_3O_4Si$: C, 51.04; H, 8.26; N, 12.75. Found: C, 50.3; H, 7.8; N, 11.8.[46]

Preparation of (*Δ*,*S*,*S*)-Bis[alaninato(2–)-*N*,*O*][(2,2,6,6-tetramethylpiperidinio)methyl]-silicate (2b). Compound **23** (500 mg, 2.70 mmol) was added at 20 °C to a stirred suspension of (*S*)-alanine (481 mg, 5.40 mmol) in dichloromethane (8 mL), and the mixture was stirred at this temperature for 48 h (evolution of hydrogen). The remaining solid was separated by filtration and discarded, *n*-pentane (30 mL) was added to the filtrate, and the resulting solution was kept undisturbed at –20 °C for 24 h (formation of crystals). The precipitate was isolated by filtration and dried in vacuo (0.01 Torr, 60 °C, 2 days) to give **2b** in 83% yield as a

colorless crystalline product (800 mg, 2.24 mmol); mp 250 °C (dec). ^{15}N VACP/MAS NMR (22 °C, ν_{rot} = 5 kHz) δ –334.3 (2 N, SiNHC), –290.3 (C_3NH); ^{29}Si VACP/MAS NMR (22 °C, ν_{rot} = 5 kHz) δ –100.5 to –98.0 (m). Upon dissolution of **2b** in CD_2Cl_2 (c = 30 mM) at 23 °C, epimerization occurred (establishment of an equilibrium, with a molar ratio **2a**:**2b** = 0.71:0.29). NMR data for **2a**: ^{1}H NMR (CD_2Cl_2, 23 °C, 300.1 MHz) δ 1.24 (d, $^3J_{HH}$ = 6.8 Hz, 6 H, NCHCH_3), 1.30 (s, 3 H, CCH_3), 1.32 (s, 6 H, CCH_3), 1.38 (br s, 2 H, SiNHC), 1.49 (s, 3 H, CCH_3), 1.56–1.92 (m, 6 H, CCH_2C), 2.35 (δ_A) and 2.60 (δ_B) (AB part of an ABX system, $^2J_{AB}$ = 16.4 Hz, $^3J_{AX}$ = 3.8 Hz, $^3J_{BX}$ = 3.5 Hz, 2 H, $SiCH_AH_BNH_X$), 3.56 (q, $^3J_{HH}$ = 6.8 Hz, 2 H, NCHCH$_3$), 5.9 (br s, 1 H, C_3NH); ^{13}C NMR (CD_2Cl_2, 23 °C, 75.5 MHz) δ 16.0 (NCCCH$_2$C), 20.1 (CCH$_3$), 20.3 (CCH$_3$), 23.6 (NCHCH$_3$), 30.0 (CCH$_3$), 31.0 (CCH$_3$), 39.5 (NCCH$_2$C), 39.7 (NCCH$_2$C), 40.6 (SiCH$_2$N), 52.4 (NCHCH$_3$), 64.9 (NCC_3), 65.3 (NCC_3), 178.9 (C=O); ^{15}N NMR (CD_2Cl_2, 23 °C) δ –337.5 (SiNHC), –298.5 (C_3NH); ^{29}Si NMR (CD_2Cl_2, 23 °C, 59.6 MHz) δ –97.1. NMR data for **2b**: ^{1}H NMR (CD_2Cl_2, 23 °C, 300.1 MHz) δ 1.19 (d, $^3J_{HH}$ = 6.8 Hz, 6 H, NCHCH_3), 1.32 (s, 6 H, CCH_3), 1.34 (s, 3 H, CCH_3), 1.39 (br s, 2 H, SiNHC), 1.55 (s, 3 H, CCH_3), 1.56–1.92 (m, 6 H, CCH_2C), 2.33 (δ_A) and 2.68 (δ_B) (AB part of an ABX system, $^2J_{AB}$ = 16.5 Hz, $^3J_{AX}$ = 3.9 Hz, $^3J_{BX}$ = 3.3 Hz, 2 H, $SiCH_AH_BNH_X$), 3.76 (A part of an AMX_3 system, $^3J_{AX}$ = 6.8 Hz, $^3J_{AM}$ = 2.1 Hz, 2 H, $H_MNCH_AC(H_x)_3$), 6.0 (br s, 1 H, C_3NH); ^{13}C NMR (CD_2Cl_2, 23 °C, 75.5 MHz) δ 16.0 (NCCCH$_2$C), 20.1 (CCH$_3$), 20.4 (CCH$_3$), 21.9 (NCHCH$_3$), 31.4 (CCH$_3$), 31.6 (CCH$_3$), 39.6 (NCCH$_2$C), 39.7 (NCCH$_2$C), 41.5 (SiCH$_2$N), 51.6 (NCHCH$_3$), 64.9 (NCC_3), 65.1 (NCC_3), 178.7 (C=O); ^{15}N NMR (CD_2Cl_2, 23 °C) δ –337.5 (SiNHC), –299.5 (C_3NH); ^{29}Si NMR (CD_2Cl_2, 23 °C, 59.6 MHz) δ –98.4. Anal. Calcd for $C_{16}H_{31}N_3O_4Si$: C, 53.75; H, 8.74; N, 11.75. Found: C, 53.0; H, 8.5; N, 11.6. [46]

Preparation of (*Λ*,*S*,*S*)-Bis[phenylalaninato(2–)-*N*,*O*][(2,2,6,6-tetramethylpiperidinio)-methyl]silicate–Dichloromethane (3a·CH_2Cl_2). Compound **23** (1.00 g, 5.39 mmol) was added at 20 °C to a stirred suspension of (*S*)-phenylalanine (1.78 g, 10.8 mmol) in dichloromethane (15 mL), and the mixture was stirred at this temperature for 48 h (evolution of hydrogen). The remaining solid was separated by filtration and discarded, *n*-pentane (35 mL) was added to the filtrate, and the resulting solution was kept undisturbed at 20 °C for 6 h (formation of crystals). The precipitate was isolated by filtration and dried in a nitrogen gas stream (20 °C, 1 h) to give **3a**·CH_2Cl_2 in 77% yield as a colorless crystalline solid (2.47 g, 4.15 mmol); mp 193 °C (dec). ^{15}N VACP/MAS NMR (22 °C, ν_{rot} = 5 kHz) δ –335.6 (SiNHC), –334.7 (SiNHC) –291.7 (C_3NH); ^{29}Si VACP/MAS NMR (22 °C, ν_{rot} = 5 kHz) δ –98.5 to –96.0 (m). Upon dissolution of **3a**·CH_2Cl_2 in CD_2Cl_2 (c = 78 mM) at 23 °C,

epimerization occurred (establishment of an equilibrium, with a molar ratio **3a**:**3b** = 0.73:0.27). NMR data for **3a**: ^{1}H NMR (CD_2Cl_2, 23 °C, 300.1 MHz) δ 1.27 (s, 3 H, CCH_3), 1.30 (s, 6 H, CCH_3), 1.40 (s, 3 H, CCH_3), 1.44 (br s, 2 H, SiNHC), 1.55–1.95 (m, 6 H, CCH_2C), 2.33 (δ_A) and 2.57 (δ_B) (AB part of an ABX system, $^{2}J_{AB}$= 16.6 Hz, $^{3}J_{AX}$ = 3.8 Hz, $^{3}J_{BX}$ = 3.5 Hz, 2 H, $SiCH_AH_BNH_X$), 2.58 (δ_A), 3.22 (δ_B), and 3.71 (δ_X) (ABX system, $^{2}J_{AB}$ = 13.1 Hz, $^{3}J_{AX}$ = 9.9 Hz, $^{3}J_{BX}$ = 3.3 Hz, 6 H, $CCH_AH_BCH_X$), 5.8 (br s, 1 H, C_3NH), 7.13–7.36 (m, 10 H, C_6H_5); ^{13}C NMR (CD_2Cl_2, 23 °C, 75.5 MHz) δ 16.0 (NCC*C*H_2C), 20.1 (C*C*H_3), 20.3 (C*C*H_3), 30.0 (C*C*H_3), 31.1 (C*C*H_3), 39.6 (NC*C*H_2C), 39.7 (NC*C*H_2C), 40.7 (Si*C*H_2N), 44.0 (NCH*C*H_2C), 58.7 (N*C*HCH$_2$C), 65.0 (N*C*C_3), 65.3 (N*C*C_3), 126.6 (C4, C_6H_5), 128.8 (C2/C6, C_6H_5), 129.7 (C3/C5, C_6H_5), 139.7 (C1, C_6H_5), 177.3 (*C*=O); ^{15}N NMR (CD_2Cl_2, 23 °C) δ –344.0 (SiNHC), –297.5 (C_3NH); ^{29}Si NMR (CD_2Cl_2, 23 °C, 59.6 MHz) δ –97.36. NMR data for **3b**: ^{1}H NMR (CD_2Cl_2, 23 °C) δ 1.30 (s, 3 H, CCH_3), 1.31 (br s, 2 H, SiNHC), 1.35 (s, 3 H, CCH_3), 1.42 (s, 3 H, CCH_3), 1.46 (s, 3 H, CCH_3), 1.55–1.95 (m, 6 H, CCH_2C), 2.25 (δ_A) and 2.67 (δ_B) (AB part of an ABX system, $^{2}J_{AB}$ = 16.5 Hz, $^{3}J_{AX}$ = 3.9 Hz, $^{3}J_{BX}$ = 3.4 Hz, 2 H, $SiCH_AH_BNH_X$), 2.44 (δ_A), 3.19 (δ_B), and 3.83 (δ_X) (ABX part of an ABXY system, $^{2}J_{AB}$ = 13.2 Hz, $^{3}J_{AX}$ = 10.0 Hz, $^{3}J_{BX}$ = 3.3 Hz, $^{3}J_{XY}$ = 1.6 Hz, 6 H, $CCH_AH_BCH_XNH_Y$), 5.9 (br s, 1 H, C_3NH), 7.13–7.36 (m, 10 H, C_6H_5); ^{13}C NMR (CD_2Cl_2, 23 °C, 75.5 MHz) δ 16.0 (NCC*C*H_2C), 20.2 (C*C*H_3), 20.4 (C*C*H_3), 31.6 (C*C*H_3), 31.7 (C*C*H_3), 39.6 (NC*C*H_2C), 39.8 (NC*C*H_2C), 41.1 (Si*C*H_2N), 42.0 (NCH*C*H_2C), 58.0 (N*C*HCH$_2$C), 65.0 (N*C*C_3), 65.2 (N*C*C_3), 126.5 (C4, C_6H_5), 128.8 (C2/C6, C_6H_5), 129.5 (C3/C5, C_6H_5), 140.1 (C1, C_6H_5), 177.1 (*C*=O); ^{15}N NMR (CD_2Cl_2, 23 °C) δ –345.0 (SiNHC), –297.5 (C_3NH); ^{29}Si NMR (CD_2Cl_2, 23 °C, 59.6 MHz) δ –97.45. Anal. Calcd for $C_{29}H_{41}Cl_2N_3O_4Si$: C, 58.58; H, 6.95; N, 7.07. Found: C, 58.2; H, 6.7; N, 7.0.

Preparation of (*Λ*,*S*,*S*)-Bis[valinato(2–)-*N*,*O*][(2,2,6,6-tetramethylpiperidinio)methyl]-silicate–Dichloromethane (4a·CH_2Cl_2). Compound **23** (500 mg, 2.70 mmol) was added at 20 °C to a stirred suspension of (*S*)-valine (633 mg, 5.40 mmol) in dichloromethane (10 mL), and the resulting mixture was stirred at this temperature for 12 h (evolution of hydrogen). The remaining solid was separated by filtration and discarded, *n*-pentane (40 mL) was added to the filtrate, and the resulting solution was kept undisturbed at 20 °C for 12 h (formation of crystals). The precipitate was isolated by filtration and dried in an argon stream (20 °C, 15 min) to give **4a**·CH_2Cl_2 in 72% yield as a colorless crystalline solid (967 mg, 1.94 mmol); mp 187 °C (dec). ^{15}N VACP/MAS NMR (22 °C, ν_{rot} = 5 kHz) δ –349.8 to –345.0 (m, SiNHC), –301.7 (br s, C_3NH); ^{29}Si VACP/MAS NMR (22 °C, ν_{rot} = 6.5 kHz) δ –98.8 to –95.6 (m); ^{1}H

NMR (CD_2Cl_2, 23 °C) δ 0.86 (δ_A), 0.92 (δ_B), 1.32 (δ_F), 1.96 (δ_M), and 3.44 (δ_X) (A_3B_3FMX system, $^3J_{AM}$ = 6.7 Hz, $^3J_{BM}$ = 7.0 Hz, $^3J_{MX}$ = 3.2 Hz, $^3J_{FX}$ = 4.1 Hz, 18 H, $C(H_A)_3C(H_B)_3CH_MCH_XNH_F$), 1.32 (s, 3 H, CCH_3), 1.33 (s, 3 H, CCH_3), 1.49 (s, 3 H, CCH_3), 1.55 (s, 3 H, CCH_3), 1.54–1.90 (m, 6 H, CCH_2C), 2.31 (δ_A) and 2.61 (δ_B) (AB part of an ABX system, $^2J_{AB}$ = 16.4 Hz, $^3J_{AX}$ = 3.9 Hz, $^3J_{BX}$ = 3.4 Hz, 2 H, $SiCH_AH_BNH_X$), 5.8 (br s, 1 H, C_3NH); ^{13}C NMR (CD_2Cl_2, 23 °C) δ 16.1 (NCC*C*H_2C), 17.1 (CH*C*H_3), 19.7 (CH*C*H_3), 20.1 (C*C*H_3), 20.4 (C*C*H_3), 30.0 (C*C*H_3), 31.1 (C*C*H_3), 32.7 (C*C*HC_2), 39.6 (NC*C*H_2C), 39.8 (NC*C*H_2C), 40.9 (Si*C*H_2N), 62.6 (SiN*C*HC_2), 65.0 (N*C*C_3), 65.3 (N*C*C_3), 177.7 (*C*=O); ^{15}N NMR (CD_2Cl_2, 23 °C) δ –350.5 (SiNHC), –292.0 (C_3NH); ^{29}Si NMR (CD_2Cl_2, 23 °C) δ –98.0. Anal. Calcd for $C_{21}H_{41}Cl_2N_3O_4Si$: C, 50.59; H, 8.29; N, 8.43. Found: C, 50.6; H, 8.1; N, 8.2.

Preparation of (*Λ*,*S*,*S*)-Bis[*tert*-leucinato(2–)-*N*,*O*][(2,2,6,6-tetramethylpiperidinio)-methyl]silicate–Dichloromethane (5a·CH_2Cl_2). Compound **23** (500 mg, 2.70 mmol) was added at 20 °C to a stirred suspension of (*S*)-*tert*-leucine (708 mg, 5.40 mmol) in dichloromethane (10 mL), and the resulting mixture was stirred at this temperature for 6 h (evolution of hydrogen). The remaining solid was separated by filtration and discarded, *n*-pentane (40 mL) was added to the filtrate, and the resulting solution was kept undisturbed at 20 °C for 12 h (formation of crystals). The precipitate was isolated by filtration and dried in an argon stream (20 °C, 15 min) to give **5a**·CH_2Cl_2 in 78% yield as a colorless crystalline solid (1.11 g, 2.11 mmol); mp 168 °C (dec). ^{15}N VACP/MAS NMR (22 °C, ν_{rot} = 5 kHz) δ –341.4 (br s, SiNHC), –292.4 (br s, C_3NH); ^{29}Si VACP/MAS NMR (22 °C, ν_{rot} = 5 kHz) δ –101.2 to –99.1 (m); ^{1}H NMR (CD_2Cl_2, 23 °C) δ 0.97 (s, 18 H, CHCC*H*$_3$), 1.315 (s, 3 H, CCH_3), 1.320 (s, 6 H, CCH_3), 1.49 (s, 3 H, CCH_3), 1.49 (s, 2 H, SiNHC), 1.57–1.92 (m, 6 H, CCH_2C), 2.27 (δ_A) and 2.58 (δ_B) (AB part of an ABX system, $^2J_{AB}$ = 16.4 Hz, $^3J_{AX}$ = 3.8 Hz, $^3J_{BX}$ = 3.4 Hz, 2 H, $SiCH_AH_BNH_X$), 3.25 (d, $^3J_{HH}$ = 1.7 Hz, 2 H, $SiNCHC_2$), 5.9 (br s, 1 H, C_3NH); ^{13}C NMR (CD_2Cl_2, 23 °C) δ 16.1 (NCC*C*H_2C), 20.3 (C*C*H_3), 20.4 (C*C*H_3), 26.4 (C(*C*H_3)$_3$), 29.9 (C*C*H_3), 31.0 (C*C*H_3), 35.2 (SiN*C*HC_2), 39.66 (NC*C*H_2C), 39.72 (NC*C*H_2C), 41.0 (Si*C*H_2N), 64.9 (N*C*C_3), 65.3 (N*C*C_3), 66.4 (CH*C*C), 176.8 (*C*=O); ^{15}N NMR (CD_2Cl_2, 23 °C) δ –340.7 (SiNHC), –292.7 (C_3NH); ^{29}Si NMR (CD_2Cl_2, 23 °C) δ –100.3. Anal. Calcd for $C_{23}H_{45}Cl_2N_3O_4Si$: C, 52.46; H, 8.61; N, 7.98. Found: C, 52.7; H, 8.3; N, 8.0.

Preparation of (*Λ*,*S*,*S*)-Bis[prolinato(2–)-*N*,*O*][(2,2,6,6-tetramethylpiperidinio)methyl]-silicate–(Bis)dichloromethane (6a·2CH_2Cl_2). Compound **23** (1.00 g, 5.39 mmol) was added

at 20 °C to a stirred suspension of (*S*)-proline (1.24 g, 10.78 mmol) in dichloromethane (15 mL). The reaction mixture was stirred at 20 °C for 5 days (evolution of hydrogen). The remaining solid was separated by filtration and discarded, the solvent of the filtrate was partially removed under reduced pressure (→ ca. 7 mL), *n*-pentane (30 mL) was added, and the resulting solution was kept undisturbed at 20 °C for 2 days (formation of crystals). The precipitate was isolated by filtration and dried in an argon gas stream (20 °C, 15 min) to give **6a**·2CH_2Cl_2 in 83% yield as a colorless crystalline product (2.59 g, 4.47 mmol); mp 122 °C (dec). ^{15}N VACP/MAS NMR (22 °C, ν_{rot} = 7 kHz) δ –332.3 (SiNHC), –324.9 (SiNHC), –293.3 (C_3NH); ^{29}Si VACP/MAS NMR (22 °C, ν_{rot} = 5 kHz) δ –97.5 to–95.0 (m); ^{1}H NMR (CD_2Cl_2, 23 °C, 300.1 MHz) δ 1.28 (s, 3 H, CCH_3), 1.29 (s, 6 H, CCH_3), 1.37–1.51 and 1.91–2.04 (m, 4 H, NCHCH_2C), 1.43 (s, 3 H, CCH_3), 1.54–1.91 (m, 6 H, CCH_2C), 1.55–1.71 (m, 4 H, $SiNCCH_2C$), 2.32 (δ_A), 2.57 (δ_B) (ABX system, $^2J_{AB}$ = 16.6 Hz, $^3J_{AX}$ = 4.0 Hz, $^3J_{BX}$ = 3.2 Hz, 2 H, $SiCH_AH_BNH_X$), 2.69–2.80 and 3.06–3.16 (m, 4 H, NCH_2C), 3.53 (m, 2 H, NCHC), 6.0 (br s, 1 H, NH); ^{13}C NMR (CD_2Cl_2, 23 °C, 75.5 MHz) δ 16.0 (NCCCH_2C), 20.1 (CCH_3), 20.3 (CCH_3), 27.1 (NCH$_2CH_2$C), 29.9 (CCH_3), 30.3 (CCH_3), 30.5 (NCHCH_2C), 39.5 (NCCH_2C), 39.6 (NCCH_2C), 40.6 (SiCH_2N), 46.7 (NCH_2C), 64.0 (NCHC), 64.8 (NCC_3), 65.3 (NCC_3), 177.3 (C=O); ^{15}N NMR (CD_2Cl_2, 23 °C) δ –332.0 (SiNHC), –298.5 (C_3NH); ^{29}Si NMR (CD_2Cl_2, 23 °C, 59.6 MHz) δ –97.8. Anal. Calcd for $C_{22}H_{39}Cl_4N_3O_4Si$: C, 45.60; H, 6.78; N, 7.25. Found: C, 45.8; H, 7.0; N, 7.4.

Preparation of (*Λ*,*S*,*S*)-Bis[prolinato(2–)-*N*,*O*][(2,2,6,6-tetramethylpiperidinio)methyl]-silicate–Hemidichloromethane (6a·½CH_2Cl_2). Compound **23** (1.00 g, 5.39 mmol) was added at 20 °C to a stirred suspension of (*S*)-proline (1.24 g, 10.78 mmol) in dichloromethane (10 mL), and the reaction mixture was stirred at this temperature for 2 days (evolution of hydrogen). The remaining solid was separated by filtration and discarded, *n*-pentane (40 mL) was added to the filtrate, and the resulting solution was kept undisturbed at 20 °C for 12 h (formation of crystals). The precipitate was isolated by filtration and dried in an argon stream (20 °C, 5 min) to give **6a**·½CH_2Cl_2 in 81% yield as a colorless crystalline product (1.98 g, 4.37 mmol); mp 122 °C (dec). ^{15}N VACP/MAS NMR (22 °C, ν_{rot} = 5 kHz) δ –328.1 (SiNHC), –324.4 (SiNHC), –322.0 (SiNHC), –321.3 (SiNHC), –301.3 (C_3NH), –290.1 (C_3NH); ^{29}Si VACP/MAS NMR (22 °C, ν_{rot} = 6.5 kHz) δ –97.0 to–93.0 (m). The NMR data in solution were similar to those obtained for **6a**·2CH_2Cl_2. Anal. Calcd for $C_{20.5}H_{36}ClN_3O_4Si$: C, 54.47; H, 8.03; N, 9.30. Found: C, 54.4; H, 8.1; N, 9.5.

Preparation of (*Δ*,*S*,*S*)-Bis[lactato(2–)-*O*^{1}*O*^{2}]|(morpholinio)methyl]silicate–Acetonitrile (7b·CH_3CN). Compound **25** (500 mg, 2.26 mmol) was added at 20 °C to a solution of (*S*)-lactic acid (407 mg, 4.52 mmol) in tetrahydrofuran (20 mL), and the mixture was stirred for 15 min at this temperature. The resulting precipitate was isolated by filtration and then recrystallized two times from boiling acetonitrile (slow cooling of a boiling saturated solution to 20 °C), and the resulting solid was isolated by filtration and dried in vacuo (0.01 Torr, 20 °C, 4 h) to give **7b**·CH_3CN in 79% yield as a colorless crystalline solid (617 mg, 1.78 mmol); mp 300 °C. ^{15}N VACP/MAS NMR (22 °C, ν_{rot} = 5 kHz) δ –323.7 (C_3NH), –130.6 (CH_3CN); ^{29}Si VACP/MAS NMR (23 °C, ν_{rot} = 5 kHz) δ –94.7. Upon dissolution of **7b**·CH_3CN in [D_6]DMSO (c = 46 mM) at 23 °C, epimerization occurred (establishment of an equilibrium, with a molar ratio major isomer:minor isomer = 0.60:0.40). NMR data for the major isomer: ^{1}H NMR ([D_6]DMSO, 23 °C, 300.1 MHz) δ 1.20 (d, $^3J_{HH}$ = 7.1 Hz , 6 H, CHCH_3), 2.08 (s, 3 H, CH_3CN), 2.52–2.60 (m, 2 H, $SiCH_2N$), 2.92–3.21 and 3.48–3.75 (m, 4 H, NCH_2C), 3.48–3.75 and 3.86–4.01 (m, 4 H, NCH_2CH_2O), 4.09 (q, $^3J_{HH}$ = 6.9 Hz , 2 H, OC$H$$CH_3$), 8.5 (br s, 1 H, NH); ^{13}C NMR ([D_6]DMSO, 23 °C, 75.5 MHz) δ 20.4 (CH$C$$H_3$), 30.6 ($C$$H_3CN$), 48.1 ($SiCH_2N$), 53.6 (N$C$$H_2C$), 63.43 (NCH$_2$$C$$H_2O$), 68.8 (O$CHCH_3$), 98.0 (CH$_3$$C$N), 176.4 ($C$=O); ^{15}N NMR ([D6]DMSO, 23 °C) δ –334.0; ^{29}Si NMR ([D_6]DMSO, 23 °C, 59.6 MHz) δ –95.94. NMR data for the minor isomer: ^{1}H NMR ([D_6]DMSO, 23 °C, 300.1 MHz) δ 1.25 (d, $^3J_{HH}$ = 6.1 Hz, 6 H, CHCH_3), 2.08 (s, 3 H, CH_3CN), 2.47–2.56 and 2.65–2.75 (m, 2 H, $SiCH_2N$), 2.92–3.21 (m, 4 H, NCH_2C), 3.48–3.75 and 3.86–4.01 (m, 4 H, NCH$_2$CH_2O), 4.09 (q, $^3J_{HH}$ = 6.9 Hz , 2 H, OC$H$$CH_3$), 8.5 (br s, 1 H, NH); ^{13}C NMR ([D_6]DMSO, 23 °C, 75.5 MHz) δ 19.9 (CH$C$$H_3$), 30.6 ($C$$H_3CN$), 49.2 ($SiCH_2N$), 55.0 (N$C$$H_2C$), 63.36 (NCH$_2$$C$$H_2$O), 68.7 (O$CHCH_3$), 98.0 (CH$_3$$C$N), 176.3 ($C$=O); ^{15}N NMR ([$D_6$]DMSO, 23 °C) δ –334.0; ^{29}Si NMR ([D_6]DMSO, 23 °C, 59.6 MHz) δ –95.98. Anal. Calcd for $C_{13}H_{22}N_2O_7Si$: C, 45.07; H, 6.40; N, 8.09. Found: C, 44.6; H, 6.2; N, 7.7.

Preparation of (*Λ*,*S*,*S*)-[(*cis*-2,6-Dimethylmorpholinio)methyl]bis[lactato(2–)-*O*^{1}*O*^{2}]-silicate (8a). Compound **29** (500 mg, 2.00 mmol) was added at 20 °C to a stirred solution of (*S*)-lactic acid (360 mg, 4.00 mmol) in tetrahydrofuran (8 mL), and the mixture was stirred for 1 min and then kept undisturbed at this temperature for 12 h. The resulting precipitate was isolated by filtration and then recrystallized from tetrahydrofuran/acetonitrile/diethyl ether (1:1:1 (v/v/v); addition of diethyl ether (20 mL) to a solution of the precipitate in tetrahydrofuran (20 mL) and acetonitrile (20 mL) at 20 °C), and the resulting solid was isolated by filtration, washed with diethyl ether (3 x 10 mL), and dried in vacuo (0.01 Torr, 20

°C, 4 h) to give **8a** in 90% yield as a colorless crystalline solid (600 mg, 1.80 mmol); mp 270 °C. ^{15}N VACP/MAS NMR (22 °C, ν_{rot} = 5 kHz) δ –331.3; ^{29}Si VACP/MAS NMR (22 °C, ν_{rot} = 5 kHz) δ –94.1. Upon dissolution of **8a** in CD_2Cl_2 (c = 40 mM) at 23 °C, epimerization occurred (establishment of an equilibrium, with a molar ratio **8a**:**8b** = 0.44:0.56). NMR data for **8a**: ^{1}H NMR (CD_2Cl_2, 24 °C, 600.1 MHz) δ 1.18 (d, $^3J_{HH}$ = 6.1 Hz, 3 H, NCH_2CHCH_3), 1.21 (d, $^3J_{HH}$ = 6.3 Hz, 3 H, NCH_2CHCH_3), 1.33 (d, $^3J_{HH}$ = 6.9 Hz, 6 H, $SiOCHCH_3$), 2.42–2.48 and 3.66–3.72 (m, 2 H, NCH_2C), 2.47–2.56 and 3.25–3.30 (m, 2 H, NCH_2C), 2.49–2.56 (m, 2 H, $SiCH_2N$), 3.84–3.91 (m, 1 H, NCH_2CHO), 4.05–4.12 (m, 1 H, NCH_2CH), 4.22 (q, $^3J_{HH}$ = 7.0 Hz, 2 H, SiOCHC), 8.9 (br s, 1 H, NH); ^{13}C NMR (CD_2Cl_2, 24 °C, 150.9 MHz) δ 18.5 (NCH_2CHCH_3), 18.85 (NCH_2CH), 20.6 ($SiOCCH_3$), 50.9 ($SiCH_2N$), 59.1 (NCH_2C), 61.4 (NCH_2C), 69.2 (NCH_2CH), 69.32 (NCH_2CH), 70.0 ($SiOCHC$), 179.2 (C=O); ^{29}Si NMR (CD_2Cl_2, 23 °C, 59.6 MHz) δ –96.22. NMR data for **8b**: ^{1}H NMR (CD_2Cl_2, 24 °C, 600.1 MHz) δ 1.17 (d, $^3J_{HH}$ = 6.2 Hz, 3 H, NCH_2CHCH_3), 1.21 (d, $^3J_{HH}$ = 6.2 Hz, 3 H, NCH_2CHCH_3), 1.35 (d, $^3J_{HH}$ = 7.1 Hz, 6 H, $SiOCHCH_3$), 2.36–2.43 and 3.66–3.72 (m, 2 H, NCH_2C), 2.47–2.56 and 3.21–3.26 (m, 2 H, NCH_2C), 2.48–2.52 and 2.90–2.95 (m, 2 H, $SiCH_2N$), 3.72–3.79 (m, 1 H, NCH_2CH), 4.28 (q, $^3J_{HH}$ = 6.9 Hz, 2 H, SiOCHC), 4.29–4.35 (m, 1 H, NCH_2CH), 9.5 (br s, 1 H, NH); ^{13}C NMR (CD_2Cl_2, 24 °C, 150.9 MHz) δ 18.6 (NCH_2CHCH_3), 18.89 (NCH_2CH), 20.1 ($SiOCHCH_3$), 51.9 ($SiCH_2N$), 58.9 (NCH_2C), 61.8 (NCH_2C), 68.7 (NCH_2CH), 69.29 (NCH_2CH), 70.1 ($SiOCHC$), 179.2 (C=O); ^{29}Si NMR (CD_2Cl_2, 23 °C, 59.6 MHz) δ –96.24. Anal. Calcd for $C_{13}H_{23}NO_7Si$: C, 46.83; H, 6.95; N, 4.20. Found: C, 47.1; H, 6.9; N, 3.8.

Preparation of (*Δ*,*S*,*S*)-[(*cis*-2,6-Dimethylmorpholinio)methyl]bis[lactato(2–)*O*^{1}*O*^{2}]-silicate (8b). Compound **29** (500 mg, 2.00 mmol) was added at 20 °C to a stirred solution of (*S*)-lactic acid (360 mg, 4.00 mmol) in tetrahydrofuran (5 mL), and the mixture was stirred for 1 min and then kept undisturbed at this temperature for 6 h. The resulting precipitate was isolated by filtration, washed with tetrahydrofuran (3 x 5 mL), and dried in vacuo (0.01 Torr, 20 °C, 1 h) to give **8b** in 88% yield as a colorless crystalline solid (583 mg, 1.76 mmol); mp 270 °C. ^{15}N VACP/MAS NMR (22 °C, ν_{rot} = 5 kHz) δ –328.4; ^{29}Si VACP/MAS NMR (22 °C, ν_{rot} = 5 kHz) δ –94.4. The solution NMR data were identical with those obtained for **8a** after equilibration.

Preparation of (*Δ*,*S*,*S*)-Bis[lactato(2–)-*O*^{1}*O*^{2}][(2,2,6,6-tetramethylpiperidinio)methyl]-silicate (9b). Compound **24** (500 mg, 1.82 mmol) was added at 20 °C to a stirred solution of

(*S*)-lactic acid (328 mg, 3.64 mmol) in acetonitrile (1 mL), and the mixture was stirred for 1 min and then kept undisturbed at this temperature for 1 h. The resulting precipitate was isolated by filtration, washed with acetonitrile (4 x 5 mL), and dried in vacuo (0.01 Torr, 20 °C, 4 h) to give **9b** in 91% yield as a colorless crystalline solid (592 mg, 1.65 mmol); mp 278 °C. ^{15}N VACP/MAS NMR (22 °C, ν_{rot} = 5 kHz) δ –290.3; ^{29}Si VACP/MAS NMR (22 °C, ν_{rot} = 5 kHz) δ –96.6. Upon dissolution of **9b** in CD_2Cl_2 (c = 56 mM) at 23 °C, epimerization occurred (establishment of an equilibrium, with a molar ratio major isomer:minor isomer = 0.77:0.23). NMR data for the major isomer: ^{1}H NMR (CD_2Cl_2, 23 °C, 300.1 MHz) δ 1.27 (s, 3 H, CCH_3), 1.33 (s, 3 H, CCH_3), 1.34 (s, 3 H, CCH_3), 1.35 (d, $^3J_{HH}$ = 7.0 Hz, 6 H, OCHC*H*$_3$), 1.46 (s, 3 H, CCH_3), 1.62–1.92 (m, 6 H, CCH_2C), 2.46 (δ_A) and 2.71 (δ_B) (AB part of an ABX system, $^2J_{AB}$ = 17.3 Hz, $^3J_{AX}$ = 4.0 Hz, $^3J_{BX}$ = 3.2 Hz, 2 H, $SiCH_AH_BNH_X$), 4.16 (q, $^3J_{HH}$ = 7.0 Hz, 2 H, OC*H*CH_3), 5.9 (br s, 1 H, NH); ^{13}C NMR (CD_2Cl_2, 23 °C, 75.5 MHz) δ 15.9 (NCC*C*H_2C), 20.1 (C*C*H_3), 20.3 (C*C*H_3), 20.7 (OCH*C*H_3), 29.9 (C*C*H_3), 30.4 (C*C*H_3), 37.4 (Si*C*H_2N), 39.3 (NC*C*H_2C), 39.5 (NC*C*H_2C), 65.7 (N*C*C_3), 66.1 (N*C*C_3), 70.7 (O*C*HCH_3), 177.3 (*C*=O); ^{15}N (CD_2Cl_2, 23 °C) δ–296.8 (C_3NH); ^{29}Si NMR (CD_2Cl_2, 23 °C, 59.6 MHz) δ –96.3. NMR data for the minor isomer: ^{1}H NMR (CD_2Cl_2, 23 °C, 300.1 MHz) δ 1.31 (s, 3 H, CCH_3), 1.32 (d, $^3J_{HH}$ = 7.0 Hz, 6 H, OCHC*H*$_3$), 1.35 (s, 3 H, CCH_3), 1.40 (s, 3 H, CCH_3), 1.50 (s, 3 H, CCH_3), 1.62–1.92 (m, 6 H, CCH_2C), 2.44 (δ_A) and 2.79 (δ_B) (AB part of an ABX system, $^2J_{AB}$ = 17.4 Hz, $^3J_{AX}$ = 4.1 Hz, $^3J_{BX}$ = 2.9 Hz, 2 H, $SiCH_AH_BNH_X$), 4.31 (q, $^3J_{HH}$ = 7.0 Hz, 2 H, OC*H*CH_3), 6.0 (br s, 1 H, NH); ^{13}C NMR (CD_2Cl_2, 23 °C, 75.5 MHz) δ 15.9 (NCC*C*H_2C), 19.5 (OCH*C*H_3), 20.1 (C*C*H_3), 20.4 (C*C*H_3), 30.9 (2 C, C*C*H_3), 38.1 (Si*C*H_2N), 39.4 (NC*C*H_2C), 39.5 (NC*C*H_2C), 65.6 (N*C*C_3), 66.0 (N*C*C_3), 70.1 (O*C*HCH_3), 177.2 (*C*=O); ^{15}N (CD_2Cl_2, 23 °C) δ –296.7; ^{29}Si NMR (CD_2Cl_2, 23 °C, 59.6 MHz) δ –97.5. Anal. Calcd for $C_{16}H_{29}NO_6Si$: C, 53.46; H, 8.13; N, 3.90. Found: C, 53.2; H, 8.1; N, 3.8.

Preparation of (*Λ*,*S*,*S*)-[(Morpholinio)methyl]bis[3-phenyllactato(2–)-*O*^{1}*O*^{2}]silicate (10a). *Method a*: Compound **25** (500 mg, 2.26 mmol) was added at 20 °C to a solution of (*S*)-3-phenyllactic acid (751 mg, 4.52 mmol) in acetonitrile (40 mL), and the mixture was kept undisturbed for 3 h at 20 °C (formation of the first crystals ca 30 min after combining the reactants). The resulting precipitate was isolated by filtration, washed with acetonitrile (2 x 10 mL), and dried in vacuo (0.01 Torr, 20 °C, 4 h) to give **10a** in 88% yield as a colorless crystalline solid (911 mg, 1.99 mmol); mp 280 °C. ^{13}C VACP/MAS NMR (22 °C, ν_{rot} = 6.7 kHz) δ 38.1 (OCH*C*H_2C), 41.4 (OCH*C*H_2C), 49.1 (N*C*H_2C), 51.8 (Si*C*H_2N), 56.1 (N*C*H_2C), 63.5 (NCH$_2$*C*H_2O, 2 C), 73.0 (OCH*C*H_2C), 73.6 (OCH*C*H_2C), 126.6 (C_6H_5), 127.8 (C_6H_5),

129.3 (C_6H_5), 130.8 (C_6H_5), 136.9 (C_6H_5), 138.6 (C_6H_5), 175.4 (*C*=O), 178.0 (*C*=O); ^{15}N VACP/MAS NMR (22 °C, ν_{rot} = 5 kHz) δ –331.5; ^{29}Si VACP/MAS NMR (23 °C, ν_{rot} = 5 kHz) δ –95.9. Anal. Calcd for $C_{23}H_{27}NO_7Si$: C, 60.38; H, 5.95; N, 3.06. Found: C, 60.0; H, 5.9; N, 3.4.

Method b: Compound **25** (500 mg, 2.26 mmol) was added at 20 °C to a solution of (*S*)-3-phenyllactic acid (751 mg, 4.52 mmol) in water (60 mL), and the mixture was kept undisturbed for 10 h at 20 °C. The resulting precipitate was isolated by filtration, washed with water (2 x 10 mL), and dried in vacuo (0.01 Torr, 20 °C, 4 h) to give **10a** in 71% yield as a colorless crystalline solid (732 mg, 1.60 mmol); mp 280 °C. The solid-state NMR data of **10a** were identical with those obtained by method a. Anal. Calcd for $C_{23}H_{27}NO_7Si$: C, 60.38; H, 5.95; N, 3.06. Found: C, 59.5; H, 5.9; N, 3.4.

Preparation of (*Λ*,*S*,*S*)-Bis[3-phenyllactato(2–)-*O*^{1}*O*^{2}][(2,2,6,6-tetramethylpiperidinio)methyl]silicate–Acetonitrile (11a·CH$_3$CN). Compound **24** (500 mg, 1.82 mmol) was added at 20 °C to a stirred solution of (*S*)-3-phenyllactic acid (605 mg, 3.64 mmol) in acetonitrile (8 mL), and the mixture was stirred for 1 min and then kept undisturbed at this temperature for 1 h. The resulting precipitate was isolated by filtration, washed with acetonitrile (2 x 10 mL), and dried in vacuo (0.01 Torr, 20 °C, 1 h) to give **11a**·CH_3CN in 85% yield as a colorless crystalline solid (850 mg, 1.54 mmol); mp 170 °C (dec; loss of CH_3CN at 86 °C). ^{15}N VACP/MAS NMR (22 °C, ν_{rot} = 5 kHz) δ –291.4 (C_3NH); ^{29}Si VACP/MAS NMR (22 °C, ν_{rot} = 5 kHz) δ –95.3. Upon dissolution of **11a**·CH_3CN in CD_2Cl_2 (c = 48 mM) at 23 °C, epimerization occurred (establishment of an equilibrium, with a molar ratio major isomer:minor isomer = 0.76:0.24). NMR data for the major isomer: ^{1}H NMR (CD_2Cl_2, 23 °C, 300.1 MHz) δ 1.24 (s, 3 H, CCH_3), 1.31 (s, 3 H, CCH_3), 1.33 (s, 3 H, CCH_3), 1.42 (s, 3 H, CCH_3), 1.60–1.91 (m, 6 H, CCH_2C), 2.41 (δ_A) and 2.69 (δ_B) (AB part of an ABX system, $^2J_{AB}$ = 17.3 Hz, $^3J_{AX}$ = 4.2 Hz, $^3J_{BX}$ = 3.3 Hz, 2 H, $SiCH_AH_BNH_X$), 2.77 (δ_A), 3.10 (δ_B), and 4.27 (δ_X) (ABX system, $^2J_{AB}$ = 14.1 Hz, $^3J_{AX}$ = 8.5 Hz, $^3J_{BX}$ = 3.8 Hz, 6 H, $CCH_AH_BCH_X$), 5.7 (br s, 1 H, NH), 7.13–7.33 (m, 10 H, C_6H_5); ^{13}C NMR (CD_2Cl_2, 23 °C, 75.5 MHz) δ 15.9 ($NCCCH_2C$), 20.0 (CCH_3), 20.3 (CCH_3), 30.0 (CCH_3), 30.5 (CCH_3), 37.4 ($SiCH_2N$), 39.3 ($NCCH_2C$), 39.4 ($NCCH_2C$), 40.9 ($OCHCH_2C$), 65.8 (NCC_3), 66.3 (NCC_3), 75.6 ($OCHCH_2C$), 126.8 (C4, C_6H_5), 128.5 (C2/C6, C_6H_5), 129.9 (C3/C5, C_6H_5), 138.5 (C1, C_6H_5), 175.9 (*C*=O); ^{29}Si NMR (CD_2Cl_2, 23 °C, 59.6 MHz) δ –96.5. NMR data for the minor isomer: ^{1}H NMR (CD_2Cl_2, 23 °C, 300.1 MHz) δ 1.23 (s, 3 H, CCH_3), 1.26 (s, 3 H, CCH_3), 1.28 (s, 3 H, CCH_3), 1.32 (s, 3 H, CCH_3), 1.60–1.91 (m, 6 H, CCH_2C), 2.26 (δ_A) and 2.74 (δ_B)

(AB part of an ABX system, $^2J_{AB}$ = 17.0 Hz, $^3J_{AX}$ = 4.0 Hz, $^3J_{BX}$ = 3.6 Hz, 2 H, $SiCH_AH_BNH_X$), 2.77 (δ_A), 3.18 (δ_B), and 4.44 (δ_X) (ABX system, $^2J_{AB}$ = 14.1 Hz, $^3J_{AX}$ = 8.5 Hz, $^3J_{BX}$ = 3.6 Hz, 6 H, $CCH_AH_BCH_X$), 5.8 (br s, 1 H, NH), 7.13–7.33 (m, 10 H, C_6H_5); ^{13}C NMR (CD_2Cl_2, 23 °C, 75.5 MHz) δ 15.9 (NCC*C*H$_2$C), 20.1 (C*C*H$_3$), 20.3 (C*C*H$_3$), 30.0 (C*C*H$_3$), 30.8 (C*C*H$_3$), 37.8 (Si*C*H$_2$N), 39.3 (NC*C*H$_2$C), 39.4 (NC*C*H$_2$C), 39.7 (OCH*C*H$_2$C), 65.8 (N*C*C$_3$), 66.3 (N*C*C$_3$), 75.1 (O*C*HCH$_2$C), 126.8 (C4, C_6H_5), 128.7 (C2/C6, C_6H_5), 129.7 (C3/C5, C_6H_5), 138.8 (C1, C_6H_5), 176.0 (*C*=O); ^{29}Si NMR (CD_2Cl_2, 23 °C, 59.6 MHz) δ –96.5. Anal. Calcd for $C_{30}H_{40}N_2O_6Si$: C, 65.19; H, 7.29; N, 5.07. Found: C, 65.0; H, 7.2; N, 4.9.

Preparation of (*Λ*,*S*,*S*)-Bis[mandelato(2–)-*O*^{1}*O*^{2}]|(2,2,6,6-tetramethylpiperidinio)-methyl]silicate (12a). Compound **24** (800 mg, 2.90 mmol) was added at 20 °C to a stirred solution of (*S*)-mandelic acid (883 mg, 5.80 mmol) in acetonitrile (2 mL), and the mixture was then kept undisturbed at this temperature for 20 min. The resulting precipitate was isolated by filtration, washed with acetonitrile (2 x 10 mL), and dried in vacuo (0.01 Torr, 20 °C, 1 h) to give **12a** in 81% yield as a colorless crystalline solid (1.13 g, 2.34 mmol); mp 308 °C. ^{15}N VACP/MAS NMR (22 °C, ν_{rot} = 5 kHz) δ –290.5; ^{29}Si VACP/MAS NMR (22 °C, ν_{rot} = 6.5 kHz) δ –94.5. Upon dissolution of **12a** in CD_2Cl_2 (*c* = 41 mM) at 23 °C, epimerization occurred (establishment of an equilibrium, with a molar ratio major isomer:minor isomer = 0.93: 0.07). NMR data for the major isomer: ^{1}H NMR (CD_2Cl_2, 23 °C, 300.1 MHz) δ 1.34 (s, 3 H, CCH_3), 1.35 (s, 3 H, CCH_3), 1.41 (s, 3 H, CCH_3), 1.55 (s, 3 H, CCH_3), 1.59–1.91 (m, 6 H, CCH_2C), 2.64 (δ_A) and 2.90 (δ_B) (AB part of an ABX system, $^2J_{AB}$ = 17.4 Hz, $^3J_{AX}$ = 4.2 Hz, $^3J_{BX}$ = 3.3 Hz, 2 H, $SiCH_AH_BNH_X$), 5.2 (s, 2 H, OCHC), 5.9 (br s, 1 H, NH), 7.22–7.35 and 7.38–7.46 (m, 10 H, C_6H_5); ^{13}C NMR (CD_2Cl_2, 23 °C, 75.5 MHz) δ 15.9 (NCC*C*H$_2$C), 20.1 (C*C*H$_3$), 20.3 (C*C*H$_3$), 30.0 (C*C*H$_3$), 30.5 (C*C*H$_3$), 37.4 (Si*C*H$_2$N), 39.1 (NC*C*H$_2$C), 39.2 (NC*C*H$_2$C), 66.0 (N*C*C$_3$), 66.5 (N*C*C$_3$), 76.4 (O*C*HC), 127.0 (C2/C6, C_6H_5), 128.2 (C4, C_6H_5), 128.5 (C3/C5, C_6H_5), 138.7 (C1, C_6H_5), 174.6 (*C*=O); ^{29}Si NMR (CD_2Cl_2, 23 °C, 59.6 MHz) δ –95.9. NMR data for the minor isomer: ^{1}H NMR (CD_2Cl_2, 23 °C, 300.1 MHz) δ 0.9 (s, 3 H, CCH_3), 1.19 (s, 3 H, CCH_3), 1.21 (s, 3 H, CCH_3), 1.24 (s, 3 H, CCH_3), 1.59–1.91 (m, 6 H, CCH_2C), 2.47 (δ_A) and 2.89 (δ_B) (AB part of an ABX system, $^2J_{AB}$ = 17.2 Hz, $^3J_{AX}$ = 4.1 Hz, $^3J_{BX}$ = 3.3 Hz, 2 H, $SiCH_AH_BNH_X$), 5.41 (s, 2 H, OCHC), 5.9 (br s, 1 H, NH), 7.28–7.43 and 7.58–7.63 (m, 10 H, C_6H_5); ^{13}C NMR (CD_2Cl_2, 23 °C, 75.5 MHz) δ 15.9 (NCC*C*H$_2$C), 20.0 (C*C*H$_3$), 20.2 (C*C*H$_3$), 30.5 (C*C*H$_3$), 30.8 (C*C*H$_3$), 37.3 (Si*C*H$_2$N), 39.0 (NC*C*H$_2$C), 39.2 (NC*C*H$_2$C), 65.7 (N*C*C$_3$), 66.1 (N*C*C$_3$), 75.1 (O*C*HC), 126.6 (C2/C6, C_6H_5), 127.9 (C4,

C_6H_5), 128.4 (C3/C5, C_6H_5), 138.7 (C1, C_6H_5), 174.6 (*C*=O); ^{15}N (CD_2Cl_2, 23 °C) δ –297.5; ^{29}Si NMR (CD_2Cl_2, 23 °C, 59.6 MHz) δ –96.4. Anal. Calcd for $C_{26}H_{33}NO_6Si$: C, 64.57; H, 6.88.; N, 2.90. Found: C, 63.9; H, 6.9; N, 3.1.

Preparation of *rac*-[(Dimethylammonio)methyl]bis[*meso*-oxolane-3,4-diolato(2–)]silicate (13). Compound **28** (500 mg, 2.79 mmol) was added at 20 °C to a stirred solution of *meso*-oxolane-3,4-diol (581 mg, 5.58 mmol) in water (2 mL), and the resulting mixture was then transferred into a beaker (diameter, 10 cm). The solution was stirred at 20 °C for 10 min (exothermic reaction) and then kept undisturbed at this temperature for 2 days. The resulting precipitate was washed with water (3 x 0.3 mL) and then dried in vacuo (0.01 Torr, 20 °C, 5 h) to give **13** in 88% yield as a colorless crystalline solid (717 mg, 2.46 mmol); mp 245 °C. ^{13}C VACP/MAS NMR (22 °C, ν_{rot} = 5 kHz) δ 44.5 (d, $^1J_{NC}$ = 9.5 Hz, N*C*H$_3$), 49.9 (d, $^1J_{NC}$ = 9.5 Hz, N*C*H$_3$), 52.9 (Si*C*H$_2$N), 73.3 (O*C*HC), 73.6 (O*C*HC), 73.9 (O*C*HC), 74.4 (O*C*HC), 75.9 (O*C*H$_2$CH), 77.50 (O*C*H$_2$CH), 77.52 (O*C*H$_2$CH), 78.3 (O*C*H$_2$CH); ^{15}N VACP/MAS NMR (22 °C, ν_{rot} = 5 kHz) δ –336.7; ^{29}Si VACP/MAS NMR (22 °C, ν_{rot} = 5.0 kHz) δ –87.0. Upon dissolution of **13** in D_2O (*c* = 435 mM) at 23 °C, the existence of three isomers was observed with a molar equilibrium ratio **13a**:**13b**:**13c** = 0.47:0.33:0.20. NMR data for **13a**: ^{1}H NMR (D_2O, 23 °C, 300.1 MHz) δ 2.41 (s, 2 H, SiCH_2N), 2.71 (s, 6 H, NCH_3), 3.30–3.47 (m, 4 H, CHCH_2O), 3.63–3.75 (m, 4 H, CHCH_2O), 4.21–4.30 (m, 4 H, OCHC$_2$); ^{13}C NMR (D_2O, 23 °C, 75.5 MHz) δ 46.6 (2 C, N*C*H$_3$), 51.6 (Si*C*H$_2$N), 72.7 (4 C, O*C*HC$_2$), 75.9 (4 C, O*C*H$_2$CH); ^{29}Si NMR (D_2O, 23 °C, 59.6 MHz) δ –88.2. NMR data for **13b**: ^{1}H NMR (D_2O, 23 °C, 300.1 MHz) δ 2.45 (s, 2 H, SiCH_2N), 2.73 (s, 6 H, NCH_3), 3.30–3.47 (m, 4 H, CHCH_2O), 3.63–3.75 (m, 4 H, CHCH_2O), 4.21–4.30 (m, 4 H, OCHC$_2$); ^{13}C NMR (D_2O, 23 °C, 75.5 MHz) δ 46.2 (2 C, N*C*H$_3$), 52.1 (Si*C*H$_2$N), 72.89 (4 C, O*C*HC$_2$), 75.9 (4 C, CH*C*H$_2$O); ^{29}Si NMR (D_2O, 23 °C, 59.6 MHz) δ –88.7. NMR data for **13c**: ^{1}H NMR (D_2O, 23 °C, 300.1 MHz) δ 2.32 (s, 2 H, SiCH_2N), 2.70 (s, 6 H, NCH_3), 3.30–3.47 (m, 4 H, CHCH_2O), 3.63–3.75 (m, 4 H, CHCH_2O), 4.21–4.30 (m, 4 H, OCHC$_2$); ^{13}C NMR (D_2O, 23 °C, 75.5 MHz) δ 46.5 (2 C, N*C*H$_3$), 50.7 (Si*C*H$_2$N), 72.93 (4 C, O*C*HC$_2$), 75.4 (4 C, CH*C*H$_2$O); ^{29}Si NMR (D_2O, 23 °C, 59.6 MHz) δ –87.4. Anal. Calcd for $C_{11}H_{21}NO_6Si$: C, 45.34; H, 7.26; N, 4.81. Found: C, 45.3; H, 7.0; N, 4.7.

Preparation of *rac*-Bis[*meso*-oxolane-3,4-diolato(2–)][(morpholinio)methyl]silicate (14). *Method a:* Compound **25** (500 mg, 2.26 mmol) was added at 20 °C to a stirred solution of *meso*-oxolane-3,4-diol (471 mg, 4.52 mmol) in acetonitrile (10 mL), and the resulting mixture

was then transferred into a beaker (diameter, 10 cm) and kept undisturbed at 20 °C for several hours (complete evaporation of the solvent). The solid residue was recrystallized from acetonitrile (40 mL) (cooling of a boiling solution of **14** to 20 °C and slow (complete) evaporation of the solvent over a period of several hours), and the solid product was washed with diethyl ether (3 x 20 mL) and then recrystallized from dichloromethane/diethyl ether/*n*-pentane (1:1:1 (v/v/v)) at 20 °C (dissolution of **14** in dichloromethane (40 mL), subsequent addition of diethyl ether (40 mL) and *n*-pentane (40 mL), and slow evaporation of the solvent over a period of 2 days). The resulting solid was washed with diethyl ether (3 x 20 mL) and dried in vacuo (0.01 Torr, 20 °C, 4 h) to give **14** in 87% yield as a colorless crystalline solid (657 mg, 1.97 mmol); mp 180 °C. ^{13}C VACP/MAS NMR (22 °C, ν_{rot} = 5 kHz) δ 52.1 (Si*C*H$_2$N), 55.1 (N*C*H$_2$C), 59.8 (N*C*H$_2$C), 64.34 (2 C, NCH$_2$*C*H$_2$O), 72.6 (O*C*HC$_2$), 73.2 (O*C*HC$_2$), 73.4 (O*C*HC$_2$), 74.0 (O*C*HC$_2$), 76.1 (CH*C*H$_2$O), 76.2 (CH*C*H$_2$O), 76.5 (CH*C*H$_2$O), 77.2 (CH*C*H$_2$O); ^{15}N VACP/MAS NMR (22 °C, ν_{rot} = 5 kHz) δ –328.8; ^{29}Si VACP/MAS NMR (22 °C, ν_{rot} = 5.0 kHz) δ –87.5. Upon dissolution of **14** in CD$_2$Cl$_2$ (*c* = 32 mM) at 23 °C, the existence of two isomers was observed, with a molar equilibrium ratio major isomer:minor isomer = 0.80:0.20. NMR data for the major isomer: ^{1}H NMR (CD$_2$Cl$_2$, 24 °C, 600.1 MHz) δ 2.52 (s, 2 H, SiCH$_2$N), 2.85–2.96 (m, 2 H, NCH$_2$C), 3.37–3.45 (m, 4 H, CHC*H*$_2$O), 3.48–3.55 (m, 2 H, NCH$_2$C), 3.58–3.68 (m, 2 H, NCH$_2$C*H*$_2$O), 3.70–3.77 (m, 4 H, CHC*H*$_2$O), 3.99–4.06 (m, 2 H, NCH$_2$C*H*$_2$O), 4.25–4.35 (m, 4 H, OCHC$_2$), 7.9 (br s, 1 H, NH); ^{13}C NMR (CD$_2$Cl$_2$, 24 °C, 150.9 MHz) δ 51.8 (Si*C*H$_2$N), 55.2 (2 C, N*C*H$_2$C), 65.4 (2 C, NCH$_2$*C*H$_2$O), 73.3 (4 C, O*C*HC$_2$), 77.1 (4 C, CH*C*H$_2$O); ^{29}Si NMR (CD$_2$Cl$_2$, 23 °C, 59.6 MHz) δ –89.2. NMR data for the minor isomer: ^{1}H NMR (CD$_2$Cl$_2$, 24 °C, 600.1 MHz) δ 1.99 (s, 2 H, SiCH$_2$N), 2.37–2.47 (m, 4 H, NCH$_2$C), 3.58–3.67 (m, 4 H, NCH$_2$C*H*$_2$O), 3.58–3.67 and 3.82–3.88 (m, 8 H, CHC*H*$_2$O), 4.12–4.18 (m, 4 H, OCHC$_2$), 7.9 (br s, 1 H, NH); ^{13}C NMR (CD$_2$Cl$_2$, 24 °C, 150.9 MHz) δ 46.2 (Si*C*H$_2$N), 57.4 (2 C, N*C*H$_2$C), 67.3 (2 C, NCH$_2$*C*H$_2$O), 71.8 (4 C, O*C*HC$_2$), 73.1 (4 C, CH*C*H$_2$O); ^{29}Si NMR (CD$_2$Cl$_2$, 23 °C, 59.6 MHz) δ –89.3. Anal. Calcd for C$_{13}$H$_{23}$NO$_7$Si: C 46.83, H 6.95, N 4.20. Found: C 46.6, H 6.8, N 4.2.

Method b: Compound **26** (500 mg, 1.87 mmol) was added at 20 °C to a stirred solution of *meso*-oxolane-3,4-diol (389 mg, 3.74 mmol) in water (6 mL) (formation of an oily precipitate), and the resulting mixture was kept undisturbed at 20 °C for 4 days (partial evaporation of water (ca. 3 mL)). The resulting oily residue was purified by crystallization from acetonitrile and then recrystallized from dichloromethane/diethyl ether/*n*-pentane as described for method a to give **14** in 53% yield as a colorless crystalline solid (330 mg, 990

μmol); mp 180 °C. The NMR data of the product were identical with those obtained for the product prepared according to method a. Anal. Calcd for $C_{13}H_{23}NO_7Si$: C, 46.83; H, 6.95; N, 4.20. Found: C, 46.4; H, 6.8; N, 4.1.

Preparation of *rac*-Bis[*meso*-oxolane-3,4-diolato(2–)][(morpholinio)methyl]silicate-–Hydrate (14·H_2O). The synthesis was performed in a beaker (diameter, 10 cm). Compound **25** (1.00 g, 4.52 mmol) was added at 20 °C to a stirred solution of *meso*-oxolane-3,4-diol (941 mg, 9.04 mmol) in water (2 mL), and the resulting mixture was stirred for a further 10 min (exothermic reaction) and then kept undisturbed at 20 °C for 2 days. The resulting precipitate was washed with water (3 x 0.3 mL) and dried in vacuo (0.01 Torr, 20 °C, 5 h) to give **14**·H_2O in 93% yield as a colorless crystalline solid (1.48 g, 4.20 mmol); mp 179 °C. ^{13}C VACP/MAS NMR (22 °C, ν_{rot} = 6 kHz) δ 52.1 (Si*C*H_2N), 55.1 (N*C*H_2C), 59.8 (N*C*H_2C), 64.3 (2 C, NCH$_2$*C*H_2O), 72.6 (O*C*HC$_2$), 73.2 (O*C*HC$_2$), 73.4 (O*C*HC$_2$), 74.0 (O*C*HC$_2$), 76.1 (CH*C*H_2O), 76.2 (CH*C*H_2O), 76.5 (CH*C*H_2O), 77.3 (CH*C*H_2O); ^{15}N VACP/MAS NMR (22 °C, ν_{rot} = 5 kHz) δ –328.1; ^{29}Si VACP/MAS NMR (22 °C, ν_{rot} = 5.0 kHz) δ –87.5. Upon dissolution of **14**·H_2O in D_2O (c = 475 mM) at 23 °C, the existence of three isomers was observed, with a molar equilibrium ratio major **14a**:**14b**:**14c** = 0.65:0.24:0.11. NMR data for **14a**: ^1H NMR (D_2O, 23 °C, 400.1 MHz) δ 1.81–2.06 (m, 2 H, NCH$_2$C), 2.37 (s, 2 H, SiCH$_2$N), 2.45–2.66 (m, 2 H, NCH$_2$C), 3.40 –3.48 (m, 4 H, CHC*H*$_2$O), 3.45–3.64 (m, 4 H, NCH$_2$C*H*$_2$O), 3.67–3.77 (m, 4 H, CHC*H*$_2$O), 4.03–4.11 (m, 4 H, OCHC$_2$); ^{13}C NMR (D_2O, 23 °C, 100.6 MHz) δ 45.8 (N*C*H$_2$C), 49.7 (SiCH$_2$N), 55.4 (N*C*H$_2$C), 65.8 (2 C, NCH$_2$*C*H$_2$O), 70.8 (4 C, O*C*HC$_2$), 71.3 (4 C, CH*C*H$_2$O); ^{29}Si NMR (D_2O, 23 °C, 79.5 MHz) δ –89.2. NMR data for **14b**: ^1H NMR (D_2O, 23 °C, 400.1 MHz) δ 2.30 (SiCH$_2$N), 2.80–2.95 (m, 2 H, NCH$_2$C), 3.22–3.35 (m, 2 H, NCH$_2$C), 3.22–3.35 (m, 4 H, CHC*H*$_2$O), 3.45–3.66 (m, 4 H, CHC*H*$_2$O), 3.45–3.66 and 3.78–3.90 (m, 4 H, NCH$_2$C*H*$_2$O), 4.2 (br s, 4 H, OCHC$_2$); ^{13}C NMR (D_2O, 23 °C, 100.6 MHz) δ 49.4 (SiCH$_2$N), 55.5 (2 C, N*C*H$_2$C), 64.1 (NCH$_2$*C*H$_2$O), 64.3 (NCH$_2$*C*H$_2$O), 72.5 (4 C, O*C*HC$_2$), 75.6 (4 C, CH*C*H$_2$O); ^{29}Si NMR (D_2O, 23 °C, 79.5 MHz) δ –88.7. NMR data for **14c**: ^1H NMR (D_2O, 23 °C, 400.1 MHz) δ 2.23 (SiCH$_2$N), 2.36–2.42 (m, 4 H, NCH$_2$C), 3.22–3.35 (m, 4 H, CHC*H*$_2$O), 3.45–3.66 (m, 4 H, CHC*H*$_2$O), 3.45–3.66 and 3.78–3.90 (m, 4 H, NCH$_2$C*H*$_2$O), 4.10–4.15 (m, 4 H, OCHC$_2$); ^{13}C NMR (D_2O, 23 °C, 100.6 MHz) δ 48.9 (SiCH$_2$N), 53.8 (2 C, N*C*H$_2$C), 63.8 (2 C, NCH$_2$*C*H$_2$O), 72.4 (4 C, O*C*HC$_2$), 75.1 (4 C, CH*C*H$_2$O); ^{29}Si NMR (D_2O, 23 °C, 79.5 MHz) δ –87.9. Anal. Calcd for $C_{13}H_{25}NO_8Si$: C, 44.43; H, 7.17; N, 3.99. Found: C, 44.3; H, 6.8; N, 3.9.

Preparation of *rac*-[(*cis*-2,6-Dimethylmorpholinio)methyl]bis[*meso*-oxolane-3,4-diolato(2–)]silicate–*meso*-Oxolane-3,4-diol (15·$C_4H_8O_3$). *meso*-Oxolane-3,4-diol (419 mg, 4.02 mmol) was added at 20 °C to a stirred solution of **29** (501 mg, 2.01 mmol) in tetrahydrofuran (4 mL), and the mixture was stirred at this temperature for 15 min. After addition of diethyl ether (10 mL) at 20 °C, the reaction mixture was kept undisturbed at this temperature for 1 day. The resulting solid was isolated by filtration, washed with diethyl ether (3 x 5 mL), and dried in an argon gas stream (20 °C, 2 h) to give **15**·$C_4H_8O_3$ in 72% yield as a colorless crystalline solid (675 mg, 1.45 mmol); mp 215 °C. ^{13}C VACP/MAS NMR (22 °C, ν_{rot} = 6 kHz) δ 18.2 (C*C*H$_3$), 19.2 (C*C*H$_3$), 51.7 (Si*C*H$_2$N), 58.1 (N*C*H$_2$C), 59.5 (NCH$_2$C), 68.8 (*C*HCH$_3$), 70.0 (*C*HCH$_3$), 72.3 (2 C, O*C*HC$_2$, $C_4H_8O_3$), 72.5 (O*C*HC$_2$), 73.0 (O*C*HC$_2$), 73.6 (O*C*HC$_2$), 73.8 (2 C, O*C*H$_2$C, $C_4H_8O_3$), 74.1 (O*C*HC), 77.2 (2 C, O*C*H$_2$C), 79.0 (2 C, O*C*H$_2$C); ^{15}N VACP/MAS NMR (22 °C, ν_{rot} = 5 kHz) δ –325.7 (C$_3$NH); ^{29}Si VACP/MAS NMR (22 °C, ν_{rot} = 5.0 kHz) δ –90.1. Upon dissolution of **15**·$C_4H_8O_3$ in CD_2Cl_2 (c = 23 mM) at 23 °C, the existence of one species was observed. Upon drying, partial loss (ca. 0.2 molar equivs) of the *meso*-oxolane-3,4-diol was observed (^{1}H and ^{13}C NMR analysis). ^{1}H NMR (CD_2Cl_2, 23 °C, 300.1 MHz) δ 1.22 (d, $^3J_{HH}$ = 6.3 Hz, 6 H, CCH$_3$), 2.32–2.48 (m, 2 H, NCH$_2$C), 2.49 (δ_A) (A part of an A$_2$X system, d, $^3J_{HH}$ = 3.6 Hz, 2 H, SiC(H$_A$)$_2$NH$_X$), 3.34–3.45 (m, 4 H, OCH$_2$C), 3.42–3.51 (m, 2 H, NCH$_2$C), 3.56–3.65 (m, 1.65 H, OCH$_2$C, $C_4H_8O_3$), 3.63–3.73 (m, 2 H, OC*H*CH$_3$), 3.67–3.76 (m, 4 H, OCH$_2$C), 3.81–3.90 (m, 2 H, OCH$_2$C, $C_4H_8O_3$), 4.10–4.19 (m, 2 H, OCHC, $C_4H_8O_3$), 4.25–4.34 (m, 4 H, OCHC), 4.5 (br s, 1.65 H, OH, $C_4H_8O_3$), 7.8 (br s, 1 H, NH); ^{13}C NMR (CD_2Cl_2, 23 °C, 75.5 MHz) δ 18.5 (2 C, CH*C*H$_3$), 51.7 (Si*C*H$_2$N), 59.6 (2 C, N*C*H$_2$C), 70.9 (2 C, *C*HCH$_3$), 71.8 (2 C, O*C*HC, $C_4H_8O_3$), 73.1 (2 C, O*C*H$_2$C, $C_4H_8O_3$), 73.3 (4 C, O*C*HC), 77.1 (4 C, O*C*H$_2$C); ^{29}Si NMR (CD_2Cl_2, 23 °C, 59.6 MHz) δ –89.3. Anal. Calcd for $C_{19}H_{35}NO_{10}Si$: C, 49.02; H, 7.58; N, 3.01. Found: C, 49.0; H, 7.4; N, 3.2.

Preparation of *rac*-Bis[*meso*-oxolane-3,4-diolato(2–)][(2,2,6,6-tetramethylpiperidinio)-methyl]silicate (16). *meso*-Oxolane-3,4-diol (379 mg, 3.64 mmol) was added at 20 °C to a stirred solution of **24** (501 mg, 1.82 mmol) in diethyl ether (10 mL), and the mixture was stirred at this temperature for 6 h. After addition of *n*-pentane (20 mL) at 20 °C, the reaction mixture was further stirred at this temperature for 1 day. The resulting solid was isolated by filtration, recrystallized from dichloromethane/diethyl ether (1:2 (v/v); addition of diethyl ether to a solution of the product in dichloromethane at 20 °C), washed with diethyl ether (3 x 5 mL), and dried in vacuo (0.01 Torr, 60 °C, 6 h) to give **16** in 82% yield as a colorless

crystalline solid (581 mg, 1.50 mmol); mp 194 °C. ^{13}C VACP/MAS NMR (22 °C, ν_{rot} = 5 kHz) δ 17.5 (NCC*C*H$_2$C), 19.3 (C*C*H$_3$), 21.1 (C*C*H$_3$), 30.1 (C*C*H$_3$), 31.6 (C*C*H$_3$), 37.7 (Si*C*H$_2$N), 38.7 (NC*C*H$_2$C), 40.3 (NC*C*H$_2$C), 63.1 (N*C*C$_3$), 63.2 (N*C*C$_3$), 71.7 (O*C*HC), 73.2 (O*C*HC), 73.4 (O*C*H$_2$C), 74.0 (O*C*HC), 74.6 (O*C*HC), 77.1 (O*C*H$_2$C), 77.8 (O*C*H$_2$C), 78.6 (O*C*H$_2$C); ^{15}N VACP/MAS NMR (22 °C, ν_{rot} = 5 kHz) δ –292.6; ^{29}Si VACP/MAS NMR (22 °C, ν_{rot} = 5.0 kHz) δ –85.0. Upon dissolution of **16** in CD$_2$Cl$_2$ (c = 102 mM) at 23 °C, the existence of three isomers was observed, with a molar equilibrium ratio **16a**:**16b**:**16c** = 0.24:0.63:0.14. NMR data for **16a**: ^{1}H NMR (CD$_2$Cl$_2$, 24 °C, 600.1 MHz) δ 1.29 (s, 6 H, CCH$_3$), 1.50 (s, 6 H, CCH$_3$), 1.53–1.65 and 1.73–1.85 (m, 6 H, CCH$_2$C), 2.43 (δ_A) (A part of an A$_2$X system, d, $^3J_{HH}$ = 2.9 Hz, 2 H, SiC(H$_A$)$_2$NH$_X$), 3.37–3.46 (m, 4 H, OCH$_2$C), 3.68–3.71 (m, 4 H, OCH$_2$C), 4.26–4.31 (m, 4 H, OCHC), 7.6 (br s, 1 H, NH); ^{13}C NMR (CD$_2$Cl$_2$, 24 °C, 150.9 MHz) δ 16.5 (NCC*C*H$_2$C), 20.9 (2 C, C*C*H$_3$), 30.0 (2 C, C*C*H$_3$), 37.4 (Si*C*H$_2$N), 39.7 (2 C, NC*C*H$_2$C), 63.6 (2 C, N*C*C$_3$), 74.0 (4 C, O*C*HC), 76.6 (4 C, O*C*H$_2$C); ^{29}Si NMR (CD$_2$Cl$_2$, 23 °C, 59.6 MHz) δ –85.3. NMR data for **16b**: ^{1}H NMR (CD$_2$Cl$_2$, 24 °C, 600.1 MHz) δ 1.29 (s, 6 H, CCH$_3$), 1.41 (s, 6 H, CCH$_3$), 1.53–1.65 and 1.73–1.85 (m, 6 H, CCH$_2$C), 2.41 (δ_A) (A part of an A$_2$X system, d, $^3J_{HH}$ = 3.1 Hz, 2 H, SiC(H$_A$)$_2$NH$_X$), 3.31–3.37 (m, 2 H, OCH$_2$C), 3.56–3.68 (m, 4 H, OCH$_2$C), 3.71–3.75 (m, 2 H, OCH$_2$C), 4.15–4.19 (m, 2 H, OCHC), 4.26–4.31 (m, 2 H, OCHC), 7.8 (br s, 1 H, NH); ^{13}C NMR (CD$_2$Cl$_2$, 24 °C, 150.9 MHz) δ 16.4 (NCC*C*H$_2$C), 20.6 (2 C, C*C*H$_3$), 30.2 (2 C, C*C*H$_3$), 38.2 (Si*C*H$_2$N), 39.8 (2 C, NC*C*H$_2$C), 63.0 (2 C, N*C*C$_3$), 73.9 (2 C, O*C*HC), 74.3 (2 C, O*C*HC), 76.0 (2 C, O*C*H$_2$C), 77.1 (2 C, O*C*H$_2$C); ^{29}Si NMR (CD$_2$Cl$_2$, 23 °C, 59.6 MHz) δ –86.1. NMR data for **16c**: ^{1}H NMR (CD$_2$Cl$_2$, 24 °C, 600.1 MHz) δ 1.29 (s, 6 H, CCH$_3$), 1.37 (s, 6 H, CCH$_3$), 1.53–1.65 and 1.73–1.85 (m, 6 H, CCH$_2$C), 2.30 (δ_A) (A part of an A$_2$X system, d, $^3J_{HH}$ = 3.0 Hz, 2 H, SiC(H$_A$)$_2$NH$_X$), 3.57–3.68 (m, 8 H, OCH$_2$C), 4.17–4.21 (m, 4 H, OCHC), 8.1 (br s, 1 H, NH); ^{13}C NMR (CD$_2$Cl$_2$, 24 °C, 150.9 MHz) δ 16.3 (NCC*C*H$_2$C), 20.6 (2 C, C*C*H$_3$), 30.2 (2 C, C*C*H$_3$), 38.3 (Si*C*H$_2$N), 39.8 (2 C, NC*C*H$_2$C), 62.9 (2 C, N*C*C$_3$), 74.2 (4 C, O*C*HC), 75.9 (4 C, O*C*H$_2$C); ^{29}Si NMR (CD$_2$Cl$_2$, 23 °C, 59.6 MHz) δ –85.7. Anal. Calcd for C$_{18}$H$_{33}$NO$_6$Si: C, 55.79; H, 8.58; N, 3.61. Found: C, 55.4; H, 8.2; N, 3.7.

Preparation of *rac*-Bis[*cis*-1,2-diphenylethene-1,2-diolato(2–)][(morpholinio)methyl]-silicate (17): *Method a:* This compound was prepared according to ref. 13. Compound **25** (500 mg, 2.26 mmol) was added dropwise within 2 min to a stirred suspension of benzoin (959 mg, 4.52 mmol) in acetonitrile (15 mL). After the mixture was stirred for a further 20 min, it was kept undisturbed at 20 °C for 2 days (formation of a precipitate ca. 30 min after

combining the reactants). The product was filtered off, washed with cold (0 °C) acetonitrile (20 mL), and dried in vacuo (0.01 Torr, 20 °C, 2 h) to give 1.00 g (1.82 mmol) of a crystalline solid (yield 81 %); mp 177 °C. ^{29}Si VACP/MAS NMR (ν_{rot} = 5 kHz) δ –86.0; ^{1}H NMR ([D$_6$]DMSO, 23 °C, 300.1 MHz) δ 2.71 (d, $^{3}J_{HH}$ = 3.2 Hz, 2 H, SiC*H*$_2$N), 2.98–3.15 and 3.30–3.41 (m, 4 H, CC*H*$_2$N), 3.57–3.71 and 3.83–3.95 (m, 4 H, CC*H*$_2$O), 7.08–7.17 (m, 4 H, H-4, C$_6$H$_5$), 7.19–7.27 (m, 8 H, H-3/H-5, C$_6$H$_5$), 7.38–7.46 (m, 8 H, H-2/H-6, C$_6$H$_5$), 8.6 (br. s, 1 H, NH); ^{13}C NMR ([D$_6$]DMSO, 23 °C, 75.5 MHz) δ 48.3 (Si*C*H$_2$N), 54.4 (C*C*H$_2$N), 63.6 (C*C*H$_2$O), 126.1 (*C*-4, C$_6$H$_5$), 126.4 (*C*-2/*C*-6, C$_6$H$_5$), 127.8 (*C*-3/*C*-5, C$_6$H$_5$) 135.2 (*C*-1, C$_6$H$_5$), 135.8 (O*C*C$_2$); ^{29}Si NMR ([D$_6$]DMSO); δ –89.6. Anal. Calcd for C$_{33}$H$_{31}$NO$_5$Si: C, 72.11; H, 5.68; N, 2.55. Found: C, 72.0; H, 5.7; N, 2.7.

Method b: Compound **26** (500 mg, 1.87 mmol) was added at 20 °C to a stirred solution of benzoin (794 mg, 3.74 mmol) in acetonitrile (30 mL). After the mixture was stirred for a further 30 min, it was kept undisturbed at 20 °C for 2 days (formation of the first crystals ca. 20 h after combining the reactants). The resulting precipitate was isolated by filtration, washed with cold (0 °C) acetonitrile (20 mL), and dried in vacuo (0.01 Torr, 20 °C, 5 h) to give **17** in 42% yield as a colorless crystalline solid (430 mg, 782 μmol); mp 177 °C. The NMR data of the product were identical with those obtained for the product prepared according to method a. Anal. Calcd for C$_{33}$H$_{31}$NO$_5$Si: C, 72.11; H, 5.68; N, 2.55. Found: C, 72.0; H, 5.8; N, 2.6.

Method c: Compound **27** (501 mg, 2.44 mmol) was added at 20 °C to a stirred solution of benzoin (1.04 g, 4.90 mmol) in acetonitrile (30 mL). After the mixture was stirred for a further 30 min, it was kept undisturbed at 20 °C for 36 days, followed by addition of diethyl ether (30 mL) and *n*-pentane (70 mL). The mixture was kept undisturbed at 20 °C for a further 16 days, and the resulting precipitate (formation of the first crystals ca. 50 days after combining the reactants) was isolated by filtration and dried in vacuo (0.01 Torr, 20 °C, 2 h) to give **17** in 35% yield as a colorless crystalline solid (466 mg, 848 μmol); mp 177 °C. The NMR data of the product were identical with those obtained for the product prepared according to method a. Anal. Calcd for C$_{33}$H$_{31}$NO$_5$Si: C, 72.11; H, 5.68; N, 2.55. Found: C, 71.0; H, 5.6; N, 2.3.

Preparation of *rac*-Bis[*cis*-1,2-diphenylethene-1,2-diolato(2–)][(2,2,6,6-tetramethyl-piperidinio)methyl]silicate–Sesqui-1,4-dioxane (18·3/2C$_4$H$_8$O$_2$). This compound was prepared according to ref. 14.

Preparation of Morpholinium *meso*-Bis[citrato(3–)-*O*^{1},*O*^{3},*O*^{6}]silicate–Dimethanol (*meso*-19·2CH$_3$OH). Tetramethoxysilane (250 mg, 1.64 mmol) and morpholine (286 mg, 3.28 mmol) were added one after another at 20 °C to a stirred solution of citric acid (630 mg, 3.28 mmol) in methanol (20 mL), and the resulting mixture was then kept undisturbed at 20 °C for 6 days (formation of a precipitate ca. 2 days after combining the reactants). The product was isolated by filtration, washed with methanol (3 x 5 mL), and dried in an argon gas stream (20 °C, 5 min) to give *meso*-**19**·2CH$_3$OH in 91% yield as a colorless crystalline solid (966 mg, 1.49 mmol); mp 168 °C. ^{13}C VACP/MAS NMR (22 °C, ν_{rot} = 6 kHz) δ 40.4 (C*C*H$_2$C), 43.9 (C*C*H$_2$C), 44.5 (N*C*H$_2$C), 45.5 (N*C*H$_2$C), 50.3 (*C*H$_3$OH), 64.9 (2 C, O*C*H$_2$C), 75.0 (O*C*C$_3$), 175.2 (*C*=O), 179.8 (*C*=O), 180.9 (*C*=O); ^{15}N VACP/MAS NMR (22 °C, ν_{rot} = 5 kHz) δ –337.5; ^{29}Si VACP/MAS NMR (22 °C, ν_{rot} = 5 kHz) δ –162.4. Anal. Calcd for C$_{22}$H$_{38}$N$_2$O$_{18}$Si: C, 40.86; H, 5.92; N, 4.33. Found: C, 40.5; H, 5.6; N, 4.4.

Preparation of Morpholinium *rac*-Bis[citrato(4–)-*O*^{1},*O*^{3},*O*^{6}]silicate–Methanol (*rac*-20·1.73CH$_3$OH). Tetramethoxysilane (1.00 g, 6.57 mmol) and morpholine (2.30 g, 26.4 mmol) were added one after another at 20 °C to a stirred solution of citric acid (2.52 g, 13.1 mmol) in tetrahydrofuran/methanol (50 mL/50 mL), and the resulting mixture was kept undisturbed at 20 °C for 20 days (formation of a precipitate ca. 10 days after combining the reactants). The product was isolated by filtration, washed with methanol (3 x 5 mL), and dried in an argon gas stream (20 °C, 5 min) to give *rac*-**20**·1.73CH$_3$OH in 75% yield as a colorless crystalline solid (4.00 g, 4.93 mmol); mp 192 °C. ^{13}C VACP/MAS NMR (22 °C, ν_{rot} = 5 kHz) δ 40.8 (4 C, C*C*H$_2$C), 42.6–46.4 (m, 8 C, N*C*H$_2$C), 63.9 (2 C, O*C*H$_2$C), 64.1 (2 C, O*C*H$_2$C), 64.3 (2 C, O*C*H$_2$C), 64.7 (2 C, O*C*H$_2$C), 74.9 (2 C, O*C*C$_3$), 174.9 (*C*=O), 176.6 (*C*=O), 178.4 (*C*=O), 178.7 (*C*=O), 180.6 (2 C, *C*=O), (^{13}C signals for the methanol molecules could not be detected because the solvate molecules were removed due to the high spinning speed used in this experiment); ^{15}N VACP/MAS NMR (22 °C, ν_{rot} = 5 kHz) δ –341.5 to –336.5 (m); ^{29}Si VACP/MAS NMR (22 °C, ν_{rot} = 5 kHz) δ –166.4. Anal. Calcd for C$_{29.73}$H$_{54.92}$N$_4$O$_{19.73}$Si: C, 43.96; H, 6.82; N, 6.90. Found: C, 43.2; H, 6.2; N, 6.5.

Preparation of Tri(*n*-propyl)ammonium (*Λ*,*S*,*S*,*S*)-*mer*-Tris[malato(2–)-*O*^{1},*O*^{2}]silicate ((*Λ*,*S*,*S*,*S*)-*mer*-21). Tetramethoxysilane (3.00 g, 19.7 mmol) and tri(*n*-propyl)amine (5.65 g, 39.4 mmol) were added one after another at 20 °C to a stirred solution of (*S*)-malic acid (7.93 g, 59.1 mmol) in tetrahydrofuran (15 mL), and the resulting mixture was stirred at 20 °C for 1 h and then kept undisturbed at 20 °C for 8 days (formation of a precipitate ca. 3 days after

combining the reactants). The product was isolated by filtration, recrystallized from acetonitrile/tetrahydrofuran/diethyl ether (1:1:3 (v/v/v); addition of diethyl ether to a solution of the product in acetonitrile/tetrahydrofuran at 20 °C), washed with diethyl ether (3 x 5 mL), and dried in vacuo (0.01 Torr, 20 °C, 4 h) to give (*Λ*,*S*,*S*,*S*)-*mer*-**21** in 89% yield as a colorless crystalline solid (12.5 g, 17.5 mmol); mp 155 °C. ^{13}C VACP/MAS NMR (22 °C, ν_{rot} = 5 kHz) δ 8.6 (C*C*H$_3$), 8.8 (C*C*H$_3$), 9.0 (C*C*H$_3$), 10.1 (C*C*H$_3$), 11.5 (C*C*H$_3$), 12.3 (C*C*H$_3$), 17.5 (2 C, C*C*H$_2$CH$_3$), 17.7 (2 C, C*C*H$_2$CH$_3$), 17.9 (2 C, C*C*H$_2$CH$_3$), 38.3 (CH*C*H$_2$C), 39.1 (CH*C*H$_2$C), 40.2 (CH*C*H$_2$C), 46.3 (N*C*H$_2$C), 48.8 (N*C*H$_2$C), 53.5 (N*C*H$_2$C), 54.0 (N*C*H$_2$C), 54.1 (N*C*H$_2$C), 54.7 (N*C*H$_2$C), 69.4 (O*C*HC$_2$), 70.0 (O*C*HC$_2$), 70.3 (O*C*HC$_2$), 170.7 (*C*=O), 171.0 (*C*=O), 172.0 (*C*=O), 179.8 (*C*=O), 180.3 (*C*=O), 181.6 (*C*=O); ^{15}N VACP/MAS NMR (22 °C, ν_{rot} = 5 kHz) δ –317.9, –317.3; ^{29}Si VACP/MAS NMR (22 °C, ν_{rot} = 5 kHz) δ –148.1. Anal. Calcd for $C_{30}H_{56}N_2O_{15}Si$: C, 50.55; H, 7.92; N, 3.93. Found: C, 50.4; H, 7.8; N, 3.9.

Preparation of Tri(*n*-butyl)ammonium (*Λ*,*S*,*S*,*S*)-*mer*-Tris[malato(2–)*O*^{1},*O*^{2}]silicate-–Diacetonitrile ((*Λ*,*S*,*S*,*S*)-*mer*-22·2CH$_3$CN). Tetramethoxysilane (5.00 g, 32.8 mmol) and tri(*n*-butyl)amine (12.2 g, 65.8 mmol) were added one after another at 20 °C to a stirred solution of (*S*)-malic acid (13.2 g, 98.4 mmol) in tetrahydrofuran (30 mL), and the resulting mixture was stirred for 30 min and then kept undisturbed at 20 °C for 2 days. Diethyl ether (100 mL) was added, and the mixture was kept undisturbed at 20 °C for a further 7 days (formation of a precipitate ca. 3 days after the addition of diethyl ether). The product was isolated by filtration, purified by a twofold recrystallization from acetonitrile (slow cooling of a boiling solution to 20 °C), washed with ancetonitrile (3 x 5 mL), and dried in an argon gas stream (20 °C, 5 min) to give (*Λ*,*S*,*S*,*S*)-*mer*-**22**·2CH$_3$CN in 86% yield as a colorless crystalline solid (24.9 g, 28.3 mmol); mp 172 °C. ^{13}C VACP/MAS NMR (22 °C, ν_{rot} = 6 kHz) δ 1.4 (2 C, *C*H$_3$CN), 14.1 (2 C, C*C*H$_3$), 14.3 (2 C, C*C*H$_3$), 14.9 (2 C, C*C*H$_3$), 20.0 (2 C, C*C*H$_2$CH$_3$), 20.8 (2 C, C*C*H$_2$CH$_3$), 21.2 (2 C, C*C*H$_2$CH$_3$), 23.2 (2 C, NCH$_2$*C*H$_2$C), 27.2 (2 C, NCH$_2$*C*H$_2$C), 28.1 (2 C, NCH$_2$*C*H$_2$C), 39.7 (CH*C*H$_2$C), 39.8 (CH*C*H$_2$C), 40.7 (CH*C*H$_2$C), 51.3 (N*C*H$_2$C), 52.6 (N*C*H$_2$C), 53.5 (N*C*H$_2$C), 54.0 (N*C*H$_2$C), 55.4 (N*C*H$_2$C), 56.0 (N*C*H$_2$C), 70.4 (3 C, O*C*HC$_2$), 114.9 (2 C, CH$_3$*C*N), 173.5 (*C*=O), 174.7 (*C*=O), 174.9 (*C*=O), 178.5 (*C*=O), 181.5 (*C*=O), 182.1 (*C*=O); ^{15}N VACP/MAS NMR (22 °C, ν_{rot} = 5 kHz) δ –318.9, –317.8; ^{29}Si VACP/MAS NMR (22 °C, ν_{rot} = 5 kHz) δ –146.3. Anal. Calcd for $C_{40}H_{74}N_4O_{15}Si$: C, 54.65; H, 8.48; N, 6.37. Found: C, 54.0; H, 8.1; N, 6.4.

Preparation of [(2,2,6,6-Tetramethylpiperidino)methyl]silane (23). This compound was prepared according to ref. 4m.

Preparation of [(2,2,6,6-Tetramethylpiperidino)methyl]trimethoxysilane (24). This compound was prepared according to ref. 4h.

Preparation of [(Morpholino)methyl]trimethoxysilane (25). This compound was prepared according to ref. 47.

Preparation of Dimethoxy[(morpholino)methyl]phenylsilane (26). This compound was prepared according to ref. 47.

Preparation of Dimethoxy(methyl)[(morpholino)methyl]silane (27). Compound **30** (18.8 g, 122 mmol) was added dropwise at 20 °C within 30 min to a solution of morpholine (27.4 g, 315 mmol) in methanol (120 mL), and the mixture was then stirred under reflux for 20 h. After the mixture was cooled to 20 °C, the solvent and the excess morpholine were removed under reduced pressure, and *n*-pentane (150 mL) was added to the residue. The resulting precipitate was filtered off and discarded, the solvent was removed from the filtrate under reduced pressure, and the liquid residue was distilled in vacuo to give **27** in 78% yield as a colorless liquid (19.5 g, 95.0 mmol); bp 60 °C, 0.5 mbar. ^{1}H NMR ($CDCl_3$, 23 °C, 300.1 MHz) δ 0.12 (s, 3 H, $SiCH_3$), 1.90 (s, 2 H, $SiCH_2N$), 2.34–2.41 (m, 4 H, CCH_2N), 3.47 (s, 6 H, OCH_3), 3.59–3.65 (m, 4 H, CCH_2O); ^{13}C NMR ($CDCl_3$, 23 °C, 75.5 MHz) δ –5.4 (Si*C*H_3), 46.9 (Si*C*H_2N), 50.2 (O*C*H_3), 57.0 (C*C*H_2N), 67.0 (C*C*H_2O); ^{29}Si NMR ($CDCl_3$, 23 °C, 59.6 MHz) δ –6.6. Anal. Calcd for $C_8H_{19}NO_3Si$: C, 46.80; H, 9.33; N, 6.82. Found: C, 46.8; H, 9.5; N, 6.9.

Preparation of [(Dimethylamino)methyl]trimethoxysilane (28). This compound was prepared according to ref. 48.

Preparation of [(*cis*-2,6-Dimethylmorpholino)methyl]trimethoxysilane (29). Compound **31** (14.8 g, 86.7 mmol) was added dropwise at 20 °C within 30 min to a stirred solution of *cis*-2,6-dimethylmorpholine (19.9 g, 173 mmol) in acetonitrile (40 mL), and the mixture was then stirred under reflux for 12 h. After the mixture was cooled to 20 °C, diethyl ether (40 mL) was added, the resulting precipitate was filtered off and discarded, the solvent of the filtrate was

removed under reduced pressure, and the residue was distilled in vacuo (Vigreux column) to give **29** in 67% yield as a colorless liquid (14.5 g, 58.1 mmol); bp 55 °C, 0.5 mbar. ^{1}H NMR (CD_2Cl_2, 23 °C, 400.1 MHz) δ 1.07 (δ_A), 1.60 (δ_M), 2.74 (δ_N), and 3.59 (δ_O) ($(A_3MNO)_2X$ system, $^{1}J_{NX} \approx 1.2$ Hz, $^{2}J_{MN} = 11.4$ Hz, $^{3}J_{AO} = 6.3$ Hz, $^{3}J_{MO} = 10.1$ Hz, $^{3}J_{NO} = 2.0$ Hz, 12 H, $(C(H_A)_3CH_OCH_MH_N)_2N_X$), 1.91 (s, 2 H, $SiCH_2N$), 3.55 (s, 9 H, OCH_3); ^{13}C NMR ([D_6]DMSO, 23 °C, 75.5 MHz) δ 18.9 (2 C, CCH_3), 42.4 ($SiCH_2N$), 50.1 (3 C, OCH_3), 62.5 (2 C, NCH_2C), 71.0 (2 C, $OCHC_2$); ^{29}Si NMR ([D_6]DMSO, 23 °C, 59.6 MHz) δ –48.1. Anal. Calcd for $C_{10}H_{23}NO_4Si$: C, 48.16; H, 9.30; N, 5.62. Found: C, 48.1; H, 8.9; N, 5.7.

Preparation of (Chloromethyl)dimethoxy(methyl)silane (30). This compound was prepared according to ref 4b.

Preparation of (Chloromethyl)trimethoxysilane (31). This compound was commercially available.

11 Appendix A: Crystal Structure Data

Table 25. Crystal Data and Experimental Parameters for the Crystal Structure Analyses of *rac*-**1**, **2b**, and **3a**·CH_2Cl_2

	rac-**1**	**2b**	**3a**·CH_2Cl_2
empirical formula	$C_{14}H_{27}N_3O_4Si$	$C_{16}H_{31}N_3O_4Si$	$C_{29}H_{41}Cl_2N_3O_4Si$
formula mass (g mol^{-1})	329.48	357.53	594.64
collection T (K)	173(2)	173(2)	173(2)
λ(Mo Kα) (Å)	0.71073	0.71073	0.71073
crystal system	orthorhombic	orthorhombic	monoclinic
space group (no.)	*Pbca* (61)	$P2_12_12_1$ (19)	$P2_1$ (4)
a (Å)	13.458(3)	9.2403(10)	10.809(4)
b (Å)	11.899(2)	10.7313(10)	12.027(4)
c (Å)	20.511(4)	18.712(2)	12.922(4)
β (deg)	90	90	112.89(4)
V (Å^3)	3284.7(11)	1855.5(3)	1547.5(9)
Z	8	4	2
D(calcd) (g cm^{-3})	1.333	1.280	1.276
μ (mm^{-1})	0.165	0.151	0.286
F(000)	1424	776	632
crystal dimensions (mm)	0.6 x 0.4 x 0.3	0.5 x 0.5 x 0.4	0.5 x 0.3 x 0.2
2θ range (deg)	3.98–49.50	4.36–53.98	4.10–52.80
index ranges	$-15 \le h \le 15$, $-13 \le k \le 13$, $-24 \le l \le 24$	$-10 \le h \le 11$, $-13 \le k \le 13$, $-23 \le l \le 23$	$-13 \le h \le 13$, $-15 \le k \le 15$, $-16 \le l \le 16$
no. of collected reflections	27792	13428	17381
no. of independent reflections	2791	3998	6311
R_{int}	0.1486	0.0274	0.0600
no. of reflections used	2791	3998	6311
no. of restraints	0	0	25
no. of parameters	212	232	386
S^a	0.853	1.045	1.056
weight parameters a/b^b	0.0281/0.0000	0.0420/0.3523	0.0762/1.3425
$R1^c$ ($I > 2\sigma(I)$)	0.0392	0.0280	0.0530
$wR2^d$ (all data)	0.0763	0.0741	0.1541
absolute structure parameter		–0.04(9)	0.05(9)
max./min. residual electron density (e Å^{-3})	+0.196/–0.236	+0.224/–0.185	+0.544/–0.272

[a] $S = \{\Sigma[w(F_o^2 - F_c^2)^2]/(n-p)\}^{0.5}$; n = no. of reflections; p = no. of parameters. [b] $w^{-1} = \sigma^2(F_o^2) + (aP)^2 + bP$, with $P = [\max(F_o^2,0) + 2F_c^2]/3$. [c] $R1 = \Sigma||F_o| - |F_c||/\Sigma|F_o|$. [d] $wR2 = \{\Sigma[w(F_o^2 - F_c^2)^2]/\Sigma[w(F_o^2)^2]\}^{.0.5}$

Table 26. Crystal Data and Experimental Parameters for the Crystal Structure Analyses of **4a**·CH_2Cl_2, **5a**·CH_2Cl_2, **6a**·$2CH_2Cl_2$, and **6a**·$½CH_2Cl_2$

	4a·CH_2Cl_2	**5a**·CH_2Cl_2	**6a**·$2CH_2Cl_2$	**6a**·$½CH_2Cl_2$
empirical formula	$C_{21}H_{41}Cl_2N_3O_4Si$	$C_{23}H_{45}Cl_2N_3O_4Si$	$C_{22}H_{39}Cl_4N_3O_4Si$	$C_{20.5}H_{36}ClN_3O_4Si$
formula mass (g mol^{-1})	498.56	526.61	579.45	452.07
collection T (K)	173(2)	173(2)	173(2)	173(2)
λ(Mo Kα) (Å)	0.71073	0.71073	0.71073	0.71073
crystal system	triclinic	orthorhombic	orthorhombic	monoclinic
space group (no.)	$P1$ (1)	$P2_12_12_1$ (19)	$P2_12_12_1$ (19)	$C2$ (5)
a (Å)	11.4543(11)	10.0371(6)	10.2471(9)	23.911(2)
b (Å)	11.8958(11)	12.1617(7)	14.7908(12)	8.2717(4)
c (Å)	19.7436(19)	22.9076(17)	18.635(2)	24.4908(19)
α (deg)	85.224(11)	90	90	90
β (deg)	82.253(11)	90	90	109.231(10)
γ (deg)	89.398(11)	90	90	90
V (Å^3)	2656.4(4)	2796.3(3)	2824.3(5)	4573.6(6)
Z	4	4	4	8
D(calcd) (g cm^{-3})	1.247	1.251	1.363	1.313
μ (mm^{-1})	0.320	0.307	0.494	0.251
F(000)	1072	1136	1224	1944
crystal dimensions (mm)	0.5 x 0.3 x 0.2	0.5 x 0.3 x 0.2	0.5 x 0.4 x 0.3	0.5 x 0.4 x 0.3
2θ range (deg)	3.88–51.80	4.44–53.90	4.84–53.84	4.12–53.84
index ranges	$-14 \le h \le 14$, $-14 \le k \le 14$, $-24 \le l \le 24$	$-12 \le h \le 11$, $-14 \le k \le 15$, $-29 \le l \le 29$	$-12 \le h \le 13$, $-18 \le k \le 18$, $-23 \le l \le 23$	$-30 \le h \le 30$, $-10 \le k \le 10$, $-31 \le l \le 30$
no. of collected reflections	37911	17499	16044	21747
no. of independent reflections	19168	6021	6026	9699
R_{int}	0.0286	0.0431	0.0352	0.0283
no. of reflections used	19168	6021	6026	9699
no. of restraints	450	0	14	20
no. of parameters	1333	317	340	565
weight parameters a/b^b	0.0368/0.0000	0.0509/0.0000	0.0576/0.1732	0.0487/1.3340
$R1^c$ ($I > 2\sigma(I)$)	0.0302	0.0347	0.0329	0.0355
$wR2^d$ (all data)	0.0666	0.0856	0.0893	0.0890
absolute structure parameter	0.00(3)	0.05(5)	0.01(5)	0.03(5)
extinction coefficient	0.0023(3)			
max./min. residual electron density, e Å^{-3}	+0.203/–0.220	+0.511/–0.476	+0.284/–0.254	+0.535/–0.375

[a] $S = \{\Sigma[w(F_o^2 - F_c^2)^2]/(n-p)\}^{0.5}$; n = no. of reflections; p = no. of parameters. [b] $w^{-1} = \sigma^2(F_o^2) + (aP)^2 + bP$, with $P = [\max(F_o^2,0) + 2F_c^2]/3$. [c] $R1 = \Sigma||F_o| - |F_c||/\Sigma|F_o|$. [d] $wR2 = \{\Sigma[w(F_o^2 - F_c^2)^2]/\Sigma[w(F_o^2)^2]\}^{0.5}$.

Table 27. Crystal Data and Experimental Parameters for the Crystal Structure Analyses of **7b**·CH_3CN, **8a**, and **9b**

	7b·CH_3CN	**8a**	**9b**
empirical formula	$C_{13}H_{22}N_2O_7Si$	$C_{13}H_{23}NO_7Si$	$C_{16}H_{29}NO_6Si$
formula mass (g mol^{-1})	346.41	331.41	359.49
collection T (K)	173(2)	173(2)	173(2)
λ(Mo Kα) (Å)	0.71073	0.71073	0.71073
crystal system	orthorhombic	orthorhombic	tetragonal
space group (no.)	$P2_12_12_1$ (19)	$P2_12_12_1$ (19)	$P4_1$ (76)
a (Å)	7.5306(5)	9.954(2)	8.0232(10)
b (Å)	12.1465(10)	10.803(2)	8.0232(10)
c (Å)	18.7734(18)	15.687(3)	28.688(3)
β (deg)	90	90	90
V ($Å^3$)	1717.2(2)	1686.9(6)	1846.7(4)
Z	4	4	4
D(calcd) (g cm^{-3})	1.340	1.313	1.293
μ (mm^{-1})	0.172	0.171	0.157
F(000)	736	712	776
crystal dimensions (mm)	0.5 x 0.3 x 0.2	0.5 x 0.4 x 0.4	0.5 x 0.4 x 0.4
2θ range (deg)	2.74–27.98	5.56–53.88	5.08–47.90
index ranges	$-9 \le h \le 9$, $-15 \le k \le 16$, $-24 \le l \le 24$	$-12 \le h \le 12$, $-13 \le k \le 13$, $-19 \le l \le 19$	$-9 \le h \le 8$, $-8 \le k \le 9$, $-32 \le l \le 31$
no. of collected reflections	16689	19169	6805
no. of independent reflections	4055	3614	2832
R_{int}	0.0317	0.0343	0.0269
no. of reflections used	4055	3614	2832
no. of restraints	0	0	1
no. of parameters	212	206	226
S^a	1.033	1.045	1.034
weight parameters a/b^b	0.0461/0.0000	0.0333/0.5708	0.0501/0.0000
$R1^c$ ($I > 2\sigma(I)$)	0.0289	0.0296	0.0259
$wR2^d$ (all data)	0.0726	0.0724	0.0667
absolute structure parameter	0.06(9)	–0.02(11)	–0.05(10)
max./min. residual electron density, e $Å^{-3}$	+0.232/–0.225	+0.253/–0.247	+0.156/–0.137

[a] $S = \{\Sigma[w(F_o^2 - F_c^2)^2]/(n-p)\}^{0.5}$; n = no. of reflections; p = no. of parameters. [b] $w^{-1} = \sigma^2(F_o^2) + (aP)^2 + bP$, with $P = [\max(F_o^2,0) + 2F_c^2]/3$. [c] $R1 = \Sigma||F_o| - |F_c||/\Sigma|F_o|$. [d] $wR2 = \{\Sigma[w(F_o^2 - F_c^2)^2]/\Sigma[w(F_o^2)^2]\}^{0.5}$.

Table 28. Crystal Data and Experimental Parameters for the Crystal Structure Analyses of **10a**, **11a**·CH_3CN, and **12a**

	10a	**11a**·CH_3CN	**12a**
empirical formula	$C_{23}H_{27}NO_7Si$	$C_{30}H_{40}N_2O_6Si$	$C_{26}H_{33}NO_6Si$
formula mass (g mol^{-1})	457.55	552.73	483.62
collection T (K)	173(2)	173(2)	173(2)
λ(Mo Kα) (Å)	0.71073	0.71073	0.71073
crystal system	monoclinic	monoclinic	orthorhombic
space group (no.)	$P2_1$ (4)	$P2_1$ (4)	$P2_12_12_1$ (19)
a (Å)	8.9712(7)	11.0878(15)	10.878(4)
b (Å)	10.8821(7)	11.2514(12)	11.036(3)
c (Å)	11.8118(9)	12.8474(17)	20.267(10)
β (deg)	109.649(9)	113.727(15)	90
V ($Å^3$)	1085.99(14)	1467.3(3)	2433.1(16)
Z	2	2	4
D(calcd) (g cm^{-3})	1.399	1.251	1.320
μ (mm^{-1})	0.154	0.125	0.139
F(000)	484	592	1032
crystal dimensions (mm)	0.5 x 0.3 x 0.1	0.5 x 0.3 x 0.1	0.3 x 0.3 x 0.2
2θ range (deg)	4.82–53.82	5.02–52.90	4.20–46.66
index ranges	$-11 \le h \le 11$, $-13 \le k \le 13$, $-15 \le l \le 14$	$-13 \le h \le 13$, $-14 \le k \le 14$, $-16 \le l \le 16$	$-12 \le h \le 12$, $-12 \le k \le 11$, $-22 \le l \le 22$
no. of collected reflections	7131	16615	9830
no. of independent reflections	4546	6021	3504
R_{int}	0.0252	0.0624	0.0768
no. of reflections used	4546	6021	3504
no. of restraints	1	1	0
no. of parameters	292	360	314
S^a	1.052	1.013	0.979
weight parameters a/b^b	0.0446/0.0000	0.0493/0.0000	0.0464/0.0000
$R1^c$ ($I > 2\sigma(I)$)	0.0275	0.0324	0.0385
$wR2^d$ (all data)	0.0686	0.0821	0.0884
absolute structure parameter	0.10(8)	–0.03(8)	–0.10(15)
max./min. residual electron density, e $Å^{-3}$	+0.183/–0.168	+0.172/–0.243	+0.182/–0.262

[a] $S = \{\Sigma[w(F_o^2 - F_c^2)^2]/(n-p)\}^{0.5}$; n = no. of reflections; p = no. of parameters. [b] $w^{-1} = \sigma^2(F_o^2) + (aP)^2 + bP$, with $P = [\max(F_o^2,0) + 2F_c^2]/3$. [c] $R1 = \Sigma||F_o| - |F_c||/\Sigma|F_o|$. [d] $wR2 = \{\Sigma[w(F_o^2 - F_c^2)^2]/\Sigma[w(F_o^2)^2]\}^{0.5}$.

Table 29. Crystal Data and Experimental Parameters for the Crystal Structure Analyses of **14**, **14**·H_2O, **15**·$C_4H_8O_3$, and **16**

	14	**14**·H_2O	**15**·$C_4H_8O_3$	**16**
empirical formula	$C_{13}H_{23}NO_7Si$	$C_{13}H_{25}NO_8Si$	$C_{19}H_{35}NO_{10}Si$	$C_{18}H_{33}NO_6Si$
formula mass (g mol^{-1})	333.41	351.43	465.57	387.54
collection T (K)	173(2)	173(2)	173(2)	173(2)
λ(Mo Kα) (Å)	0.71073	0.71073	0.71073	0.71073
crystal system	monoclinic	monoclinic	monoclinic	monoclinic
space group (no.)	$P2_1/c$ (14)	Cc (9)	$P2_1/n$ (14)	$P2_1/c$ (14)
a (Å)	9.941(2)	9.9705(8)	10.9875(8)	10.7859(11)
b (Å)	17.028(3)	16.9981(12)	8.8592(5)	30.250(4)
c (Å)	10.100(2)	10.4368(8)	22.9984(18)	18.4665(19)
β (deg)	118.66(3)	117.356(8)	99.234(9)	101.971(12)
V (Å^3)	1500.3(5)	1571.0(2)	2209.7(3)	5894.0(12)
Z	4	4	4	12
D(calcd) (g cm^{-3})	1.476	1.486	1.399	1.310
μ (mm^{-1})	0.192	0.192	0.162	0.153
F(000)	712	752	1000	2520
crystal dimensions (mm)	0.4 x 0.2 x 0.1	0.4 x 0.4 x 0.2	0.5 x 0.3 x 0.2	0.5x 0.5 x 0.15
2θ range (deg)	5.18–49.48	5.26–53.74	4.42–53.76	4.26–54.00
index ranges	$-11 \le h \le 11$, $-20 \le k \le 20$, $-11 \le l \le 11$	$-12 \le h \le 12$, $-21 \le k \le 21$, $-13 \le l \le 13$	$-13 \le h \le 13$, $-11 \le k \le 11$, $-29 \le l \le 29$	$-13 \le h \le 13$, $-38 \le k \le 38$, $-23 \le l \le 23$
no. of collected reflections	13821	9054	24039	56821
no. of independent reflections	2538	3339	4725	12673
R_{int}	0.0691	0.0313	0.0468	0.0432
max./min. transmission	0.9781/0.9489			
no. of reflections used	2538	3339	4725	12673
no. of restraints	176	3	0	0
no. of parameters	248	217	291	736
S^a	1.198	1.053	1.043	1.055
weight parameters a/b^b	0.0238/1.9472	0.0444/0.4270	0.0603/0.8159	0.0787/0.5129
$R1^c$ ($I > 2\sigma(I)$)	0.0521	0.0264	0.0385	0.0411
$wR2^d$ (all data)	0.1232	0.0692	0.1097	0.1194
absolute structure parameter		0.05(8)		
max./min. residual electron density (e Å^{-3})	+0.214/–0.250	+0.224/–0.207	+0.305/–0.422	+0.533/–0.308

[a] $S = \{\Sigma[w(F_o^2 - F_c^2)^2]/(n-p)\}^{0.5}$; n = no. of reflections; p = no. of parameters. [b] $w^{-1} = \sigma^2(F_o^2) + (aP)^2 + bP$, with $P = [\max(F_o^2,0) + 2F_c^2]/3$. [c] $R1 = \Sigma||F_o| - |F_c||/\Sigma|F_o|$. [d] $wR2 = \{\Sigma[w(F_o^2 - F_c^2)^2]/\Sigma[w(F_o^2)^2]\}^{0.5}$.

Table 30. Crystal Data and Experimental Parameters for the Crystal Structure Analyses of *meso*-**19**·2CH_3OH, *rac*-**20**·1.73CH_3OH, (*Λ*,*S*,*S*,*S*)-*mer*-**21**, and (*Λ*,*S*,*S*,*S*)-*mer*-**22**·2CH_3CN

	meso-**19**·2CH_3OH	*rac*-**20**·1.73CH_3OH	(*Λ*,*S*,*S*,*S*)-*mer*-**21**	(*Λ*,*S*,*S*,*S*)-*mer*-**22**·2CH_3CN
empirical formula	$C_{22}H_{38}N_2O_{18}Si$	$C_{29.73}H_{54.91}N_4O_{19.73}Si$	$C_{30}H_{56}N_2O_{15}Si$	$C_{40}H_{74}N_4O_{15}Si$
formula mass (g mol^{-1})	646.63	812.06	712.86	879.12
collection T (K)	173(2)	173(2)	173(2)	173(2)
λ(Mo Kα) (Å)	0.71073	0.71073	0.71073	0.71073
crystal system	monoclinic	triclinic	orthorhombic	monoclinic
space group (no.)	$P2_1/n$ (14)	$P\bar{1}$ (2)	$P2_12_12_1$ (19)	$P2_1$ (4)
a (Å)	13.2318(13)	12.3633(12)	12.2326(9)	12.5161(16)
b (Å)	6.7631(4)	12.3871(12)	15.6886(18)	15.7570(18)
c (Å)	15.7756(13)	13.3526(11)	20.0976(19)	12.7940(14)
α (deg)	90	69.329(10)	90	90
β (deg)	100.859(11)	84.253(11)	90	104.493(14)
γ (deg)	90	83.934(12)	90	90
V ($Å^3$)	1386.4(2)	1898.2(3)	3857.0(6)	2442.9(5)
Z	2	2	4	2
D(calcd) (g cm^{-3})	1.549	1.421	1.228	1.195
μ (mm^{-1})	0.175	0.148	0.126	0.113
F(000)	684	866	1536	952
crystal dimensions (mm)	0.3 x 0.3 x 0.2	0.4 x 0.3 x 0.1	0.3 x 0.1 x 0.1	0.4 x 0.4 x 0.4
2θ range (deg)	4.46–49.78	4.50–52.74	4.82–53.04	4.82–52.94
index ranges	$-15 \le h \le 15$, $-7 \le k \le 7$, $-18 \le l \le 18$	$-15 \le h \le 15$, $-15 \le k \le 15$, $-16 \le l \le 16$	$-15 \le h \le 14$, $-19 \le k \le 19$, $-25 \le l \le 25$	$-15 \le h \le 15$, $-19 \le k \le 19$, $-15 \le l \le 15$
no. of collected reflections	12658	21562	32368	18029
no. of independent reflections	2393	7269	7877	9261
R_{int}	0.0276	0.0294	0.0496	0.0382
no. of reflections used	2393	7269	7877	9261
no. of parameters	209	519	448	578
no. of restraints	0	0	0	4
S^a	1.061	1.046	0.893	0.931
weight parameters a/b^b	0.0668/0.8325	0.0652/0.5579	0.0335/0.0000	0.0423/0.0000
$R1^c$ ($I > 2\sigma(I)$)	0.0384	0.0419	0.0323	0.0371
$wR2^d$ (all data)	0.1115	0.1156	0.0660	0.0796
absolute structure parameter			+0.01(9)	–0.03(9)
max./min. residual electron density (e $Å^{-3}$)	+0.312/–0.469	+0.757/–0.535	+0.157/–0.175	+0.156/–0.146

[a] $S = \{\Sigma[w(F_o^2 - F_c^2)^2]/(n-p)\}^{0.5}$; n = no. of reflections; p = no. of parameters. [b] $w^{-1} = \sigma^2(F_o^2) + (aP)^2 + bP$, with $P = [\max(F_o^2,0) + 2F_c^2]/3$. [c] $R1 = \Sigma||F_o| - |F_c||/\Sigma|F_o|$. [d] $wR2 = \{\Sigma[w(F_o^2 - F_c^2)^2]/\Sigma[w(F_o^2)^2]\}^{0.5}$.

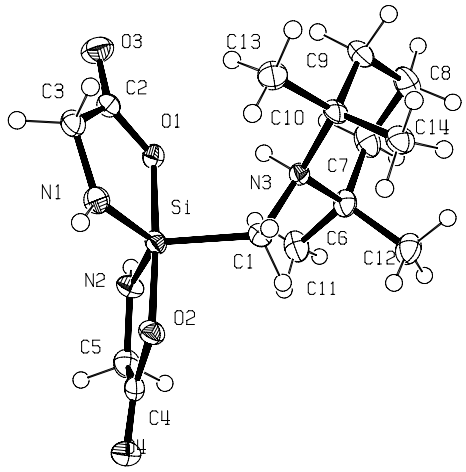

Figure 65. Crystal structure of *rac*-**1** (probability level of displacement ellipsoids 50%) showing the atomic numbering scheme.

Table 31. Atomic Coordinates (x 10^4) and Equivalent Isotropic Displacement Parameters (Å^2 x 10^3) for *rac*-**1**. U(eq) is Defined as One Third of the trace of the Orthogonalized Uij Tensor.

	x	y	z	U(eq)
C(1)	2943(2)	659(2)	5892(1)	19(1)
C(2)	719(2)	2505(2)	5984(1)	22(1)
C(3)	119(2)	1437(2)	5943(1)	24(1)
C(4)	2322(2)	–130(2)	4260(1)	22(1)
C(5)	2489(2)	1071(2)	4071(1)	27(1)
C(6)	4339(2)	2055(2)	6179(1)	23(1)
C(7)	4519(2)	3069(3)	6619(1)	32(1)
C(8)	4427(2)	2819(3)	7344(1)	37(1)
C(9)	3394(2)	2355(2)	7483(1)	29(1)
C(10)	3125(2)	1296(2)	7097(1)	22(1)
C(11)	4264(2)	2473(3)	5477(1)	29(1)
C(12)	5164(2)	1179(3)	6232(1)	32(1)
C(13)	2007(2)	1086(3)	7186(1)	31(1)
C(14)	3701(2)	276(2)	7321(1)	26(1)
N(1)	712(2)	652(2)	5574(1)	22(1)
N(2)	2155(2)	1756(2)	4613(1)	22(1)
N(3)	3300(2)	1568(2)	6363(1)	18(1)
O(1)	1628(1)	2393(2)	5738(1)	21(1)
O(2)	2044(1)	–245(2)	4872(1)	21(1)
O(3)	421(1)	3375(2)	6227(1)	34(1)
O(4)	2424(1)	–926(2)	3890(1)	29(1)
Si	1872(1)	1058(1)	5320(1)	18(1)

Table 32. Bond Lengths [Å] and Angles [deg] for *rac*-**1**.

Si–N(2)	1.713(2)	N(2)–Si–N(1)	126.59(11)
Si–N(1)	1.717(2)	N(2)–Si–O(2)	87.60(10)
Si–O(2)	1.8163(19)	N(1)–Si–O(2)	91.64(10)
Si–O(1)	1.8356(19)	N(2)–Si–O(1)	90.94(10)
Si–C(1)	1.918(2)	N(1)–Si–O(1)	86.45(10)
O(1)–C(2)	1.329(3)	O(2)–Si–O(1)	176.25(9)

O(2)–C(4)	1.318(3)	N(2)–Si–C(1)	118.10(11)
O(3)–C(2)	1.217(3)	N(1)–Si–C(1)	115.30(11)
O(4)–C(4)	1.221(3)	O(2)–Si–C(1)	90.15(9)
N(1)–C(3)	1.442(3)	O(1)–Si–C(1)	93.58(9)
N(1)–H(1N)	0.80(3)	C(2)–O(1)–Si	115.41(17)
N(2)–C(5)	1.449(3)	C(4)–O(2)–Si	115.40(17)
N(2)–H(2N)	0.87(3)	C(3)–N(1)–Si	118.71(18)
N(3)–C(1)	1.528(3)	C(3)–N(1)–H(1N)	120(2)
N(3)–C(10)	1.557(3)	O(3)–C(2)–O(1)	122.9(3)
N(3)–C(6)	1.560(3)	O(3)–C(2)–C(3)	124.3(2)
N(3)–H(3N)	0.87(3)	O(1)–C(2)–C(3)	112.8(2)
C(1)–H(1A)	0.9900	N(1)–C(3)–C(2)	106.2(2)
C(1)–H(1B)	0.9900	O(4)–C(4)–O(2)	122.9(3)
C(2)–C(3)	1.508(4)	O(4)–C(4)–C(5)	124.2(2)
C(3)–H(3A)	0.9900	O(2)–C(4)–C(5)	112.8(2)
C(3)–H(3B)	0.9900	N(2)–C(5)–C(4)	107.0(2)
C(4)–C(5)	1.497(4)	C(7)–C(6)–C(11)	108.1(2)
C(6)–C(7)	1.526(4)	C(7)–C(6)–C(12)	112.5(2)
C(6)–C(11)	1.526(3)	C(11)–C(6)–C(12)	109.7(2)
C(6)–C(12)	1.527(4)	C(7)–C(6)–N(3)	107.1(2)
C(7)–C(8)	1.523(4)	C(11)–C(6)–N(3)	106.9(2)
C(8)–C(9)	1.523(4)	C(12)–C(6)–N(3)	112.4(2)
C(9)–C(10)	1.531(4)	C(8)–C(7)–C(6)	114.2(2)
C(10)–C(14)	1.511(4)	C(7)–C(8)–C(9)	109.1(2)
C(10)–C(13)	1.536(3)	C(8)–C(9)–C(10)	114.7(2)
Si–N(1)–H(1N)	122(2)	C(14)–C(10)–C(9)	112.5(2)
C(5)–N(2)–Si	116.44(18)	C(14)–C(10)–C(13)	109.6(2)
C(5)–N(2)–H(2N)	117.7(19)	C(9)–C(10)–C(13)	107.7(2)
Si–N(2)–H(2N)	123.7(19)	C(14)–C(10)–N(3)	112.5(2)
C(1)–N(3)–C(10)	114.63(19)	C(9)–C(10)–N(3)	107.0(2)
C(1)–N(3)–C(6)	113.06(18)	C(13)–C(10)–N(3)	107.26(19)
C(10)–N(3)–C(6)	116.51(18)	C(6)–N(3)–H(3N)	103.4(18)
C(1)–N(3)–H(3N)	102.2(18)	N(3)–C(1)–Si	116.62(16)
C(10)–N(3)–H(3N)	104.8(18)	N(3)–C(1)–H(1A)	108.1

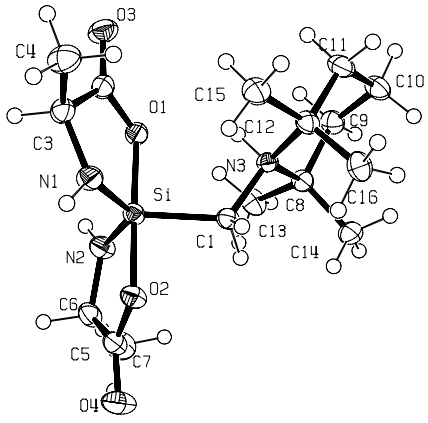

Figure 66. Crystal structure of **2b** (probability level of displacement ellipsoids 50%) showing the atomic numbering scheme.

Table 33. Atomic Coordinates (x 10^4) and Equivalent Isotropic Displacement Parameters (Å^2 x 10^3) for **2b**. U(eq) is Defined as One Third of the Trace of the Orthogonalized Uij Tensor.

	x	y	z	U(eq)
C(1)	9189(1)	4792(1)	1241(1)	21(1)
C(2)	5503(2)	5945(1)	1671(1)	25(1)
C(3)	5217(2)	4837(1)	2161(1)	27(1)
C(4)	5134(2)	5212(2)	2946(1)	37(1)
C(5)	8020(2)	1928(1)	680(1)	26(1)
C(6)	7033(2)	2497(1)	116(1)	28(1)
C(7)	7755(2)	2513(2)	–617(1)	40(1)
C(8)	10178(2)	6630(1)	516(1)	22(1)
C(9)	10222(2)	8058(1)	529(1)	27(1)
C(10)	10937(2)	8595(1)	1189(1)	30(1)
C(11)	10107(2)	8159(1)	1844(1)	30(1)
C(12)	9996(2)	6743(1)	1925(1)	24(1)
C(13)	9218(2)	6209(2)	–102(1)	31(1)
C(14)	11683(2)	6074(1)	434(1)	30(1)
C(15)	8859(2)	6464(2)	2496(1)	31(1)
C(16)	11446(2)	6180(2)	2138(1)	30(1)
N(1)	6357(1)	3947(1)	2002(1)	26(1)
N(2)	6659(2)	3726(1)	375(1)	27(1)
N(3)	9421(1)	6194(1)	1213(1)	19(1)
O(1)	6455(1)	5687(1)	1165(1)	23(1)
O(2)	8107(1)	2611(1)	1264(1)	25(1)
O(3)	4929(1)	6957(1)	1731(1)	35(1)
O(4)	8663(1)	948(1)	601(1)	40(1)
Si	7264(1)	4134(1)	1210(1)	20(1)

Table 34. Bond Lengths [Å] and Angles [deg] for **2b**.

C(1)–N(3)	1.5203(15)	C(10)–C(11)–C(12)	114.85(12)
C(1)–Si	1.9157(14)	C(16)–C(12)–C(15)	110.13(12)
C(2)–O(3)	1.2146(19)	C(16)–C(12)–C(11)	111.13(13)
C(2)–O(1)	1.3213(17)	C(15)–C(12)–C(11)	108.08(12)
C(2)–C(3)	1.525(2)	C(16)–C(12)–N(3)	112.06(11)
C(3)–N(1)	1.4522(19)	C(15)–C(12)–N(3)	106.91(11)
C(3)–C(4)	1.524(2)	C(11)–C(12)–N(3)	108.36(11)
C(5)–O(4)	1.2169(19)	H(1N)–N(1)–C(3)	115.7(12)
C(5)–O(2)	1.3189(17)	H(1N)–N(1)–Si	121.8(12)
C(5)–C(6)	1.522(2)	C(3)–N(1)–Si	117.04(10)
C(6)–N(2)	1.4472(19)	H(2N)–N(2)–C(6)	117.5(14)
C(6)–C(7)	1.526(2)	H(2N)–N(2)–Si	122.8(13)
C(8)–C(14)	1.521(2)	C(6)–N(2)–Si	117.37(10)
C(8)–C(13)	1.527(2)	H(3N)–N(3)–C(1)	104.9(10)
C(8)–C(9)	1.5331(19)	H(3N)–N(3)–C(12)	104.3(11)
C(8)–N(3)	1.5521(17)	C(1)–N(3)–C(12)	113.29(11)
C(9)–C(10)	1.516(2)	H(3N)–N(3)–C(8)	102.7(11)
C(10)–C(11)	1.519(2)	C(1)–N(3)–C(8)	112.94(10)
C(11)–C(12)	1.530(2)	C(12)–N(3)–C(8)	116.92(10)
C(12)–C(16)	1.523(2)	C(2)–O(1)–Si	115.42(9)
C(12)–C(15)	1.528(2)	C(5)–O(2)–Si	115.35(9)
C(12)–N(3)	1.5500(17)	N(2)–Si–N(1)	126.76(6)
N(1)–H(1N)	0.888(19)	N(2)–Si–O(2)	87.80(6)
N(1)–Si	1.7150(13)	N(1)–Si–O(2)	93.23(5)
N(2)–H(2N)	0.83(2)	N(2)–Si–O(1)	93.30(5)
N(2)–Si	1.7146(13)	N(1)–Si–O(1)	86.93(5)
N(3)–H(3N)	0.899(18)	O(2)–Si–O(1)	178.50(5)
O(1)–Si	1.8294(10)	N(2)–Si–C(1)	115.11(7)

O(2)–Si	1.8129(10)	N(1)–Si–C(1)	118.06(6)
N(3)–C(1)–Si	119.65(9)	O(2)–Si–C(1)	86.06(5)
O(3)–C(2)–O(1)	122.92(13)	N(1)–C(3)–C(4)	114.06(13)
O(3)–C(2)–C(3)	124.52(13)	N(1)–C(3)–C(2)	105.29(11)
O(1)–C(2)–C(3)	112.56(12)	C(4)–C(3)–C(2)	112.47(13)
O(4)–C(5)–O(2)	123.46(14)	N(2)–C(6)–C(5)	106.06(11)
O(4)–C(5)–C(6)	123.72(13)	N(2)–C(6)–C(7)	113.30(13)
O(2)–C(5)–C(6)	112.82(12)	C(5)–C(6)–C(7)	111.45(13)
C(14)–C(8)–C(13)	109.76(12)	C(9)–C(8)–N(3)	107.49(11)
C(14)–C(8)–C(9)	111.69(12)	C(10)–C(9)–C(8)	113.83(12)
C(13)–C(8)–C(9)	108.83(12)	C(9)–C(10)–C(11)	108.64(12)
C(13)–C(8)–N(3)	106.61(11)		

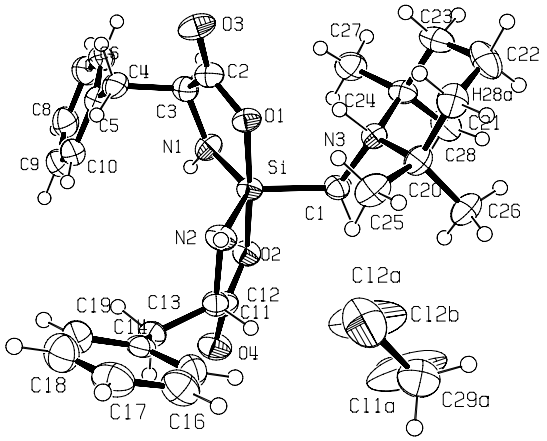

Figure 67. Crystal structure of **3a**·CH_2Cl_2 (probability level of displacement ellipsoids 50%) showing the atomic numbering scheme.

Table 35. Atomic Coordinates (x 10^4) and Equivalent Isotropic Displacement Parameters ($Å^2$ x 10^3) for **3a**·CH_2Cl_2. U(eq) is Defined as One Third of the Trace of the Orthogonalized Uij Tensor.

	x	y	z	U(eq)
C(1)	9448(3)	5718(3)	5331(3)	31(1)
C(2)	11104(3)	7534(3)	3858(3)	32(1)
C(3)	11219(3)	6506(3)	3217(3)	33(1)
C(4)	11073(4)	6817(3)	2014(3)	39(1)
C(5)	11175(4)	5787(4)	1367(3)	39(1)
C(6)	12421(4)	5300(4)	1586(3)	48(1)
C(7)	12530(5)	4348(5)	1037(4)	55(1)
C(8)	11385(5)	3859(4)	258(4)	53(1)
C(9)	10146(5)	4320(4)	28(3)	48(1)
C(10)	10051(4)	5292(4)	584(3)	45(1)
C(11)	6771(4)	5182(3)	2690(3)	34(1)
C(12)	6400(3)	6401(3)	2717(3)	32(1)
C(13)	5497(3)	6834(3)	1560(3)	35(1)
C(14)	4913(3)	7987(3)	1559(3)	33(1)
C(15)	4420(4)	8309(4)	2362(3)	43(1)
C(16)	3827(4)	9335(4)	2312(4)	50(1)
C(17)	3692(4)	10076(4)	1456(4)	53(1)
C(18)	4187(5)	9762(4)	654(4)	57(1)
C(19)	4799(4)	8724(4)	708(3)	47(1)
C(20)	9649(4)	7050(3)	6938(3)	35(1)

C(21)	10688(4)	7792(3)	7830(3)	44(1)
C(22)	11927(5)	7173(4)	8599(3)	54(1)
C(23)	12606(4)	6640(4)	7903(4)	47(1)
C(24)	11727(3)	5823(3)	7013(3)	32(1)
C(25)	8639(4)	7812(3)	6076(4)	43(1)
C(26)	8936(4)	6280(4)	7459(3)	45(1)
C(27)	12423(4)	5514(4)	6221(4)	46(1)
C(28)	11463(4)	4764(3)	7570(3)	43(1)
Cl(1A)	5072(4)	7066(4)	5477(3)	52(2)
C(29A)	4679(5)	8375(4)	5933(4)	59(1)
Cl(2A)	5368(5)	9489(5)	5447(2)	74(1)
Cl(1B)	5133(13)	7090(8)	5690(20)	125(6)
C(29B)	4679(5)	8375(4)	5933(4)	59(1)
Cl(2B)	5462(17)	9359(17)	5490(20)	102(11)
N(1)	10189(3)	5747(3)	3239(3)	35(1)
N(2)	7671(3)	6987(3)	3214(3)	35(1)
N(3)	10398(3)	6426(2)	6300(2)	28(1)
O(1)	10160(2)	7436(2)	4273(2)	30(1)
O(2)	8036(3)	4982(2)	3298(2)	34(1)
O(3)	11804(3)	8345(2)	3980(3)	43(1)
O(4)	5969(3)	4464(3)	2170(2)	46(1)
Si	9099(1)	6192(1)	3836(1)	28(1)

Table 36. Bond Lengths [Å] and Angles [deg] for **3a**·CH_2Cl_2.

C(1)–Si	1.906(3)	C(9)–C(8)–C(7)	120.5(5)
C(2)–O(3)	1.208(4)	C(8)–C(9)–C(10)	119.2(4)
C(2)–O(1)	1.330(4)	C(5)–C(10)–C(9)	121.3(4)
C(2)–C(3)	1.520(5)	O(4)–C(11)–O(2)	123.5(4)
C(3)–N(1)	1.449(5)	O(4)–C(11)–C(12)	123.7(3)
C(3)–C(4)	1.545(5)	O(2)–C(11)–C(12)	112.7(3)
C(4)–C(5)	1.523(6)	N(2)–C(12)–C(11)	105.3(3)
C(5)–C(10)	1.378(5)	N(2)–C(12)–C(13)	113.7(3)
C(5)–C(6)	1.394(6)	C(11)–C(12)–C(13)	112.4(3)
C(6)–C(7)	1.376(7)	C(14)–C(13)–C(12)	114.8(3)
C(7)–C(8)	1.387(7)	C(19)–C(14)–C(15)	118.3(4)
C(8)–C(9)	1.370(7)	C(19)–C(14)–C(13)	119.6(3)
C(9)–C(10)	1.397(7)	C(15)–C(14)–C(13)	122.0(3)
C(11)–O(4)	1.223(5)	C(16)–C(15)–C(14)	121.2(4)
C(11)–O(2)	1.308(5)	C(15)–C(16)–C(17)	121.1(4)
C(11)–C(12)	1.524(5)	C(16)–C(17)–C(18)	118.0(4)
C(12)–N(2)	1.452(4)	C(17)–C(18)–C(19)	121.1(4)
C(12)–C(13)	1.524(5)	C(14)–C(19)–C(18)	120.3(4)
C(13)–C(14)	1.523(5)	C(26)–C(20)–C(25)	110.3(3)
C(14)–C(19)	1.380(6)	C(26)–C(20)–C(21)	111.6(3)
C(14)–C(15)	1.393(5)	C(25)–C(20)–C(21)	107.7(3)
C(15)–C(16)	1.380(6)	C(26)–C(20)–N(3)	113.5(3)
C(16)–C(17)	1.383(7)	C(25)–C(20)–N(3)	106.0(3)
C(17)–C(18)	1.391(7)	C(21)–C(20)–N(3)	107.3(3)
C(18)–C(19)	1.402(7)	C(22)–C(21)–C(20)	114.0(3)
C(20)–C(26)	1.519(5)	C(23)–C(22)–C(21)	109.2(3)
C(20)–C(25)	1.525(5)	C(22)–C(23)–C(24)	114.7(3)
C(20)–C(21)	1.543(5)	C(23)–C(24)–C(27)	109.6(3)
C(20)–N(3)	1.555(4)	C(23)–C(24)–C(28)	110.7(3)
C(21)–C(22)	1.516(6)	C(27)–C(24)–C(28)	109.8(3)
C(22)–C(23)	1.507(7)	C(23)–C(24)–N(3)	107.9(3)
C(23)–C(24)	1.530(5)	C(27)–C(24)–N(3)	107.3(3)
C(24)–C(27)	1.533(5)	C(28)–C(24)–N(3)	111.5(3)
C(24)–C(28)	1.543(5)	Cl(2A)–C(29A)–Cl(1A)	111.4(4)
C(24)–N(3)	1.552(4)	H(1N)–N(1)–C(3)	117(2)

Cl(1A)–C(29A)	1.790(7)	H(1N)–N(1)–Si	123(2)
C(29A)–Cl(2A)	1.763(7)	C(3)–N(1)–Si	118.5(2)
N(1)–H(1N)	1.16(5)	H(2N)–N(2)–C(12)	101(3)
N(1)–Si	1.725(3)	H(2N)–N(2)–Si	137(3)
N(2)–H(2N)	0.96(5)	C(12)–N(2)–Si	117.3(2)
N(2)–Si	1.725(3)	H(3N)–N(3)–C(1)	103(2)
N(3)–H(3N)	1.05(4)	H(3N)–N(3)–C(24)	105(2)
O(1)–Si	1.835(2)	C(1)–N(3)–C(24)	113.4(2)
O(2)–Si	1.817(3)	H(3N)–N(3)–C(20)	104(2)
N(3)–C(1)–Si	117.9(2)	C(1)–N(3)–C(20)	112.3(3)
O(3)–C(2)–O(1)	124.0(3)	C(24)–N(3)–C(20)	117.6(3)
O(3)–C(2)–C(3)	123.2(3)	C(2)–O(1)–Si	115.7(2)
O(1)–C(2)–C(3)	112.7(3)	C(11)–O(2)–Si	116.1(2)
N(1)–C(3)–C(2)	106.0(3)	N(1)–Si–N(2)	127.31(16)
N(1)–C(3)–C(4)	113.2(3)	N(1)–Si–O(2)	91.18(14)
C(2)–C(3)–C(4)	110.7(3)	N(2)–Si–O(2)	86.98(14)
C(5)–C(4)–C(3)	110.8(3)	N(1)–Si–O(1)	86.41(13)
C(10)–C(5)–C(6)	118.3(4)	N(2)–Si–O(1)	91.76(13)
C(10)–C(5)–C(4)	121.6(4)	O(2)–Si–O(1)	175.81(12)
C(6)–C(5)–C(4)	120.1(3)	N(1)–Si–C(1)	117.40(16)
C(7)–C(6)–C(5)	121.0(4)	N(2)–Si–C(1)	115.25(16)
C(6)–C(7)–C(8)	119.7(5)	O(2)–Si–C(1)	89.68(13)

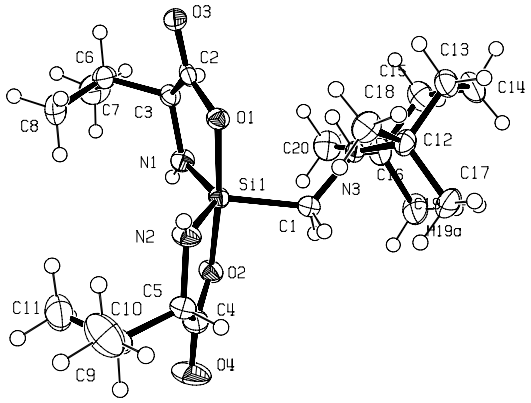

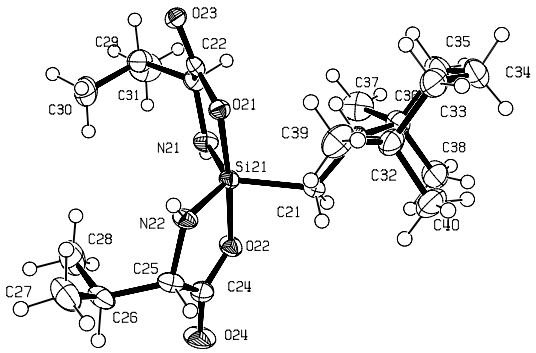

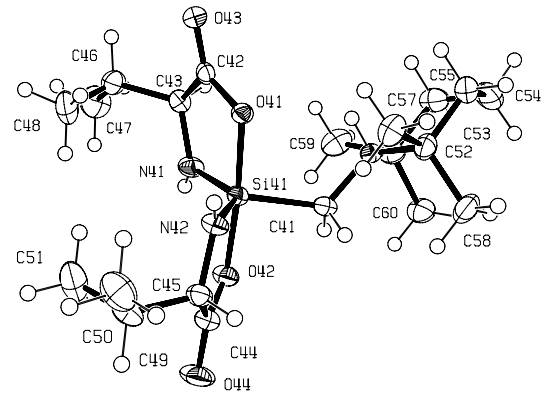

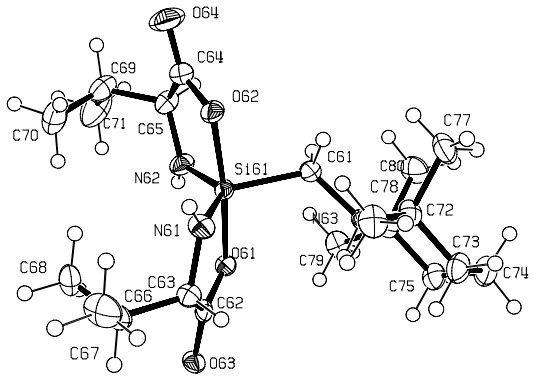

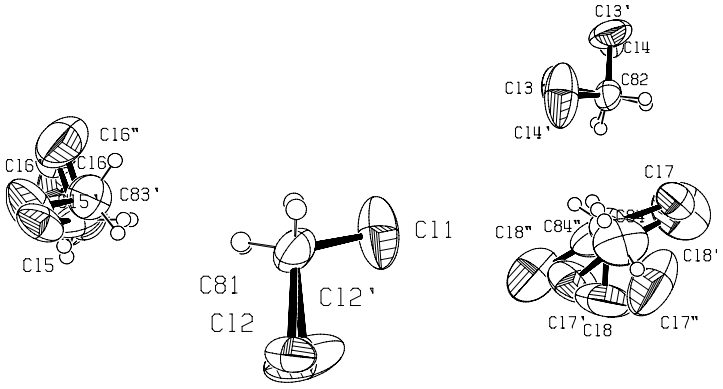

Figure 68. Crystal structure of **4a**·CH_2Cl_2 (probability level of displacement ellipsoids 50%) showing the atomic numbering scheme.

Table 37. Atomic Coordinates (x 10^4) and Equivalent Isotropic Displacement Parameters (Å^2 x 10^3) for **4a**·CH_2Cl_2. U(eq) is Defined as One Third of the Trace of the Orthogonalized Uij Tensor.

	x	y	z	U(eq)
O1	2476(1)	7795(1)	7949(1)	22(1)
N1	2911(2)	9427(1)	8528(1)	25(1)
O2	1053(1)	10465(1)	8306(1)	26(1)
N2	442(2)	8514(1)	8353(1)	27(1)
O3	3880(1)	6655(1)	8296(1)	25(1)
O4	–705(2)	11228(1)	8603(1)	52(1)
N3	2920(1)	9427(1)	6587(1)	22(1)
C1	1921(2)	9726(2)	7136(1)	28(1)
C2	3392(2)	7585(2)	8260(1)	21(1)
C3	3823(2)	8588(2)	8585(1)	22(1)
C4	–96(2)	10407(2)	8468(1)	31(1)
C5	–591(2)	9229(2)	8464(1)	28(1)
C6	4092(2)	8262(2)	9315(1)	30(1)
C7	4693(2)	9228(2)	9592(1)	48(1)
C8	2992(2)	7866(2)	9790(1)	42(1)
C9	–1452(2)	8914(2)	9112(1)	36(1)
C10	–2070(3)	7796(3)	9067(2)	60(1)
C11	–864(2)	8884(2)	9757(1)	48(1)
C12	2504(2)	8749(2)	6025(1)	27(1)
C13	3593(2)	8457(2)	5530(1)	32(1)
C14	4353(2)	9454(2)	5240(1)	40(1)
C15	4751(2)	10061(2)	5818(1)	38(1)
C16	3738(2)	10450(2)	6335(1)	29(1)
C17	1596(2)	9382(2)	5643(1)	41(1)
C18	1976(2)	7654(2)	6388(1)	34(1)
C19	3089(2)	11452(2)	6009(1)	42(1)
C20	4261(2)	10815(2)	6954(1)	39(1)
Si21	5201(1)	5009(1)	6602(1)	21(1)
O21	4483(1)	6316(1)	6829(1)	21(1)
N21	6464(2)	5572(1)	6810(1)	27(1)
O22	5988(1)	3769(1)	6297(1)	28(1)
N22	4677(1)	5147(1)	5825(1)	25(1)
O23	4874(1)	8085(1)	7029(1)	24(1)
O24	6322(2)	2721(1)	5403(1)	45(1)
N23	3584(2)	4398(1)	7939(1)	24(1)
C21	4301(2)	4015(2)	7288(1)	28(1)
C22	5176(2)	7095(2)	6981(1)	21(1)
C23	6401(2)	6671(2)	7086(1)	25(1)

C24	5846(2)	3527(2)	5676(1)	30(1)
C25	5029(2)	4331(2)	5329(1)	28(1)
C26	5621(2)	4844(2)	4625(1)	34(1)
C27	4750(2)	5553(2)	4249(1)	48(1)
C28	6716(2)	5516(3)	4681(1)	51(1)
C29	7359(2)	7514(2)	6778(1)	34(1)
C30	7435(2)	7716(2)	5997(1)	45(1)
C31	8557(2)	7159(3)	6984(2)	54(1)
C32	2230(2)	4316(2)	7942(1)	34(1)
C33	1629(2)	4777(2)	8603(1)	42(1)
C34	2031(3)	4225(2)	9250(1)	54(1)
C35	3333(2)	4368(2)	9223(1)	45(1)
C36	4064(2)	3896(2)	8600(1)	35(1)
C37	5324(2)	4318(2)	8556(1)	46(1)
C38	4041(3)	2602(2)	8675(1)	47(1)
C39	1940(2)	5091(2)	7333(1)	42(1)
C40	1811(2)	3117(2)	7883(2)	47(1)
Si41	899(1)	4966(1)	3407(1)	21(1)
O41	296(1)	3669(1)	3179(1)	21(1)
N41	2266(2)	4407(2)	3171(1)	27(1)
O42	1545(1)	6195(1)	3710(1)	28(1)
N42	58(2)	4813(2)	4195(1)	26(1)
O43	806(1)	1909(1)	2945(1)	25(1)
O44	1487(2)	7228(1)	4608(1)	45(1)
N43	–193(1)	5642(1)	2101(1)	23(1)
C41	263(2)	5988(2)	2743(1)	28(1)
C42	1081(2)	2890(2)	3006(1)	21(1)
C43	2336(2)	3314(2)	2890(1)	24(1)
C44	1136(2)	6428(2)	4336(1)	30(1)
C45	177(2)	5630(2)	4686(1)	27(1)
C46	3177(2)	2463(2)	3191(1)	34(1)
C47	4462(2)	2819(2)	2980(2)	51(1)
C48	2899(2)	2263(2)	3973(1)	45(1)
C49	448(2)	5119(2)	5394(1)	35(1)
C50	–567(2)	4401(2)	5761(1)	49(1)
C51	1597(2)	4461(3)	5336(1)	51(1)
C52	–1568(2)	5712(2)	2142(1)	29(1)
C53	–1900(2)	5306(2)	1481(1)	36(1)
C54	–1285(2)	5938(2)	836(1)	47(1)
C55	34(2)	5784(2)	813(1)	38(1)
C56	533(2)	6194(2)	1432(1)	30(1)
C57	–2052(2)	4881(2)	2734(1)	37(1)
C58	–2050(2)	6891(2)	2260(1)	39(1)
C59	1793(2)	5755(2)	1430(1)	40(1)
C60	522(2)	7484(2)	1400(1)	37(1)
Si61	–1773(1)	866(1)	1911(1)	20(1)
O61	–1176(1)	2228(1)	2061(1)	21(1)
N61	–412(2)	611(1)	1472(1)	27(1)
O62	–2351(1)	–424(1)	1654(1)	28(1)
N62	–2990(2)	1526(2)	1640(1)	29(1)
O63	329(1)	3402(1)	1695(1)	26(1)
O64	–3842(2)	–1125(1)	1204(1)	54(1)
N63	–1328(1)	564(1)	3398(1)	20(1)
C61	–2065(2)	269(2)	2853(1)	26(1)
C62	–138(2)	2469(2)	1729(1)	21(1)
C63	465(2)	1491(2)	1366(1)	24(1)
C64	–3373(2)	–338(2)	1425(1)	34(1)
C65	–3911(2)	834(2)	1460(1)	33(1)
C66	918(2)	1859(2)	612(1)	31(1)
C67	1676(2)	924(2)	289(1)	49(1)
C68	–96(2)	2199(2)	210(1)	41(1)
C69	–4414(2)	1240(2)	796(1)	40(1)

C70	–3456(3)	1376(2)	185(1)	53(1)
C71	–5118(3)	2318(3)	887(2)	66(1)
C72	–607(2)	–468(2)	3653(1)	27(1)
C73	161(2)	–72(2)	4162(1)	35(1)
C74	–515(2)	518(2)	4750(1)	38(1)
C75	–1168(2)	1524(2)	4459(1)	31(1)
C76	–2027(2)	1229(2)	3967(1)	26(1)
C77	–1382(2)	–1462(2)	3974(1)	39(1)
C78	196(2)	–826(2)	3029(1)	36(1)
C79	–2410(2)	2321(2)	3609(1)	34(1)
C80	–3093(2)	585(2)	4347(1)	40(1)
C81	–1678(2)	3507(2)	8700(2)	54(1)
Cl1	–1443(1)	4155(1)	7868(1)	89(1)
Cl2	–2022(5)	4405(5)	9371(2)	80(1)
Cl2'	–1855(5)	4596(5)	9235(3)	104(2)
C82	5016(3)	6558(2)	1233(2)	62(1)
Cl3	4806(4)	5628(4)	1984(2)	66(1)
Cl4	5389(4)	5837(3)	491(2)	76(1)
Cl3'	5151(7)	5702(5)	567(3)	113(2)
Cl4'	4711(8)	5819(9)	2022(4)	136(3)
C83'	7556(11)	1572(15)	6849(8)	96(5)
Cl5'	6923(9)	1056(9)	7675(6)	117(3)
Cl6'	8998(5)	1097(5)	6645(3)	109(2)
C83	7843(11)	1766(11)	7027(8)	84(4)
Cl5	6812(6)	1354(6)	7717(4)	75(1)
Cl6	8455(6)	617(4)	6610(2)	102(2)
C84	3715(15)	8059(11)	3071(8)	82(5)
Cl7	3188(4)	8562(5)	2315(2)	69(1)
Cl8	4364(8)	9225(5)	3365(3)	146(3)
C84'	3514(12)	8410(15)	3148(8)	117(5)
Cl7'	4924(4)	8676(4)	3315(2)	114(1)
Cl8'	3242(6)	8801(8)	2296(4)	159(3)
C83"	8220(16)	1820(20)	6790(30)	105(8)
Cl5"	9747(8)	1837(7)	6552(5)	95(2)
Cl6"	7721(13)	475(11)	6684(11)	169(8)
C84"	4420(40)	8290(30)	2900(20)	120(9)
Cl7"	3465(18)	9399(17)	3112(17)	186(9)
Cl8"	5447(14)	8149(15)	3480(13)	143(7)

Table 38. Bond Lengths [Å] and Angles [deg] for **4a**·CH_2Cl_2.

Si1–N2	1.718(2)	C17–C12–N3	112.78(16)
Si1–O2	1.8098(13)	C13–C12–N3	107.97(16)
Si1–O1	1.8275(13)	C14–C13–C12	114.47(17)
Si1–C1	1.915(2)	C13–C14–C15	110.14(18)
O1–C2	1.296(2)	C14–C15–C16	114.10(19)
N1–HN1	0.800(14)	C20–C16–C15	108.06(18)
N1–C3	1.446(2)	C20–C16–C19	109.57(17)
O2–C4	1.313(3)	C15–C16–C19	110.10(19)
N2–HN2	0.770(14)	C20–C16–N3	107.54(17)
N2–C5	1.453(2)	C15–C16–N3	108.45(16)
O3–C2	1.236(2)	C19–C16–N3	112.98(18)
O4–C4	1.221(2)	N21–Si21–N22	127.76(9)
N3–HN3	0.875(15)	N21–Si21–O21	86.81(7)
N3–C1	1.527(2)	N22–Si21–O21	90.13(7)
N3–C16	1.550(3)	N21–Si21–O22	91.83(7)
N3–C12	1.553(2)	N22–Si21–O22	86.38(7)
C2–C3	1.518(3)	O21–Si21–O22	174.37(7)
C3–C6	1.533(3)	N21–Si21–C21	117.41(9)
C4–C5	1.517(3)	N22–Si21–C21	114.67(9)

C5–C9	1.529(3)	O21–Si21–C21	97.85(7)
C6–C8	1.520(3)	O22–Si21–C21	87.63(8)
C6–C7	1.522(3)	C22–O21–Si21	115.42(11)
C9–C11	1.517(3)	HN21–N21–C23	115.3(18)
C9–C10	1.528(4)	HN21–N21–Si21	125.3(18)
C12–C18	1.522(3)	C23–N21–Si21	118.52(12)
C12–C17	1.523(3)	C24–O22–Si21	115.94(12)
C12–C13	1.533(3)	HN22–N22–C25	116.9(15)
C13–C14	1.506(3)	HN22–N22–Si21	123.7(15)
C14–C15	1.522(3)	C25–N22–Si21	119.17(13)
C15–C16	1.534(3)	HN23–N23–C21	107.8(17)
C16–C20	1.527(3)	HN23–N23–C32	99.9(16)
C16–C19	1.541(3)	C21–N23–C32	113.58(15)
Si21–N21	1.7133(18)	HN23–N23–C36	106.0(15)
Si21–N22	1.7168(17)	C21–N23–C36	112.15(14)
Si21–O21	1.8116(12)	C32–N23–C36	116.01(17)
Si21–O22	1.8242(13)	N23–C21–Si21	124.18(13)
Si21–C21	1.918(2)	O23–C22–O21	123.39(16)
O21–C22	1.305(2)	O23–C22–C23	122.82(17)
N21–HN21	0.782(15)	O21–C22–C23	113.78(15)
N21–C23	1.455(2)	N21–C23–C22	103.79(15)
O22–C24	1.313(2)	N21–C23–C29	116.22(16)
N22–HN22	0.801(14)	C22–C23–C29	112.23(17)
N22–C25	1.451(2)	O24–C24–O22	123.14(19)
O23–C22	1.232(2)	O24–C24–C25	123.06(18)
O24–C24	1.226(2)	O22–C24–C25	113.80(15)
N23–HN23	0.876(16)	N22–C25–C24	104.70(15)
N23–C21	1.528(2)	N22–C25–C26	114.75(17)
N23–C32	1.555(3)	C24–C25–C26	111.78(17)
N23–C36	1.556(3)	C28–C26–C27	111.3(2)
C22–C23	1.520(3)	C28–C26–C25	112.22(18)
C23–C29	1.524(3)	C27–C26–C25	111.18(18)
C24–C25	1.518(3)	C23–C29–C31	111.3(2)
C25–C26	1.543(3)	C23–C29–C30	112.71(18)
C26–C28	1.516(3)	C31–C29–C30	110.6(2)
C26–C27	1.529(3)	C39–C32–C40	110.15(19)
C29–C31	1.529(3)	C39–C32–C33	108.61(18)
C29–C30	1.531(3)	C40–C32–C33	110.8(2)
C32–C39	1.523(3)	C39–C32–N23	106.24(18)
C32–C40	1.527(3)	C40–C32–N23	113.09(17)
C32–C33	1.533(3)	C33–C32–N23	107.78(17)
C33–C34	1.512(4)	C34–C33–C32	114.16(19)
C34–C35	1.496(4)	C35–C34–C33	109.9(2)
C35–C36	1.535(3)	C34–C35–C36	114.3(2)
C36–C37	1.521(4)	C37–C36–C38	110.02(19)
C36–C38	1.535(3)	C37–C36–C35	108.3(2)
Si41–N42	1.7135(19)	C38–C36–C35	110.3(2)
Si41–N41	1.7151(18)	C37–C36–N23	106.73(19)
Si41–O41	1.8122(13)	C38–C36–N23	112.69(18)
Si41–O42	1.8251(14)	C35–C36–N23	108.63(16)
Si41–C41	1.923(2)	N42–Si41–N41	127.75(9)
O41–C42	1.317(2)	N42–Si41–O41	90.28(8)
N41–HN41	0.766(15)	N41–Si41–O41	86.91(7)
N41–C43	1.453(2)	N42–Si41–O42	86.44(8)
O42–C44	1.312(2)	N41–Si41–O42	91.58(7)
N42–HN42	0.776(15)	O41–Si41–O42	174.47(7)
N42–C45	1.449(2)	N42–Si41–C41	114.63(9)
O43–C42	1.231(2)	N41–Si41–C41	117.42(10)
O44–C44	1.228(2)	O41–Si41–C41	98.09(7)
N43–HN43	0.857(15)	O42–Si41–C41	87.33(7)
N43–C41	1.523(2)	C42–O41–Si41	115.04(11)
N43–C56	1.561(3)	HN41–N41–C43	118.5(16)

N43–C52	1.568(3)	HN41–N41–Si41	120.8(16)
C42–C43	1.510(3)	C43–N41–Si41	118.43(13)
C43–C46	1.530(3)	C44–O42–Si41	115.84(14)
C44–C45	1.514(3)	HN42–N42–C45	116.7(17)
C45–C49	1.546(3)	HN42–N42–Si41	124.2(17)
C46–C47	1.529(3)	C45–N42–Si41	119.01(15)
C46–C48	1.532(3)	HN43–N43–C41	108.4(13)
C49–C50	1.516(4)	HN43–N43–C56	104.2(14)
C49–C51	1.520(3)	C41–N43–C56	111.96(15)
C52–C57	1.515(3)	HN43–N43–C52	101.4(14)
C52–C53	1.524(3)	C41–N43–C52	113.26(15)
C52–C58	1.526(3)	C56–N43–C52	116.34(15)
C53–C54	1.513(4)	N43–C41–Si41	124.77(13)
C54–C55	1.514(4)	O43–C42–O41	122.58(17)
C55–C56	1.534(3)	O43–C42–C43	123.58(16)
C56–C59	1.529(3)	O41–C42–C43	113.83(15)
C56–C60	1.531(3)	N41–C43–C42	104.26(15)
Si61–N61	1.7162(18)	N41–C43–C46	115.75(15)
Si61–N62	1.7184(17)	C42–C43–C46	111.79(17)
Si61–O62	1.8144(14)	O44–C44–O42	123.1(2)
Si61–O61	1.8267(13)	O44–C44–C45	123.22(19)
Si61–C61	1.922(2)	O42–C44–C45	113.70(16)
O61–C62	1.300(2)	N42–C45–C44	104.97(16)
N61–HN61	0.779(15)	N42–C45–C49	114.85(17)
N61–C63	1.441(3)	C44–C45–C49	112.17(16)
O62–C64	1.311(3)	C47–C46–C43	111.3(2)
N62–HN62	0.775(14)	C47–C46–C48	110.78(19)
N62–C65	1.444(3)	C43–C46–C48	112.25(17)
O63–C62	1.230(2)	C50–C49–C51	111.3(2)
O64–C64	1.224(3)	C50–C49–C45	111.29(18)
N63–C61	1.520(2)	C51–C49–C45	111.75(18)
N63–C76	1.557(2)	C57–C52–C53	108.52(18)
N63–C72	1.559(2)	C57–C52–C58	110.17(18)
C62–C63	1.527(2)	C53–C52–C58	111.45(17)
C63–C66	1.538(3)	C57–C52–N43	105.81(15)
C64–C65	1.521(3)	C53–C52–N43	107.54(16)
C65–C69	1.542(3)	C58–C52–N43	113.09(17)
C66–C68	1.526(3)	C54–C53–C52	113.93(19)
C66–C67	1.532(3)	C53–C54–C55	109.02(19)
C69–C70	1.515(4)	C54–C55–C56	114.14(18)
C69–C71	1.518(3)	C59–C56–C60	110.17(19)
C72–C78	1.524(3)	C59–C56–C55	108.73(18)
C72–C73	1.527(3)	C60–C56–C55	110.43(18)
C72–C77	1.528(3)	C59–C56–N43	106.23(17)
C73–C74	1.524(3)	C60–C56–N43	112.61(16)
C74–C75	1.518(3)	C55–C56–N43	108.53(17)
C75–C76	1.534(3)	N61–Si61–N62	130.73(9)
C76–C79	1.516(3)	N61–Si61–O62	91.02(7)
C76–C80	1.523(3)	N62–Si61–O62	86.59(7)
C81–Cl2'	1.731(5)	N61–Si61–O61	86.33(7)
C81–Cl1	1.744(3)	N62–Si61–O61	90.33(7)
C81–Cl2	1.771(5)	O62–Si61–O61	173.13(7)
C82–Cl4'	1.719(9)	N61–Si61–C61	116.97(9)
C82–Cl3'	1.719(6)	N62–Si61–C61	112.22(9)
C82–Cl4	1.762(5)	O62–Si61–C61	89.50(8)
C82–Cl3	1.765(5)	O61–Si61–C61	97.35(7)
C83'–Cl6'	1.746(11)	C62–O61–Si61	115.21(11)
C83'–Cl5'	1.756(12)	HN61–N61–C63	117.5(19)
C83–Cl5	1.720(11)	HN61–N61–Si61	121.7(19)
C83–Cl6	1.747(10)	C63–N61–Si61	119.33(12)
C84–Cl7	1.743(11)	C64–O62–Si61	115.89(12)
C84–Cl8	1.756(11)	HN62–N62–C65	115.2(17)

C84'–Cl7'	1.729(11)	HN62–N62–Si61	124.6(17)
C84'–Cl8'	1.774(11)	C65–N62–Si61	118.29(14)
C83"–Cl6"	1.740(15)	C61–N63–C76	113.18(14)
C83"–Cl5"	1.749(14)	C61–N63–C72	111.89(14)
C84"–Cl7"	1.742(15)	C76–N63–C72	115.85(14)
C84"–Cl8"	1.746(15)	N63–C61–Si61	123.56(14)
N1–Si1–N2	130.18(9)	O63–C62–O61	123.91(16)
N1–Si1–O2	91.26(7)	O63–C62–C63	121.83(18)
N2–Si1–O2	86.69(7)	O61–C62–C63	114.25(16)
N1–Si1–O1	86.23(7)	N61–C63–C62	104.14(16)
N2–Si1–O1	90.67(7)	N61–C63–C66	115.24(15)
O2–Si1–O1	173.89(7)	C62–C63–C66	110.99(16)
N1–Si1–C1	117.52(10)	O64–C64–O62	123.0(2)
N2–Si1–C1	112.20(9)	O64–C64–C65	123.62(19)
O2–Si1–C1	88.83(7)	O62–C64–C65	113.38(17)
O1–Si1–C1	97.27(7)	N62–C65–C64	104.68(16)
C2–O1–Si1	115.53(11)	N62–C65–C69	115.7(2)
HN1–N1–C3	116.1(16)	C64–C65–C69	112.06(17)
HN1–N1–Si1	124.8(16)	C68–C66–C67	111.97(18)
C3–N1–Si1	119.10(12)	C68–C66–C63	111.36(17)
C4–O2–Si1	115.61(13)	C67–C66–C63	110.00(18)
HN2–N2–C5	112.8(18)	C70–C69–C71	111.7(2)
HN2–N2–Si1	126.3(18)	C70–C69–C65	111.70(19)
C5–N2–Si1	117.63(14)	C71–C69–C65	110.77(19)
HN3–N3–C1	107.1(14)	C78–C72–C73	108.38(18)
HN3–N3–C16	101.6(15)	C78–C72–C77	109.42(17)
C1–N3–C16	111.82(14)	C73–C72–C77	111.06(18)
HN3–N3–C12	105.0(13)	C78–C72–N63	106.62(16)
C1–N3–C12	113.35(15)	C73–C72–N63	108.01(15)
C16–N3–C12	116.59(15)	C77–C72–N63	113.15(17)
N3–C1–Si1	124.61(13)	C74–C73–C72	114.22(18)
O3–C2–O1	123.83(16)	C75–C74–C73	109.25(18)
O3–C2–C3	122.01(16)	C74–C75–C76	114.25(17)
O1–C2–C3	114.16(15)	C79–C76–C80	110.36(18)
N1–C3–C2	104.21(15)	C79–C76–C75	107.98(17)
N1–C3–C6	115.28(15)	C80–C76–C75	111.48(17)
C2–C3–C6	111.77(16)	C79–C76–N63	106.10(16)
O4–C4–O2	122.9(2)	C80–C76–N63	112.87(16)
O4–C4–C5	123.5(2)	C75–C76–N63	107.78(15)
O2–C4–C5	113.67(16)	Cl2'–C81–Cl1	105.6(3)
N2–C5–C4	104.52(17)	Cl2'–C81–Cl2	12.1(4)
N2–C5–C9	116.07(18)	Cl1–C81–Cl2	116.6(2)
C4–C5–C9	111.45(16)	Cl4'–C82–Cl3'	112.8(5)
C8–C6–C7	111.65(19)	Cl4'–C82–Cl4	120.2(4)
C8–C6–C3	111.58(17)	Cl3'–C82–Cl4	10.8(4)
C7–C6–C3	110.89(19)	Cl4'–C82–Cl3	8.5(5)
C11–C9–C10	110.7(2)	Cl3'–C82–Cl3	105.1(3)
C11–C9–C5	112.22(19)	Cl4–C82–Cl3	112.0(2)
C10–C9–C5	111.43(19)	Cl6'–C83'–Cl5'	112.4(9)
C18–C12–C17	110.11(18)	Cl5–C83–Cl6	112.1(8)
C18–C12–C13	108.27(17)	Cl7–C84–Cl8	105.7(8)
C17–C12–C13	111.01(18)	Cl7'–C84'–Cl8'	115.4(9)
C18–C12–N3	106.50(16)	Cl6"–C83"–Cl5"	107.6(12)

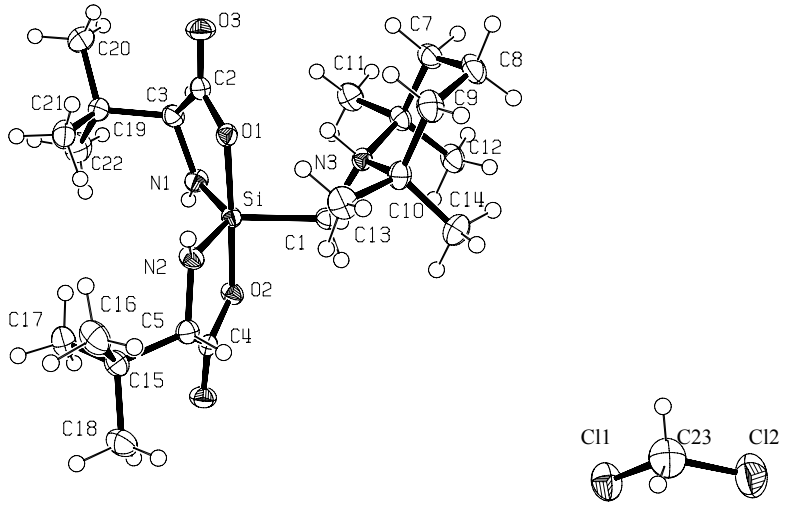

Figure 69. Crystal structure of **5a**·CH_2Cl_2 (probability level of displacement ellipsoids 50%) showing the atomic numbering scheme.

Table 39. Atomic Coordinates (x 10^4) and Equivalent Isotropic Displacement Parameters ($Å^2$ x 10^3) for **5a**·CH_2Cl_2. U(eq) is Defined as One Third of the Trace of the Orthogonalized Uij Tensor.

	x	y	z	U(eq)
Si	8453(1)	9641(1)	8990(1)	18(1)
N(2)	8540(2)	9208(1)	9700(1)	23(1)
N(1)	9385(2)	9184(1)	8414(1)	23(1)
N(3)	5790(2)	10454(1)	8663(1)	19(1)
O(2)	9702(1)	10652(1)	9174(1)	22(1)
O(1)	7264(1)	8571(1)	8787(1)	21(1)
O(4)	10966(2)	11276(1)	9897(1)	28(1)
O(3)	6828(2)	7311(1)	8106(1)	31(1)
C(1)	7184(2)	10801(2)	8851(1)	21(1)
C(4)	10080(2)	10672(1)	9726(1)	20(1)
C(5)	9291(2)	9879(2)	10110(1)	22(1)
C(2)	7593(2)	7964(2)	8327(1)	23(1)
C(3)	8994(2)	8196(2)	8109(1)	23(1)
C(6)	5438(2)	10810(2)	8029(1)	23(1)
C(7)	4069(2)	10331(2)	7879(1)	27(1)
C(8)	2995(2)	10594(2)	8320(1)	32(1)
C(9)	3399(2)	10157(2)	8916(1)	31(1)
C(10)	4711(2)	10631(2)	9143(1)	25(1)
C(11)	6472(2)	10276(2)	7629(1)	31(1)
C(12)	5464(2)	12057(2)	7954(1)	31(1)
C(13)	5158(2)	9967(2)	9673(1)	33(1)
C(14)	4549(3)	11836(2)	9312(1)	37(1)
C(19)	9954(2)	7196(2)	8198(1)	26(1)
C(21)	9852(3)	6760(2)	8820(1)	36(1)
C(22)	11378(2)	7572(2)	8080(1)	41(1)
C(20)	9598(3)	6280(2)	7767(1)	38(1)
C(15)	10147(2)	9209(2)	10550(1)	25(1)
C(16)	9241(3)	8357(2)	10847(1)	37(1)
C(18)	10690(2)	9976(2)	11025(1)	36(1)
C(17)	11289(2)	8627(2)	10241(1)	34(1)
C(23)	627(3)	3020(2)	8857(1)	49(1)
Cl(1)	1883(1)	3896(1)	8591(1)	48(1)
Cl(2)	–958(1)	3581(1)	8796(1)	70(1)

Table 40. Bond Lengths [Å] and Angles [deg] for **5a**·CH_2Cl_2.

Si–N(1)	1.7087(17)	HN1–N(1)–C(3)	117.2(17)
Si–N(2)	1.7124(16)	HN1–N(1)–Si	122.5(17)
Si–O(2)	1.8058(14)	C(3)–N(1)–Si	119.66(14)
Si–O(1)	1.8258(14)	HN3–N(3)–C(1)	104.3(14)
Si–C(1)	1.9274(19)	HN3–N(3)–C(10)	103.1(14)
N(2)–HN2	0.84(3)	C(1)–N(3)–C(10)	113.70(14)
N(2)–C(5)	1.456(2)	HN3–N(3)–C(6)	102.8(13)
N(1)–HN1	0.80(3)	C(1)–N(3)–C(6)	113.25(14)
N(1)–C(3)	1.445(3)	C(10)–N(3)–C(6)	117.54(14)
N(3)–HN3	0.93(2)	C(4)–O(2)–Si	115.86(12)
N(3)–C(1)	1.523(2)	C(2)–O(1)–Si	115.82(12)
N(3)–C(10)	1.558(2)	N(3)–C(1)–Si	116.84(12)
N(3)–C(6)	1.558(2)	O(4)–C(4)–O(2)	122.00(17)
O(2)–C(4)	1.319(2)	O(4)–C(4)–C(5)	124.93(17)
O(1)–C(2)	1.328(2)	O(2)–C(4)–C(5)	113.07(16)
O(4)–C(4)	1.218(2)	N(2)–C(5)–C(4)	104.46(15)
O(3)–C(2)	1.215(2)	N(2)–C(5)–C(15)	114.23(15)
C(4)–C(5)	1.528(3)	C(4)–C(5)–C(15)	114.76(16)
C(5)–C(15)	1.554(3)	O(3)–C(2)–O(1)	122.44(18)
C(2)–C(3)	1.519(3)	O(3)–C(2)–C(3)	124.72(18)
C(3)–C(19)	1.564(3)	O(1)–C(2)–C(3)	112.84(16)
C(6)–C(12)	1.527(3)	N(1)–C(3)–C(2)	104.27(16)
C(6)–C(11)	1.529(3)	N(1)–C(3)–C(19)	114.58(16)
C(6)–C(7)	1.531(3)	C(2)–C(3)–C(19)	112.56(16)
C(7)–C(8)	1.512(3)	C(12)–C(6)–C(11)	110.08(18)
C(8)–C(9)	1.521(3)	C(12)–C(6)–C(7)	111.64(17)
C(9)–C(10)	1.528(3)	C(11)–C(6)–C(7)	108.23(17)
C(10)–C(14)	1.524(3)	C(12)–C(6)–N(3)	112.07(16)
C(10)–C(13)	1.526(3)	C(11)–C(6)–N(3)	106.71(15)
C(19)–C(21)	1.524(3)	C(7)–C(6)–N(3)	107.89(15)
C(19)–C(22)	1.524(3)	C(8)–C(7)–C(6)	114.17(17)
C(19)–C(20)	1.532(3)	C(7)–C(8)–C(9)	109.67(17)
C(15)–C(17)	1.522(3)	C(8)–C(9)–C(10)	113.78(17)
C(15)–C(18)	1.533(3)	C(14)–C(10)–C(13)	109.71(18)
C(15)–C(16)	1.538(3)	C(14)–C(10)–C(9)	110.92(18)
C(23)–Cl(2)	1.737(3)	C(13)–C(10)–C(9)	108.97(17)
C(23)–Cl(1)	1.761(3)	C(14)–C(10)–N(3)	112.69(17)
N(1)–Si–N(2)	127.24(9)	C(13)–C(10)–N(3)	106.48(16)
N(1)–Si–O(2)	91.23(8)	C(9)–C(10)–N(3)	107.91(15)
N(2)–Si–O(2)	87.24(7)	C(21)–C(19)–C(22)	109.47(19)
N(1)–Si–O(1)	85.98(7)	C(21)–C(19)–C(20)	109.51(18)
N(2)–Si–O(1)	93.25(7)	C(22)–C(19)–C(20)	108.81(19)
O(2)–Si–O(1)	176.83(7)	C(21)–C(19)–C(3)	110.53(16)
N(1)–Si–C(1)	118.17(9)	C(22)–C(19)–C(3)	108.78(17)
N(2)–Si–C(1)	114.56(9)	C(20)–C(19)–C(3)	109.71(16)
O(2)–Si–C(1)	89.93(7)	C(17)–C(15)–C(18)	110.19(19)
O(1)–Si–C(1)	92.71(7)	C(17)–C(15)–C(16)	109.78(18)
HN2–N(2)–C(5)	118.4(16)	C(18)–C(15)–C(16)	107.83(17)
HN2–N(2)–Si	119.3(16)	C(17)–C(15)–C(5)	110.99(16)
C(5)–N(2)–Si	117.88(13)	C(18)–C(15)–C(5)	109.71(16)
Cl(2)–C(23)–Cl(1)	112.98(14)	C(16)–C(15)–C(5)	108.27(17)

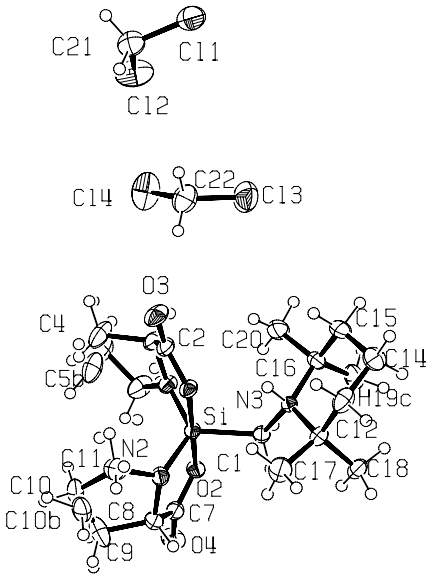

Figure 70. Crystal structure of **6a**·$2CH_2Cl_2$ (probability level of displacement ellipsoids 50%) showing the atomic numbering scheme.

Table 41. Atomic Coordinates (x 10^4) and Equivalent Isotropic Displacement Parameters ($Å^2$ x 10^3) for **6a**·$2CH_2Cl_2$. U(eq) is Defined as One Third of the Trace of the Orthogonalized Uij Tensor.

	x	y	z	U(eq)
C(1)	8757(2)	4611(1)	3029(1)	24(1)
C(7)	9071(2)	5805(1)	1403(1)	29(1)
C(8)	10420(2)	5409(1)	1317(1)	29(1)
C(9)	10889(3)	5276(2)	545(1)	50(1)
C(10)	10888(6)	4344(3)	405(2)	50(2)
C(11)	11199(2)	3910(2)	1189(1)	45(1)
C(9B)	10889(3)	5276(2)	545(1)	50(1)
C(10B)	11771(9)	4405(4)	606(4)	43(2)
C(11B)	11199(2)	3910(2)	1189(1)	45(1)
C(2)	9023(2)	2384(1)	2092(1)	29(1)
C(3)	7794(2)	2624(1)	1697(1)	32(1)
C(4)	7702(3)	2325(2)	913(1)	52(1)
C(5)	6637(8)	2965(5)	646(4)	45(2)
C(6)	6863(3)	3844(2)	1065(1)	43(1)
C(4B)	7702(3)	2325(2)	913(1)	52(1)
C(5B)	7160(20)	3153(9)	501(6)	52(3)
C(6B)	6863(3)	3844(2)	1065(1)	43(1)
C(12)	10243(2)	4293(1)	4108(1)	26(1)
C(13)	10546(2)	3552(2)	4657(1)	37(1)
C(14)	9375(3)	3254(2)	5096(1)	44(1)
C(15)	8341(3)	2902(2)	4587(1)	41(1)
C(16)	7880(2)	3598(1)	4036(1)	30(1)
C(17)	11411(2)	4399(2)	3603(1)	42(1)
C(18)	9965(2)	5200(1)	4468(1)	35(1)
C(19)	7088(2)	4348(2)	4391(1)	40(1)
C(20)	7044(2)	3114(2)	3479(1)	43(1)
C(21)	7186(2)	–2992(2)	2702(1)	46(1)
C(22)	6493(3)	304(2)	2623(2)	54(1)
N(1)	7699(2)	3607(1)	1675(1)	28(1)
N(2)	10424(2)	4505(1)	1645(1)	27(1)

N(3)	9094(2)	3964(1)	3637(1)	21(1)
O(1)	9636(1)	3103(1)	2340(1)	26(1)
O(3)	9398(2)	1612(1)	2187(1)	41(1)
O(2)	8291(1)	5286(1)	1778(1)	27(1)
O(4)	8756(2)	6536(1)	1155(1)	43(1)
Cl(1)	7068(1)	–3178(1)	3634(1)	58(1)
Cl(2)	6058(1)	–2180(1)	2408(1)	69(1)
Cl(3)	5738(1)	720(1)	3399(1)	70(1)
Cl(4)	5441(1)	287(1)	1889(1)	74(1)
Si	8964(1)	4211(1)	2059(1)	22(1)

Table 42. Bond Lengths [Å] and Angles [deg] for **6a**·$2CH_2Cl_2$.

C(1)–N(3)	1.522(2)	N(1)–C(3)–C(4)	104.91(17)
C(1)–Si	1.9142(18)	C(2)–C(3)–C(4)	116.8(2)
C(7)–O(4)	1.220(2)	N(1)–C(3)–H(3)	112.6(15)
C(7)–O(2)	1.310(2)	C(5)–C(4)–C(3)	100.1(3)
C(7)–C(8)	1.510(3)	C(4)–C(5)–C(6)	104.6(3)
C(8)–N(2)	1.470(2)	N(1)–C(6)–C(5)	106.3(3)
C(8)–C(9)	1.530(3)	N(1)–C(6)–H(6A)	110.5
C(9)–C(10)	1.403(5)	N(1)–C(6)–H(6B)	110.5
C(10)–C(11)	1.628(5)	C(18)–C(12)–C(17)	109.10(17)
C(11)–N(2)	1.459(3)	C(18)–C(12)–C(13)	111.89(16)
C(2)–O(3)	1.218(2)	C(17)–C(12)–C(13)	109.02(18)
C(2)–O(1)	1.318(2)	C(18)–C(12)–N(3)	112.55(15)
C(2)–C(3)	1.501(3)	C(17)–C(12)–N(3)	106.15(14)
C(3)–N(1)	1.458(3)	C(13)–C(12)–N(3)	107.93(15)
C(3)–C(4)	1.531(3)	C(14)–C(13)–C(12)	114.08(18)
C(4)–C(5)	1.528(6)	C(15)–C(14)–C(13)	108.44(18)
C(5)–C(6)	1.535(6)	C(14)–C(15)–C(16)	113.88(18)
C(6)–N(1)	1.467(2)	C(19)–C(16)–C(20)	109.76(19)
C(12)–C(18)	1.528(3)	C(19)–C(16)–C(15)	111.33(17)
C(12)–C(17)	1.531(3)	C(20)–C(16)–C(15)	108.35(18)
C(12)–C(13)	1.532(3)	C(19)–C(16)–N(3)	112.39(16)
C(12)–N(3)	1.547(2)	C(20)–C(16)–N(3)	106.74(14)
C(13)–C(14)	1.517(4)	C(15)–C(16)–N(3)	108.09(17)
C(14)–C(15)	1.514(3)	Cl(2)–C(21)–Cl(1)	111.70(14)
C(15)–C(16)	1.529(3)	Cl(4)–C(22)–Cl(3)	112.33(16)
C(16)–C(19)	1.525(3)	C(3)–N(1)–C(6)	107.41(16)
C(16)–C(20)	1.525(3)	C(3)–N(1)–Si	116.96(13)
C(16)–N(3)	1.547(2)	C(6)–N(1)–Si	129.43(14)
C(21)–Cl(2)	1.755(2)	C(11)–N(2)–C(8)	108.01(16)
C(21)–Cl(1)	1.763(3)	C(11)–N(2)–Si	125.14(14)
C(22)–Cl(4)	1.742(3)	C(8)–N(2)–Si	114.22(13)
C(22)–Cl(3)	1.750(3)	H(3N)–N(3)–C(1)	108.6(14)
N(1)–Si	1.7287(17)	H(3N)–N(3)–C(16)	98.5(14)
N(2)–Si	1.7381(17)	C(1)–N(3)–C(16)	113.33(14)
N(3)–H(3N)	0.90(2)	H(3N)–N(3)–C(12)	104.5(15)
N(3)–H(3N)	0.90(2)	C(1)–N(3)–C(12)	113.39(14)
O(1)–Si	1.8524(13)	C(16)–N(3)–C(12)	116.69(13)
O(2)–Si	1.8105(13)	H(3N)–N(3)–H(3N)	0(3)
N(3)–C(1)–Si	118.91(12)	C(1)–N(3)–H(3N)	108.6(14)
N(3)–C(1)–H(1A)	107.6	C(16)–N(3)–H(3N)	98.5(14)
Si–C(1)–H(1A)	107.6	C(12)–N(3)–H(3N)	104.5(15)
N(3)–C(1)–H(1B)	107.6	C(2)–O(1)–Si	115.95(12)
Si–C(1)–H(1B)	107.6	C(7)–O(2)–Si	115.88(12)
O(4)–C(7)–O(2)	124.13(19)	N(1)–Si–N(2)	126.26(8)
O(4)–C(7)–C(8)	123.04(18)	N(1)–Si–O(2)	92.78(7)
O(2)–C(7)–C(8)	112.83(16)	N(2)–Si–O(2)	88.82(7)
N(2)–C(8)–C(7)	108.09(16)	N(1)–Si–O(1)	86.48(7)

N(2)–C(8)–C(9)	105.84(18)	N(2)–Si–O(1)	91.60(7)
C(7)–C(8)–C(9)	115.91(18)	O(2)–Si–O(1)	179.25(7)
N(2)–C(8)–H(8)	106.4(15)	N(1)–Si–C(1)	117.82(8)
C(10)–C(9)–C(8)	107.5(2)	N(2)–Si–C(1)	115.92(8)
C(9)–C(10)–C(11)	102.8(3)	O(2)–Si–C(1)	87.64(7)
N(2)–C(11)–C(10)	100.2(2)	O(1)–Si–C(1)	92.74(7)
N(2)–C(11)–H(11A)	111.7	O(3)–C(2)–O(1)	123.75(19)
N(2)–C(11)–H(11B)	111.7	O(3)–C(2)–C(3)	123.88(18)
N(1)–C(3)–C(2)	107.79(16)	O(1)–C(2)–C(3)	112.36(16)

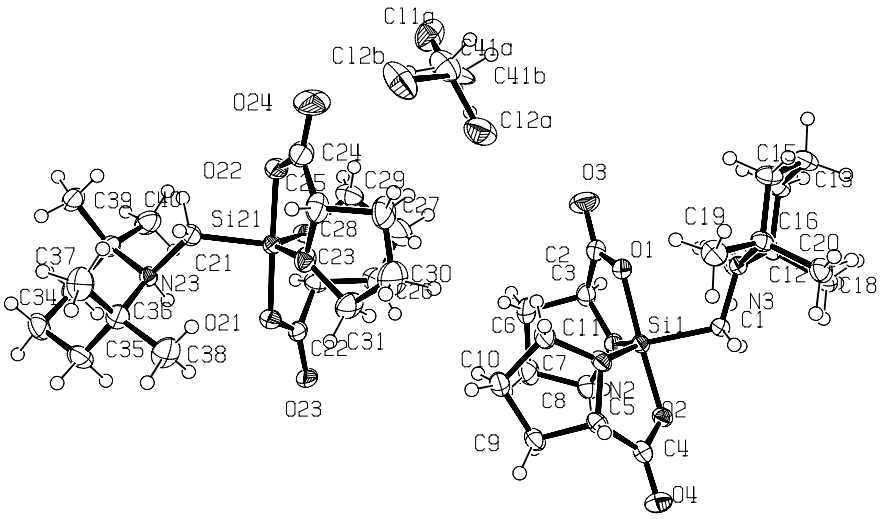

Figure 71. Crystal structure of **6a**·½CH_2Cl_2 (probability level of displacement ellipsoids 50%) showing the atomic numbering scheme.

Table 43. Atomic Coordinates (x 10^4) and Equivalent Isotropic Displacement Parameters (Å^2 x 10^3) for **6a**·½CH_2Cl_2. U(eq) is Defined as One Third of the Trace of the Orthogonalized Uij Tensor.

	x	y	z	U(eq)
Si1	9449(1)	1324(1)	5948(1)	21(1)
O1	8750(1)	524(2)	5989(1)	27(1)
O3	8370(1)	–1420(3)	6401(1)	52(1)
O2	10135(1)	2080(2)	5877(1)	24(1)
O4	10648(1)	4369(2)	5908(1)	33(1)
N1	9804(1)	–195(2)	6427(1)	25(1)
N2	9318(1)	3258(2)	6156(1)	25(1)
N3	8630(1)	21(2)	4852(1)	20(1)
C1	9209(1)	910(2)	5130(1)	23(1)
C2	8796(1)	–709(3)	6352(1)	31(1)
C3	9430(1)	–1127(3)	6675(1)	29(1)
C4	10244(1)	3618(3)	5995(1)	24(1)
C5	9811(1)	4372(3)	6252(1)	24(1)
C6	9642(1)	–688(3)	7325(1)	37(1)
C7	10287(1)	–132(3)	7450(1)	39(1)
C8	10395(1)	–213(3)	6868(1)	31(1)
C9	10069(1)	4566(3)	6918(1)	28(1)
C10	9528(1)	4324(3)	7116(1)	32(1)
C11	9029(1)	3714(3)	6576(1)	31(1)
C12	8715(1)	–1700(3)	4641(1)	23(1)
C13	8108(1)	–2534(3)	4447(1)	28(1)
C14	7615(1)	–1553(3)	4021(1)	32(1)

C15	7562(1)	94(3)	4275(1)	30(1)
C16	8135(1)	1079(3)	4440(1)	25(1)
C17	9116(1)	–2638(3)	5159(1)	31(1)
C18	8991(1)	–1661(3)	4159(1)	29(1)
C19	8065(1)	2564(3)	4785(1)	33(1)
C20	8279(1)	1629(3)	3908(1)	31(1)
Si21	8430(1)	3471(1)	9114(1)	24(1)
O21	9217(1)	3957(2)	9355(1)	27(1)
O23	10101(1)	2927(2)	9420(1)	33(1)
O22	7642(1)	2959(2)	8851(1)	32(1)
O24	6795(1)	3375(4)	8140(1)	65(1)
N21	8629(1)	1451(2)	9104(1)	29(1)
N22	8286(1)	4852(2)	8555(1)	30(1)
N23	8766(1)	4643(2)	10358(1)	22(1)
C21	8284(1)	4288(3)	9788(1)	30(1)
C22	9570(1)	2762(3)	9347(1)	26(1)
C23	9262(1)	1151(3)	9241(1)	32(1)
C24	7317(1)	3705(4)	8388(1)	40(1)
C25	7663(1)	4995(3)	8198(1)	37(1)
C26	9334(1)	182(4)	8730(1)	55(1)
C27	8722(1)	107(4)	8289(1)	56(1)
C28	8325(1)	240(3)	8666(1)	40(1)
C29	7660(1)	4827(4)	7576(1)	47(1)
C30	8230(1)	5566(5)	7602(1)	68(1)
C31	8660(1)	5270(3)	8203(1)	39(1)
C32	8653(1)	3715(3)	10867(1)	27(1)
C33	9177(1)	4067(3)	11420(1)	34(1)
C34	9299(1)	5846(3)	11541(1)	40(1)
C35	9421(1)	6622(3)	11028(1)	39(1)
C36	8912(1)	6465(3)	10458(1)	30(1)
C37	8379(1)	7472(3)	10462(1)	43(1)
C38	9127(1)	7037(3)	9967(1)	45(1)
C39	8063(1)	4190(3)	10942(1)	34(1)
C40	8657(1)	1910(3)	10737(1)	40(1)
Cl1A	6655(1)	–1633(1)	7472(1)	56(1)
C41A	6714(3)	246(5)	7144(2)	50(1)
Cl2A	7395(1)	324(1)	7003(1)	56(1)
Cl1B	6655(1)	–1633(1)	7472(1)	56(1)
C41B	6830(20)	–23(16)	7083(17)	50(7)
Cl2B	6704(4)	1751(10)	7429(3)	68(3)

Table 44. Bond Lengths [Å] and Angles [deg] for **6a**·½CH_2Cl_2.

Si1–N1	1.7378(18)	N3–C1–Si1	118.01(12)
Si1–N2	1.7387(18)	O3–C2–O1	123.3(2)
Si1–O2	1.8169(14)	O3–C2–C3	124.7(2)
Si1–O1	1.8322(14)	O1–C2–C3	112.00(17)
Si1–C1	1.9228(19)	N1–C3–C2	108.11(17)
O1–C2	1.333(3)	N1–C3–C6	105.43(17)
O3–C2	1.215(3)	C2–C3–C6	114.86(18)
O2–C4	1.311(3)	O4–C4–O2	124.32(19)
O4–C4	1.225(2)	O4–C4–C5	123.4(2)
N1–C3	1.456(3)	O2–C4–C5	112.31(17)
N1–C8	1.470(3)	N2–C5–C4	107.51(16)
N2–C5	1.453(3)	N2–C5–C9	104.88(16)
N2–C11	1.466(2)	C4–C5–C9	112.97(16)
N3–HN3	0.88(2)	C7–C6–C3	104.10(17)
N3–C1	1.517(2)	C8–C7–C6	105.40(17)
N3–C16	1.549(2)	N1–C8–C7	105.44(17)
N3–C12	1.550(3)	C10–C9–C5	103.52(16)

C2–C3	1.501(3)	C9–C10–C11	105.48(16)
C3–C6	1.546(3)	N2–C11–C10	105.89(15)
C4–C5	1.512(3)	C17–C12–C18	109.85(16)
C5–C9	1.551(3)	C17–C12–C13	107.43(17)
C6–C7	1.541(3)	C18–C12–C13	112.01(16)
C7–C8	1.533(3)	C17–C12–N3	107.73(14)
C9–C10	1.535(3)	C18–C12–N3	111.97(16)
C10–C11	1.545(3)	C13–C12–N3	107.64(15)
C12–C17	1.527(3)	C14–C13–C12	114.33(17)
C12–C18	1.530(2)	C15–C14–C13	110.34(16)
C12–C13	1.532(3)	C14–C15–C16	113.42(17)
C13–C14	1.525(3)	C20–C16–C15	111.65(16)
C14–C15	1.520(3)	C20–C16–C19	109.25(18)
C15–C16	1.529(3)	C15–C16–C19	108.77(17)
C16–C20	1.522(3)	C20–C16–N3	112.69(16)
C16–C19	1.531(3)	C15–C16–N3	107.29(16)
Si21–N22	1.7285(19)	C19–C16–N3	107.02(15)
Si21–N21	1.740(2)	N22–Si21–N21	127.44(9)
Si21–O21	1.8227(14)	N22–Si21–O21	91.51(8)
Si21–O22	1.8279(15)	N21–Si21–O21	87.58(8)
Si21–C21	1.919(2)	N22–Si21–O22	87.79(8)
O21–C22	1.304(3)	N21–Si21–O22	91.58(8)
O23–C22	1.230(2)	O21–Si21–O22	178.26(7)
O22–C24	1.300(3)	N22–Si21–C21	113.82(10)
O24–C24	1.225(3)	N21–Si21–C21	118.54(10)
N21–C23	1.459(3)	O21–Si21–C21	95.96(8)
N21–C28	1.472(3)	O22–Si21–C21	85.77(8)
N22–C25	1.462(3)	C22–O21–Si21	115.60(13)
N22–C31	1.471(3)	C24–O22–Si21	116.62(15)
N23–HN23	0.87(3)	C23–N21–C28	106.06(18)
N23–C21	1.518(2)	C23–N21–Si21	115.36(15)
N23–C36	1.549(3)	C28–N21–Si21	126.26(15)
N23–C32	1.562(2)	C25–N22–C31	109.12(16)
C22–C23	1.503(3)	C25–N22–Si21	115.10(15)
C23–C26	1.543(3)	C31–N22–Si21	128.17(15)
C24–C25	1.515(4)	HN23–N23–C21	109.1(16)
C25–C29	1.528(3)	HN23–N23–C36	101.7(18)
C26–C27	1.507(4)	C21–N23–C36	113.44(16)
C27–C28	1.530(4)	HN23–N23–C32	104.1(17)
C29–C30	1.476(4)	C21–N23–C32	111.19(15)
C30–C31	1.514(4)	C36–N23–C32	116.18(15)
C32–C40	1.528(3)	N23–C21–Si21	124.21(13)
C32–C39	1.532(3)	O23–C22–O21	123.8(2)
C32–C33	1.539(3)	O23–C22–C23	123.1(2)
C33–C34	1.510(4)	O21–C22–C23	113.10(16)
C34–C35	1.522(4)	N21–C23–C22	107.49(19)
C35–C36	1.525(3)	N21–C23–C26	106.71(18)
C36–C37	1.525(3)	C22–C23–C26	115.0(2)
C36–C38	1.530(3)	O24–C24–O22	123.1(3)
Cl1A–C41A	1.775(4)	O24–C24–C25	125.1(2)
C41A–Cl2A	1.773(6)	O22–C24–C25	111.80(18)
C41B–Cl2B	1.774(16)	N22–C25–C24	108.19(18)
N1–Si1–N2	124.24(8)	N22–C25–C29	104.98(18)
N1–Si1–O2	93.38(7)	C24–C25–C29	114.7(2)
N2–Si1–O2	88.12(7)	C27–C26–C23	105.1(2)
N1–Si1–O1	87.27(8)	C26–C27–C28	102.4(2)
N2–Si1–O1	93.43(8)	N21–C28–C27	103.49(19)
O2–Si1–O1	177.60(7)	C30–C29–C25	102.6(2)
N1–Si1–C1	119.12(9)	C29–C30–C31	107.2(2)
N2–Si1–C1	116.59(8)	N22–C31–C30	105.0(2)
O2–Si1–C1	86.03(7)	C40–C32–C39	110.21(19)
O1–Si1–C1	91.64(7)	C40–C32–C33	107.99(19)

C2–O1–Si1	115.90(13)	C39–C32–C33	111.14(17)
C4–O2–Si1	115.58(13)	C40–C32–N23	107.43(17)
C3–N1–C8	105.30(16)	C39–C32–N23	112.16(17)
C3–N1–Si1	115.76(13)	C33–C32–N23	107.75(16)
C8–N1–Si1	129.81(15)	C34–C33–C32	113.95(18)
C5–N2–C11	105.53(16)	C33–C34–C35	109.12(18)
C5–N2–Si1	114.59(12)	C34–C35–C36	114.00(19)
C11–N2–Si1	127.93(15)	C37–C36–C35	111.41(19)
HN3–N3–C1	104.9(16)	C37–C36–C38	109.5(2)
HN3–N3–C16	101.8(16)	C35–C36–C38	108.6(2)
C1–N3–C16	114.08(15)	C37–C36–N23	112.76(19)
HN3–N3–C12	103.4(17)	C35–C36–N23	107.36(17)
C1–N3–C12	113.30(14)	C38–C36–N23	107.03(17)
C16–N3–C12	117.20(14)	Cl2A–C41A–Cl1A	109.5(2)

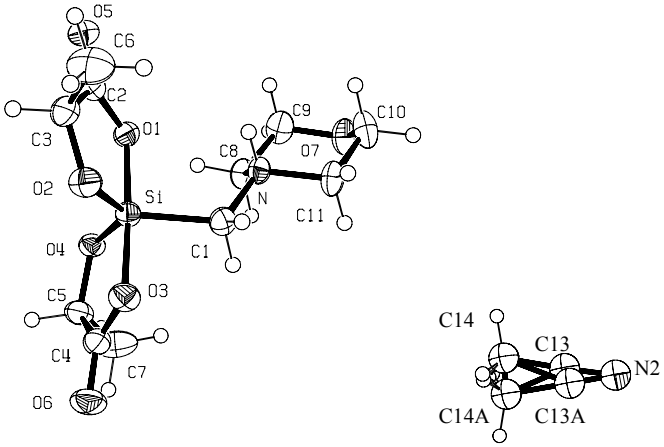

Figure 72. Crystal structure of **7b**·CH_3CN (probability level of displacement ellipsoids 50%) showing the atomic numbering scheme.

Table 45. Atomic Coordinates (x 10^4) and Equivalent Isotropic Displacement Parameters ($Å^2$ x 10^3) for **7b**·CH_3CN. U(eq) is Defined as One Third of the Trace of the Orthogonalized Uij Tensor.

	x	y	z	U(eq)
Si	3338(1)	5937(1)	2196(1)	26(1)
N	6476(2)	7030(1)	1605(1)	26(1)
O(1)	2969(1)	7384(1)	2065(1)	29(1)
O(2)	2697(2)	6078(1)	3038(1)	37(1)
O(3)	3591(2)	4474(1)	2377(1)	35(1)
O(4)	1962(1)	5640(1)	1534(1)	29(1)
O(5)	1863(2)	8865(1)	2616(1)	43(1)
O(6)	2659(2)	2848(1)	1991(1)	44(1)
O(7)	8378(2)	8216(1)	517(1)	45(1)
C(1)	5759(2)	5985(1)	1922(1)	31(1)
C(2)	2301(2)	7903(1)	2621(1)	33(1)
C(3)	2111(2)	7144(1)	3252(1)	38(1)
C(4)	2686(2)	3854(1)	1948(1)	33(1)
C(5)	1698(2)	4502(1)	1387(1)	34(1)
C(6)	3139(3)	7547(2)	3889(1)	60(1)
C(7)	2334(3)	4208(1)	649(1)	54(1)
C(8)	5675(2)	7298(1)	894(1)	32(1)
C(9)	6506(2)	8326(1)	596(1)	42(1)
C(10)	9157(2)	8012(2)	1195(1)	45(1)
C(11)	8454(2)	6963(1)	1521(1)	37(1)
N(2)	7773(3)	5026(2)	10097(1)	75(1)
C(13)	7306(6)	4827(4)	9515(2)	39(1)

C(14)	6678(7)	4544(3)	8832(2)	51(1)
N(2A)	7773(3)	5026(2)	10097(1)	75(1)
C(13A)	7776(6)	4819(4)	9544(3)	39(1)
C(14A)	7765(7)	4593(3)	8775(2)	51(1)

Table 46. Bond Lengths [Å] and Angles [deg] for **7b**·CH_3CN.

Si–O(4)	1.6582(10)	O(2)–Si–C(1)	122.31(6)
Si–O(2)	1.6616(10)	O(1)–Si–C(1)	94.64(5)
Si–O(1)	1.7971(9)	O(3)–Si–C(1)	88.88(6)
Si–O(3)	1.8188(10)	HN–N–C(11)	107.4(11)
Si–C(1)	1.8958(16)	HN–N–C(1)	105.0(10)
N–HN	0.888(17)	C(11)–N–C(1)	110.68(11)
N–C(11)	1.500(2)	HN–N–C(8)	112.1(11)
N–C(1)	1.5010(17)	C(11)–N–C(8)	108.48(11)
N–C(8)	1.5011(17)	C(1)–N–C(8)	113.03(11)
O(1)–C(2)	1.3184(17)	C(2)–O(1)–Si	114.72(9)
O(2)–C(3)	1.4251(18)	C(3)–O(2)–Si	116.91(9)
O(3)–C(4)	1.2971(19)	C(4)–O(3)–Si	113.33(9)
O(4)–C(5)	1.4242(15)	C(5)–O(4)–Si	116.28(9)
O(5)–C(2)	1.2145(17)	C(10)–O(7)–C(9)	109.35(12)
O(6)–C(4)	1.2247(17)	N–C(1)–Si	118.67(10)
O(7)–C(10)	1.423(2)	O(5)–C(2)–O(1)	123.92(14)
O(7)–C(9)	1.424(2)	O(5)–C(2)–C(3)	124.60(13)
C(2)–C(3)	1.509(2)	O(1)–C(2)–C(3)	111.46(12)
C(3)–C(6)	1.506(2)	O(2)–C(3)–C(6)	111.10(15)
C(4)–C(5)	1.510(2)	O(2)–C(3)–C(2)	107.68(11)
C(5)–C(7)	1.509(2)	C(6)–C(3)–C(2)	112.07(14)
C(8)–C(9)	1.505(2)	O(6)–C(4)–O(3)	123.20(14)
C(10)–C(11)	1.509(2)	O(6)–C(4)–C(5)	123.86(14)
N(2)–C(13)	1.174(5)	O(3)–C(4)–C(5)	112.93(12)
C(13)–C(14)	1.409(6)	O(4)–C(5)–C(7)	111.27(12)
C(13A)–C(14A)	1.470(6)	O(4)–C(5)–C(4)	107.62(12)
O(4)–Si–O(2)	123.68(6)	C(7)–C(5)–C(4)	111.12(14)
O(4)–Si–O(1)	90.74(5)	N–C(8)–C(9)	110.07(13)
O(2)–Si–O(1)	89.09(5)	O(7)–C(9)–C(8)	111.85(13)
O(4)–Si–O(3)	89.64(5)	O(7)–C(10)–C(11)	111.39(14)
O(2)–Si–O(3)	87.36(5)	N–C(11)–C(10)	110.20(13)
O(1)–Si–O(3)	175.96(5)	N(2)–C(13)–C(14)	176.7(4)
O(4)–Si–C(1)	113.83(6)		

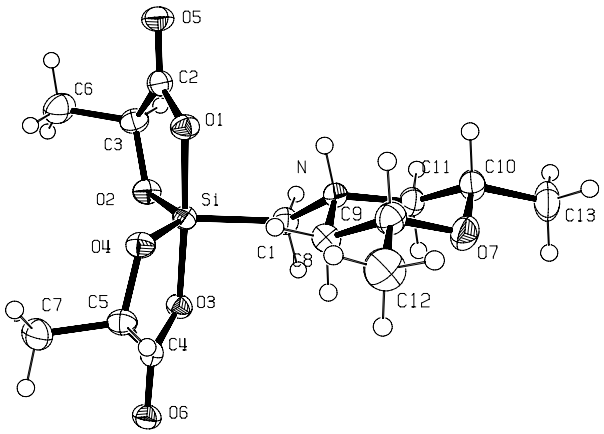

Figure 73. Crystal structure of **8a** (probability level of displacement ellipsoids 50%) showing the atomic numbering scheme.

Table 47. Atomic Coordinates (x 10^4) and Equivalent Isotropic Displacement Parameters ($Å^2$ x 10^3) for **8a**. U(eq) is Defined as One Third of the Trace of the Orthogonalized Uij Tensor.

	x	y	z	U(eq)
Si	–3620(1)	–3564(1)	–501(1)	21(1)
O(1)	–5241(1)	–3103(1)	–901(1)	26(1)
O(2)	–3496(1)	–4602(1)	–1277(1)	26(1)
O(3)	–2023(1)	–4115(1)	–77(1)	24(1)
O(4)	–4309(1)	–3819(1)	457(1)	25(1)
O(5)	–6631(1)	–3465(1)	–2005(1)	34(1)
O(6)	–1057(1)	–4692(1)	1153(1)	30(1)
O(7)	–3309(1)	1466(1)	361(1)	34(1)
N	–3508(1)	–836(1)	–551(1)	23(1)
C(1)	–2808(2)	–2018(1)	–786(1)	26(1)
C(2)	–5596(2)	–3679(2)	–1613(1)	25(1)
C(3)	–4585(2)	–4648(2)	–1873(1)	28(1)
C(4)	–2045(2)	–4367(1)	736(1)	24(1)
C(5)	–3436(2)	–4261(2)	1119(1)	26(1)
C(6)	–5203(2)	–5931(2)	–1885(1)	41(1)
C(7)	–3899(2)	–5507(2)	1457(1)	36(1)
C(8)	–3721(2)	–740(2)	397(1)	28(1)
C(9)	–4236(2)	538(2)	641(1)	31(1)
C(10)	–3212(2)	1470(2)	–556(1)	31(1)
C(11)	–2684(2)	238(2)	–864(1)	29(1)
C(12)	–4393(2)	642(2)	1602(1)	46(1)
C(13)	–2252(2)	2490(2)	–813(2)	44(1)

Table 48. Bond Lengths [Å] and Angles [deg] for **8a**.

Si–O(2)	1.6606(11)	O(1)–Si–C(1)	93.22(6)
Si–O(4)	1.6747(12)	O(3)–Si–C(1)	90.09(6)
Si–O(1)	1.8017(12)	C(2)–O(1)–Si	113.71(10)
Si–O(3)	1.8233(12)	C(3)–O(2)–Si	116.44(10)
Si–C(1)	1.9087(17)	C(4)–O(3)–Si	114.19(10)
O(1)–C(2)	1.3256(19)	C(5)–O(4)–Si	117.07(9)
O(2)–C(3)	1.432(2)	C(9)–O(7)–C(10)	110.59(12)
O(3)–C(4)	1.3048(19)	C(1)–N–C(11)	108.84(12)
O(4)–C(5)	1.4351(19)	C(1)–N–C(8)	111.55(12)
O(5)–C(2)	1.2224(19)	C(11)–N–C(8)	110.21(12)
O(6)–C(4)	1.2321(19)	N–C(1)–Si	119.33(10)
O(7)–C(9)	1.432(2)	O(5)–C(2)–O(1)	124.01(16)
O(7)–C(10)	1.442(2)	O(5)–C(2)–C(3)	123.88(15)
N–C(1)	1.5003(19)	O(1)–C(2)–C(3)	112.10(13)
N–C(11)	1.504(2)	O(2)–C(3)–C(2)	107.72(13)
N–C(8)	1.506(2)	O(2)–C(3)–C(6)	110.31(14)
C(2)–C(3)	1.508(2)	C(2)–C(3)–C(6)	111.58(15)
C(3)–C(6)	1.516(2)	O(6)–C(4)–O(3)	124.38(15)
C(4)–C(5)	1.513(2)	O(6)–C(4)–C(5)	122.82(14)
C(5)–C(7)	1.519(2)	O(3)–C(4)–C(5)	112.78(13)
C(8)–C(9)	1.522(2)	O(4)–C(5)–C(4)	107.05(12)
C(9)–C(12)	1.519(3)	O(4)–C(5)–C(7)	111.29(14)
C(10)–C(11)	1.510(2)	C(4)–C(5)–C(7)	110.42(14)
C(10)–C(13)	1.514(2)	N–C(8)–C(9)	111.04(13)
O(2)–Si–O(4)	125.25(6)	O(7)–C(9)–C(12)	108.62(15)
O(2)–Si–O(1)	89.87(6)	O(7)–C(9)–C(8)	109.89(14)
O(4)–Si–O(1)	89.49(5)	C(12)–C(9)–C(8)	110.58(15)
O(2)–Si–O(3)	88.96(6)	O(7)–C(10)–C(11)	109.87(13)
O(4)–Si–O(3)	88.65(5)	O(7)–C(10)–C(13)	108.06(15)
O(1)–Si–O(3)	176.69(6)	C(11)–C(10)–C(13)	109.68(14)

O(2)–Si–C(1)	112.81(7)	N–C(11)–C(10)	112.68(13)
O(4)–Si–C(1)	121.88(7)		

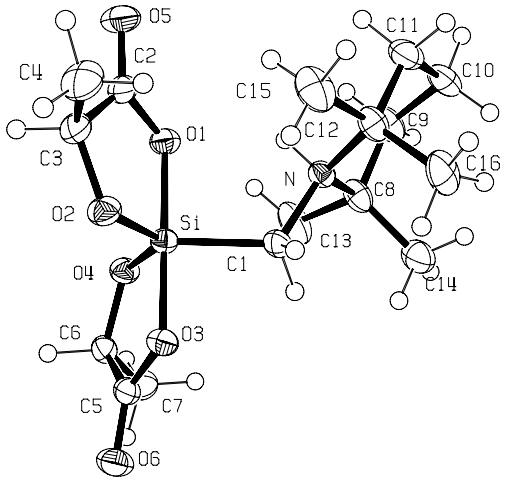

Figure 74. Crystal structure of **9b** (probability level of displacement ellipsoids 50%) showing the atomic numbering scheme.

Table 49. Atomic Coordinates (x 10^4) and Equivalent Isotropic Displacement Parameters ($Å^2$ x 10^3) for **9b**. U(eq) is Defined as One Third of the Trace of the Orthogonalized Uij Tensor.

	x	y	z	U(eq)
C(1)	11054(2)	3883(2)	4010(1)	25(1)
C(2)	6790(2)	4073(2)	4471(1)	30(1)
C(3)	6904(2)	5946(2)	4501(1)	32(1)
C(4)	5959(2)	6835(3)	4117(1)	45(1)
C(5)	12434(2)	6349(2)	4966(1)	26(1)
C(6)	11832(2)	4995(2)	5295(1)	26(1)
C(7)	13245(2)	3846(2)	5432(1)	34(1)
C(8)	11429(2)	731(2)	3910(1)	30(1)
C(9)	10459(3)	–788(2)	3738(1)	37(1)
C(10)	9922(3)	–671(2)	3231(1)	37(1)
C(11)	8807(2)	826(2)	3170(1)	36(1)
C(12)	9619(2)	2483(2)	3307(1)	30(1)
C(13)	11595(3)	631(2)	4439(1)	42(1)
C(14)	13140(2)	857(3)	3688(1)	43(1)
C(15)	8267(3)	3806(3)	3335(1)	45(1)
C(16)	10940(3)	2991(3)	2954(1)	43(1)
N	10327(2)	2283(2)	3807(1)	22(1)
O(1)	8277(1)	3361(1)	4512(1)	26(1)
O(2)	8620(1)	6375(1)	4494(1)	29(1)
O(3)	11637(1)	6320(1)	4566(1)	25(1)
O(4)	10514(1)	4121(1)	5068(1)	26(1)
O(5)	5512(2)	3280(2)	4417(1)	44(1)
O(6)	13532(2)	7331(2)	5063(1)	37(1)
Si	9986(1)	4826(1)	4543(1)	21(1)

Table 50. Bond Lengths [Å] and Angles [deg] for **9b**.

C(1)–N	1.526(2)	C(14)–C(8)–C(13)	110.03(16)
C(1)–Si	1.9090(17)	C(14)–C(8)–C(9)	112.17(16)
C(2)–O(5)	1.217(2)	C(13)–C(8)–C(9)	108.92(16)
C(2)–O(1)	1.328(2)	C(14)–C(8)–N	112.43(15)
C(2)–C(3)	1.508(3)	C(13)–C(8)–N	106.33(13)
C(3)–O(2)	1.419(2)	C(9)–C(8)–N	106.72(14)
C(3)–C(4)	1.516(3)	C(10)–C(9)–C(8)	113.87(15)
C(5)–O(6)	1.214(2)	C(11)–C(10)–C(9)	109.19(15)
C(5)–O(3)	1.313(2)	C(10)–C(11)–C(12)	114.15(15)
C(5)–C(6)	1.518(2)	C(15)–C(12)–C(16)	110.22(16)
C(6)–O(4)	1.427(2)	C(15)–C(12)–C(11)	108.41(16)
C(6)–C(7)	1.513(2)	C(16)–C(12)–C(11)	111.04(15)
C(8)–C(14)	1.518(3)	C(15)–C(12)–N	106.52(13)
C(8)–C(13)	1.526(2)	C(16)–C(12)–N	112.82(15)
C(8)–C(9)	1.528(2)	C(11)–C(12)–N	107.63(13)
C(8)–N	1.555(2)	H–N–C(1)	105.2(13)
C(9)–C(10)	1.520(3)	H–N–C(12)	100.1(13)
C(10)–C(11)	1.508(3)	C(1)–N–C(12)	113.98(12)
C(11)–C(12)	1.532(3)	H–N–C(8)	105.0(13)
C(12)–C(15)	1.520(3)	C(1)–N–C(8)	112.54(12)
C(12)–C(16)	1.520(3)	C(12)–N–C(8)	117.82(12)
C(12)–N	1.552(2)	H–N–H	0(4)
N–H	0.89(2)	C(1)–N–H	105.2(13)
N–H	0.89(2)	C(12)–N–H	100.1(13)
O(1)–Si	1.8077(11)	C(8)–N–H	105.0(13)
O(2)–Si	1.6624(12)	C(2)–O(1)–Si	113.96(10)
O(3)–Si	1.7875(11)	C(3)–O(2)–Si	117.20(10)
O(4)–Si	1.6643(12)	O(5)–C(2)–C(3)	125.41(16)
N–C(1)–Si	117.91(11)	O(1)–C(2)–C(3)	111.64(13)
O(5)–C(2)–O(1)	122.95(17)	C(5)–O(3)–Si	113.93(10)
O(2)–C(3)–C(2)	107.43(13)	C(6)–O(4)–Si	115.76(10)
O(2)–C(3)–C(4)	111.12(16)	O(2)–Si–O(4)	119.94(7)
C(2)–C(3)–C(4)	113.40(15)	O(2)–Si–O(3)	89.47(5)
O(2)–C(3)–H(3)	108.2	O(4)–Si–O(3)	90.32(6)
O(6)–C(5)–O(3)	124.37(17)	O(2)–Si–O(1)	88.96(5)
O(6)–C(5)–C(6)	123.58(16)	O(4)–Si–O(1)	90.97(5)
O(3)–C(5)–C(6)	112.05(13)	O(3)–Si–O(1)	178.32(6)
O(4)–C(6)–C(7)	112.00(14)	O(2)–Si–C(1)	121.60(7)
O(4)–C(6)–C(5)	107.69(13)	O(4)–Si–C(1)	118.40(7)
C(7)–C(6)–C(5)	111.05(14)	O(3)–Si–C(1)	87.87(6)
O(4)–C(6)–H(6)	108.7	O(1)–Si–C(1)	92.45(6)

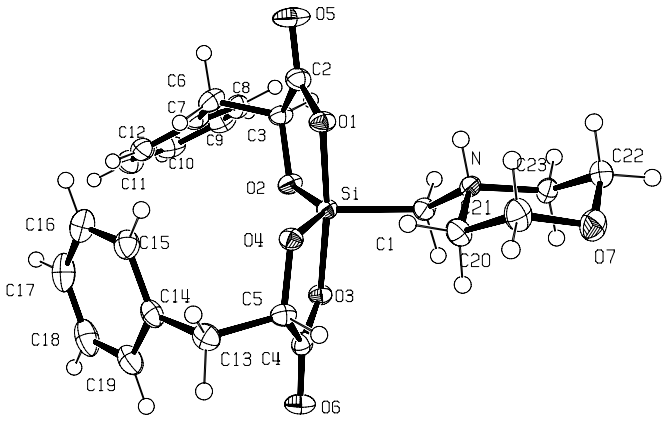

Figure 75. Crystal structure of **10a** (probability level of displacement ellipsoids 50%) showing the atomic numbering scheme.

Table 51. Atomic Coordinates (x 10^4) and Equivalent Isotropic Displacement Parameters ($Å^2$ x 10^3) for **10a**. U(eq) is Defined as One Third of the Trace of the Orthogonalized Uij Tensor.

	x	y	z	U(eq)
Si	1428(1)	9823(1)	5675(1)	16(1)
O(1)	1441(1)	11438(1)	6012(1)	21(1)
O(2)	1568(1)	9494(1)	7085(1)	21(1)
O(3)	1668(1)	8184(1)	5465(1)	18(1)
O(4)	2858(1)	10085(1)	5099(1)	19(1)
O(5)	1413(2)	12697(1)	7505(1)	35(1)
O(6)	2817(1)	6894(1)	4534(1)	27(1)
O(7)	–2365(1)	11315(1)	1082(1)	30(1)
N	–1164(1)	10792(1)	3631(1)	17(1)
C(1)	–704(2)	9828(2)	4604(1)	19(1)
C(2)	1429(2)	11672(2)	7095(1)	24(1)
C(3)	1430(2)	10505(2)	7804(1)	21(1)
C(4)	2601(2)	7925(1)	4844(1)	20(1)
C(5)	3371(2)	9074(2)	4565(1)	20(1)
C(6)	2783(2)	10520(2)	9006(1)	26(1)
C(7)	2705(2)	9536(1)	9892(1)	22(1)
C(8)	1317(2)	9298(2)	10135(2)	28(1)
C(9)	1289(2)	8441(2)	10999(2)	32(1)
C(10)	2647(3)	7814(2)	11641(2)	34(1)
C(11)	4037(2)	8034(2)	11416(2)	35(1)
C(12)	4066(2)	8881(2)	10537(1)	28(1)
C(13)	5175(2)	8981(2)	5003(2)	25(1)
C(14)	5896(2)	8726(2)	6337(2)	24(1)
C(15)	6126(2)	9680(2)	7166(2)	29(1)
C(16)	6749(2)	9450(2)	8392(2)	35(1)
C(17)	7143(2)	8268(2)	8808(2)	37(1)
C(18)	6923(2)	7309(2)	7993(2)	38(1)
C(19)	6306(2)	7533(2)	6762(2)	31(1)
C(20)	–154(2)	10732(2)	2842(1)	23(1)
C(21)	–774(2)	11594(2)	1772(1)	28(1)
C(22)	–3329(2)	11517(2)	1807(1)	25(1)
C(23)	–2883(2)	10642(2)	2866(1)	22(1)

Table 52. Bond Lengths [Å] and Angles [deg] for **10a**.

Si–O(2)	1.6665(11)	C(2)–O(1)–Si	113.85(10)
Si–O(4)	1.6668(10)	C(3)–O(2)–Si	116.05(9)
Si–O(1)	1.8015(11)	C(4)–O(3)–Si	114.36(9)
Si–O(3)	1.8229(11)	C(5)–O(4)–Si	117.25(9)
Si–C(1)	1.9052(14)	C(21)–O(7)–C(22)	108.60(12)
O(1)–C(2)	1.3080(19)	HN–N–C(20)	110.7(11)
O(2)–C(3)	1.4197(18)	HN–N–C(1)	107.9(12)
O(3)–C(4)	1.3156(18)	C(20)–N–C(1)	112.01(11)
O(4)–C(5)	1.4193(18)	HN–N–C(23)	106.7(11)
O(5)–C(2)	1.217(2)	C(20)–N–C(23)	109.32(11)
O(6)–C(4)	1.216(2)	C(1)–N–C(23)	110.07(11)
O(7)–C(21)	1.418(2)	N–C(1)–Si	117.71(10)
O(7)–C(22)	1.423(2)	O(5)–C(2)–O(1)	124.94(15)
N–HN	0.91(2)	O(5)–C(2)–C(3)	122.91(14)
N–C(20)	1.5040(18)	O(1)–C(2)–C(3)	112.15(14)
N–C(1)	1.5075(19)	O(2)–C(3)–C(2)	107.56(12)
N–C(23)	1.5116(18)	O(2)–C(3)–C(6)	111.25(13)
C(2)–C(3)	1.521(2)	C(2)–C(3)–C(6)	110.87(13)
C(3)–C(6)	1.527(2)	O(6)–C(4)–O(3)	124.22(14)
C(4)–C(5)	1.517(2)	O(6)–C(4)–C(5)	124.34(14)

C(5)–C(13)	1.528(2)	O(3)–C(4)–C(5)	111.44(13)
C(6)–C(7)	1.515(2)	O(4)–C(5)–C(4)	107.64(12)
C(7)–C(8)	1.393(2)	O(4)–C(5)–C(13)	111.44(13)
C(7)–C(12)	1.398(2)	C(4)–C(5)–C(13)	112.36(13)
C(8)–C(9)	1.389(3)	C(7)–C(6)–C(3)	115.30(14)
C(9)–C(10)	1.380(3)	C(8)–C(7)–C(12)	118.04(15)
C(10)–C(11)	1.381(3)	C(8)–C(7)–C(6)	121.76(15)
C(11)–C(12)	1.395(3)	C(12)–C(7)–C(6)	120.12(15)
C(13)–C(14)	1.515(2)	C(9)–C(8)–C(7)	120.98(16)
C(14)–C(15)	1.394(2)	C(10)–C(9)–C(8)	120.35(17)
C(14)–C(19)	1.395(2)	C(9)–C(10)–C(11)	119.72(17)
C(15)–C(16)	1.388(3)	C(10)–C(11)–C(12)	120.14(17)
C(16)–C(17)	1.380(3)	C(11)–C(12)–C(7)	120.76(16)
C(17)–C(18)	1.388(3)	C(14)–C(13)–C(5)	113.38(12)
C(18)–C(19)	1.392(3)	C(15)–C(14)–C(19)	118.76(16)
C(20)–C(21)	1.521(2)	C(15)–C(14)–C(13)	120.30(15)
C(22)–C(23)	1.514(2)	C(19)–C(14)–C(13)	120.92(16)
O(2)–Si–O(4)	129.43(6)	C(16)–C(15)–C(14)	120.71(17)
O(2)–Si–O(1)	89.76(5)	C(17)–C(16)–C(15)	120.34(18)
O(4)–Si–O(1)	88.53(5)	C(16)–C(17)–C(18)	119.56(17)
O(2)–Si–O(3)	87.35(5)	C(17)–C(18)–C(19)	120.46(18)
O(4)–Si–O(3)	88.22(5)	C(18)–C(19)–C(14)	120.17(18)
O(1)–Si–O(3)	172.80(5)	N–C(20)–C(21)	111.09(12)
O(2)–Si–C(1)	112.72(6)	O(7)–C(21)–C(20)	111.19(14)
O(4)–Si–C(1)	117.81(6)	O(7)–C(22)–C(23)	110.77(12)
O(1)–Si–C(1)	94.27(6)	N–C(23)–C(22)	111.03(12)
O(3)–Si–C(1)	92.94(6)		

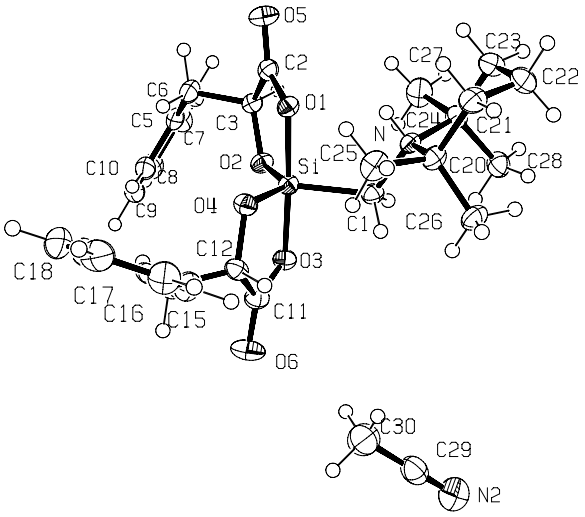

Figure 76. Termical ellipsoids (probability level of displacement 50%) of **11a**·CH_3CN with labels.

Table 53. Atomic Coordinates (x 10^4) and Equivalent Isotropic Displacement Parameters ($Å^2$ x 10^3) for **11a**·CH_3CN. U(eq) is Defined as One Third of the Trace of the Orthogonalized Uij Tensor.

	x	y	z	U(eq)
C(1)	754(2)	–402(1)	339(1)	24(1)
C(2)	–2173(2)	–2303(1)	–950(1)	23(1)
C(3)	–2867(1)	–1217(1)	–1632(1)	23(1)
C(4)	–3912(2)	–1591(1)	–2792(1)	29(1)
C(5)	–4696(2)	–555(1)	–3477(1)	27(1)
C(6)	–5707(2)	–60(2)	–3238(1)	34(1)
C(7)	–6423(2)	905(2)	–3855(2)	39(1)

C(8)	–6125(2)	1389(2)	–4710(2)	38(1)
C(9)	–5126(2)	913(2)	–4961(2)	36(1)
C(10)	–4419(2)	–60(2)	–4346(1)	31(1)
C(11)	854(2)	158(2)	–2282(1)	28(1)
C(12)	1200(2)	–1160(1)	–2240(1)	25(1)
C(13)	1033(2)	–1650(2)	–3397(1)	31(1)
C(14)	1686(2)	–2829(2)	–3384(1)	26(1)
C(15)	2931(2)	–3112(2)	–2559(2)	33(1)
C(16)	3548(2)	–4176(2)	–2598(2)	39(1)
C(17)	2936(2)	–4974(2)	–3470(2)	41(1)
C(18)	1706(2)	–4708(2)	–4295(2)	43(1)
C(19)	1078(2)	–3644(2)	–4250(2)	36(1)
C(20)	2346(1)	–1791(1)	1840(1)	25(1)
C(21)	2438(2)	–2594(2)	2830(2)	33(1)
C(22)	2100(2)	–1978(2)	3726(2)	39(1)
C(23)	687(2)	–1523(2)	3172(2)	36(1)
C(24)	462(2)	–633(1)	2212(1)	27(1)
C(25)	2417(2)	–2567(2)	887(2)	34(1)
C(26)	3465(2)	–887(2)	2223(1)	32(1)
C(27)	–1028(2)	–450(2)	1561(2)	39(1)
C(28)	1140(2)	548(2)	2671(2)	33(1)
C(29)	4641(2)	3145(2)	–354(2)	43(1)
C(30)	4068(3)	2098(3)	–1013(2)	64(1)
N	960(1)	–1198(1)	1350(1)	21(1)
N(2)	5099(2)	3962(2)	167(2)	58(1)
O(1)	–883(1)	–2248(1)	–651(1)	23(1)
O(2)	–1894(1)	–481(1)	–1752(1)	24(1)
O(3)	119(1)	374(1)	–1720(1)	25(1)
O(4)	403(1)	–1780(1)	–1780(1)	25(1)
O(5)	–2736(1)	–3116(1)	–709(1)	33(1)
O(6)	1233(1)	904(1)	–2764(1)	41(1)
Si	–331(1)	–931(1)	–1145(1)	21(1)

Table 54. Bond Lengths [Å] and Angles [deg] for **11a**·CH_3CN.

C(1)–N	1.5176(19)	O(6)–C(11)–O(3)	124.94(15)
C(1)–Si	1.8949(16)	O(6)–C(11)–C(12)	123.69(14)
C(2)–O(5)	1.2165(19)	O(3)–C(11)–C(12)	111.36(14)
C(2)–O(1)	1.3243(18)	O(4)–C(12)–C(13)	111.98(13)
C(2)–C(3)	1.520(2)	O(4)–C(12)–C(11)	107.43(12)
C(3)–O(2)	1.4167(18)	C(13)–C(12)–C(11)	112.75(13)
C(3)–C(4)	1.534(2)	C(14)–C(13)–C(12)	115.96(13)
C(4)–C(5)	1.508(2)	C(19)–C(14)–C(15)	118.01(16)
C(5)–C(10)	1.389(2)	C(19)–C(14)–C(13)	119.70(15)
C(5)–C(6)	1.392(2)	C(15)–C(14)–C(13)	122.19(15)
C(6)–C(7)	1.390(3)	C(16)–C(15)–C(14)	121.32(17)
C(7)–C(8)	1.380(3)	C(17)–C(16)–C(15)	120.02(18)
C(8)–C(9)	1.381(3)	C(18)–C(17)–C(16)	119.47(18)
C(9)–C(10)	1.392(3)	C(17)–C(18)–C(19)	120.58(18)
C(11)–O(6)	1.215(2)	C(14)–C(19)–C(18)	120.59(17)
C(11)–O(3)	1.3105(19)	C(26)–C(20)–C(21)	110.63(14)
C(11)–C(12)	1.528(2)	C(26)–C(20)–C(25)	109.93(14)
C(12)–O(4)	1.4281(18)	C(21)–C(20)–C(25)	108.70(13)
C(12)–C(13)	1.524(2)	C(26)–C(20)–N	112.76(13)
C(13)–C(14)	1.508(2)	C(21)–C(20)–N	108.34(12)
C(14)–C(19)	1.390(2)	C(25)–C(20)–N	106.32(12)
C(14)–C(15)	1.397(2)	C(22)–C(21)–C(20)	114.09(14)
C(15)–C(16)	1.390(3)	C(21)–C(22)–C(23)	108.66(15)
C(16)–C(17)	1.382(3)	C(22)–C(23)–C(24)	113.58(14)
C(17)–C(18)	1.381(3)	C(28)–C(24)–C(23)	111.32(14)

C(18)–C(19)	1.398(3)	C(28)–C(24)–C(27)	110.40(15)
C(20)–C(26)	1.525(2)	C(23)–C(24)–C(27)	108.48(14)
C(20)–C(21)	1.529(2)	C(28)–C(24)–N	111.80(12)
C(20)–C(25)	1.532(2)	C(23)–C(24)–N	108.43(12)
C(20)–N	1.5572(18)	C(27)–C(24)–N	106.23(13)
C(21)–C(22)	1.514(3)	N(2)–C(29)–C(30)	179.4(3)
C(22)–C(23)	1.525(3)	H–N–C(1)	107.7(12)
C(23)–C(24)	1.530(2)	H–N–C(24)	102.7(12)
C(24)–C(28)	1.523(2)	C(1)–N–C(24)	113.18(11)
C(24)–C(27)	1.536(2)	H–N–C(20)	101.5(13)
C(24)–N	1.5571(19)	C(1)–N–C(20)	112.55(11)
C(29)–N(2)	1.131(3)	C(24)–N–C(20)	117.49(11)
C(29)–C(30)	1.441(3)	C(1)–N–H	107.7(12)
O(1)–Si	1.8131(11)	C(24)–N–H	102.7(12)
O(2)–Si	1.6667(11)	C(20)–N–H	101.5(13)
O(3)–Si	1.8017(12)	C(2)–O(1)–Si	114.46(10)
O(4)–Si	1.6654(11)	C(3)–O(2)–Si	117.78(9)
N–C(1)–Si	119.49(10)	C(11)–O(3)–Si	114.24(11)
O(5)–C(2)–O(1)	124.53(14)	C(12)–O(4)–Si	115.37(9)
O(5)–C(2)–C(3)	123.96(13)	O(4)–Si–O(2)	124.49(6)
O(1)–C(2)–C(3)	111.51(13)	O(4)–Si–O(3)	89.82(5)
O(2)–C(3)–C(2)	107.52(11)	O(2)–Si–O(3)	88.19(5)
O(2)–C(3)–C(4)	111.43(12)	O(4)–Si–O(1)	90.15(5)
C(2)–C(3)–C(4)	110.44(12)	O(2)–Si–O(1)	88.72(5)
C(5)–C(4)–C(3)	112.84(13)	O(3)–Si–O(1)	176.22(5)
C(10)–C(5)–C(6)	118.41(15)	O(4)–Si–C(1)	115.79(7)
C(10)–C(5)–C(4)	121.17(15)	O(2)–Si–C(1)	119.65(6)
C(6)–C(5)–C(4)	120.42(15)	O(3)–Si–C(1)	89.33(6)
C(7)–C(6)–C(5)	120.81(16)	O(1)–Si–C(1)	94.08(6)
C(8)–C(7)–C(6)	119.83(18)	C(8)–C(9)–C(10)	119.57(17)
C(7)–C(8)–C(9)	120.33(18)	C(5)–C(10)–C(9)	121.05(16)

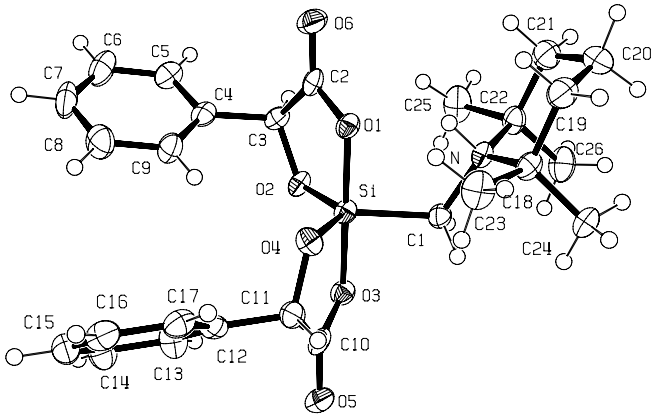

Figure 77. Crystal structure of **12a** (probability level of displacement ellipsoids 50%) showing the atomic numbering scheme.

Table 55. Atomic Coordinates (x 10^4) and Equivalent Isotropic Displacement Parameters ($Å^2$ x 10^3) for **12a**. U(eq) is Defined as One Third of the Trace of the Orthogonalized Uij Tensor.

	x	y	z	U(eq)
C(1)	4089(3)	2955(3)	726(1)	25(1)
C(2)	6826(3)	4825(3)	1058(2)	26(1)
C(3)	7501(2)	4195(2)	495(2)	24(1)
C(4)	8261(3)	5105(2)	112(1)	26(1)
C(5)	9544(3)	5094(3)	162(2)	32(1)

C(6)	10232(3)	5970(3)	–159(2)	43(1)
C(7)	9673(3)	6852(3)	–532(2)	44(1)
C(8)	8399(3)	6849(3)	–592(2)	42(1)
C(9)	7705(3)	5989(3)	–268(2)	33(1)
C(10)	4035(3)	3803(3)	–920(2)	30(1)
C(11)	3976(3)	5130(3)	–728(1)	28(1)
C(12)	4601(2)	5955(3)	–1222(1)	27(1)
C(13)	5447(3)	5527(3)	–1679(2)	38(1)
C(14)	6000(3)	6306(3)	–2129(2)	41(1)
C(15)	5712(3)	7523(3)	–2120(2)	36(1)
C(16)	4877(3)	7964(3)	–1668(2)	35(1)
C(17)	4331(3)	7181(3)	–1219(2)	32(1)
C(18)	2767(2)	3750(3)	1690(2)	26(1)
C(19)	2916(3)	4078(3)	2419(2)	36(1)
C(20)	3341(3)	3044(3)	2857(2)	40(1)
C(21)	4559(3)	2554(3)	2609(2)	37(1)
C(22)	4537(3)	2131(3)	1890(2)	28(1)
C(23)	2607(3)	4907(3)	1283(2)	38(1)
C(24)	1676(3)	2886(3)	1574(2)	38(1)
C(25)	5879(3)	1952(3)	1658(2)	42(1)
C(26)	3811(3)	960(3)	1801(2)	40(1)
N	4007(2)	3176(2)	1470(1)	22(1)
O(1)	5613(2)	4824(2)	952(1)	24(1)
O(2)	6593(2)	3629(2)	88(1)	25(1)
O(3)	4664(2)	3156(2)	–486(1)	25(1)
O(4)	4525(2)	5239(2)	–87(1)	27(1)
O(5)	3546(2)	3380(2)	–1406(1)	42(1)
O(6)	7313(2)	5260(2)	1539(1)	37(1)
Si	5129(1)	3987(1)	229(1)	22(1)

Table 56. Bond Lengths [Å] and Angles [deg] for **12a**.

C(1)–N	1.530(4)	O(5)–C(10)–O(3)	123.9(3)
C(1)–Si	1.896(3)	O(5)–C(10)–C(11)	124.2(3)
C(2)–O(6)	1.208(3)	O(3)–C(10)–C(11)	111.9(3)
C(2)–O(1)	1.337(3)	O(4)–C(11)–C(12)	111.2(2)
C(2)–C(3)	1.525(4)	O(4)–C(11)–C(10)	107.2(2)
C(3)–O(2)	1.430(3)	C(12)–C(11)–C(10)	113.1(3)
C(3)–C(4)	1.515(4)	C(17)–C(12)–C(13)	118.4(3)
C(4)–C(9)	1.383(4)	C(17)–C(12)–C(11)	119.3(3)
C(4)–C(5)	1.399(4)	C(13)–C(12)–C(11)	122.3(3)
C(5)–C(6)	1.384(4)	C(12)–C(13)–C(14)	120.9(3)
C(6)–C(7)	1.375(5)	C(15)–C(14)–C(13)	119.7(3)
C(7)–C(8)	1.391(5)	C(16)–C(15)–C(14)	120.1(3)
C(8)–C(9)	1.380(4)	C(15)–C(16)–C(17)	119.9(3)
C(10)–O(5)	1.214(3)	C(12)–C(17)–C(16)	120.9(3)
C(10)–O(3)	1.324(4)	C(23)–C(18)–C(19)	109.6(3)
C(10)–C(11)	1.516(4)	C(23)–C(18)–C(24)	110.3(3)
C(11)–O(4)	1.433(3)	C(19)–C(18)–C(24)	112.0(3)
C(11)–C(12)	1.515(4)	C(23)–C(18)–N	106.6(2)
C(12)–C(17)	1.385(4)	C(19)–C(18)–N	106.3(2)
C(12)–C(13)	1.389(4)	C(24)–C(18)–N	111.9(2)
C(13)–C(14)	1.389(5)	C(20)–C(19)–C(18)	114.8(3)
C(14)–C(15)	1.379(5)	C(21)–C(20)–C(19)	109.9(3)
C(15)–C(16)	1.378(4)	C(20)–C(21)–C(22)	114.3(3)
C(16)–C(17)	1.388(4)	C(26)–C(22)–C(21)	112.3(3)
C(18)–C(23)	1.530(4)	C(26)–C(22)–N	111.9(2)
C(18)–C(19)	1.530(4)	C(21)–C(22)–N	107.6(2)
C(18)–C(24)	1.540(4)	C(26)–C(22)–C(25)	110.1(3)
C(18)–N	1.555(4)	C(21)–C(22)–C(25)	108.3(3)

C(19)–C(20)	1.518(4)	N–C(22)–C(25)	106.3(2)
C(20)–C(21)	1.517(4)	H–N–C(22)	105.2(16)
C(21)–C(22)	1.529(4)	C(1)–N–C(22)	113.7(2)
C(22)–C(26)	1.526(4)	H–N–C(18)	100.4(16)
C(22)–N	1.545(4)	C(1)–N–C(18)	113.3(2)
C(22)–C(25)	1.546(4)	C(22)–N–C(18)	118.1(2)
O(1)–Si	1.811(2)	C(1)–N–H	103.5(16)
O(2)–Si	1.666(2)	C(22)–N–H	105.2(17)
O(3)–Si	1.787(2)	C(18)–N–H	100.4(16)
O(4)–Si	1.659(2)	C(2)–O(1)–Si	114.71(18)
N–C(1)–Si	117.60(19)	C(3)–O(2)–Si	117.24(16)
O(6)–C(2)–O(1)	124.3(3)	C(10)–O(3)–Si	114.05(17)
O(6)–C(2)–C(3)	125.0(3)	C(11)–O(4)–Si	116.40(17)
O(1)–C(2)–C(3)	110.7(2)	O(4)–Si–O(2)	120.70(11)
O(2)–C(3)–C(4)	111.8(2)	O(4)–Si–O(3)	90.14(10)
O(2)–C(3)–C(2)	107.4(2)	O(2)–Si–O(3)	90.57(10)
C(4)–C(3)–C(2)	110.1(2)	O(4)–Si–O(1)	90.18(10)
C(9)–C(4)–C(5)	118.8(3)	O(2)–Si–O(1)	88.94(10)
C(9)–C(4)–C(3)	120.9(2)	O(3)–Si–O(1)	179.51(10)
C(5)–C(4)–C(3)	120.2(3)	O(4)–Si–C(1)	117.98(12)
C(6)–C(5)–C(4)	120.0(3)	O(2)–Si–C(1)	121.28(12)
C(7)–C(6)–C(5)	120.9(3)	O(3)–Si–C(1)	87.35(11)
C(6)–C(7)–C(8)	119.2(3)	O(1)–Si–C(1)	92.84(11)
C(9)–C(8)–C(7)	120.4(3)	C(8)–C(9)–C(4)	120.7(3)

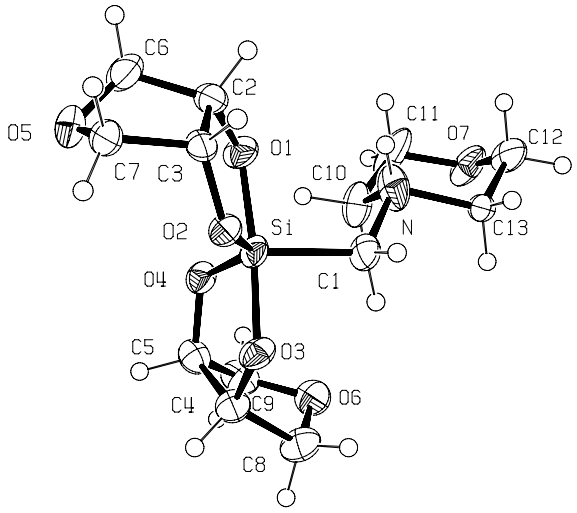

Figure 78. Crystal structure of **14** (probability level of displacement ellipsoids 50%) showing the atomic numbering scheme.

Table 57. Atomic Coordinates (x 10^4) and Equivalent Isotropic Displacement Parameters (Å^2 x 10^3) for **14** U(eq) is Defined as One Third of the Trace of the Orthogonalized Uij Tensor.

	x	y	z	U(eq)
C(1)	2148(3)	1783(2)	4632(4)	38(1)
N	2417(4)	1485(2)	6130(4)	46(1)
C(10)	2876(11)	645(5)	6136(11)	47(3)
C(11)	2912(7)	305(5)	7502(9)	64(3)
O(7)	1449(5)	293(4)	7432(7)	50(2)
C(12)	883(7)	1071(4)	7309(7)	45(2)
C(13)	756(7)	1478(4)	5940(8)	29(2)

O(3)	2721(2)	1985(1)	2373(2)	33(1)
C(4)	2566(3)	1298(2)	1551(4)	34(1)
C(8)	1056(4)	862(2)	1081(4)	44(1)
O(6)	1376(3)	278(1)	2214(3)	44(1)
C(9)	2849(4)	–15(2)	2556(4)	42(1)
C(5)	3795(4)	704(2)	2625(4)	34(1)
O(4)	4560(2)	1042(1)	4084(2)	31(1)
O(2)	4442(2)	2844(1)	4237(2)	31(1)
C(3)	5637(3)	3178(2)	5568(3)	32(1)
C(7)	7075(4)	3321(2)	5424(4)	39(1)
O(5)	7948(2)	2618(1)	5940(3)	45(1)
C(6)	7812(4)	2396(2)	7234(4)	48(1)
C(2)	6155(3)	2555(2)	6834(3)	35(1)
O(1)	5229(2)	1894(1)	6246(2)	36(1)
C(10A)	3349(10)	709(5)	6768(10)	33(2)
C(11A)	2245(7)	29(4)	6041(7)	33(2)
O(7A)	1064(5)	46(3)	6461(7)	37(1)
C(12A)	247(7)	770(4)	5950(8)	37(2)
C(13A)	1246(9)	1465(5)	6668(10)	33(2)

Table 58. Bond Lengths [Å] and Angles [deg] for **14**.

Si–O(4)	1.682(2)	C(1)–N–C(10)	103.6(4)
Si–O(2)	1.702(2)	H–N–C(13A)	96(3)
Si–O(1)	1.739(2)	C(1)–N–C(13A)	125.5(4)
Si–O(3)	1.758(2)	C(10)–N–C(13A)	105.3(5)
Si–C(1)	1.913(3)	H–N–C(10A)	100(3)
C(1)–N	1.493(4)	C(1)–N–C(10A)	119.2(4)
N–H	0.85(4)	C(10)–N–C(10A)	22.2(4)
N–C(10)	1.500(9)	C(13A)–N–C(10A)	103.9(5)
N–C(13A)	1.503(7)	H–N–C(13)	114(3)
N–C(10A)	1.565(9)	C(1)–N–C(13)	102.3(4)
N–C(13)	1.569(7)	C(10)–N–C(13)	107.0(5)
C(10)–C(11)	1.481(10)	C(13A)–N–C(13)	24.7(3)
C(11)–O(7)	1.421(7)	C(10A)–N–C(13)	115.1(5)
O(7)–C(12)	1.422(8)	C(11)–C(10)–N	104.4(7)
C(12)–C(13)	1.497(8)	O(7)–C(11)–C(10)	113.1(6)
O(3)–C(4)	1.400(3)	C(11)–O(7)–C(12)	110.1(5)
C(4)–C(8)	1.532(4)	O(7)–C(12)–C(13)	111.5(6)
C(4)–C(5)	1.556(4)	C(12)–C(13)–N	105.9(5)
C(8)–O(6)	1.433(4)	C(4)–O(3)–Si	115.48(18)
O(6)–C(9)	1.423(4)	O(3)–C(4)–C(8)	113.7(3)
C(9)–C(5)	1.523(4)	O(3)–C(4)–C(5)	107.7(2)
C(5)–O(4)	1.417(4)	C(8)–C(4)–C(5)	103.1(2)
O(2)–C(3)	1.418(3)	O(6)–C(8)–C(4)	106.2(3)
C(3)–C(7)	1.525(4)	C(9)–O(6)–C(8)	104.2(2)
C(3)–C(2)	1.547(4)	O(6)–C(9)–C(5)	105.7(3)
C(7)–O(5)	1.424(4)	O(4)–C(5)–C(9)	112.7(3)
O(5)–C(6)	1.428(4)	O(4)–C(5)–C(4)	108.1(2)
C(6)–C(2)	1.520(4)	C(9)–C(5)–C(4)	103.3(2)
C(2)–O(1)	1.395(3)	C(5)–O(4)–Si	117.36(18)
C(10A)–C(11A)	1.520(8)	C(3)–O(2)–Si	117.76(18)
C(11A)–O(7A)	1.427(7)	O(2)–C(3)–C(7)	111.8(2)
O(7A)–C(12A)	1.430(7)	O(2)–C(3)–C(2)	107.7(2)
C(12A)–C(13A)	1.490(9)	C(7)–C(3)–C(2)	103.4(3)
O(4)–Si–O(2)	130.78(10)	O(5)–C(7)–C(3)	105.4(2)
O(4)–Si–O(1)	90.63(11)	C(7)–O(5)–C(6)	104.3(3)
O(2)–Si–O(1)	89.05(10)	O(5)–C(6)–C(2)	106.1(3)
O(4)–Si–O(3)	89.57(10)	O(1)–C(2)–C(6)	112.2(3)

O(2)–Si–O(3)	85.51(10)	O(1)–C(2)–C(3)	108.2(2)
O(1)–Si–O(3)	172.98(10)	C(6)–C(2)–C(3)	103.3(2)
O(4)–Si–C(1)	112.20(12)	C(2)–O(1)–Si	117.21(19)
O(2)–Si–C(1)	116.84(13)	C(11A)–C(10A)–N	107.3(6)
O(1)–Si–C(1)	95.17(13)	O(7A)–C(11A)–C(10A)	110.3(6)
O(3)–Si–C(1)	91.26(13)	C(11A)–O(7A)–C(12A)	108.4(5)
N–C(1)–Si	117.5(2)	O(7A)–C(12A)–C(13A)	112.3(5)
H–N–C(1)	107(3)	C(12A)–C(13A)–N	107.0(5)
H–N–C(10)	121(3)		

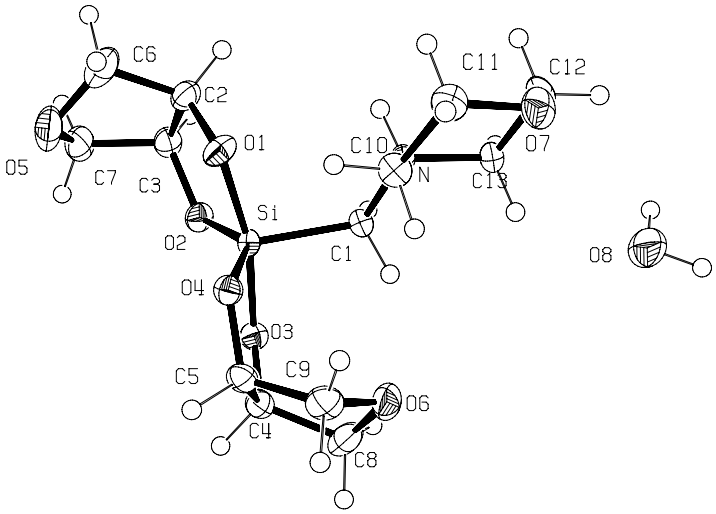

Figure 79. Crystal structure of **14**· H_2O (probability level of displacement ellipsoids 50%) showing the atomic numbering scheme.

Table 59. Atomic Coordinates (x 10^4) and Equivalent Isotropic Displacement Parameters ($Å^2$ x 10^3) for **14**·H_2O. U(eq) is Defined as One Third of the Trace of the Orthogonalized Uij Tensor.

	x	y	z	U(eq)
Si(1)	8935(1)	619(1)	5637(1)	18(1)
O(1)	10371(1)	664(1)	7394(1)	28(1)
O(2)	9452(1)	–329(1)	5532(1)	25(1)
O(3)	7824(1)	539(1)	3765(1)	23(1)
O(4)	9436(1)	1541(1)	5385(1)	23(1)
O(5)	12995(2)	–178(1)	7341(2)	48(1)
O(6)	6104(1)	2092(1)	3657(2)	37(1)
O(7)	6651(1)	2166(1)	8972(1)	35(1)
N	7431(1)	986(1)	7436(1)	19(1)
C(1)	7227(2)	659(1)	6014(2)	20(1)
C(2)	11074(2)	–45(1)	8030(2)	28(1)
C(3)	10577(2)	–669(1)	6808(2)	28(1)
C(4)	7540(2)	1243(1)	2981(2)	25(1)
C(5)	8589(2)	1888(1)	4010(2)	25(1)
C(6)	12770(2)	4(1)	8569(2)	42(1)
C(7)	12024(2)	–836(1)	6691(2)	39(1)
C(8)	5957(2)	1571(1)	2520(2)	36(1)
C(9)	7477(2)	2504(1)	4009(2)	33(1)
C(10)	8074(2)	1804(1)	7688(2)	26(1)
C(11)	8118(2)	2150(1)	9049(2)	31(1)
C(12)	6081(2)	1387(1)	8822(2)	30(1)
C(13)	5931(2)	1006(1)	7452(2)	23(1)
O(8)	2580(2)	1418(1)	5971(2)	53(1)

Table 60. Bond Lengths [Å] and Angles [deg] for **14**·H_2O.

Si(1)–O(4)	1.7007(11)	O(1)–Si(1)–C(1)	99.27(6)
Si(1)–O(2)	1.7114(11)	O(3)–Si(1)–C(1)	93.78(6)
Si(1)–O(1)	1.7333(12)	C(2)–O(1)–Si(1)	117.00(10)
Si(1)–O(3)	1.7528(11)	C(3)–O(2)–Si(1)	117.22(10)
Si(1)–C(1)	1.9168(14)	C(4)–O(3)–Si(1)	116.04(9)
O(1)–C(2)	1.3997(19)	C(5)–O(4)–Si(1)	117.37(9)
O(2)–C(3)	1.4120(19)	C(7)–O(5)–C(6)	104.09(14)
O(3)–C(4)	1.4026(18)	C(9)–O(6)–C(8)	103.69(12)
O(4)–C(5)	1.4166(18)	C(12)–O(7)–C(11)	109.63(12)
O(5)–C(7)	1.430(3)	HN–N–C(10)	110.3(12)
O(5)–C(6)	1.432(3)	HN–N–C(13)	109.3(12)
O(6)–C(9)	1.427(2)	C(10)–N–C(13)	108.85(10)
O(6)–C(8)	1.434(2)	HN–N–C(1)	107.3(12)
O(7)–C(12)	1.421(2)	C(10)–N–C(1)	111.53(10)
O(7)–C(11)	1.427(2)	C(13)–N–C(1)	109.54(10)
N–HN	0.93(2)	N–C(1)–Si(1)	118.97(9)
N–C(10)	1.5029(17)	O(1)–C(2)–C(6)	111.00(13)
N–C(13)	1.5030(16)	O(1)–C(2)–C(3)	107.31(12)
N–C(1)	1.5086(17)	C(6)–C(2)–C(3)	102.80(14)
C(2)–C(6)	1.520(2)	O(2)–C(3)–C(7)	111.76(13)
C(2)–C(3)	1.555(2)	O(2)–C(3)–C(2)	108.05(11)
C(3)–C(7)	1.528(2)	C(7)–C(3)–C(2)	103.63(14)
C(4)–C(8)	1.529(2)	O(3)–C(4)–C(8)	113.41(12)
C(4)–C(5)	1.554(2)	O(3)–C(4)–C(5)	107.88(12)
C(5)–C(9)	1.525(2)	C(8)–C(4)–C(5)	103.29(13)
C(10)–C(11)	1.520(2)	O(4)–C(5)–C(9)	112.39(13)
C(12)–C(13)	1.513(2)	O(4)–C(5)–C(4)	107.72(12)
O(8)–HO1	0.96(2)	C(9)–C(5)–C(4)	103.04(13)
O(8)–HO2	0.96(2)	O(5)–C(6)–C(2)	105.19(15)
O(4)–Si(1)–O(2)	137.66(5)	O(5)–C(7)–C(3)	105.96(14)
O(4)–Si(1)–O(1)	87.96(5)	O(6)–C(8)–C(4)	105.47(13)
O(2)–Si(1)–O(1)	89.01(5)	O(6)–C(9)–C(5)	105.99(13)
O(4)–Si(1)–O(3)	88.79(5)	N–C(10)–C(11)	110.43(12)
O(2)–Si(1)–O(3)	84.85(5)	O(7)–C(11)–C(10)	111.44(12)
O(1)–Si(1)–O(3)	166.88(5)	O(7)–C(12)–C(13)	111.34(12)
O(4)–Si(1)–C(1)	110.58(6)	N–C(13)–C(12)	110.69(12)
O(2)–Si(1)–C(1)	111.59(6)	HO1–O(8)–HO2	103(3)

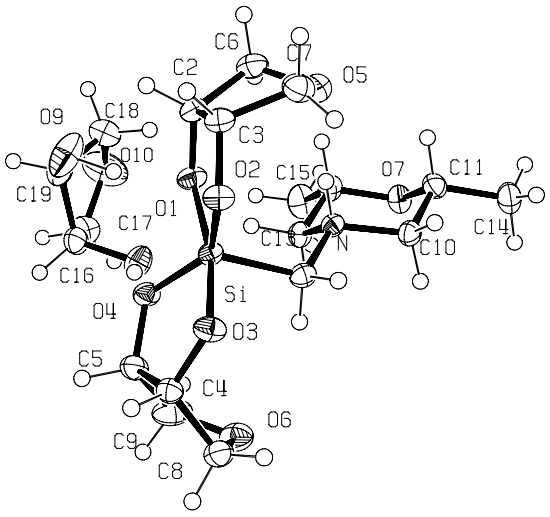

Figure 80. Crystal structure of **15**·$C_4H_8O_3$ (probability level of displacement ellipsoids 50%) showing the atomic numbering scheme.

Table 61. Atomic Coordinates (x 10^4) and Equivalent Isotropic Displacement Parameters ($Å^2$ x 10^3) for **15**·$C_4H_8O_3$. U(eq) is Defined as One Third of the Trace of the Orthogonalized Uij Tensor.

	x	y	z	U(eq)
Si	11213(1)	3754(1)	1139(1)	20(1)
N	8605(1)	3169(2)	687(1)	21(1)
O(1)	10390(1)	3978(1)	1733(1)	26(1)
O(2)	11386(1)	5652(1)	1128(1)	26(1)
O(3)	12312(1)	3627(1)	678(1)	27(1)
O(4)	11869(1)	2214(1)	1514(1)	25(1)
O(5)	8533(1)	6202(1)	1198(1)	34(1)
O(6)	11774(1)	333(1)	318(1)	36(1)
O(7)	6196(1)	1872(1)	637(1)	27(1)
C(1)	9887(1)	3158(2)	541(1)	24(1)
C(2)	10184(2)	5468(2)	1912(1)	26(1)
C(3)	10706(2)	6533(2)	1474(1)	26(1)
C(4)	13053(1)	2326(2)	725(1)	25(1)
C(5)	12702(2)	1356(2)	1239(1)	28(1)
C(6)	8814(2)	5825(2)	1815(1)	31(1)
C(7)	9537(2)	7203(2)	1117(1)	33(1)
C(8)	12757(2)	1277(2)	196(1)	30(1)
C(9)	12114(2)	–48(2)	928(1)	40(1)
C(10)	7647(1)	3244(2)	143(1)	24(1)
C(11)	6361(2)	3205(2)	304(1)	26(1)
C(12)	7060(2)	1831(2)	1176(1)	27(1)
C(13)	8370(1)	1816(2)	1044(1)	24(1)
C(14)	5410(2)	3176(2)	–254(1)	34(1)
C(15)	6802(2)	409(2)	1503(1)	39(1)
C(16)	10945(2)	211(2)	2723(1)	32(1)
C(17)	10078(2)	–849(2)	2965(1)	42(1)
C(18)	9437(2)	1584(2)	3111(1)	43(1)
C(19)	10810(2)	1628(2)	3084(1)	34(1)
O(8)	10482(1)	442(2)	2118(1)	37(1)
O(9)	11236(2)	2972(2)	2872(1)	55(1)
O(10)	9137(2)	34(2)	3149(1)	64(1)

Table 62. Bond Lengths [Å] and Angles [deg] for **15**·$C_4H_8O_3$.

Si–O(2)	1.6926(12)	HN–N–C(1)	111.1(12)
Si–O(4)	1.7103(11)	C(13)–N–C(1)	111.64(12)
Si–O(3)	1.7353(11)	HN–N–C(10)	105.8(12)
Si–O(1)	1.7653(11)	C(13)–N–C(10)	109.38(12)
Si–C(1)	1.9120(16)	C(1)–N–C(10)	111.77(11)
N–HN	0.89(2)	C(2)–O(1)–Si	117.16(9)
N–C(13)	1.4983(19)	C(3)–O(2)–Si	118.03(9)
N–C(1)	1.4995(19)	C(4)–O(3)–Si	117.21(9)
N–C(10)	1.5020(18)	C(5)–O(4)–Si	116.96(9)
O(1)–C(2)	1.4114(19)	C(6)–O(5)–C(7)	102.75(12)
O(2)–C(3)	1.4113(18)	C(8)–O(6)–C(9)	104.12(13)
O(3)–C(4)	1.4054(19)	C(11)–O(7)–C(12)	111.08(12)
O(4)–C(5)	1.4149(18)	N–C(1)–Si	118.08(10)
O(5)–C(6)	1.442(2)	O(1)–C(2)–C(6)	110.67(13)
O(5)–C(7)	1.451(2)	O(1)–C(2)–C(3)	106.61(12)
O(6)–C(8)	1.428(2)	C(6)–C(2)–C(3)	103.78(13)
O(6)–C(9)	1.433(2)	O(2)–C(3)–C(7)	112.70(13)
O(7)–C(11)	1.4348(19)	O(2)–C(3)–C(2)	108.24(12)
O(7)–C(12)	1.4358(18)	C(7)–C(3)–C(2)	102.63(13)
C(2)–C(6)	1.519(2)	O(3)–C(4)–C(8)	113.03(13)

C(2)–C(3)	1.555(2)	O(3)–C(4)–C(5)	107.45(12)
C(3)–C(7)	1.530(2)	C(8)–C(4)–C(5)	102.83(13)
C(4)–C(8)	1.524(2)	O(4)–C(5)–C(9)	113.07(14)
C(4)–C(5)	1.559(2)	O(4)–C(5)–C(4)	107.47(12)
C(5)–C(9)	1.525(2)	C(9)–C(5)–C(4)	103.42(12)
C(10)–C(11)	1.516(2)	O(5)–C(6)–C(2)	104.12(12)
C(11)–C(14)	1.520(2)	O(5)–C(7)–C(3)	106.49(13)
C(12)–C(15)	1.516(2)	O(6)–C(8)–C(4)	105.74(12)
C(12)–C(13)	1.518(2)	O(6)–C(9)–C(5)	106.91(13)
C(16)–O(8)	1.4179(19)	N–C(10)–C(11)	110.65(12)
C(16)–C(17)	1.507(3)	O(7)–C(11)–C(10)	110.56(13)
C(16)–C(19)	1.525(2)	O(7)–C(11)–C(14)	107.96(14)
C(17)–O(10)	1.415(3)	C(10)–C(11)–C(14)	109.68(13)
C(18)–O(10)	1.418(3)	O(7)–C(12)–C(15)	107.41(14)
C(18)–C(19)	1.521(3)	O(7)–C(12)–C(13)	110.12(12)
C(19)–O(9)	1.395(2)	C(15)–C(12)–C(13)	110.52(14)
O(8)–HO8	1.08(3)	N–C(13)–C(12)	110.82(12)
O(9)–HO9	1.00(3)	O(8)–C(16)–C(17)	107.68(15)
O(2)–Si–O(4)	139.55(6)	O(8)–C(16)–C(19)	111.35(14)
O(2)–Si–O(3)	87.97(5)	C(17)–C(16)–C(19)	100.93(14)
O(4)–Si–O(3)	88.75(5)	O(10)–C(17)–C(16)	107.59(16)
O(2)–Si–O(1)	88.44(5)	O(10)–C(18)–C(19)	105.68(16)
O(4)–Si–O(1)	85.79(5)	O(9)–C(19)–C(18)	115.28(17)
O(3)–Si–O(1)	166.84(6)	O(9)–C(19)–C(16)	116.42(15)
O(2)–Si–C(1)	109.74(6)	C(18)–C(19)–C(16)	100.62(15)
O(4)–Si–C(1)	110.70(6)	HO8–O(8)–C(16)	108.5(13)
O(3)–Si–C(1)	93.80(6)	HO9–O(9)–C(19)	105.1(18)
O(1)–Si–C(1)	99.33(6)	C(17)–O(10)–C(18)	109.13(15)
HN–N–C(13)	106.9(12)	HN–N–C(1)	111.1(12)

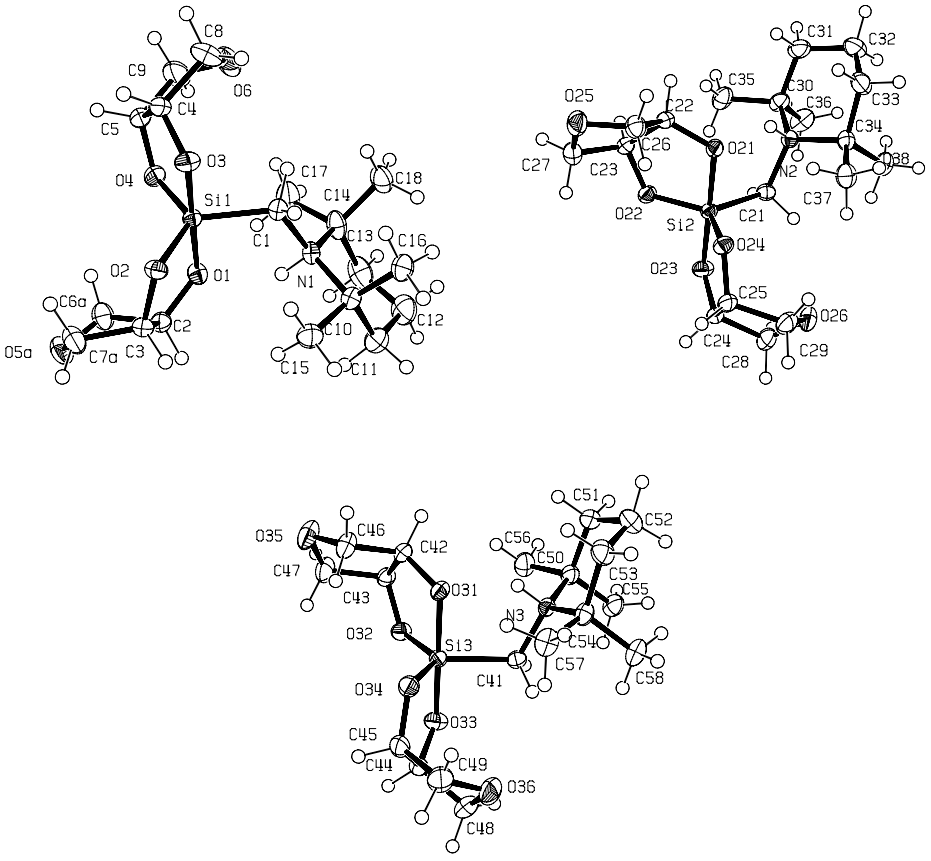

Figure 81. Crystal structure of **16** (probability level of displacement ellipsoids 50%) showing the atomic numbering scheme.

Table 63. Atomic Coordinates (x 10^4) and Equivalent Isotropic Displacement Parameters ($Å^2$ x 10^3) for **16**. U(eq) is Defined as One Third of the Trace of the Orthogonalized Uij Tensor.

	x	y	z	U(eq)
Si(1)	–2203(1)	941(1)	3953(1)	19(1)
O(1)	–1236(1)	562(1)	3575(1)	24(1)
O(2)	–2389(1)	1239(1)	3166(1)	23(1)
O(3)	–3171(1)	1308(1)	4302(1)	29(1)
O(4)	–1001(1)	1035(1)	4675(1)	28(1)
C(1)	–3368(1)	476(1)	4056(1)	23(1)
C(2)	–812(1)	725(1)	2960(1)	24(1)
C(3)	–1701(1)	1107(1)	2628(1)	23(1)
C(4)	–2650(2)	1487(1)	4995(1)	32(1)
C(5)	–1270(2)	1313(1)	5238(1)	33(1)
C(6A)	487(1)	950(1)	3147(1)	34(1)
O(5A)	439(1)	1282(1)	2589(1)	37(1)
C(7A)	–799(2)	1469(1)	2476(1)	35(1)
C(6B)	487(1)	950(1)	3147(1)	34(1)
O(5B)	410(13)	1360(5)	2967(9)	52(3)
C(7B)	–799(2)	1469(1)	2476(1)	35(1)
C(8)	–3302(2)	1312(1)	5597(1)	47(1)
O(6)	–2610(1)	927(1)	5879(1)	46(1)
C(9)	–1310(2)	1053(1)	5941(1)	47(1)
C(10)	–4146(1)	–106(1)	3056(1)	27(1)
C(11)	–3766(2)	–542(1)	2745(1)	40(1)
C(12)	–3449(2)	–906(1)	3317(1)	47(1)
C(13)	–2379(2)	–749(1)	3921(1)	44(1)
C(14)	–2690(1)	–333(1)	4332(1)	33(1)
C(15)	–4138(2)	248(1)	2468(1)	35(1)
C(16)	–5466(1)	–140(1)	3232(1)	37(1)
C(17)	–1478(2)	–163(1)	4827(1)	49(1)
C(18)	–3677(2)	–426(1)	4798(1)	37(1)
N(1)	–3126(1)	26(1)	3741(1)	22(1)
Si(2)	2220(1)	–710(1)	1006(1)	18(1)
N(2)	2833(1)	–1650(1)	1069(1)	20(1)
O(21)	1091(1)	–1080(1)	1268(1)	21(1)
O(22)	2352(1)	–454(1)	1828(1)	24(1)
O(23)	3326(1)	–349(1)	769(1)	27(1)
O(24)	1132(1)	–558(1)	259(1)	23(1)
O(25)	–537(1)	–410(1)	2355(1)	34(1)
O(26)	2846(1)	–647(1)	–877(1)	36(1)
C(21)	3314(1)	–1197(1)	895(1)	22(1)
C(22)	665(1)	–954(1)	1905(1)	21(1)
C(23)	1596(1)	–604(1)	2319(1)	23(1)
C(24)	2939(1)	–133(1)	90(1)	26(1)
C(25)	1532(1)	–256(1)	–229(1)	27(1)
C(26)	–602(1)	–708(1)	1747(1)	28(1)
C(27)	731(2)	–238(1)	2503(1)	32(1)
C(28)	3630(2)	–302(1)	–499(1)	36(1)
C(29)	1589(2)	–472(1)	–968(1)	34(1)
C(30)	3631(1)	–1871(1)	1767(1)	27(1)
C(31)	2917(2)	–2291(1)	1918(1)	36(1)
C(32)	2534(2)	–2596(1)	1255(1)	40(1)
C(33)	1716(2)	–2341(1)	625(1)	35(1)
C(34)	2394(1)	–1942(1)	376(1)	25(1)
C(35)	3657(2)	–1554(1)	2415(1)	34(1)
C(36)	4987(1)	–1970(1)	1687(1)	36(1)
C(37)	1457(1)	–1670(1)	–185(1)	31(1)
C(38)	3481(1)	–2082(1)	13(1)	33(1)
Si(3)	2465(1)	2671(1)	987(1)	19(1)
O(31)	1328(1)	2306(1)	1257(1)	22(1)
O(32)	2629(1)	2922(1)	1816(1)	24(1)

O(33)	3571(1)	3026(1)	740(1)	30(1)
O(34)	1372(1)	2825(1)	243(1)	27(1)
N(3)	3061(1)	1731(1)	1072(1)	20(1)
C(41)	3535(1)	2179(1)	869(1)	22(1)
C(42)	913(1)	2436(1)	1896(1)	23(1)
C(43)	1864(1)	2781(1)	2306(1)	23(1)
C(44)	3189(2)	3238(1)	58(1)	31(1)
C(45)	1780(2)	3117(1)	–256(1)	32(1)
C(46)	–340(1)	2690(1)	1739(1)	32(1)
O(35)	–252(1)	2992(1)	2340(1)	42(1)
C(47)	1019(2)	3152(1)	2491(1)	35(1)
C(48)	3865(2)	3060(1)	–531(1)	41(1)
O(36)	3076(1)	2714(1)	–899(1)	42(1)
C(49)	1821(2)	2889(1)	–989(1)	41(1)
C(50)	3874(1)	1523(1)	1776(1)	25(1)
C(51)	3153(2)	1118(1)	1967(1)	33(1)
C(52)	2735(2)	797(1)	1328(1)	39(1)
C(53)	1915(2)	1040(1)	682(1)	35(1)
C(54)	2594(1)	1426(1)	400(1)	25(1)
C(55)	5214(1)	1410(1)	1684(1)	31(1)
C(56)	3958(2)	1856(1)	2406(1)	33(1)
C(57)	1653(1)	1692(1)	–172(1)	32(1)
C(58)	3661(1)	1270(1)	33(1)	33(1)

Table 64. Bond Lengths [Å] and Angles [deg] for **16**.

Si(1)–O(4)	1.6803(10)	C(11)–C(10)–C(16)	110.93(12)
Si(1)–O(2)	1.6873(9)	C(15)–C(10)–N(1)	106.98(10)
Si(1)–O(3)	1.7377(10)	C(11)–C(10)–N(1)	109.26(12)
Si(1)–O(1)	1.7847(9)	C(16)–C(10)–N(1)	112.25(10)
Si(1)–C(1)	1.9199(13)	C(12)–C(11)–C(10)	113.91(12)
O(1)–C(2)	1.3983(14)	C(13)–C(12)–C(11)	108.26(13)
O(2)–C(3)	1.4150(14)	C(12)–C(13)–C(14)	114.23(13)
O(3)–C(4)	1.3951(16)	C(17)–C(14)–C(18)	109.66(13)
O(4)–C(5)	1.4153(16)	C(17)–C(14)–N(1)	106.56(11)
C(1)–N(1)	1.5244(16)	C(18)–C(14)–N(1)	112.55(12)
C(2)–C(6A)	1.5317(19)	C(17)–C(14)–C(13)	108.90(14)
C(2)–C(3)	1.5441(18)	C(18)–C(14)–C(13)	111.98(12)
C(3)–C(7A)	1.5287(18)	N(1)–C(14)–C(13)	106.98(12)
C(4)–C(8)	1.5271(18)	H(1N)–N(1)–C(1)	100.7(10)
C(4)–C(5)	1.554(2)	H(1N)–N(1)–C(14)	104.2(10)
C(5)–C(9)	1.5263(19)	C(1)–N(1)–C(14)	114.18(10)
C(6A)–O(5A)	1.433(2)	H(1N)–N(1)–C(10)	104.8(10)
O(5A)–C(7A)	1.425(2)	C(1)–N(1)–C(10)	113.24(10)
C(8)–O(6)	1.423(2)	C(14)–N(1)–C(10)	117.20(10)
O(6)–C(9)	1.435(2)	O(24)–Si(2)–O(22)	121.99(5)
C(10)–C(15)	1.5255(18)	O(24)–Si(2)–O(23)	91.24(5)
C(10)–C(11)	1.5278(19)	O(22)–Si(2)–O(23)	90.32(4)
C(10)–C(16)	1.5291(19)	O(24)–Si(2)–O(21)	89.65(4)
C(10)–N(1)	1.5471(17)	O(22)–Si(2)–O(21)	88.76(4)
C(11)–C(12)	1.515(2)	O(23)–Si(2)–O(21)	178.96(5)
C(12)–C(13)	1.507(3)	O(24)–Si(2)–C(21)	117.46(5)
C(13)–C(14)	1.543(2)	O(22)–Si(2)–C(21)	120.54(5)
C(14)–C(17)	1.520(2)	O(23)–Si(2)–C(21)	89.21(5)
C(14)–C(18)	1.529(2)	O(21)–Si(2)–C(21)	90.85(5)
C(14)–N(1)	1.5429(16)	H(2N)–N(2)–C(21)	101.2(10)
N(1)–H(1N)	0.889(16)	H(2N)–N(2)–C(30)	103.9(10)
Si(2)–O(24)	1.6782(9)	C(21)–N(2)–C(30)	114.22(10)
Si(2)–O(22)	1.6825(9)	H(2N)–N(2)–C(34)	103.6(11)
Si(2)–O(23)	1.7375(9)	C(21)–N(2)–C(34)	113.49(9)

Si(2)–O(21)	1.7932(9)	C(30)–N(2)–C(34)	117.75(10)
Si(2)–C(21)	1.9259(13)	C(22)–O(21)–Si(2)	114.50(7)
N(2)–H(2N)	0.888(17)	C(23)–O(22)–Si(2)	118.72(8)
N(2)–C(21)	1.5222(15)	C(24)–O(23)–Si(2)	115.22(8)
N(2)–C(30)	1.5445(16)	C(25)–O(24)–Si(2)	116.54(8)
N(2)–C(34)	1.5462(15)	C(26)–O(25)–C(27)	105.59(10)
O(21)–C(22)	1.4022(14)	C(28)–O(26)–C(29)	103.70(11)
O(22)–C(23)	1.4130(14)	N(2)–C(21)–Si(2)	115.12(8)
O(23)–C(24)	1.3985(15)	O(21)–C(22)–C(26)	114.08(10)
O(24)–C(25)	1.4126(15)	O(21)–C(22)–C(23)	108.02(9)
O(25)–C(26)	1.4288(16)	C(26)–C(22)–C(23)	102.92(10)
O(25)–C(27)	1.4365(18)	O(22)–C(23)–C(27)	111.78(10)
O(26)–C(28)	1.4307(19)	O(22)–C(23)–C(22)	107.63(9)
O(26)–C(29)	1.4322(19)	C(27)–C(23)–C(22)	104.02(11)
C(22)–C(26)	1.5307(18)	O(23)–C(24)–C(28)	112.40(12)
C(22)–C(23)	1.5474(17)	O(23)–C(24)–C(25)	108.32(10)
C(23)–C(27)	1.5308(18)	C(28)–C(24)–C(25)	103.34(11)
C(24)–C(28)	1.5309(17)	O(24)–C(25)–C(29)	111.58(11)
C(24)–C(25)	1.555(2)	O(24)–C(25)–C(24)	108.42(10)
C(25)–C(29)	1.5247(17)	C(29)–C(25)–C(24)	103.00(11)
C(30)–C(36)	1.5297(19)	O(25)–C(26)–C(22)	105.05(11)
C(30)–C(35)	1.5299(19)	O(25)–C(27)–C(23)	107.11(10)
C(30)–C(31)	1.539(2)	O(26)–C(28)–C(24)	105.38(11)
C(31)–C(32)	1.520(2)	O(26)–C(29)–C(25)	105.51(11)
C(32)–C(33)	1.517(2)	C(36)–C(30)–C(35)	109.54(12)
C(33)–C(34)	1.5297(18)	C(36)–C(30)–C(31)	112.42(12)
C(34)–C(38)	1.5252(17)	C(35)–C(30)–C(31)	107.71(11)
C(34)–C(37)	1.5289(19)	C(36)–C(30)–N(2)	112.47(10)
Si(3)–O(34)	1.6810(10)	C(35)–C(30)–N(2)	107.30(10)
Si(3)–O(32)	1.6844(9)	C(31)–C(30)–N(2)	107.16(11)
Si(3)–O(33)	1.7360(10)	C(32)–C(31)–C(30)	114.64(11)
Si(3)–O(31)	1.7950(9)	C(33)–C(32)–C(31)	109.11(12)
Si(3)–C(41)	1.9239(13)	C(32)–C(33)–C(34)	113.14(13)
O(31)–C(42)	1.4030(13)	C(38)–C(34)–C(37)	108.18(11)
O(32)–C(43)	1.4119(14)	C(38)–C(34)–C(33)	111.85(11)
O(33)–C(44)	1.3965(16)	C(37)–C(34)–C(33)	109.79(12)
O(34)–C(45)	1.4123(16)	C(38)–C(34)–N(2)	112.94(11)
N(3)–H(3N)	0.912(16)	C(37)–C(34)–N(2)	107.40(10)
N(3)–C(41)	1.5204(15)	C(33)–C(34)–N(2)	106.58(10)
N(3)–C(50)	1.5437(16)	O(34)–Si(3)–O(32)	122.81(5)
N(3)–C(54)	1.5448(15)	O(34)–Si(3)–O(33)	91.01(5)
C(42)–C(46)	1.5293(18)	O(32)–Si(3)–O(33)	90.59(5)
C(42)–C(43)	1.5463(18)	O(34)–Si(3)–O(31)	89.61(5)
C(43)–C(47)	1.5293(18)	O(32)–Si(3)–O(31)	88.58(4)
C(44)–C(48)	1.5278(18)	O(33)–Si(3)–O(31)	179.14(5)
C(44)–C(45)	1.553(2)	O(34)–Si(3)–C(41)	117.19(5)
C(45)–C(49)	1.5281(19)	O(32)–Si(3)–C(41)	119.99(5)
C(46)–O(35)	1.4256(17)	O(33)–Si(3)–C(41)	89.33(5)
O(35)–C(47)	1.4262(19)	O(31)–Si(3)–C(41)	90.90(5)
C(48)–O(36)	1.429(2)	C(42)–O(31)–Si(3)	114.61(7)
O(36)–C(49)	1.431(2)	C(43)–O(32)–Si(3)	118.68(8)
C(50)–C(56)	1.5273(18)	C(44)–O(33)–Si(3)	115.45(9)
C(50)–C(55)	1.5287(18)	C(45)–O(34)–Si(3)	116.49(9)
C(50)–C(51)	1.5316(19)	H(3N)–N(3)–C(41)	101.5(10)
C(51)–C(52)	1.522(2)	H(3N)–N(3)–C(50)	103.3(9)
C(52)–C(53)	1.519(2)	C(41)–N(3)–C(50)	114.15(10)
C(53)–C(54)	1.5266(19)	H(3N)–N(3)–C(54)	103.3(10)
C(54)–C(58)	1.5259(17)	C(41)–N(3)–C(54)	113.86(9)
C(54)–C(57)	1.5329(19)	C(50)–N(3)–C(54)	117.78(9)
O(4)–Si(1)–O(2)	121.77(5)	N(3)–C(41)–Si(3)	114.88(8)
O(4)–Si(1)–O(3)	91.22(5)	O(31)–C(42)–C(46)	113.92(11)
O(2)–Si(1)–O(3)	90.25(5)	O(31)–C(42)–C(43)	107.79(10)

O(4)–Si(1)–O(1)	90.09(5)	C(46)–C(42)–C(43)	102.98(10)
O(2)–Si(1)–O(1)	88.86(4)	O(32)–C(43)–C(47)	112.01(11)
O(3)–Si(1)–O(1)	178.67(5)	O(32)–C(43)–C(42)	107.91(9)
O(4)–Si(1)–C(1)	117.30(5)	C(47)–C(43)–C(42)	103.84(11)
O(2)–Si(1)–C(1)	120.93(5)	O(33)–C(44)–C(48)	112.66(12)
O(3)–Si(1)–C(1)	88.59(5)	O(33)–C(44)–C(45)	108.25(11)
O(1)–Si(1)–C(1)	91.02(5)	C(48)–C(44)–C(45)	103.06(12)
C(2)–O(1)–Si(1)	114.06(7)	O(34)–C(45)–C(49)	111.35(12)
C(3)–O(2)–Si(1)	117.94(8)	O(34)–C(45)–C(44)	108.46(11)
C(4)–O(3)–Si(1)	115.43(9)	C(49)–C(45)–C(44)	103.41(12)
C(5)–O(4)–Si(1)	116.25(9)	O(35)–C(46)–C(42)	105.13(11)
N(1)–C(1)–Si(1)	116.60(8)	C(46)–O(35)–C(47)	106.01(10)
O(1)–C(2)–C(6A)	114.31(11)	O(35)–C(47)–C(43)	107.48(11)
O(1)–C(2)–C(3)	107.82(10)	O(36)–C(48)–C(44)	105.73(12)
C(6A)–C(2)–C(3)	102.78(10)	C(48)–O(36)–C(49)	103.89(12)
O(2)–C(3)–C(7A)	111.90(10)	O(36)–C(49)–C(45)	105.33(12)
O(2)–C(3)–C(2)	107.69(9)	C(56)–C(50)–C(55)	108.93(12)
C(7A)–C(3)–C(2)	104.04(11)	C(56)–C(50)–C(51)	107.79(11)
O(3)–C(4)–C(8)	112.01(12)	C(55)–C(50)–C(51)	112.58(11)
O(3)–C(4)–C(5)	108.30(11)	C(56)–C(50)–N(3)	107.77(10)
C(8)–C(4)–C(5)	103.32(12)	C(55)–C(50)–N(3)	112.51(10)
O(4)–C(5)–C(9)	111.37(13)	C(51)–C(50)–N(3)	107.05(11)
O(4)–C(5)–C(4)	108.55(10)	C(52)–C(51)–C(50)	114.50(11)
C(9)–C(5)–C(4)	103.08(12)	C(53)–C(52)–C(51)	109.34(12)
O(5A)–C(6A)–C(2)	104.72(13)	C(52)–C(53)–C(54)	113.28(12)
C(7A)–O(5A)–C(6A)	106.02(12)	C(58)–C(54)–C(53)	111.99(11)
O(5A)–C(7A)–C(3)	107.56(12)	C(58)–C(54)–C(57)	107.98(11)
O(6)–C(8)–C(4)	105.33(13)	C(53)–C(54)–C(57)	109.92(12)
C(8)–O(6)–C(9)	103.96(13)	C(58)–C(54)–N(3)	113.00(11)
O(6)–C(9)–C(5)	105.58(13)	C(53)–C(54)–N(3)	106.49(10)
C(15)–C(10)–C(11)	107.31(11)	C(57)–C(54)–N(3)	107.35(10)
C(15)–C(10)–C(16)	109.91(12)		

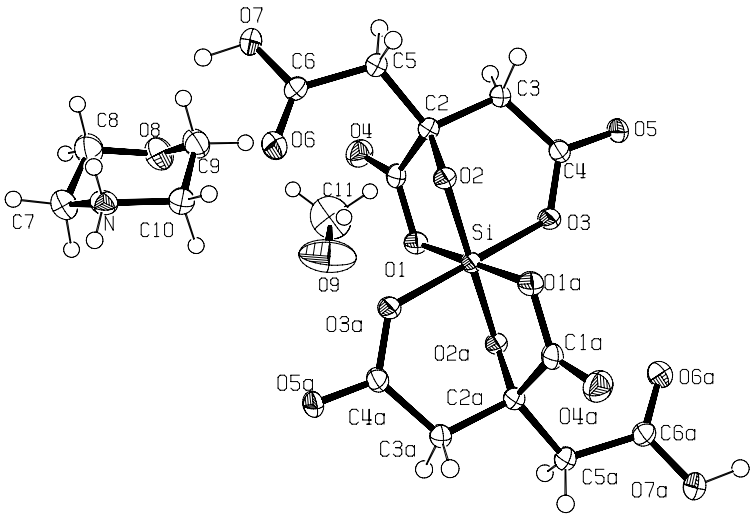

Figure 82. Crystal structure of *meso*-**19**·2CH_3OH (probability level of displacement ellipsoids 50%) showing the atomic numbering scheme.

Table 65. Atomic Coordinates (x 10^4) and Equivalent Isotropic Displacement Parameters ($Å^2$ x 10^3) for *meso*-**19**·2CH_3OH. U(eq) is Defined as One Third of the Trace of the Orthogonalized Uij Tensor.

	x	y	z	U(eq)
Si	10000	5000	10000	19(1)
C(1)	10323(1)	5678(3)	8460(1)	21(1)
C(2)	9915(1)	7592(3)	8797(1)	20(1)
C(3)	10823(1)	8912(3)	9199(1)	21(1)
C(4)	11436(2)	8113(3)	10035(1)	21(1)
C(5)	9234(2)	8737(3)	8067(1)	22(1)
C(6)	8467(2)	7465(3)	7475(1)	22(1)
O(1)	10433(1)	4269(2)	9043(1)	23(1)
O(2)	9386(1)	7001(2)	9458(1)	19(1)
O(3)	11189(1)	6459(2)	10348(1)	22(1)
O(4)	10539(1)	5495(2)	7750(1)	30(1)
O(5)	12187(1)	9066(2)	10416(1)	26(1)
O(6)	7970(1)	6144(2)	7719(1)	30(1)
O(7)	8403(1)	7935(2)	6650(1)	29(1)
C(7)	8132(2)	908(3)	4916(1)	32(1)
C(8)	8900(2)	2110(4)	4533(2)	37(1)
C(9)	9502(2)	3725(3)	5830(2)	33(1)
C(10)	8802(2)	2577(3)	6298(1)	29(1)
C(11)	12072(3)	2188(5)	7052(2)	67(1)
O(8)	9788(1)	2544(2)	5159(1)	37(1)
O(9)	11347(2)	1672(3)	7539(2)	80(1)
N	7863(1)	1972(3)	5674(1)	26(1)

Table 66. Bond Lengths [Å] and Angles [deg] for *meso*-**19**·2CH_3OH.

Si–O(2)	1.7203(12)	O(1)–Si–O(3)	90.46(6)
Si–O(2)A	1.7203(12)	O(1)A–Si–O(3)	89.54(6)
Si–O(1)	1.7835(13)	O(2)–Si–O(3)A	88.65(6)
Si–O(1)A	1.7835(13)	O(2)A–Si–O(3)A	91.35(6)
Si–O(3)	1.8509(13)	O(1)–Si–O(3)A	89.54(6)
Si–O(3)A	1.8509(13)	O(1)A–Si–O(3)A	90.46(6)
C(1)–O(4)	1.213(2)	O(3)–Si–O(3)A	180.0
C(1)–O(1)	1.313(2)	O(4)–C(1)–O(1)	123.90(18)
C(1)–C(2)	1.535(3)	O(4)–C(1)–C(2)	124.43(17)
C(2)–O(2)	1.419(2)	O(1)–C(1)–C(2)	111.65(16)
C(2)–C(5)	1.533(3)	O(2)–C(2)–C(5)	113.16(15)
C(2)–C(3)	1.535(3)	O(2)–C(2)–C(3)	108.48(15)
C(3)–C(4)	1.512(3)	C(5)–C(2)–C(3)	108.67(15)
C(4)–O(5)	1.241(2)	O(2)–C(2)–C(1)	105.76(14)
C(4)–O(3)	1.289(2)	C(5)–C(2)–C(1)	111.12(15)
C(5)–C(6)	1.511(3)	C(3)–C(2)–C(1)	109.56(15)
C(6)–O(6)	1.214(3)	C(4)–C(3)–C(2)	113.67(16)
C(6)–O(7)	1.327(2)	O(5)–C(4)–O(3)	120.18(17)
C(7)–N	1.494(3)	O(5)–C(4)–C(3)	119.06(17)
C(7)–C(8)	1.514(3)	O(3)–C(4)–C(3)	120.76(16)
C(8)–O(8)	1.416(3)	C(6)–C(5)–C(2)	114.09(16)
C(9)–O(8)	1.432(3)	O(6)–C(6)–O(7)	123.20(18)
C(9)–C(10)	1.504(3)	O(6)–C(6)–C(5)	124.41(18)
C(10)–N	1.490(3)	O(7)–C(6)–C(5)	112.39(17)
C(11)–O(9)	1.382(4)	C(1)–O(1)–Si	112.39(12)
O(2)–Si–O(2)A	180.000(1)	C(2)–O(2)–Si	109.54(11)
O(2)–Si–O(1)	89.67(6)	C(4)–O(3)–Si	127.69(12)
O(2)A–Si–O(1)	90.33(6)	N–C(7)–C(8)	109.85(18)
O(2)–Si–O(1)A	90.33(6)	O(8)–C(8)–C(7)	111.33(19)
O(2)A–Si–O(1)A	89.67(6)	O(8)–C(9)–C(10)	110.33(18)

O(1)–Si–O(1)A	180.00(4)	N–C(10)–C(9)	109.36(18)
O(2)–Si–O(3)	91.35(6)	C(8)–O(8)–C(9)	109.30(17)
O(2)A–Si–O(3)	88.65(6)	C(10)–N–C(7)	111.47(16)

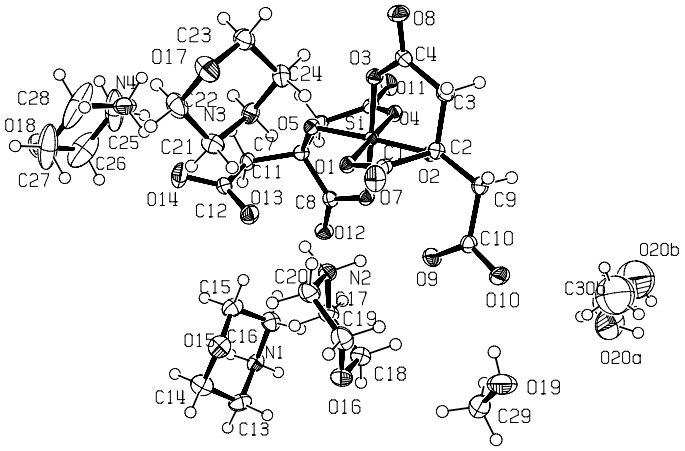

Figure 83. Crystal structure of *rac*-**20**·1.73CH_3OH (probability level of displacement ellipsoids 50%) showing the atomic numbering scheme.

Table 67. Atomic Coordinates (x 10^4) and Equivalent Isotropic Displacement Parameters ($Å^2$ x 10^3) for *rac*-**20**·1.73CH_3OH. U(eq) is Defined as One Third of the Trace of the Orthogonalized Uij Tensor.

	x	y	z	U(eq)
Si	3202(1)	4603(1)	2013(1)	16(1)
O(1)	2948(1)	3092(1)	2757(1)	19(1)
O(2)	1984(1)	4990(1)	2578(1)	18(1)
O(3)	2577(1)	4555(1)	877(1)	20(1)
O(4)	3425(1)	6126(1)	1266(1)	20(1)
O(5)	4425(1)	4144(1)	1515(1)	18(1)
O(6)	3890(1)	4686(1)	3117(1)	18(1)
O(7)	1539(1)	2011(1)	3453(1)	31(1)
O(8)	1285(1)	4301(1)	–28(1)	31(1)
O(9)	1842(1)	3640(1)	4877(1)	27(1)
O(10)	141(1)	3470(1)	5596(1)	30(1)
O(11)	4347(1)	7585(1)	230(1)	29(1)
O(12)	5572(1)	4892(1)	3484(1)	25(1)
O(13)	5494(1)	2292(1)	3293(1)	28(1)
O(14)	6759(1)	1780(1)	2216(1)	38(1)
C(1)	1913(2)	2957(2)	3057(2)	20(1)
C(2)	1236(1)	4123(2)	2782(2)	19(1)
C(3)	720(2)	4340(2)	1720(2)	22(1)
C(4)	1552(2)	4395(2)	790(2)	21(1)
C(5)	4345(2)	6559(2)	823(2)	21(1)
C(6)	5417(1)	5819(2)	1013(2)	19(1)
C(7)	5301(1)	4589(2)	1824(2)	18(1)
C(8)	4956(1)	4711(1)	2911(2)	19(1)
C(9)	390(1)	4118(2)	3690(2)	20(1)
C(10)	835(2)	3706(2)	4800(2)	20(1)
C(11)	6338(1)	3802(2)	1844(2)	21(1)
C(12)	6178(2)	2529(2)	2513(2)	21(1)
O(15)	7187(1)	1766(1)	5860(1)	34(1)
C(13)	7885(2)	2626(2)	7008(2)	33(1)
C(14)	8003(2)	1633(2)	6589(2)	35(1)
C(15)	7333(2)	2794(2)	4946(2)	31(1)
C(16)	7206(2)	3860(2)	5262(2)	30(1)

N(1)	7987(1)	3733(2)	6081(2)	25(1)
O(16)	3545(1)	1368(1)	7114(1)	34(1)
C(17)	4472(2)	2751(2)	5597(2)	28(1)
C(18)	3786(2)	2553(2)	6630(2)	32(1)
C(19)	2939(2)	1045(2)	6417(2)	35(1)
C(20)	3566(2)	1191(2)	5355(2)	31(1)
N(2)	3880(1)	2409(1)	4846(2)	25(1)
O(17)	3371(1)	–103(1)	1090(1)	37(1)
C(21)	4393(2)	522(2)	2231(2)	30(1)
C(22)	4394(2)	–224(2)	1547(2)	37(1)
C(23)	3119(2)	1067(2)	433(2)	31(1)
C(24)	3065(2)	1873(2)	1063(2)	27(1)
N(3)	4120(1)	1748(1)	1559(2)	24(1)
O(18)	10025(1)	866(2)	905(2)	50(1)
C(26)	9733(3)	1958(3)	955(3)	71(1)
C(25)	8921(3)	2602(2)	210(3)	92(2)
N(4)	7939(2)	1964(3)	424(2)	72(1)
C(28)	8243(2)	754(4)	473(4)	104(2)
C(27)	9092(3)	236(2)	1191(4)	83(1)
O(19)	401(2)	2754(2)	7758(2)	49(1)
C(29)	1342(2)	3045(3)	8069(2)	48(1)
C(30A)	825(8)	9594(6)	5605(7)	180(6)
O(20A)	634(3)	8424(4)	6280(4)	110(2)

Table 68. Bond Lengths [Å] and Angles [deg] for *rac*-**20**·1.73CH_3OH.

Si–O(5)	1.7140(13)	C(2)–O(2)–Si	110.44(11)
Si–O(2)	1.7156(13)	C(4)–O(3)–Si	129.19(13)
Si–O(3)	1.7910(14)	C(5)–O(4)–Si	127.21(12)
Si–O(6)	1.8125(13)	C(7)–O(5)–Si	110.43(11)
Si–O(1)	1.8266(13)	C(8)–O(6)–Si	112.50(12)
Si–O(4)	1.8319(13)	O(7)–C(1)–O(1)	123.42(17)
O(1)–C(1)	1.312(2)	O(7)–C(1)–C(2)	124.87(16)
O(2)–C(2)	1.426(2)	O(1)–C(1)–C(2)	111.60(14)
O(3)–C(4)	1.326(2)	O(2)–C(2)–C(9)	112.29(15)
O(4)–C(5)	1.305(2)	O(2)–C(2)–C(1)	106.86(14)
O(5)–C(7)	1.422(2)	C(9)–C(2)–C(1)	110.54(15)
O(6)–C(8)	1.320(2)	O(2)–C(2)–C(3)	106.92(14)
O(7)–C(1)	1.222(2)	C(9)–C(2)–C(3)	112.50(15)
O(8)–C(4)	1.219(2)	C(1)–C(2)–C(3)	107.43(15)
O(9)–C(10)	1.251(2)	C(4)–C(3)–C(2)	113.44(15)
O(10)–C(10)	1.265(2)	O(8)–C(4)–O(3)	120.24(18)
O(11)–C(5)	1.237(2)	O(8)–C(4)–C(3)	120.79(16)
O(12)–C(8)	1.219(2)	O(3)–C(4)–C(3)	118.96(16)
O(13)–C(12)	1.244(2)	O(11)–C(5)–O(4)	119.67(17)
O(14)–C(12)	1.263(2)	O(11)–C(5)–C(6)	119.33(16)
C(1)–C(2)	1.534(3)	O(4)–C(5)–C(6)	121.00(15)
C(2)–C(9)	1.519(3)	C(5)–C(6)–C(7)	113.59(15)
C(2)–C(3)	1.538(3)	O(5)–C(7)–C(11)	110.14(14)
C(3)–C(4)	1.517(3)	O(5)–C(7)–C(8)	107.67(14)
C(5)–C(6)	1.519(3)	C(11)–C(7)–C(8)	112.86(16)
C(6)–C(7)	1.538(2)	O(5)–C(7)–C(6)	106.77(14)
C(7)–C(11)	1.523(3)	C(11)–C(7)–C(6)	112.32(15)
C(7)–C(8)	1.527(3)	C(8)–C(7)–C(6)	106.77(14)
C(9)–C(10)	1.526(3)	O(12)–C(8)–O(6)	124.01(19)
C(11)–C(12)	1.537(2)	O(12)–C(8)–C(7)	124.56(17)
O(15)–C(14)	1.428(3)	O(6)–C(8)–C(7)	111.24(15)
O(15)–C(15)	1.432(3)	C(2)–C(9)–C(10)	114.76(15)
C(13)–N(1)	1.495(3)	O(9)–C(10)–O(10)	123.91(18)
C(13)–C(14)	1.510(3)	O(9)–C(10)–C(9)	119.35(17)

C(15)–C(16)	1.510(3)	O(10)–C(10)–C(9)	116.73(16)
C(16)–N(1)	1.487(3)	C(7)–C(11)–C(12)	112.77(15)
N(1)–HN1B	0.92(3)	O(13)–C(12)–O(14)	124.06(18)
N(1)–HN1A	0.93(3)	O(13)–C(12)–C(11)	119.37(16)
O(16)–C(18)	1.430(3)	O(14)–C(12)–C(11)	116.57(17)
O(16)–C(19)	1.432(3)	C(14)–O(15)–C(15)	109.39(15)
C(17)–N(2)	1.495(3)	N(1)–C(13)–C(14)	108.88(19)
C(17)–C(18)	1.502(3)	O(15)–C(14)–C(13)	110.63(18)
C(19)–C(20)	1.508(3)	O(15)–C(15)–C(16)	111.39(18)
C(20)–N(2)	1.496(2)	N(1)–C(16)–C(15)	109.50(17)
N(2)–HN2B	0.91(3)	HN1B–N(1)–HN1A	107(2)
N(2)–HN2A	0.93(3)	HN1B–N(1)–C(16)	111.3(15)
O(17)–C(23)	1.425(3)	HN1A–N(1)–C(16)	110.4(15)
O(17)–C(22)	1.430(3)	HN1B–N(1)–C(13)	108.4(15)
C(21)–N(3)	1.488(3)	HN1A–N(1)–C(13)	107.7(14)
C(21)–C(22)	1.512(3)	C(16)–N(1)–C(13)	111.54(15)
C(23)–C(24)	1.508(3)	C(18)–O(16)–C(19)	110.23(16)
C(24)–N(3)	1.491(3)	N(2)–C(17)–C(18)	109.17(16)
N(3)–HN3A	0.90(3)	O(16)–C(18)–C(17)	111.17(18)
N(3)–HN3B	0.91(3)	O(16)–C(19)–C(20)	111.53(17)
O(18)–C(26)	1.385(4)	N(2)–C(20)–C(19)	109.77(18)
O(18)–C(27)	1.407(4)	HN2B–N(2)–HN2A	110(2)
C(26)–C(25)	1.451(6)	HN2B–N(2)–C(17)	107.0(15)
C(25)–N(4)	1.469(5)	HN2A–N(2)–C(17)	108.0(14)
N(4)–C(28)	1.486(5)	HN2B–N(2)–C(20)	110.8(14)
C(28)–C(27)	1.435(6)	HN2A–N(2)–C(20)	110.2(14)
O(19)–C(29)	1.396(3)	C(17)–N(2)–C(20)	110.86(16)
C(30A)–O(20A)	1.440(8)	C(23)–O(17)–C(22)	110.72(15)
O(5)–Si–O(2)	176.59(7)	N(3)–C(21)–C(22)	108.62(18)
O(5)–Si–O(3)	89.04(6)	O(17)–C(22)–C(21)	111.87(18)
O(2)–Si–O(3)	92.66(6)	O(17)–C(23)–C(24)	111.46(18)
O(5)–Si–O(6)	88.87(6)	N(3)–C(24)–C(23)	109.43(16)
O(2)–Si–O(6)	89.53(6)	HN3A–N(3)–HN3B	110(2)
O(3)–Si–O(6)	177.11(6)	HN3A–N(3)–C(21)	108.8(15)
O(5)–Si–O(1)	88.88(6)	HN3B–N(3)–C(21)	110.7(15)
O(2)–Si–O(1)	88.14(6)	HN3A–N(3)–C(24)	110.1(15)
O(3)–Si–O(1)	90.80(6)	HN3B–N(3)–C(24)	106.5(15)
O(6)–Si–O(1)	91.15(6)	C(21)–N(3)–C(24)	110.84(15)
O(5)–Si–O(4)	92.18(6)	C(26)–O(18)–C(27)	108.1(2)
O(2)–Si–O(4)	90.82(6)	O(18)–C(26)–C(25)	112.6(3)
O(3)–Si–O(4)	88.67(6)	C(26)–C(25)–N(4)	110.2(2)
O(6)–Si–O(4)	89.42(6)	C(25)–N(4)–C(28)	109.8(2)
O(1)–Si–O(4)	178.80(6)	C(27)–C(28)–N(4)	110.5(2)
C(1)–O(1)–Si	112.26(11)	O(18)–C(27)–C(28)	112.5(3)

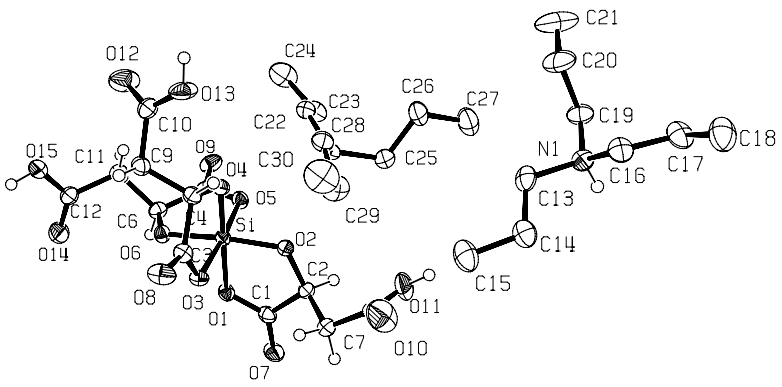

Figure 84. Crystal structure (probability level of displacement ellipsoids 50%) of (*Λ*,*S*,*S*,*S*)-*mer*-**21** showing the atomic numbering scheme.

Table 69. Atomic Coordinates (x 10^4) and Equivalent Isotropic Displacement Parameters (Å^2 x 10^3) for (*Λ*,*S*,*S*,*S*)-*mer*-**21**. U(eq) is Defined as One Third of the Trace of the Orthogonalized Uij Tensor.

	x	y	z	U(eq)
Si	2011(1)	7287(1)	2113(1)	18(1)
O(1)	1244(1)	6997(1)	2862(1)	22(1)
O(2)	2953(1)	6503(1)	2342(1)	22(1)
O(5)	1272(1)	6528(1)	1614(1)	23(1)
O(6)	953(1)	8018(1)	1968(1)	22(1)
O(3)	2662(1)	8121(1)	2607(1)	21(1)
O(4)	2824(1)	7588(1)	1448(1)	22(1)
O(7)	1291(1)	6187(1)	3766(1)	36(1)
O(9)	–252(1)	6362(1)	1026(1)	32(1)
O(8)	3733(1)	9253(1)	2495(1)	35(1)
O(11)	4551(1)	4999(1)	3023(1)	48(1)
O(10)	5601(2)	6080(1)	3337(1)	69(1)
O(14)	–1318(1)	9152(1)	1782(1)	40(1)
O(15)	–473(1)	9721(1)	902(1)	39(1)
O(13)	4023(1)	8620(1)	216(1)	45(1)
O(12)	2339(1)	8986(1)	–63(1)	56(1)
C(1)	1682(2)	6418(1)	3229(1)	25(1)
C(2)	2737(2)	6072(1)	2945(1)	25(1)
C(5)	344(2)	6793(1)	1387(1)	25(1)
C(6)	46(2)	7679(1)	1627(1)	24(1)
C(3)	3268(2)	8625(1)	2260(1)	25(1)
C(4)	3352(2)	8372(1)	1533(1)	23(1)
C(7)	3662(2)	6205(1)	3449(1)	34(1)
C(8)	4709(2)	5767(1)	3268(1)	39(1)
C(11)	–297(2)	8244(1)	1051(1)	29(1)
C(12)	–752(2)	9078(1)	1293(1)	28(1)
C(9)	2864(2)	9064(1)	1085(1)	26(1)
C(10)	3019(2)	8884(1)	355(1)	28(1)
N(1)	9248(1)	3894(1)	1669(1)	29(1)
C(13)	8733(2)	4746(1)	1818(1)	34(1)
C(14)	9078(2)	5111(1)	2482(1)	38(1)
C(15)	8375(2)	5870(1)	2670(1)	49(1)
C(16)	10473(2)	3944(1)	1613(1)	34(1)
C(17)	11007(2)	3085(1)	1511(1)	42(1)
C(18)	12239(2)	3153(2)	1581(1)	56(1)
C(19)	8710(2)	3473(1)	1080(1)	36(1)
C(20)	8906(2)	3911(2)	413(1)	54(1)
C(21)	8271(3)	3452(2)	–127(1)	81(1)
C(22)	3404(2)	6004(1)	531(1)	29(1)
C(23)	2494(2)	5356(1)	512(1)	37(1)
C(24)	1721(2)	5558(2)	–65(1)	53(1)
C(25)	4508(2)	5077(1)	1306(1)	34(1)
C(26)	5161(2)	4637(1)	765(1)	47(1)
C(27)	5307(2)	3695(1)	928(1)	50(1)
C(28)	5072(2)	6580(1)	1032(1)	31(1)
C(29)	5713(2)	6765(2)	1656(1)	46(1)
C(30)	6582(2)	7438(2)	1516(1)	62(1)
N(2)	4143(1)	5965(1)	1135(1)	26(1)

Table 70. Bond Lengths [Å] and Angles [deg] for (*Λ*,*S*,*S*,*S*)-*mer*-**21**.

Si–O(4)	1.7328(12)	O(5)–Si–O(1)	92.09(6)
Si–O(2)	1.7472(13)	O(3)–Si–O(1)	87.43(5)
Si–O(6)	1.7537(13)	C(1)–O(1)–Si	115.67(11)
Si–O(5)	1.8007(12)	C(2)–O(2)–Si	116.03(11)

Si–O(3)	1.8249(12)	C(5)–O(5)–Si	115.13(11)
Si–O(1)	1.8300(12)	C(6)–O(6)–Si	114.56(10)
O(1)–C(1)	1.287(2)	C(3)–O(3)–Si	113.39(10)
O(2)–C(2)	1.4138(19)	C(4)–O(4)–Si	114.19(10)
O(5)–C(5)	1.292(2)	O(7)–C(1)–O(1)	123.16(17)
O(6)–C(6)	1.409(2)	O(7)–C(1)–C(2)	123.68(16)
O(3)–C(3)	1.288(2)	O(1)–C(1)–C(2)	113.14(14)
O(4)–C(4)	1.400(2)	O(2)–C(2)–C(1)	108.11(14)
O(7)–C(1)	1.235(2)	O(2)–C(2)–C(7)	111.31(15)
O(9)–C(5)	1.231(2)	C(1)–C(2)–C(7)	109.36(14)
O(8)–C(3)	1.232(2)	O(9)–C(5)–O(5)	123.49(17)
O(11)–C(8)	1.315(3)	O(9)–C(5)–C(6)	123.26(18)
O(10)–C(8)	1.205(3)	O(5)–C(5)–C(6)	113.23(15)
O(14)–C(12)	1.207(2)	O(6)–C(6)–C(5)	108.12(15)
O(15)–C(12)	1.324(2)	O(6)–C(6)–C(11)	111.60(15)
O(13)–C(10)	1.326(2)	C(5)–C(6)–C(11)	111.07(14)
O(12)–C(10)	1.192(2)	O(8)–C(3)–O(3)	123.35(16)
C(1)–C(2)	1.512(3)	O(8)–C(3)–C(4)	123.10(16)
C(2)–C(7)	1.531(3)	O(3)–C(3)–C(4)	113.54(15)
C(5)–C(6)	1.516(2)	O(4)–C(4)–C(3)	108.43(14)
C(6)–C(11)	1.516(2)	O(4)–C(4)–C(9)	111.77(15)
C(3)–C(4)	1.518(2)	C(3)–C(4)–C(9)	110.77(14)
C(4)–C(9)	1.533(2)	C(8)–C(7)–C(2)	114.09(15)
C(7)–C(8)	1.499(3)	O(10)–C(8)–O(11)	123.4(2)
C(11)–C(12)	1.503(3)	O(10)–C(8)–C(7)	124.0(2)
C(9)–C(10)	1.506(2)	O(11)–C(8)–C(7)	112.6(2)
N(1)–HN1	0.85(2)	C(12)–C(11)–C(6)	111.39(14)
N(1)–C(16)	1.505(3)	O(14)–C(12)–O(15)	123.91(18)
N(1)–C(19)	1.506(3)	O(14)–C(12)–C(11)	124.02(17)
N(1)–C(13)	1.508(2)	O(15)–C(12)–C(11)	112.06(16)
C(13)–C(14)	1.512(3)	C(10)–C(9)–C(4)	112.99(15)
C(14)–C(15)	1.518(3)	O(12)–C(10)–O(13)	122.68(17)
C(16)–C(17)	1.511(3)	O(12)–C(10)–C(9)	124.9(2)
C(17)–C(18)	1.517(4)	O(13)–C(10)–C(9)	112.37(16)
C(19)–C(20)	1.525(3)	HN1–N(1)–C(16)	105.1(14)
C(20)–C(21)	1.515(4)	HN1–N(1)–C(19)	106.9(14)
C(22)–C(23)	1.507(3)	C(16)–N(1)–C(19)	113.58(16)
C(22)–N(2)	1.515(2)	HN1–N(1)–C(13)	106.8(14)
C(23)–C(24)	1.530(3)	C(16)–N(1)–C(13)	112.56(15)
C(25)–N(2)	1.503(2)	C(19)–N(1)–C(13)	111.27(16)
C(25)–C(26)	1.516(3)	N(1)–C(13)–C(14)	113.28(16)
C(26)–C(27)	1.524(3)	C(13)–C(14)–C(15)	111.00(19)
C(28)–N(2)	1.505(3)	N(1)–C(16)–C(17)	113.22(16)
C(28)–C(29)	1.506(3)	C(16)–C(17)–C(18)	110.76(19)
C(29)–C(30)	1.524(3)	N(1)–C(19)–C(20)	115.15(17)
N(2)–HN2	0.89(2)	C(21)–C(20)–C(19)	109.6(2)
O(4)–Si–O(2)	90.91(6)	C(23)–C(22)–N(2)	115.64(15)
O(4)–Si–O(6)	96.70(6)	C(22)–C(23)–C(24)	109.59(18)
O(2)–Si–O(6)	172.35(6)	N(2)–C(25)–C(26)	114.47(15)
O(4)–Si–O(5)	92.17(6)	C(25)–C(26)–C(27)	110.39(18)
O(2)–Si–O(5)	90.68(6)	N(2)–C(28)–C(29)	113.77(16)
O(6)–Si–O(5)	88.25(6)	C(28)–C(29)–C(30)	110.1(2)
O(4)–Si–O(3)	88.50(6)	HN2–N(2)–C(25)	109.4(12)
O(2)–Si–O(3)	94.24(6)	HN2–N(2)–C(28)	105.1(13)
O(6)–Si–O(3)	86.77(6)	C(25)–N(2)–C(28)	113.64(16)
O(5)–Si–O(3)	175.02(6)	HN2–N(2)–C(22)	106.3(14)
O(4)–Si–O(1)	175.27(6)	C(25)–N(2)–C(22)	113.45(15)
O(2)–Si–O(1)	86.98(5)	C(28)–N(2)–C(22)	108.36(14)
O(6)–Si–O(1)	85.49(6)	O(5)–Si–O(1)	92.09(6)

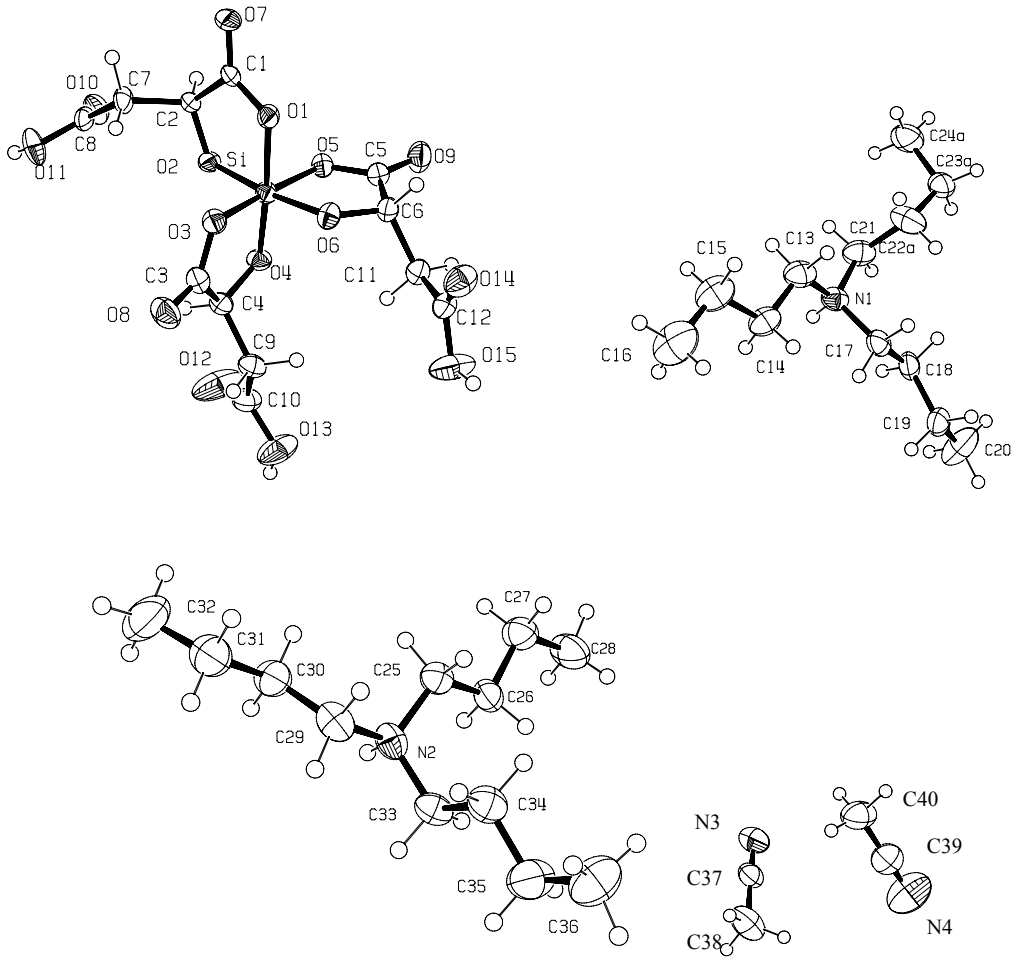

Figure 85. Crystal structure of (*Λ*,*S*,*S*,*S*)-*mer*-**22**·2CH_3CN (probability level of displacement ellipsoids 50%) showing the atomic numbering scheme.

Table 71. Atomic Coordinates (x 10^4) and Equivalent Isotropic Displacement Parameters ($Å^2$ x 10^3) for (*Λ*,*S*,*S*,*S*)-*mer*-**22**·2CH_3CN. U(eq) is Defined as One Third of the Trace of the Orthogonalized Uij Tensor.

	x	y	z	U(eq)
Si	7772(1)	4374(1)	2065(1)	24(1)
O(3)	8264(1)	4769(1)	959(1)	28(1)
O(4)	8482(1)	5163(1)	2889(1)	28(1)
O(5)	7374(1)	3875(1)	3186(1)	28(1)
O(6)	8858(1)	3647(1)	2281(1)	29(1)
O(1)	6947(1)	3593(1)	1141(1)	27(1)
O(2)	6594(1)	4995(1)	1802(1)	25(1)
O(8)	9462(1)	5707(1)	620(1)	45(1)
O(12)	9770(2)	6935(1)	3983(2)	81(1)
O(13)	11462(2)	6463(1)	4455(2)	65(1)
O(9)	7830(1)	2843(1)	4386(1)	45(1)
O(15)	11961(1)	3397(1)	4286(2)	64(1)
O(14)	11067(1)	2446(1)	3109(1)	45(1)
O(7)	5242(1)	3329(1)	172(1)	39(1)
O(10)	4440(1)	6227(1)	988(2)	41(1)
O(11)	5194(2)	6697(1)	–299(2)	46(1)
C(3)	8965(2)	5391(1)	1221(2)	32(1)
C(4)	9077(2)	5703(1)	2370(2)	29(1)
C(5)	8015(2)	3265(1)	3642(2)	30(1)

C(6)	8993(1)	3131(1)	3190(1)	28(1)
C(1)	5928(1)	3792(1)	743(1)	25(1)
C(2)	5659(1)	4677(1)	1063(1)	23(1)
C(9)	10271(2)	5789(1)	2993(2)	33(1)
C(10)	10451(2)	6449(1)	3864(2)	38(1)
C(11)	10057(2)	3325(1)	4042(2)	32(1)
C(12)	11056(2)	3006(1)	3739(2)	33(1)
C(7)	5338(2)	5237(1)	68(2)	30(1)
C(8)	4937(2)	6097(1)	322(2)	28(1)
N(1)	1107(2)	8071(1)	–82(2)	37(1)
C(13)	169(2)	8551(2)	173(2)	47(1)
C(14)	–776(2)	8699(2)	–807(2)	45(1)
C(15)	–1593(2)	9350(2)	–584(3)	61(1)
C(16)	–2554(2)	9498(2)	–1555(3)	83(1)
C(17)	781(2)	7214(1)	–564(2)	39(1)
C(18)	1721(2)	6749(1)	–839(2)	41(1)
C(19)	1319(2)	6034(1)	–1633(2)	45(1)
C(20)	2229(3)	5643(2)	–2038(3)	83(1)
C(21)	2106(2)	8049(2)	872(2)	50(1)
C(22A)	1976(2)	7478(2)	1785(2)	61(1)
C(23A)	3042(3)	7264(3)	2656(4)	46(1)
C(24A)	3471(4)	8034(3)	3312(5)	62(2)
C(22B)	1976(2)	7478(2)	1785(2)	61(1)
C(23B)	3198(10)	7788(11)	2539(9)	85(6)
C(24B)	3302(15)	7412(17)	3617(11)	142(12)
N(2)	6618(2)	5787(1)	3904(2)	39(1)
C(25)	7538(2)	5894(1)	4906(2)	39(1)
C(26)	8009(2)	5068(1)	5416(2)	44(1)
C(27)	9049(2)	5190(2)	6287(2)	51(1)
C(28)	9478(3)	4376(2)	6850(2)	68(1)
C(29)	6169(2)	6632(2)	3440(2)	45(1)
C(30)	6907(2)	7062(1)	2857(2)	47(1)
C(31)	6459(2)	7912(2)	2393(3)	62(1)
C(32)	7172(3)	8292(2)	1722(4)	95(1)
C(33)	5713(2)	5204(2)	4038(2)	43(1)
C(34)	5121(2)	5484(2)	4857(2)	47(1)
C(35)	4240(2)	4851(2)	4938(3)	64(1)
C(36)	3640(3)	5072(2)	5774(3)	74(1)
N(3)	3869(2)	2705(2)	3835(2)	69(1)
C(37)	4533(2)	2529(2)	3428(2)	47(1)
C(38)	5391(2)	2279(2)	2915(3)	75(1)
N(4A)	3381(3)	197(2)	2311(3)	104(1)
C(39A)	2938(2)	782(2)	1900(3)	59(1)
C(40A)	2389(2)	1523(2)	1372(3)	68(1)

Table 72. Bond Lengths [Å] and Angles [deg] for (*Λ*,*S*,*S*,*S*)-*mer*-**22**·2CH_3CN.

Si–O(4)	1.7255(13)	O(2)–Si–O(1)	86.55(6)
Si–O(2)	1.7317(13)	O(6)–Si–O(1)	87.29(6)
Si–O(6)	1.7463(14)	O(3)–Si–O(1)	88.46(7)
Si–O(3)	1.7911(16)	O(5)–Si–O(1)	89.88(7)
Si–O(5)	1.8099(16)	C(3)–O(3)–Si	113.62(14)
Si–O(1)	1.8350(13)	C(4)–O(4)–Si	113.71(12)
O(3)–C(3)	1.301(2)	C(5)–O(5)–Si	114.67(14)
O(4)–C(4)	1.403(3)	C(6)–O(6)–Si	116.13(11)
O(5)–C(5)	1.294(2)	C(1)–O(1)–Si	115.66(9)
O(6)–C(6)	1.3945(18)	C(2)–O(2)–Si	117.08(9)
O(1)–C(1)	1.2876(16)	HO13–O(13)–C(10)	116(3)
O(2)–C(2)	1.4000(16)	HO15–O(15)–C(12)	103(2)
O(8)–C(3)	1.211(3)	HO11–O(11)–C(8)	112(3)

O(12)–C(10)	1.184(3)	O(8)–C(3)–O(3)	124.5(2)
O(13)–HO13	0.83(4)	O(8)–C(3)–C(4)	122.79(18)
O(13)–C(10)	1.302(3)	O(3)–C(3)–C(4)	112.70(18)
O(9)–C(5)	1.230(3)	O(4)–C(4)–C(9)	112.11(17)
O(15)–HO15	0.91(4)	O(4)–C(4)–C(3)	109.17(15)
O(15)–C(12)	1.325(3)	C(9)–C(4)–C(3)	112.17(18)
O(14)–C(12)	1.196(3)	O(9)–C(5)–O(5)	122.4(2)
O(7)–C(1)	1.2199(16)	O(9)–C(5)–C(6)	123.67(16)
O(10)–C(8)	1.192(3)	O(5)–C(5)–C(6)	113.93(17)
O(11)–HO11	0.74(3)	O(6)–C(6)–C(5)	107.54(12)
O(11)–C(8)	1.325(3)	O(6)–C(6)–C(11)	112.36(12)
C(3)–C(4)	1.523(3)	C(5)–C(6)–C(11)	110.43(14)
C(4)–C(9)	1.514(3)	O(7)–C(1)–O(1)	124.74(12)
C(5)–C(6)	1.494(3)	O(7)–C(1)–C(2)	122.77(8)
C(6)–C(11)	1.526(2)	O(1)–C(1)–C(2)	112.49(7)
C(1)–C(2)	15.152	O(2)–C(2)–C(1)	107.93(6)
C(2)–C(7)	1.519(2)	O(2)–C(2)–C(7)	111.04(12)
C(9)–C(10)	1.499(3)	C(1)–C(2)–C(7)	109.74(9)
C(11)–C(12)	1.486(3)	C(10)–C(9)–C(4)	113.49(17)
C(7)–C(8)	1.508(3)	O(12)–C(10)–O(13)	122.8(2)
N(1)–H(1N)	0.84(3)	O(12)–C(10)–C(9)	124.4(2)
N(1)–C(17)	1.498(3)	O(13)–C(10)–C(9)	112.8(2)
N(1)–C(13)	1.500(3)	C(12)–C(11)–C(6)	112.80(18)
N(1)–C(21)	1.513(3)	O(14)–C(12)–O(15)	123.1(2)
C(13)–C(14)	1.511(4)	O(14)–C(12)–C(11)	125.22(19)
C(14)–C(15)	1.525(3)	O(15)–C(12)–C(11)	111.6(2)
C(15)–C(16)	1.516(5)	C(8)–C(7)–C(2)	111.92(17)
C(17)–C(18)	1.500(3)	O(10)–C(8)–O(11)	123.66(18)
C(18)–C(19)	1.516(3)	O(10)–C(8)–C(7)	124.79(19)
C(19)–C(20)	1.497(4)	O(11)–C(8)–C(7)	111.5(2)
C(21)–C(22A)	1.515(4)	H(1N)–N(1)–C(17)	104.4(18)
C(22A)–C(23A)	1.546(5)	H(1N)–N(1)–C(13)	108.7(17)
C(23A)–C(24A)	1.496(6)	C(17)–N(1)–C(13)	113.42(18)
C(23B)–C(24B)	1.478(16)	H(1N)–N(1)–C(21)	104.5(17)
N(2)–H(2N)	0.87(3)	C(17)–N(1)–C(21)	113.34(18)
N(2)–C(33)	1.501(3)	C(13)–N(1)–C(21)	111.7(2)
N(2)–C(25)	1.503(3)	N(1)–C(13)–C(14)	113.0(2)
N(2)–C(29)	1.507(3)	C(13)–C(14)–C(15)	111.8(2)
C(25)–C(26)	1.507(3)	C(16)–C(15)–C(14)	112.5(2)
C(26)–C(27)	1.500(3)	N(1)–C(17)–C(18)	112.85(18)
C(27)–C(28)	1.503(4)	C(17)–C(18)–C(19)	111.84(19)
C(29)–C(30)	1.488(4)	C(20)–C(19)–C(18)	112.6(2)
C(30)–C(31)	1.515(3)	N(1)–C(21)–C(22A)	114.2(2)
C(31)–C(32)	1.508(5)	C(21)–C(22A)–C(23A)	116.5(3)
C(33)–C(34)	1.494(4)	C(24A)–C(23A)–C(22A)	110.6(4)
C(34)–C(35)	1.510(4)	H(2N)–N(2)–C(33)	104.4(17)
C(35)–C(36)	1.495(4)	H(2N)–N(2)–C(25)	107.0(16)
N(3)–C(37)	1.120(3)	C(33)–N(2)–C(25)	114.2(2)
C(37)–C(38)	1.446(4)	H(2N)–N(2)–C(29)	107.4(18)
N(4A)–C(39A)	1.135(4)	C(33)–N(2)–C(29)	111.62(19)
C(39A)–C(40A)	1.435(4)	C(25)–N(2)–C(29)	111.59(18)
O(4)–Si–O(2)	89.68(6)	N(2)–C(25)–C(26)	113.95(18)
O(4)–Si–O(6)	96.54(7)	C(27)–C(26)–C(25)	112.57(19)
O(2)–Si–O(6)	173.39(7)	C(26)–C(27)–C(28)	112.7(2)
O(4)–Si–O(3)	90.30(7)	C(30)–C(29)–N(2)	112.5(2)
O(2)–Si–O(3)	95.39(7)	C(29)–C(30)–C(31)	112.6(2)
O(6)–Si–O(3)	86.82(7)	C(32)–C(31)–C(30)	111.1(3)
O(4)–Si–O(5)	91.76(7)	C(34)–C(33)–N(2)	114.81(19)
O(2)–Si–O(5)	90.56(7)	C(33)–C(34)–C(35)	110.6(2)
O(6)–Si–O(5)	87.04(7)	C(36)–C(35)–C(34)	113.7(2)
O(3)–Si–O(5)	173.71(7)	N(3)–C(37)–C(38)	178.4(3)
O(4)–Si–O(1)	175.90(7)	N(4A)–C(39A)–C(40A)	179.2(4)

12 Appendix B: Formula Index

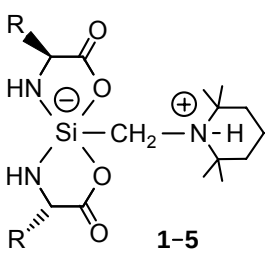

1–**5**

	R
1	H
2	Me
3	CH_2Ph
4	*i*-Pr
5	*t*-Bu

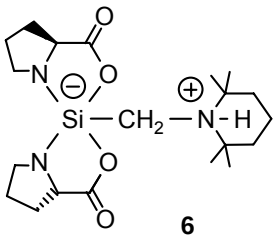

6

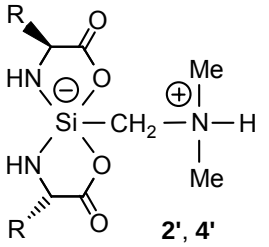

2', **4'**

	R
2'	Me
4'	*i*-Pr

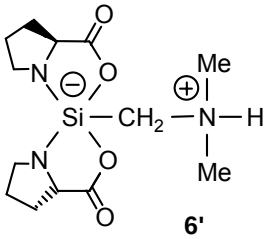

6'

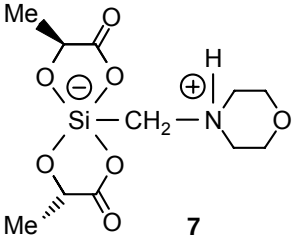

7

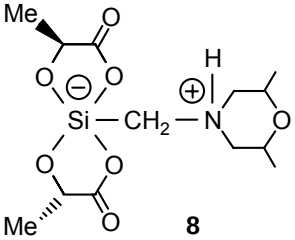

8

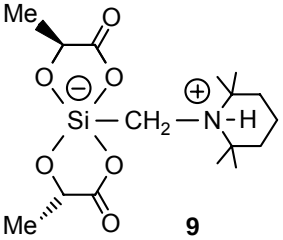

9

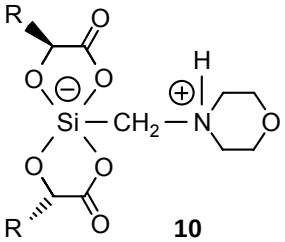

10

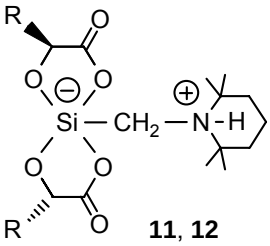

11, **12**

	R
10, **11**	CH_2Ph
12	Ph

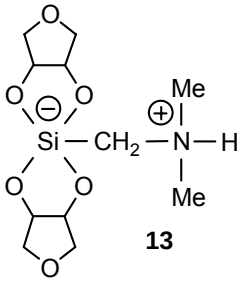

13

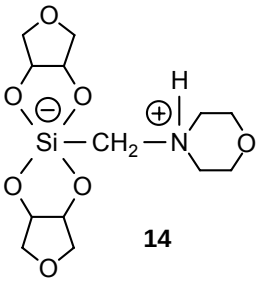

14

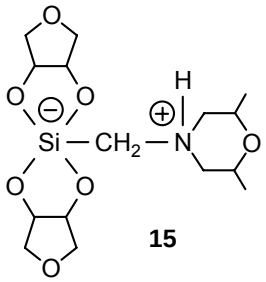

15

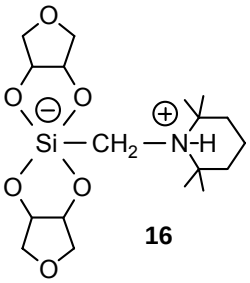

16

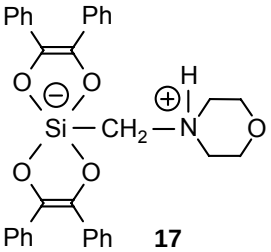

17

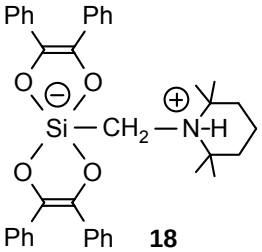

18

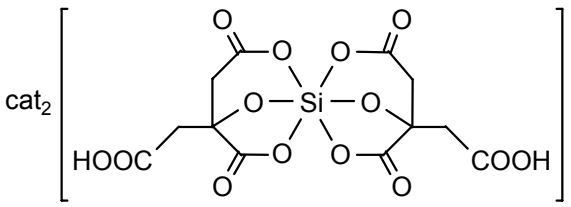

19

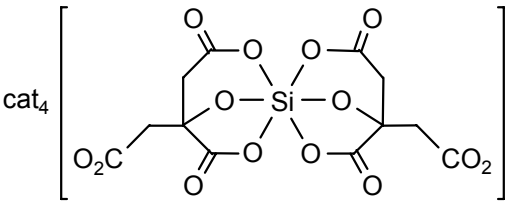

20

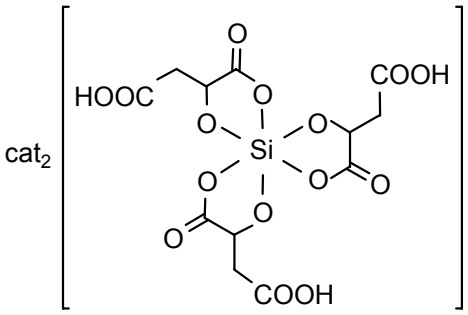

21, **22**

	cat ⊕
19, **20**	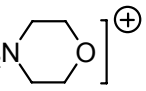
21	$[HN(n\text{-}Pr)_3]^{\oplus}$
22	$[HN(n\text{-}Bu)_3]^{\oplus}$

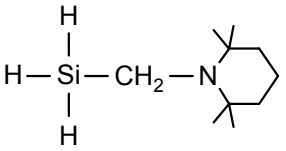

23

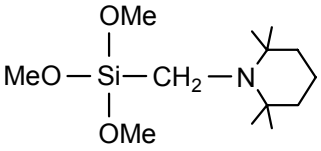

24

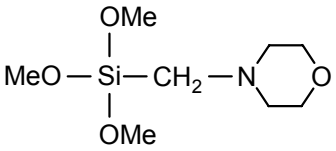

25

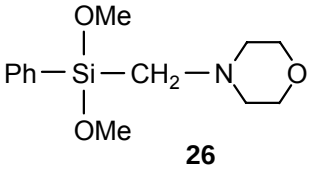

26

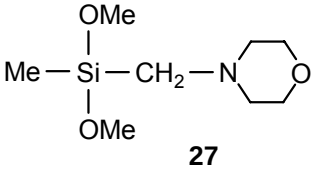

27

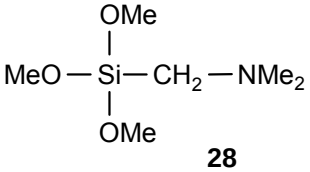

28

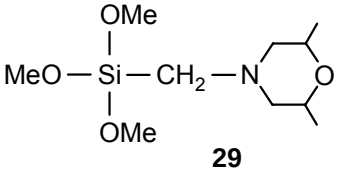

29

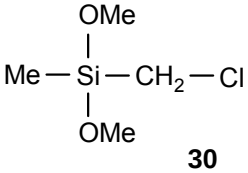

30

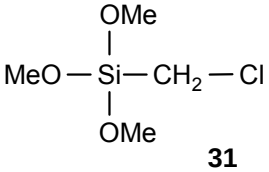

31

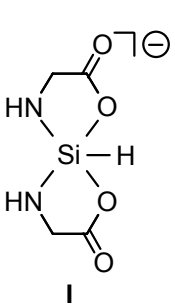

I

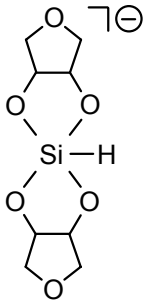

II

13 References and Notes

(1) Angel, R. J.; Ross, N. L.; Seifert, F.; Fliervoet, T. F. *Nature* **1996**, *384*, 441–444, and literature cited therein.

(2) Selected reviews dealing with compounds of higher-coordinate silicon: (a) Tandura, S. N.; Voronkov, M. G.; Alekseev, N. V. *Top. Curr. Chem.* **1986**, *131*, 99–189. (b) Sheldrick, W. S. In *The Chemistry of Organic Silicon Compounds*; Patai, S., Rappoport, Z., Eds.; Wiley: Chichester, U.K., **1989**; Part 1, pp 227–303. (c) Bassindale, A. R.; Taylor, P. G. In *The Chemistry of Organic Silicon Compounds*; Patai, S., Rappoport, Z., Eds.; Wiley: Chichester, U.K., **1989**; Part 1, pp 839–892. (d) Corriu, R. J. P.; Young, J. C. In *The Chemistry of Organic Silicon Compounds*; Patai, S., Rappoport, Z., Eds.; Wiley: Chichester, U.K., **1989**; Part 2, pp 1241–1288. (e) Holmes, R. R. *Chem. Rev.* **1990**, *90*, 17–31. (f) Chuit, C.; Corriu, R. J. P.; Reye, C.; Young, J. C. *Chem. Rev.* **1993**, *93*, 1371–1448. (g) Tacke, R.; Becht, J.; Lopez–Mras, A.; Sperlich, J. *J. Organomet. Chem.* **1993**, *446*, 1–8. (h) Verkade, J. G. *Coord. Chem. Rev.* **1994**, *137*, 233–295. (i) Tacke, R.; Dannappel, O. In *Tailor-made Silicon-Oxygen Compounds—From Molecules to Materials*; Corriu, R., Jutzi, P., Eds.; Vieweg: Braunschweig-Wiesbaden, Germany, **1996**; pp 75–86. (j) Lukevics, E.; Pudova, O. A. *Chem. Heterocycl. Compd. (Engl. Transl.)* **1996**, *32*, 1381–1418. (k) Holmes, R. R. *Chem. Rev.* **1996**, *96*, 927–950. (l) Kost, D.; Kalikhman, I. In *The Chemistry of Organic Silicon Compounds*; Rappoport, Z., Apeloig, Y., Eds.; Wiley: Chichester, U.K., **1998**; Vol. 2, Part 2, pp 1339–1445. (m) Pestunovich, V.; Kirpichenko, S.; Voronkov, M. In *The Chemistry of Organic Silicon Compounds*; Rappoport, Z., Apeloig, Y., Eds.; Wiley: Chichester, U.K., **1998**; Vol. 2, Part 2, pp 1447–1537. (n) Chuit, C.; Corriu, R. J. P.; Reye, C. In *Chemistry of Hypervalent Compounds*; Akiba, K., Ed.; Wiley-VCH: New York, **1999**; pp 81–146. (o) Tacke, R.; Pülm, M.; Wagner, B. *Adv. Organomet. Chem.* **1999**, *44*, 221–273. (p) Brook, M. A. *Silicon in Organic, Organometallic, and Polymer Chemistry*; Wiley: New York, **2000**; pp 97–114. (q) Tacke, R.; Seiler, O. In *Silicon Chemistry: From the Atom to Extended Systems*; Jutzi, P., Schubert, U., Eds.; Wiley-VCH: Weinheim, Germany, **2003**; pp 324–337. (r) Kost, D.; Kalikhman, I. *Adv. Organomet. Chem.* **2004**, *50*, 1–106.

(3) Bertrand, G. *Nature* **2004**, *305*, 783–785.

(4) Selected publications dealing with pentacoordinate silicon compounds: (a) Strohmann, C.; Tacke, R.; Mattern, G.; Kuhs, W. F. *J. Organomet. Chem*. **1991**, *403*, 63–71. (b) Tacke, R.; Sperlich, J.; Strohmann, C.; Mattern, G. *Chem. Ber*. **1991**, *124*, 1491–1496.

(c) Tacke, R.; Wiesenberger, F.; Lopez–Mras, A.; Sperlich, J.; Mattern, G. *Z. Naturforsch.* **1992**, *47b*, 1370–1376. (d) Tacke, R.; Becht, J.; Mattern, G.; Kuhs, W. F. *Chem. Ber.* **1992***, 125*, 2015–2018. (e) Tacke, R.; Lopez–Mras, A.; Sheldrick, W. S.; Sebald, A. *Z. Anorg. Allg. Chem.* **1993**, *619*, 347–358. (f) Tacke, R.; Mühleisen, M.; Jones, P. G. *Angew. Chem.* **1994***, 106*, 1250–1252; *Angew. Chem. Int. Ed. Engl*. **1994**, *33*, 1186–1188. (g) Tacke, R.; Mühleisen, M.; Lopez–Mras, A.; Sheldrick, W. S. *Z. Anorg. Allg. Chem.* **1995**, *621*, 779–788. (h) Tacke, R.; Becht, J.; Dannappel, O.; Ahlrichs, R.; Schneider, U.; Sheldrick, W. S.; Hahn, J.; Kiesgen, F. *Organometallics* **1996**, *15*, 2060–2077. (i) Pülm, M.; Tacke, R. *Organometallics* **1997**, *16*, 5664–5668. (j) Tacke, R.; Heermann, J.; Pülm, M.; Richter, I. *Organometallics* **1998**, *17*, 1663–1668. (k) Tacke, R.; Bertermann, R.; Biller, A.; Dannappel, O.; Pülm, M.; Willeke, R. *Eur. J. Inorg. Chem*. **1999**, 795–805. (l) Kost, D.; Kalikhman, I.; Krivonos, S.; Bertermann, R.; Burschka, C.; Neugebauer, R. E.; Pülm, M.; Willeke, R.; Tacke, R. *Organometallics* **2000**, *19*, 1083–1095. (m) Tacke, R.; Mallak, M.; Willeke, R. *Angew. Chem.* **2001**, *113*, 2401–2403; *Angew. Chem. Int. Ed.* **2001**, *40*, 2339–2341. (n) Richter, I.; Burschka, C.; Tacke, R. *J. Organomet. Chem.* **2002**, *646*, 200–203. (o) Tacke, R.; Bertermann, R.; Biller, A.; Burschka, C.; Penka, M. *Can. J. Chem.* **2003**, *81*, 1315–1325. (p) Bertermann, R.; Biller, A.; Kaupp, M.; Penka, M.; Seiler, O.; Tacke, R. *Organometallics* **2003**, *22*, 4104–4110.

(5) Selected publications dealing with hexacoordinate silicon compounds: (a) Tacke, R.; Stewart, A.; Becht, J.; Burschka, C.; Richter, I. *Can. J. Chem.* **2000**, *78*, 1380–1387. (b) Tacke, R.; Willeke, M.; Penka, M. *Z. Anorg. Allg. Chem.* **2001**, *627*, 1236–1240. (c) Richter, I.; Penka, M.; Tacke, R. *Inorg. Chem.* **2002**, *41*, 3950–3955. (d) Tacke, R.; Penka, M.; Popp, F.; Richter, I. *Eur. J. Inorg. Chem.* **2002**, 1025–1028. (e) Tacke, R.; Richter I. (inventors), PCT Int. Pat. Appl. WO 03/061640 A1 (applicant: Julius-Maximilians-Universitaet Wuerzburg), 31.07.2003; *Chem. Abstr. 139*, 154995 (**2003**). (f) Biller, A.; Burschka, C.; Penka, M.; Tacke, R. *Inorg. Chem.* **2002**, *41*, 3901–3908. (g) Seiler, O.; Burschka, C.; Penka, M.; Tacke, R. *Z. Anorg. Allg. Chem.* **2002**, *628*, 2427–2434. (h) Seiler, O.; Burschka, C.; Penka, M.; Tacke, R. *Silicon Chem.* **2002**, *1*, 355–365. (i) Seiler, O.; Penka, M.; Tacke, R. *Inorg. Chim. Acta* **2004**, *357*, 1955–1958. (j) Seiler, O.; Burschka, C.; Schwahn, D.; Tacke, R. *Inorg. Chem.* **2005**, *44*, 2318–2325. (k) Seiler, O.; Burschka, C.; Fischer, M.; Penka, M.; Tacke, R. *Inorg. Chem.* **2005**, *44*, 2337–2346.

(6) Laine, R. M.; Blohowiak, K. Y.; Robinson, T. R.; Hoppe, M. L.; Nardi, P.; Kampf, J.; Uhm, J. *Nature* **1991**, *353*, 642–644.

(7) Nielsen, F. H.; Poellot, R. *J. Trace Elem. Exp. Med.* **2004**, *17*, 137–149.

(8) Basile-Doelsch, I.; Meunier, J. D.; Parron, C. *Nature* **2005**, *433*, 399–402.

(9) Tacke, R. *Angew. Chem.* **1999**, *111*, 3197–3200. *Angew. Chem. Int. Ed.* **1999**, *38*, 3015–3017.

(10) (a) *Silicon and Siliceous Structures in Biological Systems*; Bendz, G., Lindqvist, I., Eds.; Plenum, New York, USA, **1978**. (b) Kröger, N.; Deutzmann, R.; Bergsdorf, C.; Sumper, M. *Proc. Natl. Acad. Sci. USA* **2000**, *97*, 14133–14138. (c) Weaver, J. C.; Morse, D. E. *Micr. Res. Tech.* **2003**, *62*, 356–367. (d) Bond, R.; McAuliffe, J. C. *Aust. J. Chem.* **2003**, *56*, 7–11. (e) Poulsen, N.; Sumper, M.; Kröger, N. *Proc. Natl. Acad. Sci. USA* **2003**, *100*, 12075–12080. (f) Luckarift, H. R.; Spain, J. C.; Naik, R. R.; Stone, M. O. *Nature Biotech.* **2004**, *22*, 211–213. (g) Balton, D.; Paine, G.; Patwardan, S. V.; Perry, C. C.; *J. Mater. Chem.* **2004**, *14*, 2231–2241. (h) Wenzl, S.; Deutzmann, R.; Hett, R.; Hochmuth, E.; Sumper, M. *Angew. Chem. Int. Ed.* **2004**, *43*, 5933–5936.

(11) Sumper, M.; Kröger, N. *J. Mater. Chem.* **2004**, *14*, 2059–2065.

(12) Dannappel, O. *Doctoral Thesis*, University of Karlsruhe, **1995**.

(13) Pfrommer, B. *Doctoral Thesis*, University of Würzburg, **1998**.

(14) Richter, I. *Doctoral Thesis*, University of Würzburg, **1998**.

(15) (a) Tacke, R.; Bertermann, R.; Burschka, C.; Dragota, S.; Penka, M.; Richter, I. *J. Am. Chem. Soc.* **2004**, *126*, 14493–14505. (b) Tacke, R.; Bertermann, R.; Burschka, C.; Dragota, S. *Organometallics*, submitted.

(16) The crystal structure analyses were performed by Dr. Christian Burschka, Institute of Inorganic Chemistry, University of Würzburg.

(17) Sheldrick, G. M. SHELXS-97; University of Göttingen: Göttingen, Germany, 1997; Sheldrick, G. M. *Acta Crystallogr., Sect. A* **1990**, *46*, 467–473.

(18) Sheldrick, G. M. SHELXL-97; University of Göttingen: Göttingen, Germany, 1997.

(19) The hydrogen-bonding systems were analyzed by using the program system PLATON: Spek, A. L., PLATON; University of Utrecht: Utrecht, The Netherlands, 1998.

(20) In the case of **2b**, an additional intermolecular N1–H1···O3 interaction could be discussed (N1–H 0.888 Å, H···O3 2.637 Å, N1···O3 3.405 Å, N1–H···O3 145.21 deg) that leads to a cross-linkage of the chains built up by the N2–H···O4 hydrogen bonds to give a two-dimensional network. However, the H···O3 distance is slightly longer than the default cutoff value implemented in the program system PLATON.

(21) Kupče, Ē.; Lukevics, E. *J. Magn. Reson.* **1988**, *76*, 63–73.

(22) (a) IUPAC, *Nomenclatur der Anorganischen Chemie*, 1. Aufl., Verlag Chemie, Weinheim, **1994**, I-10.7.2, pp 224–227.

(23) Brorson, M.; Damhus, T.; Schäfer, C. E. *Inorg. Chem.* **1983**, *22*, 1569–1573.

(24) The computational studies were performed by Martin Penka, Institute of Inorganic Chemistry, University of Würzburg.

(25) Program system TURBOMOLE: Ahlrichs, R.; Bär, M.; Häser, M.; Horn, H.; Kömel, C. *Chem. Phys. Lett*. **1989**, *162*, 165–169. Optimized TZP+ basis sets (with additional polarization functions) used for the anionic model species **I**: Si, (13s10p1d)/[8s6p1d]; F and O, (11s7p1d)/[7s4p1d]; H, (6s2p)/[4s2p].

(26) (a) Schäfer, A.; Horn, H.; Ahlrichs, R. *J. Chem. Phys*. **1992**, *97*, 2571–2577. (b) Schäfer, A.; Huber, C.; Ahlrichs, R. *J. Chem. Phys*. **1994**, *100*, 5829–5835.

(27) (a) Weigend, F.; Häser, M. *Theor. Chem. Acc.* **1997**, *97*, 331–340. (b) Weigend, F.; Häser, M.; Patzelt, H.; Ahlrichs, R. *Chem. Phys. Lett.* **1998**, *294*, 143–152.

(28) Publications dealing with zwitterionic λ^5*Si*-silicates containing ligands that derive from α-hydroxycarboxylic acids: (a) Tacke, R.; Lopez-Mras, A.; Jones, P. G. *Organometallics* **1994**, *13*, 1617–1623. (b) Mühleisen, M.; Tacke, R. *Organometallics* **1994**, *13*, 3740–3742. (c) Mühleisen, M.; Tacke, R. *Chem. Ber.* **1994**, *127*, 1615–1617. (d) Tacke, R.; Heermann, J.; Pülm, M. *Organometallics* **1997**, *16*, 5648–5652. (e) Tacke, R.; Pfrommer, B.; Pülm, M.; Bertermann, R. *Eur. J. Inorg. Chem.* **1999**, 807–816.

(29) (a) Tacke, R.; Bertermann, R.; Burschka, C.; Dannappel, O.; Dragota, S.; Penka, M. *Organometallics*, submitted. (b) Tacke, R.; Bertermann, R.; Burschka, C.; Dragota, S. *Angew. Chem. Int. Ed.* **2005**, *44*, 5292–5295. *Angew. Chem.* **2005**, *117*, 5426–5429.

(30) (a) Benner, K.; Klüfers, P.; Schuhmacher, J. *Z. Anorg. Allg. Chem.* **1999**, *625*, 541–543. (b) Kinrade, S. D.; Deguns, E. W.; Gillson, A.-M. E.; Knight, C. T. G. *J. Am. Chem. Soc. Dalton Trans.* **2003**, 3713–3716. (c) Lambert, J. B.; Lu, G.; Singer, S. R.; Kolb, V. M. *J. Am. Chem. Soc.* **2004**, *126*, 9611–9625. (d) Klüfers, P.; Kopp, F.; Vogt, M. *Chem. Eur. J.* **2004**, *10*, 4538–4545. (e) Kinrade, D. S.; Balec, R. J.; Schach, A. S.; Wang, J.; Knight, C. T. G *J. Am. Chem. Soc. Dalton Trans.* **2004**, 3241–3243.

(31) (a) Twinning and disorder in the crystal structure of **14**: Refinement of the morpholinio group in the structure of **14** could only be achieved with a model of disorder, splitting the atoms C10 to C13 and atom O7. The conformation shown in Figure 35 is occupied to 52%. The residual 48% of electron density was assigned to a second part of the

morpholinio ring (also showing the chair conformation) generated by a local mirror plane running through atom N. This disorder could partially be resolved by considering additional but mostly weaker reflections that lead to a larger triclinic cell space group $P\bar{1}$, (a = 9.941 Å, b = 17.727 Å, c = 19.783 Å, α = 116.379 deg, β = 104.021 deg, γ = 90.816 deg, Z = 8). With this larger cell only two out of four crystallographically independent molecules show the same type of disorder. The other two are not disordered. The twofold axis in this case has to be taken account for by a twin matrix −1 0 0 0 −1 0 1 1 1. (b) Disorder in the crystal structure of **16**: The crystallographic unit cell given in Table 1 contains three crystallographically independent molecules. Those two molecules containing Si2 and Si3 are characterized by an almost identical structure. The structure of the third molecule containing Si1 is also very similar, except for a partial disorder of the oxygen atom O5. The position of O5 is occupied to 89%; the rest of the electron density (11%) is found to occupy the alternative position of the two possible envelope conformations of the oxolane ring.

(32) (a) Muetterties, E. L.; Guggenberger, L. J. *J. Am. Chem. Soc.* **1974**, *96*, 1748–1756. (b) Holmes, R. R.; Deiters, J. A. *J. Am. Chem. Soc.* **1977**, *99*, 3318–3326. (c) The degree of distortion was calculated by using the dihedral angle method described in refs 32a and 32b. All nine dihedral angles and the values for the reference geometry of the ideal square pyramid given in ref 32a were considered for this calculation.

(33) The distortions of the trigonal-bipyramidal Si-coordination polyhedra of the three independent molecules found in the crystal lattice of **16** do not satisfy the criteria of true Berry-type distortions as defined in ref 32.

(34) (a) Tacke, R.; Burschka, C., Richter, I.; Wagner, B.; Willeke, R. *J. Am. Chem. Soc.* **2000**, *122*, 8480–8485. (b) Refs. 4o, and 5c,d,e.

(35) From the ^{1}H NMR spectra obtained, the coalescence temperature T_C and the exchange rate k_C at the coalescence point were extracted, and the values for the activation free enthalpy $\Delta G^{\ddagger}$ for the isomerization processes were calculated by using the Eyring equation ($\Delta G^{\ddagger}$ = 19.14 T_C [10.32 + log (T_C/k_C)] [J mol^{-1}]). Weber, U.; Thiele, H. *NMR spectroscopy: modern spectral analysis*, Wiley-VCH: Weinheim, 1998, pp. 339–361.

(36) (a) Program system TURBOMOLE: Ahlrichs, R.; Bär, M.; Häser, M.; Horn, H.; Kömel, C. *Chem. Phys. Lett*. **1989**, *162*, 165–169. Optimized TZP+ basis sets (with additional polarization functions) used for the anionic model species **II**: Si, (13s10p1d)/[8s6p1d]; O and C, (11s7p1d)/[7s4p1d]; H, (6s2p)/[4s2p]. (b) TZP basis set: Schäfer, A.; Horn, H.; Ahlrichs, R. *J. Chem. Phys*. **1992**, *97*, 2571.

(37) (a) Tacke, R.; Bertermann, R.; Biller, A.; Dannappel, O.; Penka, M.; Pülm, M.; Willeke, R. *Z. Anorg. Allg. Chem*. **2000**, *626*, 1159–1173. (b) See refs. 4i,k. (c) Tacke, R.; Pülm, M.; Richter, I.; Wagner, B.; Willeke, R. *Z. Anorg. Allg. Chem.* **1999**, *625*, 2169–2177.

(38) Dragota, S.; Bertermann, R.; Burschka, C.; Heermann, J.; Penka, M.; Richter, I.; Wagner, B.; Tacke, R. *Silicon Chem.* **2002**, *1*, 291–297.

(39) (a) Sperlich, J.; Becht, J.; Mühleisen, M.; Lopez-Mras, A.; Sheldrick, W. S.; Sebald, A. *Z. Anorg. Allg. Chem.* **1993**, *619*, 347–358. (b) Tacke, R.; Ulmer, B.; Wagner, B.; Arlt, M. *Organometallics* **2000**, *19*, 5297–5309. (c) Richter, I.; Penka, M.; Tacke, R. *J. Am. Chem. Soc.* **2002**, *21*, 3050–3053.

(40) Arlt, M.; Wurziger, H.; Tacke, R.; Abufarag, A.; Ulmer, B. (Merck Patent GmbH); Ger. Pat. Appl. DE 199 39 815 A1, 1999.

(41) Tacke, R.; Bertermann, R.; Burschka, C.; Dragota, S. *Z. Anorg. Allg. Chem.* **2004**, *630*, 2006–2012.

(42) Zelewsky, A.; Knof, U. *Angew. Chem.* **1999**, *111*, 312–333. *Angew. Chem. Int. Ed.* **1999**, *38*, 302–322.

(43) The composition of this solvate was deduced from the crystal structure analysis. However, the methanol content of the bulk material might differ from that of the single crystal studied, because the product loses part of the methanol very easily at ambient conditions. This problem also explains the poor quality of the elemental analysis.

(44) (a) Program WIN-DAISY 4.05; Bruker-Franzen GmbH: Bremen, Germany, 1998. (b) Weber, U.; Germanus, A.; Thiele, H. *Fresenius J. Anal. Chem.* **1997**, *359*, 46–49.

(45) (a) Braun, S.; Kalinowski, H.-O.; Berger, S. *150 and More Basic NMR Experiments*, Wiley-VCH: Weinheim, Germany, 1998, pp. 136–139. (b) Braun, S.; Kalinowski, H.-O.; Berger, S. *150 and More Basic NMR Experiments*, Wiley-VCH: Weinheim, Germany, 1998, pp. 140–143.

(46) Apart from some remaining dichloromethane (solvent for the synthesis), the sample was NMR-spectroscopically pure. The dichloromethane could not be totally removed in vacuo at 60 °C, and drying at higher temperatures resulted in a partial decomposition. These problems, together with the hydrolytic sensitivity of the sample, are responsible for the unsatisfactory results obtained in the elemental analyses.

(47) Sperlich, J.; Becht, J.; Mühleisen, M.; Wagner, S. A.; Mattern, G.; Tacke, R. *Z. Naturforsch. B* **1993**, *48*, 1693–1706.

(48) Tacke, R.; Lopez-Mras, A.; Sperlich, J.; Strohmann, C.; Kuhs, W. F.; Mattern, G.; Sebald, A. *Chem. Ber*. **1993**, *126*, 851–861.

Danksagung

Herrn Prof. Dr. R. Tacke gilt mein herzlicher Dank für die interessante Themenstellung, den gewährten wissenschaftlichen Freiraum, seine stete Diskussionsbereitschaft, die ausgezeichneten Arbeitsbedingungen und die Tagungs-Einladungen.

Für die Aufnahme von NMR-Spektren, die Einarbeitung in die praktischen Aspekte der Festkörper- und Lösungs-NMR-Spektroskopie, die Hilfe bei Spezialmessungen danke ich dem Herrn Dr. R. Bertermann. Für die Aufnahme von Lösungs-NMR-Spektren danke ich Frau M.-L. Schäfer, sowie den Herrn Dr. I. Richter und Dr. O. Seiler für die Aufnahme von zahlreichen Festkörper-Spektren. Für die Durchführung einer Vielzahl von Kristallstrukturanalysen sowie wissenschaftliche Diskussionen über die Röntgenbeugung und die freundliche Unterstützung gilt mein Dank Herrn Dr. C. Burschka.

Frau R. Schedl und Herrn C.-P. Kneis danke ich für die Durchführung der Elementaranalysen sowie DSC-Messungen. Herrn B. Fertig danke ich für die stets schnelle Reparatur und Anfertigung von Glasgeräten. Den Angestellten aus der Chemikalienausgabe und der Werkstatt danke ich ebenfalls für die kompetente Unterstützung und Hilfe. Unseren Sekretärinnen Frau S. Estenfelder, Frau I. Pross und Frau L. Tietze sei an dieser Stelle aus gleichem Grunde ebenfalls vielfach gedankt.

Allen aktuellen Kollegen in unserer Arbeitsgruppe sowie den ehemaligen, die ich im Laufe der Jahre kennenlernen durfte und ganz besonders Herrn Dr. I. Richter gilt mein außerordentlicher Dank für die freundliche Arbeitsatmosphäre und die gute Zusammenarbeit.

Dem Fitness Show-Team Wöhrle danke ich für die Freundlichkeit und für eine wirklich hervorragende sportliche Zeit. Zahlreiche gelungene Auftritte und Stammtisch-Abende werden mir in Erinnerung bleiben.

Ganz besonders möchte ich meinem Freund danken, der mir während dieser ganzen Zeit seine Unterstützung schenkte.

Vor allem danke ich meiner Mutter, die mir mein Studium ermöglicht und mich stets unterstützt hat. Meinem Bruder danke ich ebenfalls für seine Unterstützung.

Lebenslauf

Persönliche Daten

Simona Olimpia Dragota
geboren am 11.09.1977 in Sibiu (Hermannstadt), Rumänien
rumänisch, ledig

Bildungsweg

Doktorarbeit

seit 11 2000 Bayerische Julius-Maximilians-Universität Würzburg; Arbeitskreis Prof. Dr. R. Tacke; „Contributions to the Chemistry of Higher-Coordinate Silicon: Synthesis, Structure, and Stereodynamics of New Silicon(IV) Complexes with $Si O_2N_2C$, $Si O_4C$, or $Si O_6$ Skeletons"

Studium

06 2000 Abschluss: Diplom-Chemikerin
Mittelnote der Diplom-Prüfung: 9.40 von 10 (Gesamturteil: sehr gut)
Diplomarbeit: „Synthese und Reaktionen ausgewählter Tetrafluoride der 6. Hauptgruppe"

1996–2000 Studium der Chemie (Diplom) an der Babeş-Bolyai-Universität Cluj-Napoca (Klausenburg), Fakultät für Chemie und Chemisches Ingenieurwesen, Rumänien

04–09 1999 Auslandssemester an der Bayerischen Julius-Maximilians-Universität Würzburg

11–12 1998 Forschungspraktikum an der Universität Bremen, Institut für Anorganische und Physikalische Chemie; Arbeitskreis Prof. Dr. R. Mews

Tätigkeiten

seit 11 2000 Wissenschaftliche Mitarbeiterin am Institut für Anorganische Chemie der Universität Würzburg

Schulbildung

15.07.1996 Allgemeine Hochschulreife (Abitur; Gesamturteil: gut)

1992–1996 „Gheorghe-Lazăr" Kolleg, Sibiu (Hermannstadt), Rumänien

1984–1992 Grund- und Hauptschule, Sibiu (Hermannstadt), Rumänien

Wissenschaftliche Veröffentlichungen und Konferenzbeiträge in Posterform

1. Dragota, S.; Bertermann, R.; Burschka, C.; Heermann, J.; Penka, M.; Richter, I.; Wagner, B.; Tacke, R. Zwitterionic Spirocyclic λ^5*Si*-Silicates with Two *cis*-1,2-Diphenylethene-1,2-diolato(2–) Ligands: Synthesis and Structural Characterization *Silicon Chem.* **2002**, *1*, 291–297.

2. Tacke, R.; Bertermann, R.; Burschka, C.; Dragota, S.; Penka, M.; Richter, I. Spirocyclic Zwitterionic λ^5*Si*-Silicates with Two Bidentate Ligands Derived from α-Amino Acids or α-Hydroxycarboxylic Acids: Synthesis, Structure, and Stereodynamics *J. Am. Chem. Soc.* **2004**, *126*, 14493–14505.

3. Tacke, R.; Bertermann, R.; Burschka, C.; Dragota, S. Hexacoordinate Silicon(IV) Complexes with *Si*O_6 Skeletons and Multidentate Ligands Derived from Citric Acid or Malic Acid *Z. Anorg. Allg. Chem.* **2004**, *630*, 2006–2012.

4. Tacke, R.; Bertermann, R.; Burschka, C.; Dragota, S. Diastereo- and Enantiomerically Pure Zwitterionic Spirocyclic λ^5*Si*-[(Ammonio)methyl]silicates with an *Si*O_2N_2C Skeleton Containing Two Bidentate Chelate Ligands Derived from α-Amino Acids, *Organometallics*, eingereicht.

5. Tacke, R.; Bertermann, R.; Burschka, C.; Dragota, S. A Zwitterionic Spirocyclic Pentacoordinate Silicon Compound with a Remarkable Stability in Aqueous Solution, Synthesized in Water via Si–O and Si–C Bond Cleavage, *Angew. Chem. Int. Ed.* **2005**, *44*, 5292–5295; *Angew. Chem.* **2005**, *117*, 5426–5429.

6. Tacke, R.; Bertermann, R.; Burschka, C.; Dragota, S.; Dannappel, O.; Penka, M. Zwitterionic Spirocyclic λ^5*Si*-[(Ammonio)methyl]silicates Containing Two Bidentate *meso*-Oxolane-3,4-diolato(2–) Ligands: Chemistry in Aqueous and Nonaqueous Solution, *Organometallics*, eingereicht.

7. Dragota, S.; Bertermann, R.; Burschka, C.; Tacke, R. Twofold Deprotonated α-Amino Acids as Bidentate Ligands of Pentacoordinate Silicon *13th International Symposium on Organosilicon Chemistry – 35th Organosilicon Symposium*, Guanajuato, Mexico, August 25–30, 2002; No. P2-46.

8. Penka, M.; Dragota, S.; Bertermann, R.; Burschka, C.; Tacke, R. Spirocyclic Zwitterionic λ^5*Si*-Silicates with Two Bidentate Ligands Derived from α-Amino Acids: Synthesis, Structure and Stereodynamics *37th Silicon Symposium*, Philadelphia, PA, USA, , May 20–22, 2004; No. P39.

9. Dragota, S.; Bertermann, R.; Burschka, C.; Penka, M.; Tacke, R. Chemistry of Zwitterionic λ^5*Si*-[(Ammonio)methyl]silicates containing Two Bidentate *meso*-Oxolane-3,4-diolato(2–) Ligands in

Aqueous Solution *14th International Symposium on Organosilicon Chemistry – 35th Organosilicon Symposium*, Würzburg, Germany, August 31–05, 2005; No. P160.

Erklärung

Hiermit erkläre ich an Eides statt, dass ich die Dissertation

Contributions to the Chemistry of Higher-Coordinate Silicon:
Synthesis, Structure, and Stereodynamics of New Silicon(IV) Complexes
with *Si*O_2N_2C, *Si*O_4C, or *Si*O_6 Skeletons

selbständig angefertigt und keine anderen als die von mir angegebenen Quellen und Hilfsmittel benutzt habe.

Ich erkläre außerdem, dass diese Dissertation weder in gleicher oder anderer Form bereits in einem anderen Prüfungsverfahren vorgelegen hat.

Ich habe früher außer den mit dem Zulassungsgesuch urkundlich vorgelegten Graden keine weiteren akademischen Grade erworben oder zu erwerben versucht.

Würzburg, den

_____

(Simona Olimpia Dragota)